

Antisense Oligonucleotide-mediated Alternative Splicing Strategies to Treat the Type-1 Fibrillinopathies

Jessica M. Cale

Bachelor of Science (Honours)

This thesis is presented for the degree of
Doctor of Philosophy

Centre for Molecular Medicine and Innovative Therapeutics,
Murdoch University

2021

Declaration

I, declare that:

This thesis is my own account of my research except where other sources are acknowledged.

The thesis contains as its main content, work that has not been previously submitted for a degree at any other university

In the future, no part of this thesis will be used in a submission in my name, for any other degree or diploma in any university or other tertiary institution without the prior approval of Murdoch University and where applicable, any partner institution responsible for the joint-award of this degree.

This thesis does not contain any material previously published or written by another person, except where due reference has been made in the text.

This thesis does not violate or infringe any copyright, trademark, patent, or other rights whatsoever of any person.

This thesis contains published work and work prepared for publication, some of which has been co-authored. All co-authors, where stated and certified by my principal Supervisor or Executive Author, have agreed that the works presented in this thesis represent substantial contributions from myself

The research involving human data reported in this thesis was assessed and approved by the Murdoch University Human Research Ethics Committee Approval numbers: 2013_156 and 2017_2017; and The University of Western Australia Human Research Ethics Committee. Approval number: RA4/1/2295.

The work described in this thesis was funded by the Australian Government National Health and Medical Research Council, and a Research training Program scholarship was kindly provided Murdoch University.

Signature:

Date: 02/03/2021

Abstract

The type-1 fibrillinopathies are a family of connective tissue disorders of which Marfan syndrome is the most common, affecting between 2-3 in 10,000 individuals. Marfan syndrome is a multisystem disorder characterised by ocular, skeletal and cardiovascular abnormalities and can be caused by any one of over 2800 unique mutations reported across the fibrillin-1 (*FBNI*) gene. *FBNI* encodes the large extracellular glycoprotein, fibrillin-1; the fibrillin-1 monomers aggregate to form the backbone of microfibrils. Fibrillin-1 has both structural and regulatory roles, including the regulation of transforming growth factor-beta. This regulation is critical in maintaining extracellular matrix stability and dysregulation of this function is one of the keystones of the Marfan syndrome pathogenesis. Mutations in *FBNI* can result in reduced fibrillin-1 expression, loss-of-function or the production of two different fibrillin-1 proteins that are unable to interact to form functional microfibrils. The result in all three cases is a lack of functional microfibrils and destabilisation of the extracellular matrix. The current standard of care relies heavily on surgical intervention and lifelong use of medications to slow disease progression, thus the need for new therapeutic options that target the cause of disease.

This thesis focused on developing a suite of short synthetic nucleic acid sequences, known as antisense oligonucleotides, to selectively manipulate *FBNI* pre-mRNA splicing. We hypothesised that the removal of an amenable mutation-associated exon would result in one of the following scenarios. For missense mutations, removing the mutation-associated exon from affected and unaffected transcripts would eliminate the aberrant sequence and restore homogeneity between fibrillin-1 monomers. For splice-site and in-frame deletion mutations, excluding the mutation-associated exon from the remaining healthy transcripts would restore the domain periodicity and monomer homogeneity. Lastly, for mutations resulting in a premature termination codon, excluding the mutation-associated exon from the affected transcripts would restore the reading frame, rescuing transcript functionality. The mutation-associated exon would also need to be removed from the unaffected transcripts to maintain monomer homogeneity. For each of these scenarios, we hypothesised that the internally truncated proteins produced would be capable of forming functional microfibrils, thereby reducing the severity or slowing the progression of the Marfan syndrome phenotype.

As an initial proof-of-concept for this project, antisense oligonucleotide sequences targeting *FBNI* exon 52 were assessed. A promising sequence induced dose-dependent exon skipping in healthy control cells allowing us to observe the formation of healthy fibrillin-1 fibres with 0% exon skipping, loss of extruded fibrillin-1 fibres with 50% skipping; mimicking the disease-like state, and subsequent re-appearance of extracellular fibrillin-1 fibres with greater than 80% skipping indicating that the internally truncated fibrillin-1 monomers are capable of forming aggregates. Similarly, we demonstrate that *FBNI* exons 47 and 59 can be efficiently excluded,

and sufficient skipping can result in fibrillin-1 fibre formation. However, many of the *FBNI* exons targeted were not as readily excised from the mature mRNA.

Comparison of three antisense oligonucleotide chemistries revealed the promising efficacy of the newer thiophosphoramidate morpholino oligomer chemistry. Similar to the commonly used phosphorodiamidate morpholino oligomer, the thiophosphoramidate morpholino oligomer sequences resulted in efficient and consistent *FBNI* exon 52 skipping. Both chemistries also had little effect on paraspeckle protein distribution, an indicator of toxicity, unlike the third, 2'OMe-PS, chemistry that caused gross paraspeckle protein disruption. Therefore, thiophosphoramidate morpholino oligomer should be included in the repertoire of chemistries routinely used in studies developing antisense therapeutics.

Lastly, while we demonstrate that >80% exon skipping can lead to fibrillin-1 microfibril-like formations in vitro, we could not confirm the functionality of these fibres nor the effect of exon skipping on the Marfan syndrome phenotype. Nevertheless, this study demonstrates proof-of-concept and lays a solid foundation for further development of antisense oligonucleotides to treat the type-1 fibrillinopathies.

Plain-language summary

Marfan syndrome is a rare disease of the connective tissue or ‘glue’ that holds our cells together and allows us to move. Those affected by Marfan syndrome are usually extremely tall with long arms, legs, fingers and toes. However, this disease also causes the progressive growth of the aorta, the largest blood-carrying vessel in the body. If left untreated, the aorta can continue to expand, eventually leading to death. Marfan syndrome affects those of all ethnicities and genders equally and yet there is no effective therapy targeting the cause of disease and no cure. Currently, treatment of Marfan syndrome relies heavily on corrective surgery and lifelong use of drugs to slow the aorta's growth.

Marfan syndrome has no cure; however, it does have a known genetic cause, an error in the DNA or building blocks of life that direct the synthesis of an essential protein called fibrillin-1. In a healthy individual, these fibrillin-1 proteins form a supportive scaffold between the cells in our body. However, for an individual with Marfan syndrome, the error in one copy of the fibrillin-1 gene makes a protein that prevents normal formation of the scaffold, leading to the symptoms associated with Marfan syndrome. Knowing the cause of the disease is essential. It allows for the use of synthetic alternatives of these building blocks of life called antisense oligonucleotides (AOs) to act like genetic white-out to mask the disease-causing part of the gene message and remove it from the final product.

We hypothesised that by using this genetic white-out, we could force cells to produce fibrillin-1 proteins that do not have the error and can therefore make a more functional scaffold. We anticipate that the ability to form the scaffold would reduce the severity or slow the progression of Marfan syndrome symptoms. In this thesis, we successfully identified and optimised several AOs that efficiently remove regions containing known fibrillin-1 errors. However, we also found that many regions of the fibrillin-1 gene message could not be efficiently removed and require further optimisation in genetic white-out design. We also demonstrated that removing the region containing the error can lead to the formation of a fibrillin-1 scaffold. However, further investigation is needed to assess the functionality of the re-established scaffold and to confirm that removing the error is beneficial for individuals with Marfan syndrome. This study lays a foundation for further development of AOs to treat Marfan syndrome.

Table of Contents

Declaration	i
Abstract	ii
Plain-language summary	iv
Table of Contents	v
List of Figures	viii
List of Tables	x
Science Communication	xi
Acknowledgements	xiii
List of Abbreviations	xiv
Chapter 1 Introduction and Literature Review	1
1.1 A review of the type-1 fibrillinopathies: pathophysiology, diagnosis and novel therapeutic strategies	2
1.1.1 Introduction to the type-1 fibrillinopathies	3
1.1.2 The spectrum of type-1 fibrillinopathies.....	4
1.1.3 Genotype-phenotype correlations	9
1.1.4 Models of pathogenesis.....	11
1.1.5 Life expectancy and current treatments	14
1.2 Gene expression and the splicing process	15
1.2.1 Splice sites and exon definition	16
1.2.2 Regulation of splicing	16
1.2.3 Alternative splicing.....	19
1.3 Altering exon selection as a genetic therapy	20
1.3.1 Antisense oligonucleotides	20
1.3.2 Chemistries	21
1.3.3 Delivery	22
1.3.4 Application of antisense oligonucleotides	23
1.4 Summary, final remarks, significance, and aims	28
1.4.1 Aims of this study:	28
Chapter 2 Materials and Methodology	30
2.1 Materials	31
2.1.1 General reagents.....	31
2.1.2 Buffers and solutions	33
2.2 Methods	33
2.2.1 Antisense oligonucleotide design and synthesis	33
2.2.2 Cell culture.....	34
2.2.3 Transfection	36
2.2.4 Cell harvesting and RNA extraction	37
2.2.5 Polymerase chain reaction and gel electrophoresis.....	38
2.2.6 Amplicon identity and mutation confirmation.....	41
2.2.7 Immunofluorescent staining analysis.....	42
Chapter 3 Proof-of-concept: Antisense Oligonucleotide-mediated Skipping of Fibrillin-1 Exon 52	45

3.1	Introduction.....	47
3.2	Results.....	50
3.2.1	The <i>FBNI</i> transcript and antisense oligonucleotide design	50
3.2.2	Evaluation of AOs to induce exon 52 skipping from <i>FBNI</i> transcripts.....	52
3.2.3	PMO52 induces efficient exon 52 skipping and an increase in fibrillin-1 immunofluorescent staining	54
3.3	Discussion.....	55
3.4	Materials and methods	59
3.4.1	Design and synthesis of antisense oligonucleotides.....	59
3.4.2	Cell culture and transfection	60
3.4.3	RNA extraction and RT-PCR analysis.....	61
3.4.4	Immunofluorescence.....	61
Chapter 4	Multiple Mutations One Drug.....	62
4.1	Introduction.....	63
4.1.1	The complexity of the type 1 fibrillinopathies	63
4.1.2	Mutation classification and pathogenesis.....	65
4.1.3	Aims and rationale	67
4.2	Confirming mutations in patient cells	69
4.3	AO design and synthesis	71
4.4	AO-mediated selection of <i>FBNI</i> exon 52	72
4.4.1	Assessment of AO-mediated inclusion of exon 52	72
4.4.2	Assessment of AO-mediated exclusion of exon 52 in patient fibroblasts.....	74
4.4.3	Optimisation of post-transfection incubation period.....	75
4.4.4	Evaluation of PMO52-mediated exon skipping and fibrillin-1 morphology	77
4.5	Targeting Exon 59.....	80
4.5.1	Exon 59 exclusion screening and optimisation	80
4.5.2	The effect of exon 59 skipping on fibrillin-1 morphology.....	83
4.6	Discussion.....	86
Chapter 5	Multi-exon Skipping Strategy	89
5.1	Fibrillin-1 mutation landscape.....	90
5.1.1	Multi-exon skipping strategy	91
5.2	Confirmation of patient mutations	93
5.2.1	Confirming the MFS ^{Δ47} mutation.....	93
5.2.2	Confirming the MFS ^{Δ45-47} mutation	95
5.3	Antisense oligonucleotide design.....	96
5.4	Identifying candidate AOs for <i>FBNI</i> exons 45, 46 and 47	97
5.4.1	Exon 45 and 46	97
5.4.2	Exon 47	98
5.5	Evaluation of PMO47-mediated exon skipping.....	100
5.6	Triple-exon skipping	103
5.6.1	Identification of promising cocktails	103
5.6.2	Evaluation of PMO cocktails for triple exon skipping.....	107
5.7	Discussion.....	111
Chapter 6	Alternative Targets and Antisense Oligonucleotide Chemistries.....	117
6.1	Introduction.....	118
6.1.1	Fibrillin-1 structure and potential targets.....	118
6.1.2	Antisense oligonucleotide chemistries	119
6.2	Additional <i>FBNI</i> targets	121
6.2.1	Antisense oligonucleotide design.....	121

6.2.2	Screening of 2'OMe-PS AOs	123
6.2.3	Promising sequences	128
6.3	Alternative AO chemistry	129
6.3.1	Delivery method optimisation.....	130
6.3.2	Comparison between TMO and 2'OMe-PS AOs	131
6.3.3	TMO, 2'OMe-PS and PMO chemistry comparison	135
6.4	Discussion.....	141
Chapter 7	Final Discussion and Conclusions.....	149
7.1	Current knowledge and splice-switching strategies.....	150
7.2	Main findings and study limitations.....	151
7.2.1	Proof-of-concept	151
7.2.2	Recalcitrant <i>FBNI</i> exons	153
7.2.3	Multi-exon skipping.....	154
7.2.4	Alternative chemistry.....	155
7.3	Unanswered questions and future challenges.....	156
7.3.1	The function of the fibrillin-1 isoforms created	156
7.3.2	Fibroblast and animal models in therapy development.....	158
7.3.3	Clinical trials for rare diseases	160
7.4	Final remarks and conclusions	161
Appendices.....		163
References.....		192

List of Figures

Figure 1.1: Domain Structure of the fibrillin-1 preproprotein.	4
Figure 1.2: The type-1 fibrillinopathies and associated regions in <i>FBN1</i>	10
Figure 1.3: Schematic of TGF- β regulation and dysregulation in Marfan syndrome	13
Figure 1.4: Simplified schematic of major spliceosome assembly and the mRNA splicing process.	18
Figure 1.5: Schematic exploring the possible outcomes of alternative splicing.	19
Figure 1.6: Possible applications of antisense oligonucleotides to modify gene expression.	24
Figure 1.7: Schematic of fibrillin-1 from splicing to microfibril formation	27
Figure 2.1: Antisense oligonucleotide nomenclature	34
Figure 2.2: Primer nomenclature	38
Figure 3.1: Schematic of <i>FBN1</i> pre-mRNA highlighting the region between exons 47 and 54 as well as AO binding sites	51
Figure 3.2: Evaluation of AOs designed to induce <i>FBN1</i> exon 52 skipping.	53
Figure 3.3: Evaluation of AO cocktails designed to induce <i>FBN1</i> exon 52 skipping.	54
Figure 3.4: Efficiency and effect of PMO52	55
Figure 3.5: Nomenclature of antisense oligonucleotides	60
Figure 4.1 Confirmation of patient cell line mutations	70
Figure 4.2: Evaluation of AO sequences designed to induce exon 52 inclusion.	73
Figure 4.3: Evaluation of AOs designed to induce skipping of <i>FBN1</i> exon 52	75
Figure 4.4: Exon 52 skipping efficiency and fibrillin-1 fibre formation post-transfection.	76
Figure 4.5: AO-mediated <i>FBN1</i> exon 52 skipping across three replicates.	77
Figure 4.6: Evaluation of PMO52-mediated exon 52 skipping and fibrillin-1 morphology	79
Figure 4.7: Schematic of <i>FBN1</i> pre-mRNA structure highlighting exons 56 to 62 and the binding sites of antisense oligonucleotides targeted to exon 59.	81
Figure 4.8: Evaluation of AO sequences targeting exon 59	83
Figure 4.9: Evaluation of PMO59-mediated exon 59 skipping and fibrillin-1 morphology.	84
Figure 5.1: Distribution of <i>FBN1</i> mutations by exon and type	90
Figure 5.2: Mutation confirmation in MFS ^{Δ47} fibroblasts	95
Figure 5.3: Mutation confirmation in MFS ^{Δ45-47} fibroblasts	96
Figure 5.4: Evaluation of AOs designed to induce skipping of <i>FBN1</i> exon 45 and 46.	98
Figure 5.5: Evaluation of AOs designed to induce <i>FBN1</i> exon 47 skipping.	99
Figure 5.6: PMO47 mediated exon 47 skipping	100
Figure 5.7: Evaluation of PMO47-mediated exon 47 skipping and fibrillin-1 morphology	102
Figure 5.8: Evaluation of five-AO cocktails designed to induce exon 45-47 skipping.	104
Figure 5.9: Evaluation of additional cocktails designed to induce exon 45-47 skipping.	106
Figure 5.10: Optimisation of PMO concentration required to induce exon 45-47 skipping	108
Figure 5.11: Evaluation of triple exon skipping mediated by a PMO cocktail.	110
Figure 6.1: Fibrillin-1 gene map.	119
Figure 6.2: Chemical representation of PMO, TMO and 2'OMe-PS compounds	121
Figure 6.3: Evaluation of 2'OMe PS AOs targeting specific <i>FBN1</i> exons for removal.	124
Figure 6.4: Evaluation of micro-walking AOs.	125
Figure 6.5: Evaluation of overlapping-AO cocktails targeting <i>FBN1</i> exon 16 and 32	127
Figure 6.6: Evaluation of PMO32 and PMO39 in healthy control and MFS patient fibroblasts	129
Figure 6.7: Optimisation of TMO delivery in healthy control fibroblasts.	131
Figure 6.8: Comparison of exon 52 skipping efficiency of 2'OMe-PS and TMO chemistries	132
Figure 6.9: Evaluation of skipping efficiency and NONO immunofluorescence staining after transfection with TMO and 2'OMe-PS AOs.	134
Figure 6.10: Evaluation of two AO sequences targeting <i>FBN1</i> exon 52 as the 2'OMe-PS, TMO and PMO chemistries.	136

Figure 6.11: Comparison of AO chemistry efficacy in control and MFS patient fibroblasts.....	137
Figure 6.12: Fibrillin-1 morphology and abundance after transfection with TMOs, 2'OMe-PS AOs or PMOs	139
Figure 6.13: SFPQ staining in fibroblasts after treatment with TMO, 2'OMe-PS AOs or PMOs ...	141

List of Supplementary Figures

Figure A2.1: Enlarged immunofluorescence staining images from Figure 4.6.....	169
Figure A2.2: Enlarged immunofluorescence staining images from Figure 4.9 part c.....	170
Figure A2.3: Enlarged immunofluorescence staining images from Figure 4.9 part d.	171
Figure A2.4: Enhancer and silencer motifs that are predicted to be altered by synonymous <i>FBNI</i> mutations.....	172
Figure A3.1: The location of predicted regulatory splicing motifs and AO annealing sites targeted to remove <i>FBNI</i> exons 45, 46 and 47.....	173
Figure A3.2: Enlarged immunofluorescence staining images from Figure 5.7.....	174
Figure A3.3: Enlarged immunofluorescence staining images from Figure 5.11.....	175
Figure A3.4: In silico prediction of the <i>FBNI</i> exon 45 mRNA secondary structure using the RNAfold web server ²¹⁷	176
Figure A3.5: In silico prediction of the <i>FBNI</i> exon 46 mRNA secondary structure using the RNAfold web server. ²¹⁷	176
Figure A3.6: In silico prediction of the <i>FBNI</i> exon 47 mRNA secondary structure using the RNAfold web server ²¹⁷	177
Figure A4.1: The location of predicted splicing motifs and AO annealing sites.	180
Figure A4.2: Enlarged immunofluorescence staining images from Figure 6.9.....	181
Figure A4.3: Enlarged immunofluorescence staining images from Figure 6.12 part a.....	182
Figure A4.4: Enlarged immunofluorescence staining images from Figure 6.12 part b.	183
Figure A4.5: Enlarged immunofluorescence staining images from Figure 6.12 part c.....	184
Figure A4.6: Blanket AO Python script.....	189
Figure A4.7: In silico prediction of the <i>FBNI</i> exon 32 mRNA secondary structure using the RNAfold web server ²¹⁷	190
Figure A4.8: In silico prediction of the <i>FBNI</i> exon 39 mRNA secondary structure using the RNAfold web server ²¹⁷	191

List of Tables

Table 1.1: Scoring of the systemic features of Marfan syndrome.....	7
Table 1.2: <i>FBNI</i> Mutation groups according to fibrillin-1 synthesis and deposition.	13
Table 2.1: List of reagents used in this study and their suppliers.....	31
Table 2.2: Composition of buffers made in-house.....	33
Table 2.3: Cell culture media and buffers.....	36
Table 2.4: List of primer sets.	39
Table 2.5: List of antibodies, details and dilutions.....	44
Table 3.1: Sequences and binding co-ordinates of control and <i>FBNI</i> exon 52 AOs.....	52
Table 4.1: <i>FBNI</i> mutation groups according to fibrillin-1 synthesis and deposition.....	66
Table 4.2: Antisense oligonucleotide sequences used in this study.....	71
Table 5.1: List of antisense oligonucleotides used in Chapter 5.....	97
Table 5.2: Cocktails of 2'OMe-PS AOs designed to induce triple-exon skipping 2'OMe-PS AO cocktails.	103
Table 5.3: Optimal triple-exon skipping cocktails.	107
Table 6.1: List of antisense oligonucleotides used in Section 6.2.....	122
Table 6.2: Overlapping AO cocktails.....	126
Table 6.3: Optimal exon 52 AO identified in the original screen and details of 20-mer versions used in chemistry comparison experiments.....	130
Table 7.1: Alignment of the optimal AOs targeting <i>FBNI</i> exons 47, 52 and 59 with the mouse <i>Fbn1</i>	160

List of Supplementary Tables

Table A1.1: A full list of antisense oligonucleotides used in this study.	164
Table A1.2: Details of all Marfan syndrome patient cell lines used in this study.....	168
Table A3.1: Donor splice site scores of human <i>FBNI</i> exon 47.....	177
Table A4.1: The skipping efficiencies of 2'OMe-PS AOs assessed in this thesis.....	185
Table A4.2: Proportion of effective <i>FBNI</i> 2'OMe-PS AO based on binding site.....	187
Table A4.3: The splice site scores for <i>FBNI</i> exons 27 and 49.....	187

Science Communication

Publications arising from this thesis

Cale, J. M., Fletcher, S. & Wilton, S. D. A Review of the Type-1 Fibrillinopathies: Pathophysiology, Diagnosis and Novel Therapeutic Strategies. *J Genet Syndr Gene Ther* **9**, 7 (2018). doi:10.4172/2157-7412.1000323.

Cale, J. M., Greer, K., Fletcher, S. & Wilton, S. D. Proof-of-concept: Antisense oligonucleotide mediated skipping of Fibrillin-1 exon 52. *International Journal of Molecular Sciences*. Submitted.

Conference Oral Presentations

Cale, J. M., Greer, K., Fletcher, S. & Wilton, S. D. Novel therapeutic strategies for Marfan syndrome using antisense oligonucleotides. *1st Perth RNA Salon* (2018). Perth, Australia.

Cale, J. M., Greer, K., Fletcher, S. & Wilton, S. D. Novel therapeutic strategies for Marfan syndrome using antisense oligonucleotides. *2nd International Symposium on Functional Nucleic Acids: From Laboratory to Targeted Molecular Therapy* (2018). Perth, Australia. 2nd place winner.

Wilton S.D., Cale J.M., Aung-htut M.T. Personalized medicines: Splice switching antisense oligomers to treat rare inherited diseases. *Bioinnovation Showcase* (2018). Perth, Australia.

Cale, J. M., Fletcher, S. & Wilton, S. D. Rescue of Fibrillin-1 Microfibril Formation in Individuals with Marfan Syndrome Caused by Exon 59 Mutations. *5th Science on the Swan conference* (2019). Perth, Australia.

Cale, J. M., Fletcher, S. & Wilton, S. D. Rescue of Fibrillin-1 Microfibril Formation in Individuals with Marfan Syndrome Caused by Exon 59 Mutations. *29th Combined Biological Sciences Meeting* (2019). Perth, Australia. 1st place winner.

Cale, J. M. Genetic Therapy for Marfan Syndrome. *Three Minute Thesis -Murdoch University* (2019). Perth, Australia. Finalist.

Cale, J. M. Genetic Therapy for Marfan Syndrome. *Perron Institute Three Minute Thesis* (2020). Perth, Australia.

Cale, J. M., Fletcher, S. & Wilton, S. D. Rescue of Fibrillin-1 Microfibril Formation in Fibroblasts from individuals with Marfan Syndrome. *Human Genome conference* (2020). International virtual conference.

Conference Poster Presentations

Cale, J. M., Greer, K., Fletcher, S. & Wilton, S. D. A genetic medicine to treat Marfan syndrome. *Inaugural Murdoch University Annual Research Symposium (MARS)* (2017). Perth, Australia.

Cale, J. M., Greer, K., Fletcher, S. & Wilton, S. D. Novel therapeutic strategy for Marfan syndrome using antisense oligonucleotides. *39th Annual Lorne Genome conference* (2018). Melbourne, Australia.

Cale, J. M., Greer, K., Fletcher, S. & Wilton, S. D. Novel therapeutic strategy for Marfan syndrome using antisense oligonucleotides. *10th International research symposium on Marfan syndrome and related disorders* (2018). Amsterdam, The Netherlands.

Cale, J. M., Greer, K., Fletcher, S. & Wilton, S. D. A Novel Therapeutic Strategy for Marfan Syndrome Utilising Antisense Oligonucleotides. *28th Combined Biological Sciences Meeting* (2018). Perth, Australia.

Cale, J. M., Greer, K., Fletcher, S. & Wilton, S. D. Novel therapeutic strategies for Marfan syndrome using antisense oligonucleotides. *2nd International Symposium on Functional Nucleic Acids: From Laboratory to Targeted Molecular Therapy* (2018). Perth, Australia.

Cale, J. M., Fletcher, S. & Wilton, S. D. Rescue of Fibrillin-1 Microfibril Formation in Individuals with Marfan Syndrome Caused by Exon 59 Mutations. *Symposium of Western Australian Neuroscience* (2019). Perth, Australia.

Cale, J. M., Fletcher, S. & Wilton, S. D. Rescue of Fibrillin-1 Microfibril Formation in Fibroblasts from individuals with Marfan Syndrome. *41st Annual Lorne Genome conference* (2020). Melbourne, Australia.

Cale, J. M., Fletcher, S. & Wilton, S. D. Rescue of Fibrillin-1 Microfibril Formation in Fibroblasts from individuals with Marfan Syndrome. *Human Genome conference* (2020). International virtual conference.

Cale, J. M., Fletcher, S. & Wilton, S. D. Rescue of Fibrillin-1 Microfibril Formation in Fibroblasts from Individuals with Marfan Syndrome. *29½ Combined Biological Sciences Meeting* (2020). Perth, Australia. 1st place winner.

Acknowledgements

No thesis comes together without the love and support of others; therefore, I would like to acknowledge those who supported me throughout this PhD. Firstly, I would like to thank Murdoch University for providing the financial support that allowed me the privilege of pursuing a Doctor of Philosophy.

I would like to express my sincerest gratitude to my supervisors, Steve and Sue; your support and guidance throughout my PhD have been invaluable. I appreciate the opportunity you gave me to carry out this exciting project and feel honoured to have been a part of the Molecular Therapy laboratory. Steve, your ability to come up with novel ideas inspires me to continue research and thank you for always finding time to discuss excellent results. Sue, you have been an incredible mentor throughout my PhD, supporting me through stressful times and providing invaluable advice.

I was advised early in my studies that intelligence alone is not enough to complete a PhD; although this may help, it is achieved through enthusiasm and perseverance. For myself, it was the conversations with colleagues that crystallised ideas and motivated me. I would like to thank the entire CMMIT group that I have had the privilege to work alongside. I would especially like thank Abbie, Kane, Kristin and Loren for patiently teaching me all I needed to know in the laboratory and providing the informal mentorship that allowed me to grow and learn.

To my family and friends (second family), no words can express how much your love, support, encouragement and understanding of my social absence over the last few years, means to me. A special thanks to my parents, you are the best role models a daughter could have, and I continually aspire to exceed your expectations. I appreciate your encouragement, assistance and evening phone calls throughout my PhD. Lastly, thank you Sarsha, my emotional support even when far from home

List of Abbreviations

Units

°C	Centigrade Celsius
µg	Microgram, 10 ⁻⁶ g
µl	Microlitre, 10 ⁻⁶ L
µm	Micrometre, 10 ⁻⁶ m
µmol	Micromole, 10 ⁻⁶ mole
b	Bases
bp	Base pairs
g	Gram
h	Hour(s)
Hz	Hertz
IU	International units
kbp	Kilo base pair
kDa	Kilodalton
l	Litre
min	Minute(s)
ml	Millilitre, 10 ⁻³ L
mm	Millimetre, 10 ⁻³ m
mmol	Millimole, 10 ⁻³ mole
ng	Nanogram, 10 ⁻⁹ g
rpm	Rotations per minute
sec	Second(s)

Abbreviations

2'OMe	2'-O-methyl modified oligonucleotide
ACMID	Acromicric dysplasia
ADAMTSL	A disintegrin and metalloproteinase with a thrombospondin motif-like protein
AO	Antisense oligonucleotide
Cas9	CRISPR associated protein 9
cbEFG	Calcium binding epidermal growth factor
cMFS	Classical Marfan syndrome
CRISPR	Clustered regularly interspaced short palindromic repeats
DMD	Duchenne muscular dystrophy
<i>DMD</i>	Dystrophin gene
DMEM	Dulbecco's Modified Eagle Medium
DMSO	Dimethyl sulfoxide
DNA	Deoxyribonucleic acid
DTT	Dithiothreitol
ECM	Extracellular matrix
EDTA	Ethylenediaminetetraacetic acid
EGF-like	Epidermal growth factor-like
ELS	Ectopia lentis syndrome
ESE	Exonic splice enhancer

ESS	Exonic splice silencer
<i>FBN1</i>	Fibrillin-1 gene
<i>FBN2</i>	Fibrillin-2 gene
<i>FBN3</i>	Fibrillin-3 gene
FBS	Foetal bovine serum
FDA	United states food and Drug administration
FL	Full-length transcript
GPHYSD2	Geleophysic dysplasia-2
IF	Immunofluorescence staining
IgG	Immunoglobulin G
ISE	Intronic splice enhancer
ISS	Intronic splice silencer
LLC	Large latent complex
LNA	Locked nucleic acid
LTBPs	Latent-transforming growth factor beta-binding proteins
MASS	Mitral valve, Aorta, Skin, Skeletal
MFLS	Marfan lipodystrophy syndrome
MFS	Marfan syndrome
MIM	Online Mendelian Inheritance in Man reference number
MOE	2'-O-methoxyethyl modified oligonucleotide
mRNA	Messenger ribonucleic acid
nMFS	Neonatal Marfan syndrome
NMD	Nonsense mediated decay
PBS	Phosphate-buffered saline
PCR	Polymerase Chain Reaction
PMO	Phosphorodiamidate morpholino oligomer
PPMO	Peptide conjugated phosphorodiamidate morpholino oligomer
pre-mRNA	Precursor messenger ribonucleic acid
PS	Phosphorothioate backbone
PTC	Premature termination codon
RNA	Ribonucleic acid
RT-PCR	Reverse Transcription Polymerase Chain Reaction
siRNA	Small interfering ribonucleic acid
SMA	Spinal muscular atrophy
SSKS	Stiff skin syndrome
TB	Transforming growth factor beta binding protein-like
TGF- β	Transforming growth factor beta
UMD	Universal mutation database
WB	Western blot
WMS2	Weill-Marchesani syndrome-2

*This thesis is dedicated to my parents
For their endless love, support and encouragement*

Chapter 1
Introduction and Literature Review

1.1 A review of the type-1 fibrillinopathies: pathophysiology, diagnosis and novel therapeutic strategies

The following is a modified version of the published review:

Cale, J. M., Fletcher, S. & Wilton, S. D. A Review of the Type-1 Fibrillinopathies: Pathophysiology, Diagnosis and Novel Therapeutic Strategies. *J Genet Syndr Gene Her* **9**, 7 (2018). doi:10.4172/2157-7412.100032

Attribution:

JC developed the concept, reviewed the literature, interpreted the findings, designed figures, and wrote the manuscript. SDW and SF developed the concept, edited the manuscript and provided supervision. All authors critically reviewed and approved the final version.

1.1.1 Introduction to the type-1 fibrillinopathies

The type-1 fibrillinopathies are a family of heritable connective tissue disorders characterised by skeletal, ocular and cardiovascular abnormalities. These diseases are caused by mutations in the fibrillin-1 gene (*FBNI*),¹ with over 2800 unique mutations, spread throughout the entire *FBNI* sequence, described in the Human Gene Mutation Database to date.² The majority of reported variants are either missense or nonsense single nucleotide variants; however, insertion, deletion, duplication and splicing mutations have also been described.²⁻⁴

Fibrillin-1 is one of three distinct genes in the fibrillin family, along with fibrillin-2 and fibrillin-3, all of which share extensive sequence similarities; with parallel domain structure and complete conservation of all cysteine residues.⁵ The fibrillins are large genes; *FBNI* consists of 66 exons spanning over 200Kb.⁶ While exon 1 of *FBNI* does not directly contribute to the translated product, the exon numbering system used in this thesis is based on the full 66-exon transcript ([NM_000138.5](#), [LRG_778t1](#)) in which the translation start site located in exon 2. The remaining 65 exons encode a 2871 amino acid pre-pro-protein that is cleaved by the protease furin into the large glycoprotein fibrillin-1 and the protein hormone asprosin.^{7,8}

All three fibrillin proteins are expressed during early embryogenesis and development,^{5,9} however fibrillin-2 and fibrillin-3 expression declines soon after birth.^{5,10} Fibrillin-1 and 2, in particular, have a diphasic expression pattern with fibrillin-2 appearing first followed by fibrillin-1, which continues to be expressed throughout life.⁹ Fibrillin-1 is expressed in the majority of connective tissues and has both structural¹¹ and regulatory roles.¹² As a major structural element of microfibrils, fibrillin-1 acts as a backbone to which other microfibril associated proteins bind,^{11,13} while also being essential for the stability of elastic fibres.^{14,15} In addition, fibrillin-1, in microfibril form, sequesters transforming growth factor-beta (TGF- β) regulating its bioavailability and thus activity.^{12,16} This regulation is critical to maintaining extracellular matrix stability.¹⁶

The assembly of fibrillin-1 into microfibrils is initiated immediately after translation and secretion when fibrillin-1 monomers aggregate into multimer units, bound by disulphide bonds between the first four cysteine residues at the N-terminus.¹⁷ Since the expression of fibrillin-1 and fibrillin-2 is diphasic, the majority of microfibrils observed are homopolymers containing either fibrillin-1 or fibrillin-2.¹⁸ However, Charbonneau¹⁸ demonstrated that the two fibrillins can form heteropolymers. Mutation studies performed in a mouse model have also shown that microfibrils can assemble in the absence of either fibrillin-1 or fibrillin-2 suggesting that each can compensate for the absence of the other.^{5,19}

The structure of fibrillin-1 is complex and highly repetitive, consisting of a large number of cysteine-rich domains (Figure 1.1). These include 47 epidermal growth factor (EGF)-like

domains, seven TGF- β binding protein-like (TB) domains and two hybrid domains^{20,21} (Figure 1.1). The hybrid domains share similarities with both the EGF-like and TB domains and have been shown to play an integral role in fibrillin-1 folding and microfibril assembly.^{21,22} Of the 47 EGF-like domains, 43 contain a consensus sequence for calcium-binding that is essential for protein stability and protection from proteolysis.²³ These repeats are, therefore, further denoted as cbEGF-like domains.²¹ Each EGF-like, cbEGF-like, TB and hybrid domain has 6-8 highly conserved cysteines that form disulphide bonds in specific patterns, assisting in protein folding and enhancing protein function.^{20,24} Mutations that disrupt these bonds are the most common cause of the type-1 fibrillinopathy, Marfan syndrome (MFS).²⁵

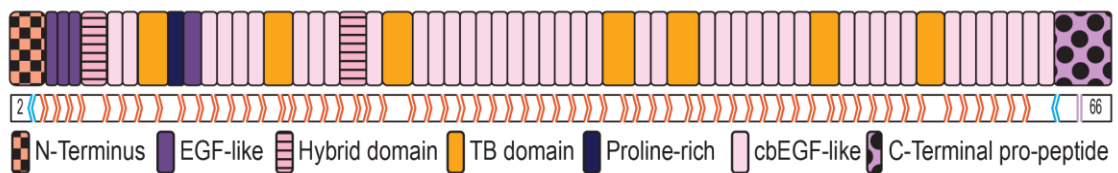


Figure 1.1: Domain Structure of the fibrillin-1 preproprotein.

Fibrillin-1 consists of four EGF-like domains and 43 calcium-binding EGF-like (cbEGF-like) domains interspaced with seven TGF- β binding protein-like (TB) domains and two hybrid domains. A proline-rich region toward the N-terminus has been implicated in the assembly and specificity of fibrillin-1 multimers.²⁰

1.1.2 The spectrum of type-1 fibrillinopathies

Marfan syndrome

Marfan syndrome (MFS, MIM [154700](#)) is the most common of the type-1 fibrillinopathies,²⁶ with an estimated prevalence of 2-3 in 10,000 individuals that remains consistent across gender, ethnicity and geographical distribution.^{27,28} MFS is inherited in an autosomal dominant manner, with approximately 25% to 30% of mutations arising *de novo*.^{29,30} However, despite being consistently described as an autosomal dominant condition, twelve cases of homozygous mutations have been recorded in the universal mutation database.³ A number of these cases have an unequivocal autosomal recessive inheritance pattern, with relatives of the proband being asymptomatic heterozygous carriers.^{31,32} This suggests that the inheritance pattern of selected mutations causing MFS is complex and still not fully understood.

Clinical features

Marfan syndrome is a multisystem disorder characterised by skeletal, cardiovascular and ocular abnormalities.^{33,34} The most noticeable features include increased height with dolichostenomelia and arachnodactyly; the disproportionate overgrowth of long bones and digits respectively, as well as joint hypermobility.³³ Spinal deformities such as scoliosis and dural ectasia, and chest wall deformities are also common features.^{33,34}

Ocular manifestations include myopia or near-sightedness, and ectopia lentis, which is the displacement of the crystalline lens from its natural location.³⁴ Such features generally present early in disease progression and are therefore critical diagnostic indicators, especially in children. However, these features are also common to a multitude of other diseases, including several other type-1 fibrillinopathies.³³

Cardiovascular abnormalities are the most common cause of death of MFS patients, especially in the most severe form, neonatal Marfan syndrome (nMFS), which is characterised by the early onset of cardiovascular manifestations.^{35,36} Death is typically the result of progressive aortic root enlargement and aortic aneurysm, that can eventuate into aortic regurgitation, dissection or rupture.³⁷ Other cardiovascular features include mitral valve prolapse and mitral regurgitation.³⁴ Due to their late-onset and progressive nature, key cardiovascular features are often not present or noticeable in younger patients. However, with advances in technology, features such as aortic enlargement can now be readily detected in suspected MFS patients using echocardiography, allowing for much needed early intervention and symptom management.²⁷

Diagnostic Odyssey

The diagnosis of MFS and delineation from other type-1 fibrillinopathies is challenging for several reasons, including the large size of *FBNI*, number of unique mutations and the lack of defined mutation hotspots.^{30,38} These characteristics mean that, despite progress in understanding the genetic basis of MFS, as well as advances in genetic testing techniques, there is still no efficient, time and cost-effective molecular test for MFS.^{26,39} Molecular diagnosis is most often reserved for patients who have either a clinical diagnosis or a relative with a confirmed diagnosis.⁴⁰

Difficulties in diagnosis also arise from the extensive phenotypic overlap between MFS and the other type-1 fibrillinopathies, as well as the phenotypic variability observed both between and within affected families.^{30,38} The progressive nature of MFS, in particular the late onset of cardiovascular features also adds to the challenge, especially in the diagnosis of children for whom the symptoms have not fully developed.⁴¹

To overcome these limitations, the diagnosis of MFS is based on a well-defined set of criteria, known as the Ghent nosology and supplemented with molecular testing when appropriate.^{27,40} These criteria were first described by Beighton et al.⁴² in 1988 under the umbrella term of the Berlin nosology that encompassed the diagnosis of several connective tissue disorders. The Berlin nosology outlines features considered major or minor in the MFS phenotype, organised according to the organ system involved. The requirements of diagnosis varied, depending on the presence of an affected relative and were based on the involvement of at least two organ systems with a number of major and minor manifestations.⁴²

These diagnostic criteria were subsequently updated in 1996 and reworked into the Ghent nosology that is more specific to the diagnosis of Marfan syndrome.⁴³ The updated criteria provide a more stringent diagnosis for relatives of MFS individuals as well as revised skeletal involvement and further delineation of MFS and MFS-like disorders.⁴³ In 2010, the Ghent nosology was revised again due to concerns about the sensitivity of diagnosis, especially concerning age-dependent manifestations and the resulting potential for misdiagnosis of children.³⁴ The revised criteria place more emphasis on aortic root aneurysm and ectopia lentis, with less focus on features such as flat feet and pulmonary artery dilation that are common to other type-1 fibrillinopathies.³⁴ Based on the updated Ghent nosology,³⁴ a diagnosis of Marfan syndrome is given upon an individual fulfilling one of the seven scenarios described below. The scoring of systemic features is summarised in Table 1.1.

In the absence of family history, a diagnosis of Marfan syndrome is given if;

- 1) Aortic Root Dilatation Z score ≥ 2 AND Ectopia Lentis OR
- 2) Aortic Root Dilatation Z score ≥ 2 AND FBN1 mutation OR
- 3) Aortic Root Dilatation Z score ≥ 2 AND Systemic Score ≥ 7 pts OR
- 4) Ectopia lentis AND a *FBN1* mutation associated with Aortic Root Dilatation

In the presence of family history, a diagnosis of Marfan syndrome is given if:

(Family history is defined as a parent, child or sibling diagnosed with Marfan syndrome based on scenarios 1-4)

- 5) Family history AND Ectopia lentis OR
- 6) Family history AND Systemic Score ≥ 7 pts OR
- 7) Family history AND Aortic Root Dilatation Z score of either ≥ 2 (>20 yrs. Old) or ≥ 3 (<20 yrs. Old)

Due to the extensive overlap between the many connective tissue disorders, a caveat was added to the updated Ghent nosology. This caveat stipulates that in the presence of any features suggestive of other connective tissue disorders, such as Shprintzen Goldberg syndrome, Loeys-Dietz syndrome, or vascular Ehlers Danlos syndrome, these diagnoses must first be excluded; including by performing additional genetic testing as appropriate.³⁴

Table 1.1: Scoring of the systemic features of Marfan syndrome

A score of ≥ 7 out of a total of 20 possible points is indicative of systemic involvement. Adapted from Loeys et al. ³⁴

Feature	Description	Score
Positive wrist AND thumb sign	• Thumb sign is positive if the thumb-tip protrudes past the fifth finger when making a fist around the clenched thumb ⁴⁴	3
Positive wrist OR thumb sign	• Wrist sign is positive if thumb and fifth finger overlap when grasping the wrist with the opposite hand ⁴⁵	1
Pectus carinatum	• Protruding breastbone/chest	2
Pectus excavatum OR chest asymmetry	• Sunken or asymmetric breastbone/chest	1
Hindfoot deformity	• Hindfoot deformities in combination with forefoot abduction and lowering of midfoot	2
Pes planus	• Flat foot only	1
Pneumothorax	• Any spontaneous pneumothorax (collapsed lung)	2
Dural ectasia	• Expansion of the dural sac surrounding the spinal cord	2
Protrusio acetabuli	• Deformity of the acetabulum leading to the progressive migration of the femoral head into the pelvic cavity ⁴⁶	2
Reduced upper segment/lower segment ratio AND increased arm span/height ratio AND no severe scoliosis	• The upper segment (Hips to head) of the body is shorter than the lower segment (Hips to feet) • The arm span exceeds the height • No evidence of severe scoliosis	1
Scoliosis OR thoracolumbar kyphosis	• Scoliosis is the excessive sideways curvature of the spine • Kyphosis is the excessive forward curvature of the spine	1
Reduced elbow extension	• Elbow extension is reduced if the angle between the upper and lower arm at full extension is $\leq 170^\circ$ ⁴⁷	1
Facial features <i>Presence of at least 3 of 5 facial features</i>	• Dolichocephaly; disproportionately narrow and long head • Enophthalmos; posterior displacement of the eyeball within the eye socket ⁴⁸ • Down-slanting palpebral fissures; the area between the open eyelids is down-slanting • malar hypoplasia; underdeveloped or flattened cheekbones • retrognathia; posterior placement of either of both jaws in relation to the forehead	1
Skin striae	• Stretch marks on the skin not associated with pregnancy or weight changes	1
Myopia	• Near-sightedness	1
Mitral valve prolapse	• Bulge in the mitral valve leading to improper closure between the upper and lower-left chambers of the heart	1

To be considered as a diagnostic criterion, an *FBNI* mutation must conform to one of the following rules;³⁴ previously reported mutation known to result in Marfan syndrome, or if not yet reported, the mutation must be *de novo* with the proven absence of both the mutation and disease phenotype in parents and fall under one of the following mutation categories. A nonsense mutation, an insertion or deletion; either in- or out-of-frame, a splice site mutation; either directly affecting the donor/acceptor splice sites or confirmed to alter splicing at the mRNA/cDNA level, a missense mutation; affecting or creating a cysteine residue or a missense mutation affecting the consensus sequence of an EGF-like domain.³⁴

In short, the current diagnosis of a suspected Marfan syndrome patient without a diagnosed relative depends on the presence of aortic root dilatation AND ectopia lentis, an *FBNI* mutation or systemic phenotype.³⁴ Individuals with a first-degree relative diagnosed with MFS, are diagnosed based on their family history plus the presence of at least one of the following; ectopia lentis, systemic involvement or aortic root dilatation.³⁴ For a full description of the revised Ghent nosology and possible differential diagnoses, please refer to Loeys et al.³⁴

Due to the considerable phenotypic variability of the type-1 fibrillinopathies, affected individuals are often informally classified according to where they sit on the 'Marfan spectrum'.⁴ At one end are those diagnosed with neonatal Marfan syndrome, the most severe form of MFS, characterised by its early onset and life expectancy of less than 24 months.⁴⁹ At the other end of the spectrum are those who do not fully meet the Ghent nosology or have additional features not observed in the Marfan phenotype. Such patients are most often diagnosed with other type-1 fibrillinopathies, as described below.

Marfan lipodystrophy syndrome

Marfan lipodystrophy syndrome (MFLS, MIM 616914); also known as the marfanoid-progeroid-lipodystrophy syndrome, is an extremely rare autosomal dominant disease, with less than ten reported cases globally.⁵⁰ The phenotype of MFLS is characterised by congenital lipodystrophy, the severe lack of fat in the subcutaneous tissues, as well as premature birth and disproportionate growth in relation to weight gain.⁵¹ Affected individuals also have distinctive facial features, including protruding eyes, down-slanting palpebral fissures and a posteriorly positioned lower jaw resulting in a severe overbite.⁵¹ Other features overlap with Marfan syndrome including long limbs and digits, hyperextensible joints and myopia.^{51,52} Due to these similarities, there are cases in which individuals fulfil the Ghent nosology but, due to the characteristic lack of subcutaneous fat tissue, are more accurately diagnosed with MFLS.⁵²

MASS Syndrome

MASS syndrome (MIM 604308) is the diagnosis given to individuals who have a phenotype involving the Mitral valve, Aorta, Skeleton and Skin, but do not fulfil the Ghent nosology.⁵³ Despite not meeting the diagnostic criteria of MFS, the MASS phenotype shares several features with MFS, including disproportionately long limbs, chest deformities, mitral valve prolapse and aortic root dilation.^{43,53} Loeys et al.³⁴ suggests caution in the diagnosis of MASS syndrome due to its ambiguity, the lack of understanding of the underlying mutations and the potential for disease progression into classic MFS.

Ectopia lentis syndrome

Ectopia lentis syndrome (ELS, MIM 129600) is an autosomal dominant disorder characterised by dislocation of the lens due to abnormal stretching of the zonular fibres.⁵⁴ While ectopia lentis is a key feature of the MFS phenotype, ELS describes patients who have ectopia lentis but lack the cardiovascular involvement typical of MFS.³⁴ Lens dislocation is often severe in ELS patients and can result in acute or chronic impaired vision.⁵⁴ Much like MFS, ELS is caused by numerous mutations throughout *FBNI*, with approximately 38% of mutations that result in ELS also identified in MFS patients.⁵⁵

Stiff skin syndrome

Stiff skin syndrome (SSKS, MIM [184900](#)) is another extremely rare autosomal dominant disorder, characterised by thick and hardened skin that leads to reduced joint mobility.⁵⁶ Due to its rarity, the exact cause and pathogenesis of SSKS remain unknown. Using pulse-chase analysis, Loeys et al.⁵⁶ determined that while SSKS patients have normal levels of fibrillin-1 secretion, they have increased deposition of fibrillin-1 and elastin in the dermis. The group also observed that patient microfibrils were noticeably shorter than those seen in control samples.⁵⁶

Other type-1 fibrillinopathies

Weill-Marchesani syndrome 2 (WMS2, MIM [608328](#)), acromicric dysplasia (ACMID, MIM [102370](#)) and geleophysic dysplasia 2 (GPHYSD2, MIM [614185](#)) are three autosomal dominant disorders characterised by short stature, brachydactyly; short digits, and limited joint movement.^{57,58} While all three disorders share skeletal phenotypes, WMS2 patients also present with lens abnormalities, including glaucoma and ectopia lentis.⁵⁸ GPHYSD2 differs from ACMID as affected patients have additional cardiovascular abnormalities that lower life expectancy.⁵⁷ The ACMID phenotype is characterised by unique craniofacial features including a rounded face, with distinctive well-defined eyebrows and eyelashes, bulbous nose and a small mouth with thick lips.⁵⁷

1.1.3 Genotype-phenotype correlations

Several studies have attempted to correlate mutations in particular regions of *FBNI* with specific phenotypes. Such studies have proved difficult due to the high frequency of unique mutations; approximately 60%³, and the extensive phenotypic variability between and within affected families.^{4,59} Despite these challenges, one trend that is well accepted is the association of neonatal MFS (nMFS) with mutations within exons 25-33 (Figure 1.2).²⁵ However, while the entire exon 25-33 region is often quoted as associated with nMFS, Booms et al.⁴⁹ reported that evidence supports the presence of two nMFS hotspots. The first encompasses exons 25-28 and

mainly consists of missense mutations and in-frame insertions.⁴⁹ The second hotspot spans exons 32 and 33, in which splice site mutations resulting in exon skipping most often lead to nMFS.⁴⁹

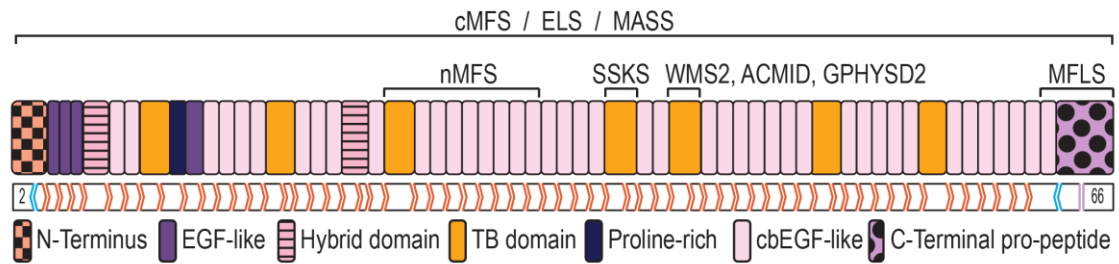


Figure 1.2: The type-1 fibrillinopathies and associated regions in FBN1.

In particular, the 'neonatal' (nMFS) region that spans exons 25-33, is associated with the most severe form of Marfan syndrome. cMFS: classic Marfan syndrome. ELS: ectopia lentis syndrome. nMFS: neonatal Marfan syndrome. MASS: MASS syndrome. SSKS: stiff skin syndrome. WMS2: Weill-Marchesani syndrome 2. ACMID: acromicric dysplasia. GPHYSD2: geleophysic dysplasia 2. MFLS: Marfan lipodystrophy syndrome.

Several of the studies attempting to unravel genotype-phenotype associations have noted that the type of mutation, rather than its location, influences the resulting phenotype.^{25,49,60,61} A good illustration of this trend is that missense mutations within exons 32 and 33 are most often associated with the classic MFS phenotype,³ while donor or acceptor splice site mutations within the same region lead to the severe and early onset phenotype of nMFS.⁴⁹ Other examples are the association of premature protein truncating mutations with severe skeletal phenotypes and cysteine substitutions with ectopia lentis.^{25,62}

While mutations causing MFS and ELS are found throughout the *FBN1* sequence, many of the mutations associated with other type-1 fibrillinopathies are clustered within specific regions of *FBN1* that have different functions (Figure 1.2). For example, MFLS is associated with mutations that affect the 3' most exons of *FBN1*.^{51,52,63-65} The C-terminal region of the fibrillin-1 pre-pro-protein is known to be cleaved by furin to allow for fibrillin-1 secretion and microfibril assembly⁶⁶. However, in 2016 Romere et al.⁷ reported that this cleaved product is a protein hormone involved in glucose homeostasis that they named asprosin. Asprosin is secreted by adipose tissue and recruited by the liver where it can activate pathways to rapidly increase circulating glucose levels.⁷ While asprosin was not extensively studied, Romere et al.⁷ confirmed that the mutations associated with MFLS disrupted asprosin function, most likely resulting in the observed lipodystrophy phenotype. Mutations causing MFLS, identified to date include 2bp, 8bp and 20bp deletions in *FBN1* exon 65,^{51,65} as well as mutations resulting in early fibrillin-1 truncation and loss of the C-terminus.⁶⁴

The majority of mutations that have been associated with WMS2, ACMID and GPHYSD2 are within exons 42 and 43 of *FBN1* (Figure 1.2).^{57,67} It is theorised that it is the nature of these mutations that results in the phenotypic differences between these diseases. For example, mutations leading to GPHYSD2 have been shown to more specifically affect residues with

structural roles, such as the cysteines involved in disulphide bond formation. At the same time, ACMID mutations are distributed throughout exons 42 and 43.⁵⁷ Le Goff et al.⁵⁷ also suggests that short stature and digits are associated with the disruption of the 5th TB domain, encoded by exons 42 and 43 specifically. In contrast, mutations in the other TB domains lead to different phenotypes; mutations within the 4th TB domain are associated with SSKS, which shares phenotypic similarity with WMS2, ACMID and GPHYSD2, but lacks the short stature and digits.⁵⁶

1.1.4 Models of pathogenesis

The Marfan phenotype, in particular the cardiovascular manifestations, have been observed to worsen progressively with age. The reason for this remains unknown, as the mechanism behind the pathogenesis of MFS, and the other type-1 fibrillinopathies is still not fully understood. Based on current knowledge, this progression has been attributed to both the compounding weakness of microfibrils and the continuing dysregulation of transforming growth factor-beta (TGF- β).

Four main models of MFS pathogenesis have been proposed to date. The first is the dominant-negative model that describes mutations resulting in an altered protein that acts antagonistically against the wild-type protein.⁶⁸ In the case of MFS, this model suggests that aberrant fibrillin-1 monomers bind incorrectly with wild-type monomers, forming semi- or non-functional multimers preventing microfibril assembly. The lack of functional microfibrils leads to disorganisation of the extracellular matrix and the observed disease phenotype.⁶⁸ Therefore, according to this model, the severity of the phenotype depends on the level of functional fibrillin-1 expression.⁶⁸

The dominant-negative model came under question after the identification of homozygous mutations and an autosomal recessive form of MFS. In 2007, de Vries et al.³¹ studied two related individuals who harboured homozygous c.1453C>T mutation (p.Arg485Cys) and presented with classic MFS. Hilhorst-Hofstee et al.³² similarly identified a homozygous c.7454A>T mutation (p.Asp2485Val) in three related individuals diagnosed with MFS. Both groups observed that in the heterozygous state, these mutations did not have a dominant-negative effect, conflicting with the dominant-negative model.^{31,32} It was suggested by de Vries et al.³¹ that in such cases the pathogenesis is more in line with a haploinsufficiency model. That is, a lack of microfibrils or fibrillin-1 resulting from protein degradation, intermolecular cross-linking, or reduced fibrillin-1 synthesis.^{31,69}

The second model suggests that mutations in *FBNI* increase the sensitivity of fibrillin-1 to proteolysis, resulting in a steady decline in microfibrils, parallel to the progression of disease severity.²³ This model is particularly relevant to mutations affecting cbEGF-like repeats, as calcium is involved in the formation of microfibrils, and specifically in their stabilisation and protection from proteolysis.¹⁵

The third model suggests that the major role of fibrillin-1 is to maintain tissue homeostasis and therefore, MFS is the result of a loss of homeostasis.¹⁵ This model was based on findings from two mouse models showing that MFS, which caused a typical phenotype in the vesicular tissue and resulted in death, did not affect elastic fibres in other tissues.¹⁵ Therefore, the authors concluded that the primary role of fibrillin-1 was not in the assembly of elastic fibres, rather in maintaining homeostasis of existing elastic fibres.¹⁵ The model also suggests a critical threshold of functional microfibrils required for tissue homeostasis.¹⁵ Therefore mutations in *FBNI* result in MFS because they reduce microfibril abundance below the threshold. This hypothesis was based on observations of the two mouse models showing that the outcome of both dominant negative and loss-of-function mutations is a similar decrease in the abundance of functional microfibrils.⁷⁰

The fourth model was proposed in the early 2000s, in light of more recent research that linked decreased fibrillin-1 deposition with the dysregulation of TGF- β ; a multifunctional cytokine with a role in cell signalling and survival.⁷¹ The study by Neptune et al.⁷¹ identified that the dysregulation of TGF- β leads to apoptosis in the lung during development, however when TGF- β activation was neutralised lung apoptosis was reduced, and alveolar development was rescued. Several other studies have now supported these findings, providing more evidence that TGF- β dysregulation is the leading cause of pathogenesis in Marfan syndrome, favouring the fourth model and directing research focus.^{13,72}

Mutations in *FBNI* lead to an increase in active TGF- β by disrupting the interaction between latent TGF- β binding protein (LTBP) and fibrillin-1.⁷³ In the absence of organised microfibril lattices, the large latent complex (LLC); made up of TGF- β , latency-associated protein and LTBP, is unable to anchor to microfibrils and as a result, the components of the LLC remain uncomplexed.⁷³ This leaves TGF- β free to bind to its receptor, activating a phosphorylation cascade and a number of downstream effects.^{73,74} One such effect is increased expression of matrix metalloproteinases leading to the degradation of elastin and the resulting loss of extracellular matrix stability.¹⁶ A schematic of this process is outlined in Figure 1.3.

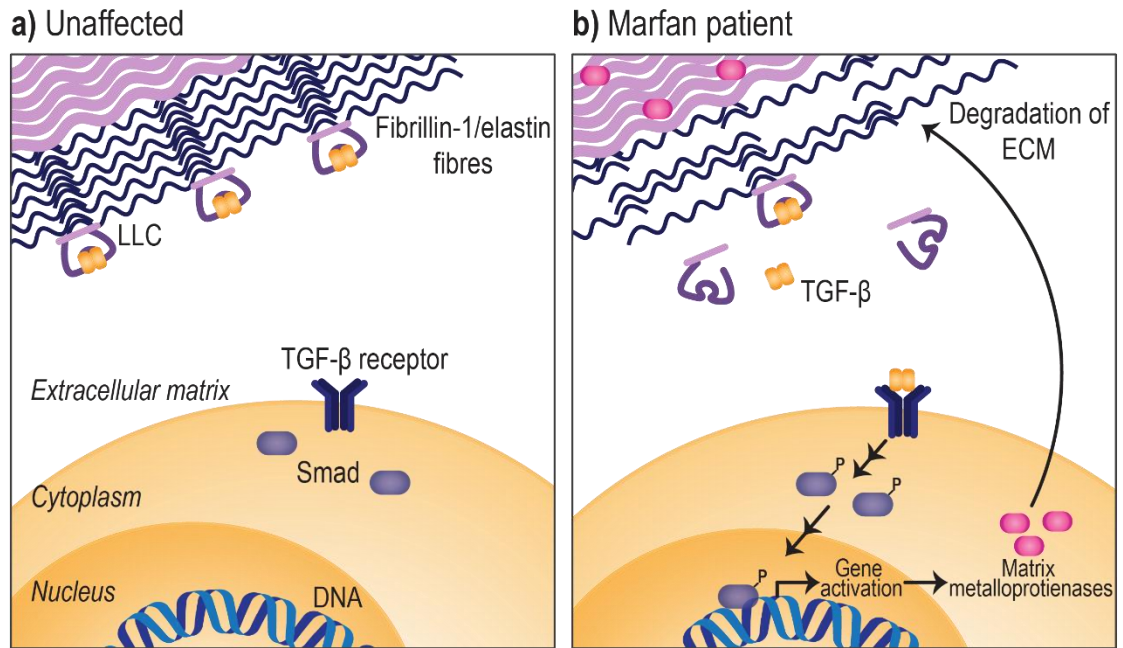


Figure 1.3: Schematic of TGF- β regulation and dysregulation in Marfan syndrome

a) In a healthy individual, fibrillin-1 monomers aggregate into multimer units that make up the backbone of microfibrils that are most often associated with elastic fibres. Functional microfibrils bind to the large latent complex (LLC) sequestering TGF- β in the extracellular matrix (ECM) regulating its signalling cascade. b) In an individual with Marfan syndrome, the loss of functional microfibrils releases TGF- β that binds to its receptor on the plasma membrane. Bound to its receptor TGF- β activates a signalling cascade including the phosphorylation (P) of Smad leading to the activation of matrix metalloproteinase expression. Matrix metalloproteinases are then secreted from the cell and lead to elastolysis or degradation of elastin further decreasing the stability of the ECM. Figure adapted from Ramachandra et al.¹⁶ and Benke et al.⁷³

The initial disruption of the LTBP and fibrillin-1 interaction, could be the result of several different factors and is likely dependent on the type and position of a mutation. Aoyama et al.⁶⁹ suggests that most *FBNI* mutations can be categorised into five groups depending on their effects on fibrillin-1 synthesis and deposition. This group⁶⁹ also suggests that *FBNI* mutations alter synthesis and deposition in different ways, supporting the dominant-negative, haploinsufficiency and protein degradation models,⁶⁹ all of which are likely to result in the dysregulation of TGF- β . This work is summarised in Table 1.2

Table 1.2: *FBNI* Mutation groups according to fibrillin-1 synthesis and deposition.

The majority of *FBNI* mutations can be classified into five groups. These groups describe the relationship between pathogenesis and the observed synthesis and deposition of fibrillin-1 protein. Adapted from Aoyama et al.⁶⁹

Group	Synthesis	Deposition	Pathogenesis
Healthy control	100%	100%	Healthy
I	<70%	\geq 35%	Haploinsufficiency
II	<70%	<35%	Dominant negative
III	\geq 70%	35-70%	Loss of function or degradation
IV	\geq 70%	<35%	Dominant negative
V	\geq 70%	\geq 70%	Loss of function

1.1.5 Life expectancy and current treatments

In 1972, the mean age of death for Marfan patients was predicted to be 32 years, with cardiovascular complications associated with aortic dilation the primary cause.³⁵ A continuation of this study in 1995 found that the mean age of death had increased significantly to 41 years; more specifically increasing from 30 to 44 years for females and 33 to 39 years for males.^{35,75} Additionally the median cumulative probability of survival which Silverman et al.⁷⁵ define as “the age at which 50% of patients are predicted to be still alive”, was found to have increased by several decades for both the male and female cohorts; increasing to 74 years for females and 70 years for males. The increased survival was attributed to an overall increase in life expectancy for the general population, an increase in the proportion of individuals diagnosed with milder phenotypes due to increased molecular genetic testing, and significant advances in medical intervention, specifically cardiovascular surgery.⁷⁵ While life expectancy has likely further increased since the mid-1990s, a considerable burden on the livelihood and quality of life²⁸ remains for individuals diagnosed with MFS for whom there is currently no cure.

The management of Marfan syndrome is multidisciplinary, involving geneticists, ophthalmologists, orthopaedists and cardiologists.³³ The majority of current treatment options are designed to treat particular clinical features with a focus on slowing aorta growth.^{76,77} Current standard of care consists of lifelong use of β -adrenergic receptor blockers^{76,78} or angiotensin II receptor type 1 blockers^{79,80} that slow the progressive aortic dilation and reduce the associated complications.^{27,33} These drugs are coupled with numerous surgical interventions aimed at correcting major abnormalities in the chest, eye, spine and cardiovascular system.^{27,33}

The progressive nature of type-1 fibrillinopathies means that constant re-evaluation is required throughout life. For example, ocular features such as lens dislocation are most often managed with corrective lenses, however with increasing severity comes additional surgical intervention such as aphakia or removal of the lens.⁸¹ Similarly, progressive scoliosis is initially managed with bracing, however patients are monitored throughout development, and surgical stabilisation is often needed.⁸²

Following the implication of TGF- β dysregulation in the pathogenesis of MFS, research into TGF- β antagonism has been the main research focus for potential therapeutics. The most notable outcome of which is trials into the repurposing of Losartan, a drug that is currently used to treat hypertension.⁷² Studies in mouse models have shown that treatment with Losartan can prevent aortic root aneurysm, as well as partially rescue lung structure.⁷⁹ However, clinical trials comparing Losartan with β -blockers demonstrated that while treatment with Losartan significantly reduces aortic dilation, there was no significant difference in the outcome between the two treatment groups.^{83,84}

Novel therapeutic strategies

Therapeutics such as cell or gene replacement for MFS are unlikely to be effective for two reasons; the dominant inheritance of MFS and the large size of *FBNI*. Gene therapy can be especially useful for recessive diseases where replacing the defective gene in appropriate tissues has a significant therapeutic benefit. However, in the case of Marfan syndrome, the presence of wild-type fibrillin-1 protein would have little to no impact on the dominant-negative effect of the affected protein.⁸⁵ Allele-specific down-regulation of the mutated fibrillin-1 protein has also been proposed as a possible therapy.⁸⁵ While the dominant-negative pathogenesis model supports the validity of this therapeutic approach, Marfan syndrome has also been linked to a lack of fibrillin-1.³¹

The applications of genome editing technologies such as the CRISPR/Cas9 system have expanded in recent years to a wide range of diseases.⁸⁶ Of particular interest is a series of proof-of-concept experiments by Zeng et al.⁸⁷ who report some success in creating and correcting *FBNI* mutations using the more recently established Base Editor system. The Base Editor system utilises a modified Cas9 protein and is presented as a safer alternative for genome editing, as it edits at specific sites without the formation of double-strand breaks. Zeng et al.⁸⁷ demonstrate that the Base Editor system can efficiently correct pathogenic *FBNI* mutations with minimal off target effects, signalling a possible future in genome editing-based therapies for MFS. However, Zeng et al.⁸⁷ also outlines some of the limitations and cautions of genome editing, including ethical issues and varying efficiency, specificity and off-target effects. In particular given that genome editing is most effectively achieved at the embryonic stage uncertainty about efficiency or possible undesirable outcomes is unacceptable and presents a serious ethical obstacle.

Despite the many advances in the field of medicine and drug development, the current treatment pipeline for the type-1 fibrillinopathies would benefit significantly from the development of novel and effective therapies, especially if such therapies could treat the cause of disease rather than its symptoms. Considering the current shift towards more personalised medicine, we suggest that antisense oligonucleotides may be an appropriate therapeutic approach for MFS with the potential to treat many mutation types by targeting the pre-mRNA directly and altering the splicing process.

1.2 Gene expression and the splicing process

The first step in protein expression is the transcription of DNA to produce a complete sense strand transcript called precursor messenger RNA (pre-mRNA). This pre-mRNA contains both coding (exonic) and non-coding (intronic) regions and requires processing before the mature mRNA can be translated into protein. Processing of pre-mRNA includes 5' capping, splicing,

tagging with exon junction complexes, cleavage and polyadenylation of the 3'-end and finally, export to the cytoplasm for translation.⁸⁸

Of particular relevance to this work is splicing, a highly complex and coordinated process that takes place for all multi-exon human gene transcripts. During the splicing process introns are removed, and the exons are re-joined or spliced together to form an uninterrupted coding sequence. Ninety-five percent of multi-exon genes undergo an additional process called alternative splicing⁸⁹ that allows for further diversification of gene expression in a highly regulated, tissue and/or development-specific manner.

1.2.1 Splice sites and exon definition

The splicing process is tightly regulated and relies on a large number of *cis* and *trans*-acting elements to remain precise. Within the transcript, six main features; 5' and 3' splice-sites, polypyrimidine tract, branchpoint and splicing silencer and enhancer-binding sites, determine how an exon is defined.^{90,91} Referred to as the exon definition model, these features determine which sequences are defined as exonic and highlight the exon/intron junctions. This definition enables the spliceosome to recognise those sequences that should be retained or excluded during the splicing process.

Exon boundaries are defined by the canonical 5' (donor) and 3' (acceptor) splice sites GU and AG, respectively. The spliceosome recognises these splice sites, along with the branchpoint and polypyrimidine tract, and binds to the intron-exon junction, allowing the intron to be removed and the exons to be joined seamlessly. Additional sequences with the potential to be used as a donor or acceptor site can often be found within the exon or intron. Such sequences are known as cryptic splice sites and can be activated or created as the result of mutations, leading to abnormal splicing.

1.2.2 Regulation of splicing

The splicing process is mediated by a complex of small nuclear RNAs (snRNA) and ribonuclear proteins called the spliceosome of which there are two; the major and minor. The majority of introns; those defined by the canonical GU/AG splice sites are spliced by the major spliceosome.⁹² However, a small proportion of introns have different splice site and branchpoint sequences and are instead spliced by the minor spliceosome.⁹³ Such introns; referred to as U12 type introns are estimated to make up only 0.15% to 0.5% of all introns.⁹⁴⁻⁹⁶

The major spliceosome predominates and is made up of an estimated 170 distinct proteins.⁹² The main building blocks of which are the small nuclear ribonucleoproteins (snRNPs) U1, U2, U3, U4/U6 and U5.⁹² The current consensus of splicing depicts a step-by-step process ultimately resulting in the production of an intron lariat and exon-exon ligation (Figure 1.4).

The process begins with the recognition of *cis*-acting elements on the pre-mRNA by the U1 snRNP and supporting proteins (Figure 1.4.a). U1 binds to the GU of the 5' splice site, while splicing factor 1 (SF1) and U2 auxiliary factors (U2AF) 1 (35 kDa subunit) and 2 (65 kDa subunit), bind to the branch point, 3' splice site and polypyrimidine tract respectively. These interactions form the spliceosome complex-E (Figure 1.4.b). Binding of the U2 snRNP to the branch point displaces SF1 and forms spliceosome complex-A (Figure 1.4.c).

Following the formation of complex-A, a pre-assembled tri-snRNP complex of U4/U6/U5 is recruited with U5 binding 5' and U6 binding to U2 to form spliceosome complex B (Figure 1.4.d). Complex-B is inactive and must undergo conformational changes resulting in the displacement of U1 and U4 to enter an active state. Following activation, the first cleavage event takes place, producing complex-C and releasing the first exon. Release of the first exon allows the 5' splice site to bind to the branch point leading to the second cleavage event that results in the excision of an intron lariat and ligation of the exons (Figure 1.4.e). At this point, the remaining spliceosome proteins are dissociated and recycled for further rounds of splicing.⁹⁷ This process is reviewed in more detail by Wahl et al.⁹² and Becerra et al.⁹⁸

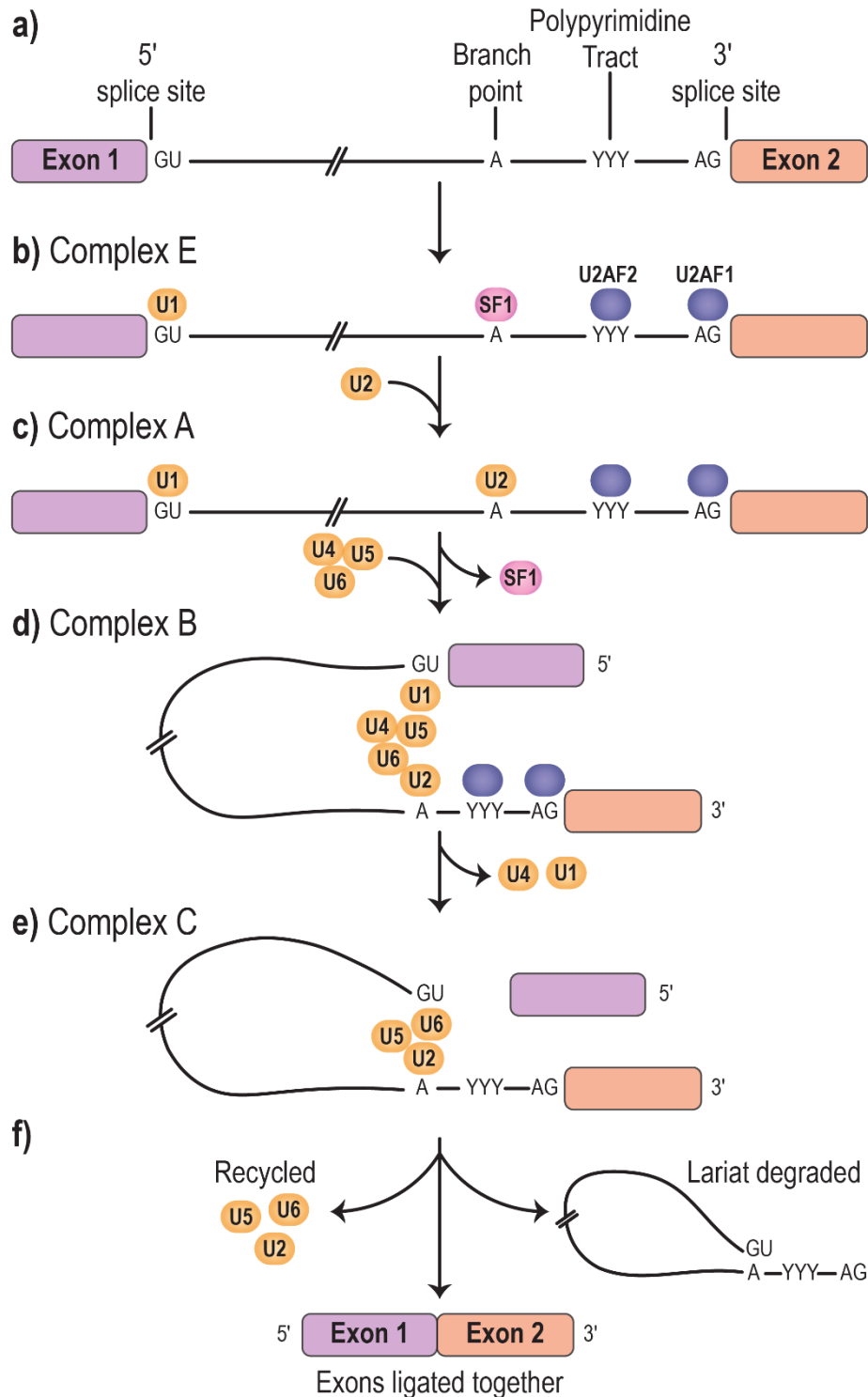


Figure 1.4: Simplified schematic of major spliceosome assembly and the mRNA splicing process.

Including; a) the regulatory elements within the pre-mRNA. b) The binding of U1, splicing factor 1(SF1) and U2 auxiliary factor 35 kDa (U2AF1) and 65 kDa (U2AF2) subunits to form complex E. c) the binding of U2 resulting in SF1 displacement and the formation of complex A. d) Recruitment of U4/5/6 to form complex B. e) After activation of complex B the formation of complex C results in the cleavage of the first exon. F) The second cleavage results in a free intron lariat that is degraded, dissociation of the spliceosome proteins that are recycled and the ligation of the exons. Figure adapted from Douglas et al.,⁹⁹ Becerra et al.⁹⁸ and Wahl et al.⁹²

1.2.3 Alternative splicing

One of the main advantages of eukaryotic genomes is the diversity of proteins that are produced from the DNA template. The mechanism by which diversity is increased is through alternative splicing. A process that can give rise to a plethora of unique RNA transcripts that may be translated into a variety of different proteins from a single DNA template (gene). An extreme example of alternative splicing and its role in genetic complexity are the Neurexins, a family of proteins involved in intercellular signalling and cell adhesion during synaptogenesis.¹⁰⁰ There are over 1000 unique neurexin proteins produced from three homologous genes through the use of different promoters and alternative splicing.¹⁰⁰ While not all genes are alternatively spliced to the same extent as the neurexins, alternative transcripts can be detected for more than 90% of human multi-exon genes.^{89,101} Some of the possible alternative splicing outcomes are shown in Figure 1.5, the result of which can be manifold, including changes to expression, isoform selection and function. However, this list is not exhaustive and for many genes a combination of alternative splicing will occur.

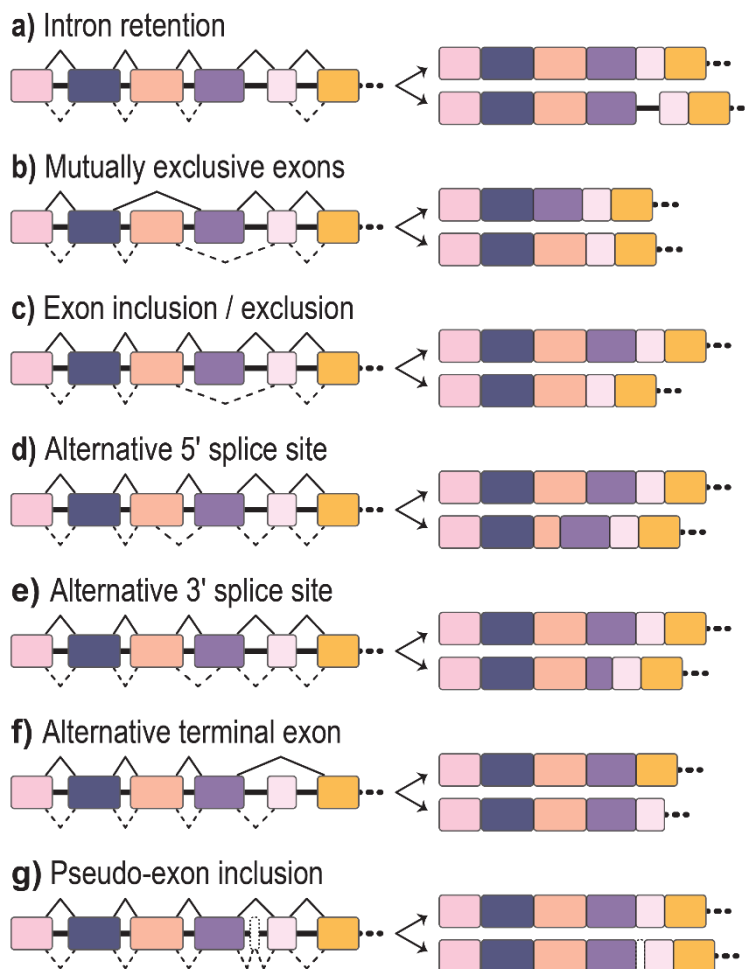


Figure 1.5: Schematic exploring the possible outcomes of alternative splicing.

Boxes represent exons, interspaced by introns represented by a black line. The solid and dashed lines above and below indicate the splice sites being utilised.

A critical factor in determining if an exon is retained or excluded from the final transcript is the balance between positive and negative splicing factors and their respective binding domains. Splicing factors are *trans*-acting proteins that bind to *cis*-acting sequences within the pre-mRNA.¹⁰² Enhancer sequences occur within the exons (exonic splicing enhancer, ESE) and introns (intronic splicing enhancer, ISE) and recruit positive splicing factors; most commonly members of the serine/arginine-rich (SR) protein family.¹⁰³ Positive splicing factors enhance the recognition of the exon by the spliceosome, resulting in the exon being retained in the final transcript.¹⁰⁴ Silencer sequences can similarly be found in either the exon (exonic splicing silencer, ESS) or intron (intronic splicing silencer, ISS), however, recruit negative splicing factors; such as heterogeneous ribonucleoprotein particles (hnRNPs), reducing the recognition of the exon, resulting in its removal with the flanking introns.¹⁰⁴

The delicate balance between enhancer and silencer sequences can be shifted by polymorphisms or disease-causing variants, resulting in the exclusion of an otherwise included exon, or vice versa. This precarious balance is explored further in chapter 4 of this thesis in the context of a single nucleotide variation in exon 52 of *FBN1* that results in the removal of exon 52 from transcripts and ultimately Marfan syndrome. Mutations can cause aberrant splicing in several ways, often resulting in a disease phenotype. Mutations can disrupt the consensus donor or acceptor splice sites, the adjacent sequences, create or activate a cryptic splice site or disrupt an enhancer or silencer sequence.

1.3 Altering exon selection as a genetic therapy

1.3.1 Antisense oligonucleotides

Antisense oligonucleotides (AOs) are single-stranded nucleic acid analogues that can be used to manipulate gene expression to include¹⁰⁵ or exclude^{106,107} an exon, induce transcript degradation,^{108–110} transcription inhibition¹¹¹ or inhibit translation.¹¹² Antisense oligonucleotides are typically between 15-30 bases long and are designed to be complementary to the “sense” RNA transcript of interest, and thus bind specifically to the targeted sequence through Watson-Crick base pairing. There are two broad classes of AOs; those that promote the degradation of targeted mRNA, such as ribonuclease H (RNase H)-dependent oligonucleotides or siRNAs, and those that physically block or inhibit the splicing or translational machinery, commonly referred to as steric-blocker oligonucleotides.¹¹³

The first reports of the practical applications of antisense oligonucleotides to alter gene expression were released in the late 1970s. In 1977 Paterson et al.¹¹⁴ reported their use of single-stranded DNA-AOs to inhibit translation of complementary RNA in a cell-free system. In 1978 Zamecnik and Stephenson¹¹⁵ reported that DNA-AOs could inhibit Rous sarcoma virus

replication in chicken embryos. Finally in 1979, Donis-Keller¹¹⁶ demonstrated site-specific cleavage of RNA by RNase H through the creation of an RNA/DNA heteroduplex. These reports are considered the foundation of the antisense oligonucleotide platform from which the many currently known applications stem.

Of particular interest is the report by Zamecnik and Stephenson¹¹⁵ who introduced chemical modifications into the AO to improve its biological activity, and concluded that the increased activity was a result of decreased nuclease susceptibility that consequently increased the AO half-life.¹¹⁵ Since the 1970s great strides have been made in the field with a major contributor to this success being the many generations of chemical modifications. Such modifications not only alter the dependency on RNase H but also aim at increasing specificity, affinity, efficiency and stability while decreasing off-target effects, cost of synthesis and toxicity.

1.3.2 Chemistries

Antisense oligonucleotides can be modified in several ways depending on the desired outcome. The early AOs were RNase H dependent phosphodiester (PO) DNA nucleotides and therefore negatively charged. While PO-AOs effectively demonstrated proof-of-concept, they are highly susceptible to nucleases and thus have limited half-lives. To reduce nuclease susceptibility, while retaining the negative charge and the ability to recruit RNase-H, the non-bridging oxygen was replaced with sulphur to produce a phosphorothioate (PS) linkage.¹¹⁷ The PS modification also increases the affinity of the AO for serum proteins such as heparin, allowing the AO to be maintained in circulation for longer and delaying removal by the liver.¹¹⁷ These benefits, in conjunction with the relatively low cost of synthesis and their efficiency have made the PS chemistry one of the more commonly used. However, the affinity of PS-AO to serum proteins, as well as several other off-target effects, have also been linked with increased toxicity.^{113,118}

Modifications of the Ribose sugar moiety can allow the AO to more closely resemble RNA than DNA, thus increasing RNA binding affinity.¹¹⁹ Two of the most common 2'-ribose modifications are 2'-*O*-methyl (2'OMe) and 2'-*O*-methoxyethyl (MOE).¹¹⁷ When bound to RNA, the 2'OMe-AOs and MOE-AOs do not support RNase H and therefore the RNA strand is not cleaved,¹¹⁷ allowing these compounds to be used for steric blockade applications. The increased similarity to RNA as a result of 2'-ribose modifications also increases the stability and thus strength of AO-RNA hybridisation, allowing for shorter AO sequences without losing efficiency.¹¹⁷ The PS and 2'OMe modifications are often used in conjunction forming 2'OMe-PS AOs that are nuclease and RNase-H resistant, as well as relatively efficient and cost-effective to synthesise.

To overcome the undesirable off-target effects of the PS backbone, a series of neutrally charged chemistries were developed, the most well-known of which are the phosphorodiamidate

morpholino oligomers (PMO) and peptide nucleic acids. Of particular interest is the PMO chemistry, in which the deoxyribose sugar and negative charge are replaced with a backbone of morpholine rings joined by phosphorodiamidate linkages.¹²⁰ The neutral charge of the PMO chemistry allows the AO to bind to RNA or DNA with higher specificity and affinity, while not recruiting RNase H, thereby making these compounds excellent steric blockers.¹¹³ The complete replacement of the ribose ring with a morpholine ring means that PMOs are not recognised by and thus resistant to the majority of natural enzymes¹²¹ making them an excellent choice for *in vivo* applications. Also, due to their neutral charge, PMOs are less likely to interact with proteins and thus have shown limited off-target effects or non-specific binding.^{118,122} Due to these advantages PMOs have been studied extensively in animal models and clinical trials, and are recognised as both safe and effective in a clinical setting.^{123–125}

1.3.3 Delivery

For an AO to induce the desired outcome, it must first enter the target cells and for many applications, enter the nucleus. Oligonucleotides are unable to diffuse through the lipid membrane alone and are believed to be actively transported into the cell through endocytosis,^{126,127} however the exact mechanism of nuclear delivery remains unresolved. The uptake of an AO has been shown to vary depending on temperature, cell type, AO structure and AO concentration.^{126–128}

Delivery limitations can be overcome more easily in an *in vitro* system through the use of various commercially available transfection reagents. One of the more common delivery mechanisms used is the encapsulation of negatively charged AOs such as 2'OMe-PS, with a cationic lipid-based reagent. Forming a positively charged liposome that has a high affinity for the negatively charged cell membrane allows the AO to be efficiently delivered into the cell. While liposome delivery is efficient for negatively charged AOs, e.g. 2'OMe-PS, neutrally charged AOs, the uncharged PMOs require different delivery mechanisms.

In an *in vitro* model, PMO delivery is commonly achieved through electroporation-based devices such as Nucleofector™ Technology (Lonza) or the Neon™ Transfection System (Thermo Fisher Scientific). Both systems allow for the efficient delivery of PMOs by subjecting cells to short pulses of electricity, altering the permeability of the cell membrane temporarily. Non-electroporation-based delivery methods are also available. An example of which is Endo-Porter (Gene Tool, LLC) a novel peptide that can deliver AOs into a cell through an endocytosis-mediated process.¹²⁹ Endo-Porter is designed to allow for efficient delivery without the membrane damage associated with electroporation.¹²⁹ Other delivery methods include gymnosis or 'naked' delivery, that relies on the natural properties of cells to promote uptake of the AO without the addition of a transfection reagent.¹³⁰ However, PMOs are notorious for having poor cellular and nuclear uptake due to their neutral charge.¹¹³ Lastly the hybridization of PMOs to sense-strand DNA or RNA-like leashes coupled with cationic liposomes can result in robust PMO delivery.¹³¹

Delivery of AOs *in vivo*, is much more complex and is one of the major limitations of antisense therapies. If not successfully delivered to the target tissue or cells the most therapeutically active compounds can become inert. Along with poor cellular uptake rapid renal clearance of PMOs act as a significant challenge.¹³² Therefore PMOs can be conjugated with cell-penetrating peptides (CPP) to improve uptake and kinetic behaviours.¹³³ Various CPPs have been developed, one type called arginine-rich peptides have been shown to greatly increase cellular uptake.^{134,135} However, some arginine-rich peptides are also associated with toxicity at higher concentrations, with increased toxicity with the each additional arginine.^{133,134} Other arginine-rich CPPs have been shown to successfully increase PMO efficiency with no signs of toxicity.¹³⁶

1.3.4 Application of antisense oligonucleotides

Blocking of transcription and translation

Steric blockade AOs can be used to physically block the binding of transcription or translation machinery, disrupting the initiation of either process. Binding of an AO, to double-stranded DNA can prevent the binding of a transcription factor (TF) as well as inhibiting recognition and initiation by RNA polymerase II (Pol)¹¹³ (Figure 1.6.a). Antisense peptide nucleic acids are particularly useful for this application as the polyamide modified backbone increases their flexibility, which in turn increases their affinity for double-stranded DNA.^{113,137} Translation can be similarly inhibited by targeting translation initiation sites; physically blocking and competing with the binding of translational machinery, or preventing the movement of the ribosome along the mRNA (Figure 1.6.d).^{112,138}

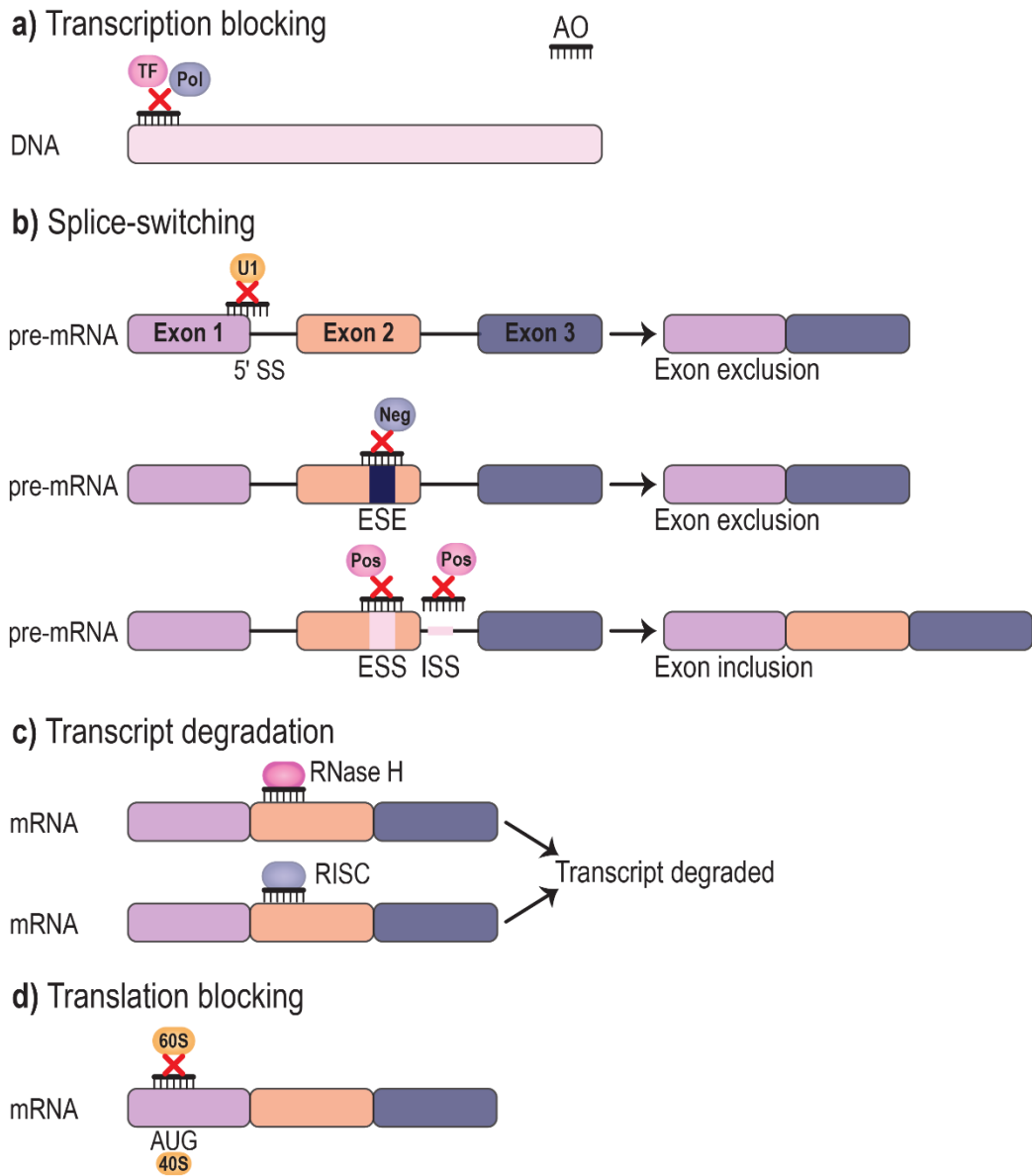


Figure 1.6: Possible applications of antisense oligonucleotides to modify gene expression.

a) transcription blocking,¹¹¹ b) splice-switching; exclusion^{106,107} or inclusion,¹⁰⁵ c) transcript degradation; via RNase-H activation^{108,109} or siRNAs¹¹⁰ and d) translation blocking.¹¹²

Splice switching

Manipulation of pre-mRNA splicing is now becoming a common application of AOs. An AO can be designed to bind; and therefore mask or activate splice sites, or splicing enhancer/silencer sequences, redirecting the spliceosome and ultimately resulting in exclusion or inclusion of the target sequence (Figure 1.6.b). The most common splice switching application is exon exclusion. Commonly referred to as exon skipping, an AO is designed to target the donor, acceptor or ESE sequences to decrease recognition by the spliceosome and lead to exon exclusion. Conversely, by targeting splicing silencers, most often those that are intronic (ISS), the exon recognition can be enhanced, leading to exon inclusion.¹³⁹ Retention of an exon is particularly relevant in cases where exon exclusion from the mature mRNA is a result of a disease-causing mutation.

Notable examples of splice-switching AOs are eteplirsen, golodirsen and nusinersen marketed as Exondys51™, Vyondys53™ and SPINRAZA®, respectively. Both eteplirsen and golodirsen are PMOs, licenced to Sarepta Therapeutics, that were granted accelerated approval by the United States Food and drug authority (FDA) as a treatment for Duchenne muscular dystrophy in 2016^{140,141} and 2019¹⁴² respectively. Eteplirsen and golodirsen are designed to induce skipping of dystrophin exon 51 and 53, respectively, to restore the mRNA reading frame around frame-shifting deletions that flank the target exons.^{143,144} Removal of the exons from transcripts with these amenable deletions allows translation of internally truncated dystrophin isoforms, similar to those characteristic of the milder Becker's muscular dystrophy.^{123,144} Nusinersen is an FDA approved MOE-AO, licenced to Biogen for the treatment of spinal muscular atrophy that targets an intronic silencer element, ISS-N1, to induce the inclusion of SMN2 exon seven, resulting in a functional full-length transcript.¹⁴⁵

Transcript degradation

RNase H-dependent AOs function by forming a heteroduplex between the DNA-like AO and RNA target, recruiting the endogenous RNase-H enzyme that binds to and cleaves at the RNA target (Figure 1.6.c).^{146,147} The most commonly used chemistry for this application is DNA modified with a phosphorothioate backbone that increases nuclease resistance while retaining RNase H dependent activity. RNase H-dependent AOs can be extremely efficient, often achieving between 80% and 95% mRNA and protein down-regulation.¹¹³ Added to this efficiency, RNase H-dependent AOs are not limited to targeting the 5'-region or initiation codon to induce downregulation of protein expression, while steric blockade AOs do have this limitation^{113,138}

To date the FDA has approved two RNase H-dependent AOs. The first; Vitravene also known as fomivirsen, is a 21-mer phosphorothioate oligodeoxynucleotide designed to disrupt the replication of cytomegalovirus (CMV) to treat patients with CMV retinitis.¹⁴⁸ The second; Kynamro also known as mipomersen, is designed to treat familial hypercholesterolemia by inhibiting apolipoprotein B.¹⁴⁹ Although the FDA had approved both drugs, Vitravene has been withdrawn from the market and Kynamro is only prescribed in special cases as there have been several reports of adverse side-effects.¹⁴⁸⁻¹⁵⁰

Applications of antisense oligonucleotides for the type-1 fibrillinopathies

As discussed, *FBNI* is translated into the fibrillin-1 preproprotein that is cleaved by furin into asprosin and a fibrillin-1 monomer. Fibrillin-1 monomers are secreted from the cell and rapidly aggregated into multimer units to form the backbone of fibrillin-1 microfibrils (Figure 1.7.a).¹⁷ Mutations in *FBNI* disrupt microfibrils' formation, either through the expression of abnormal fibrillin-1 monomers (Figure 1.7.b and d) or decreased fibrillin-1 expression (Figure 1.7.c). This disruption ultimately leads to disease, either Marfan syndrome or another type-1 fibrillinopathy.

This study aims to induce the exclusion of exons harbouring disease-causing mutations from the *FBNI* pre-mRNA, along with the corresponding exon from the transcript encoded by the healthy allele. We hypothesise that this will have different effects depending on the mutation type but ultimately result in an increase, or rescue of fibrillin-1 microfibrils (Figure 1.7.e). Firstly, mutations resulting in altered *FBNI* splicing often lead to a dominant-negative interaction between the wild-type and mutant proteins (Figure 1.7.b).^{69,151} Therefore, we hypothesise that removing the mutation-associated exon from both alleles' transcripts will re-establish transcript homogeneity. This should negate the dominant-negative interaction and allow monomers to form microfibrils correctly.

In contrast, nonsense and frameshift mutations, often result in transcript degradation and thus a reduction in fibrillin-1 abundance (Figure 1.7.c). We hypothesise that removing exons associated with a nonsense or frameshift mutation will bypass the premature termination site, re-framing the transcript. The result of which should be the expression of a truncated fibrillin-1 protein.

As with the other mutation types, the effect of a missense mutation depends on the nucleotide and exon affected. Some missense mutations result in a dominant-negative effect, while others result in loss of function or the production of abnormal microfibrils (Figure 1.7.d).^{68,69,152} We hypothesise that removing the affected exon from both alleles will remove the aberrant sequence and restore transcript homogeneity allowing monomers to form functional microfibrils.

Lastly, we hypothesise that fibrillin-1 is amenable to the removal of target exons for two main reasons. (1) The highly repetitive nature of fibrillin-1 that suggests domain periodicity is vital for microfibril formation and function. (2) The in-frame nature of the *FBNI* exons means that most exons can be removed without altering the reading frame. The exceptions to this are the exons at the N- and C- terminals; exons 2, 3, 64, 65 and 66. The removal of any of these exons would disrupt the reading-frame and likely result in no functional protein production.

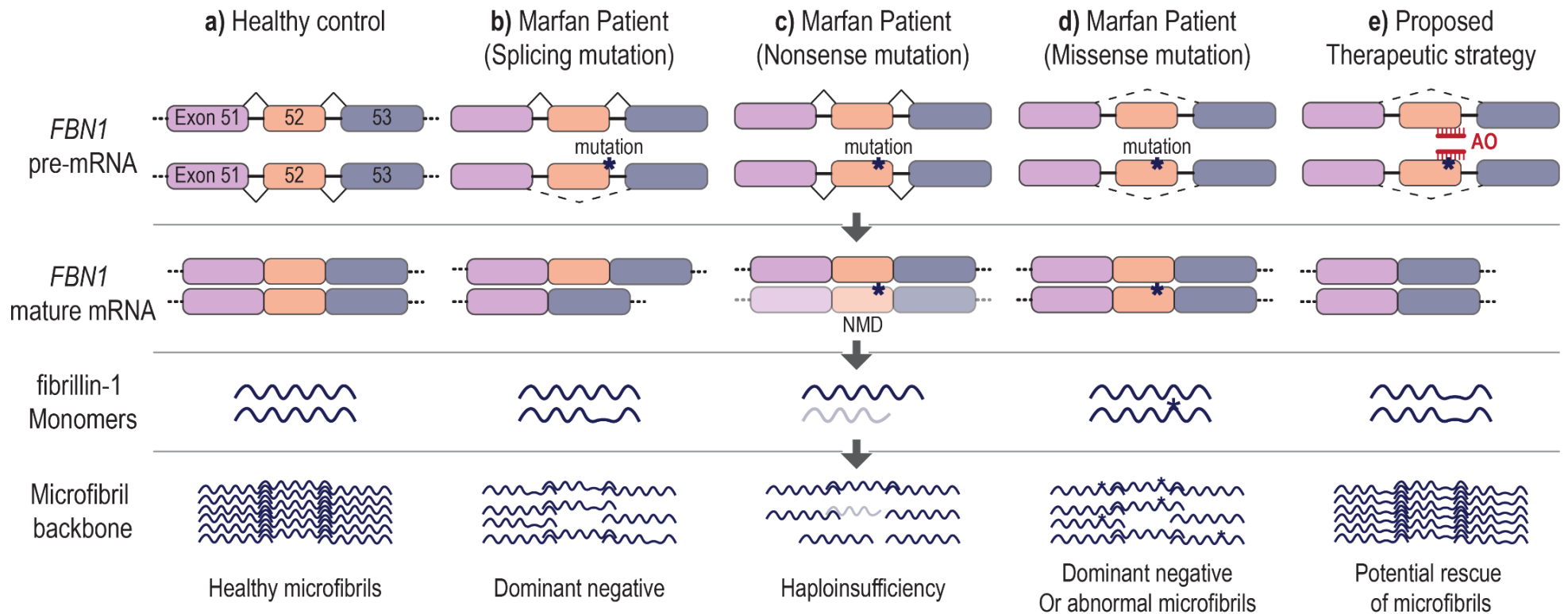


Figure 1.7: Schematic of fibrillin-1 from splicing to microfibril formation

a) a healthy control. b) a Marfan syndrome patient with a splice site mutation resulting in exon skipping and a dominant-negative effect on microfibril formation. c) a Marfan syndrome patient with a nonsense mutation resulting in nonsense-mediated decay and fibrillin-1 haploinsufficiency. NMD: Nonsense-mediated decay. d) a Marfan syndrome patient with a missense mutation resulting in a dominant-negative effect on microfibril formation or the formation of abnormal microfibrils. e) the proposed therapeutic strategy to induce exon exclusion from all transcripts using antisense oligonucleotides, potentially restoring the formation of functional microfibrils.

1.4 Summary, final remarks, significance, and aims

In summary, the type-1 fibrillinopathies are a family of connective tissue disorders, of which Marfan syndrome is the most common, with a prevalence of 2-3 in 10,000 individuals. These diseases are caused by mutations in the fibrillin-1 gene that encodes for the fibrillin-1 protein, a major component of the extracellular matrix microfibrils, providing both structural and regulatory support. The type-1 fibrillinopathies have variable ages of onset and are progressive, affecting multiple body systems with major clinical manifestations in the skeletal, ocular and cardiovascular systems.

The current standard of care relies heavily on surgical intervention and lifelong use of drugs to slow disease progression. We propose that antisense oligonucleotides could present a novel therapeutic strategy for the type-1 fibrillinopathies, by mediating the alteration of exon selection of both the unaffected and disease-causing pre-mRNA transcripts to force the translation of identical fibrillin-1 monomers that can form functional microfibrils. This proposed treatment alone or in conjunction with currently accepted symptomatic management could facilitate the production and maintenance of functional microfibrils, ultimately decreasing phenotypic severity and progression.

1.4.1 Aims of this study:

The overall focus of this study is to develop therapeutic alternative splicing strategies for the type-1 fibrillinopathies using antisense oligonucleotides. To achieve this, the following specific aims were addressed and constitute the results chapters of this thesis

1. To demonstrate proof-of-concept using *FBNI* exon 52 as a model.
 - a. Design, screen and optimise 2'OMe-PS AO sequences to induce the exclusion of exon 52 from fibrillin-1 mRNA in healthy control fibroblasts.
 - b. Evaluate the efficacy of lead sequences as the clinically applicable PMO chemistry in both healthy control and appropriate patient derived fibroblasts.
 - c. Determine the effects of exon skipping on the fibrillin-1 protein using immunofluorescence staining.
2. To evaluate the applicability of AO-mediated skipping to other *FBNI* exons.
 - a. Design, screen and optimise a series of 2'OMe-PS AO sequences to induce skipping of *FBNI* exons; 15, 16, 22, 26, 27, 31, 32, 39, 44, 45, 46, 47, 49 and 59 in healthy control fibroblasts.
 - b. Evaluate the efficacy of lead sequences as the clinically applicable PMO chemistry in both healthy control and appropriate patient derived fibroblasts.

- c. Determine the effects of efficient exon skipping on the fibroin-1 protein using immunofluorescence staining.
 3. To investigate the feasibility of triple-exon skipping.
 - a. Optimise cocktails of 2'OMe-PS AO sequences to induce exon 45, 46 and 47 exclusion.
 - b. Evaluate the efficacy of lead sequences as the clinically applicable PMO chemistry in both healthy control and appropriate patient derived fibroblasts.
 - c. Determine the effects of efficient exon skipping on the fibroin-1 protein using immunofluorescence staining.
 4. Investigate the effect of AO design and chemistry on AO efficiency
 - a. Compare the efficacy of the 2'OMe-PS, PMO and TMO chemistries using exon 52 as a model.
 - b. Investigate the impact of each chemistry on paraspeckle protein sequestration

Chapter 2
Materials and Methodology

2.1 Materials

2.1.1 General reagents

Table 2.1: List of reagents used in this study and their suppliers

Reagent	Supplier (Location)
100 bp molecular size marker	Geneworks (SA, Australia)
Acetic acid, glacial (CH ₃ COOH)	BDH Laboratories (Radnor, PA, USA)
Acetone (C ₃ H ₆ O)	Honeywell Research Chemicals (SA, Australia)
Agarose powder (molecular biology grade)	Scientifix (VIC, Australia)
Amaxa™ P3 primary cell 4D-Nucleofector™ X Kit S	Lonza (VIC, Australia)
AmpliAq Gold™ DNA Polymerase with Gold Buffer and MgCl ₂	Applied Biosystems (VIC, Australia)
Analar glycerol	Sigma Chemicals (NSW, Australia)
Anti-SFPQ antibody (ab38148)	Abcam (Melbourne, Australia)
Baxter sterile water	Baxter Healthcare (NSW, Australia)
Deoxynucleotide triphosphates (dNTPs)	Life Technologies (VIC, Australia)
Diffinity RapidTip®	Sigma-Aldrich (NSW, Australia)
Dimethyl sulfoxide (DMSO; C ₂ H ₆ OS)	Sigma Chemicals (NSW, Australia)
Dulbecco's modified Eagle's Medium (DMEM)	Life Technologies (VIC, Australia)
Endo-Porter	Gene Tools (Philomath, OR, USA)
Ethanol (C ₂ H ₅ OH)	Sigma-Aldrich (NSW, Australia)
Ethylenediaminetetraacetic acid (EDTA)	Sigma-Aldrich (NSW, Australia)
Foetal bovine serum (FBS)	Scientifix (VIC, Australia)
GlutaMAX™ Supplement	Thermo Fisher Scientific (VIC, Australia)
Hoechst 33342	Sigma-Aldrich (NSW, Australia)
Horse serum (HS)	Life Technologies (VIC, Australia)
IgG Alexa Fluor 488 goat anti-mouse (A-11001)	Thermo Fisher Scientific (VIC, Australia)
IgG Alexa Fluor 488 goat anti-rabbit (A-11008)	Thermo Fisher Scientific (VIC, Australia)
IgG Alexa Fluor 568 goat anti-mouse (A-11004)	Thermo Fisher Scientific (VIC, Australia)
Isopropanol (C ₃ H ₈ O)	Sigma-Aldrich (NSW, Australia)
Lipofectamine™ 3000 Transfection Reagent	Life Technologies (VIC, Australia)
MagMAX™ -96 Total RNA Isolation Kit	Applied Biosystems (VIC, Australia)
Methanol (CH ₃ OH)	Rowe Scientific (WA, Australia)
Mouse anti-fibrillin-1 monoclonal antibody, clone 26 (mAB2502)	EMD Millipore Corporation (Temecula, CA, USA)
Neon™ Transfection System 10 µl Kit	Thermo Fisher Scientific (VIC, Australia)
Opti-MEM® Reduced Serum Medium	Life Technologies (VIC, Australia)

Reagent	Supplier (Location)
ProLong™ Gold antifade reagent	Thermo Fisher Scientific (VIC, Australia)
PureLink™ Genomic DNA Mini Kit	Thermo Fisher Scientific (VIC, Australia)
RedSafe™ Nucleic Acid Staining Solution	iNtRON Biotechnologies (South Korea)
Sterile-filtered Water (tissue culture grade)	Sigma-Aldrich (NSW, Australia)
SuperScript™ III One-Step RT-PCR System with Platinum™ Taq DNA Polymerase	Life Technologies (VIC, Australia)
SuperScript™ IV First-Strand Synthesis System	Life Technologies (VIC, Australia)
TaKaRa LA Taq® DNA Polymerase (Mg2+ plus buffer)	Scientifix (VIC, Australia)
Triton X-100	Sigma-Aldrich (NSW, Australia)
Trizma base	Sigma-Aldrich (NSW, Australia)
Trypan Blue	Sigma-Aldrich (NSW, Australia)
Trypsin	Life Technologies (VIC, Australia)
TURBO DNase	Ambion (Austin, TX, USA)
Tween 20	Sigma-Aldrich (NSW, Australia)

2.1.2 Buffers and solutions

Table 2.2: Composition of buffers made in-house

Buffer	pH	Composition
1x PBS Autoclaved	7.4	137 mM NaCl 2.7 mM KCl 10 mM Sodium Phosphate dibasic 2 mM Potassium Phosphate monobasic
1x TAE	8.2	20 mM Trizma base 40 mM Acetic Acid 1 mM EDTA
2% Agarose		8 g Agarose powder Make to 400 ml with 1 x TAE Boiled to dissolve and stored at 65°C
Gel-loading buffer		0.5% Bromophenol blue 0.25% Xylene cyanol FF 30% glycerol In water 1% SDS in 1mM EDTA
1 x PBST (Tween-20)	7.4	137 mM NaCl 2.7 mM KCl 10 mM Sodium Phosphate dibasic 2 mM Potassium Phosphate monobasic 0.1% Tween-20
1 x PBST (Triton-X)	7.4	137 mM NaCl 2.7 mM KCl 10 mM Sodium Phosphate dibasic 2 mM Potassium Phosphate monobasic 0.1% Triton-X
Post-stain buffer		10 µl RedSafe 250 ml water

2.2 Methods

2.2.1 Antisense oligonucleotide design and synthesis

Antisense oligonucleotides (AO) were designed to anneal to acceptor and donor splice sites, as well as potential splicing factor motifs predicted *in silico* using SpliceAid.^{153,154} For initial screening AOs with 2'-*O*-methyl (2'OMe) modified bases on a phosphorothioate backbone (PS) were used. The 2'OMe-PS AOs were either synthesised in-house on an Expedite 8909 or Akta OligoPilot plus10 using the 1 µmol thioate synthesis protocol or purchased from TriLink Biotechnologies, LLC (San Diego, CA, USA). After screening, AO sequences found to mediate optimal skipping were purchased from Gene Tools (Philomath, OR, USA) as phosphorodiamidate morpholino oligomers (PMO). Thiophosphorodiamidate morpholino oligomers (TMO) were kindly provided by Professor Marvin Caruthers and Ondřej Kostov from the University of Colorado Boulder, USA.

A minimum of one AO sequence, completely unrelated to *FBNI*, was used per chemistry as a sham treatment to observe sequence-independent chemistry-related effects. A full list of all the AO sequences used in this study and their details is provided in Table A1.1, as well as in respective chapters. AO nomenclature is derived from Mann et al.¹⁵⁵ and includes the species ('H' for homo sapiens), exon number, acceptor (A) or donor (D) splice site and coordinates (xx/yy). Exonic coordinates are denoted by '+' while intronic coordinates by '-'. Therefore, FBNI H52A(+29+53) describes an oligomer annealing to the human FBNI mRNA between bases 29 and 53 of exon 52 (Figure 2.1)

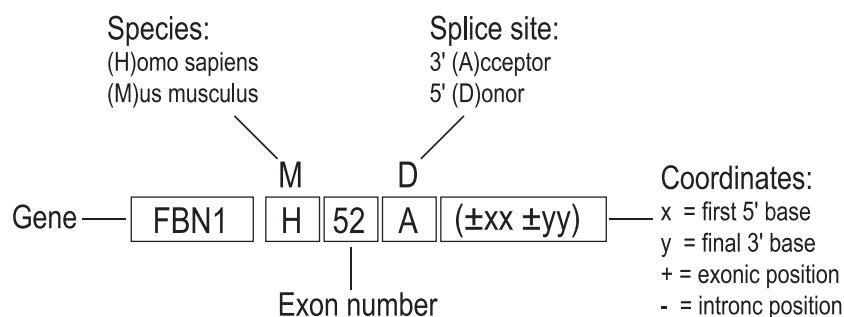


Figure 2.1: Antisense oligonucleotide nomenclature

An AOs name includes information on the gene, species, exon number, splice site and sequence coordinates. Adapted from Mann et al.¹⁵⁵

2.2.2 Cell culture

Cell lines

The use of human cells for this research was approved by the Murdoch University Human Ethics Committee; approval numbers 2013_156 and 2017_101 and The University of Western Australia Human Research Ethics Committee; approval number RA4/1/2295. Healthy control fibroblasts were cultured from a dermal biopsy of a healthy volunteer taken after informed consent.

A total of eight patient cell lines were used in this study. The following cell lines were obtained from the NIGMS Human Genetic Cell Repository at the Coriell Institute for Medical Research (Camden, NJ, USA): GM21936, GM21932, GM21940, GM21934, GM21941, GM21952, GM21992, GM21937. The mutation profile of each patient cell line was confirmed using Sanger sequencing. Mutation nomenclature was determined with respect to the *FBNI* gene Locus Reference Genomic sequence transcript 1 ([LRG_778t1](#)) and NCBI Reference Sequence ([NM_000138.5](#)) in which the translation start codon is in the second of 66 exons. A full list of the Marfan syndrome patient cell lines used in this study and their details is provided in Table A1.2.

Cell resurrection, maintenance and freezing conditions

Cells were resurrected from liquid nitrogen by thawing at 37°C, transferring into 9 ml of pre-warmed 10%-HS DMEM and centrifuging for 3 minutes at 1,000 g. Cell pellets were gently resuspended in growth medium and maintained in T75 cm² flasks at 37°C and 5% CO₂. The composition of growth media is described in Table 2.3. Media was replaced every 2-4 days as necessary.

Once at 80% confluence, cells were passaged for further expansion, freezing or use in experiments. Passaging involved, washing cells with 1x PBS, incubation with 1x trypsin for 2-4 minutes followed by inactivation with 10% FCS DMEM and centrifugation at 1,000 g for 3 minutes. Cell pellets were resuspended in growth media. As required, cells were counted by mixing 5 µl of cell suspension with 45 µl of trypan blue before 10 µl of the mixture was loaded into a haemocytometer.

For expansion, 3x10⁵ or 7x10⁵ cells were re-seeded into a T75 or T175 flask respectively with growth medium. For freezing, aliquots containing approximately 1x10⁶ cells and 10% DMSO were made up to 1 ml with 10% HS DMEM and transferred to cryovials for cryopreservation. Vials were kept at -80°C, allowing them to come to temperature before being stored in liquid nitrogen vapour phase. When required for 2'OMe-PS AOs transfection, fibroblasts were seeded into 24 well plates with 15,000 cells per well and incubated for 24 hours at 37 °C and 5% CO₂. For Nucleofection and Neon transfections, cells were transfected immediately.

Table 2.3: Cell culture media and buffers

Solutions were prepared in a Class II biological safety hood under aseptic conditions. Prepared solutions were stored at 4°C and warmed to 37°C when required.

Reagent (Cell type/purpose)	Composition
10% FCS DMEM (growth medium for healthy control fibroblasts)	High-glucose(4.5 g/L) DMEM 10% foetal bovine serum
15% FCS DMEM + GlutaMAX (Growth medium for patient fibroblasts)	High-glucose(4.5 g/L) DMEM 15% foetal bovine serum 1% GlutaMAX
5% FCS DMEM (Nucleofection transfection medium)	High Glucose DMEM 5% foetal bovine serum
Opti-MEM (Lipofectamine 3000 transfection medium)	100% Opti-MEM
10% HS DMEM (Temporary and cryo-storage medium)	High Glucose DMEM 10% Horse serum
1x trypsin (Detachment of adherent cells)	1% Trypsin 1x PBS
1 × Phosphate buffered saline (PBS) (Washing buffer, Autoclaved and filter sterilised)	pH 7.4 137 mM NaCl 2.7 mM KCl 10 mM Sodium Phosphate dibasic 2 mM Potassium Phosphate monobasic

2.2.3 Transfection

Transfection with 2'OMe-PS AOs

The initial screening 2'OMe-PS AOs were delivered as cationic lipoplexes using Lipofectamine® 3000 transfection reagent in Opti-MEM™ reduced serum. This reagent was used according to the manufacturer's instructions. In brief, 3 µl of Lipofectamine 3000 reagent and sufficient AO for a final concentration of 400 nM were incubated together in 50 µl of Opti-MEM for 10 min to allow for complexes to be formed. The transfection master mix was then diluted in Opti-MEM to a volume of 1 ml. The master mix was serially diluted to obtain concentrations of 200 nM, 100 nM and 50 nM in 1 ml each. These concentrations were used for the majority of experiments; however, higher and lower concentrations were obtained in the same manner.

The final transfection mixture was applied to fibroblasts seeded into 24-well plates 24 hours prior. Transfections were performed in duplicate with 500 µl of transfection mixture added to each well. Cells were incubated for a further 24 hours at 37°C and 5% CO₂ unless stated otherwise.

Transfection with PMOs

Phosphorodiamidate morpholino oligomers were delivered via Nucleofection using the Amaxa 4D-Nucleofector and P3 Primary Cell, 16-well Nucleocuvette™ kit (Lonza). Due to the

requirement of hyper-confluence for protein studies and to avoid cell growth post-transfection, 3×10^5 fibroblasts were used per treatment group. Cells were pelleted then resuspended in 19 μL of P3 solution(82%)-supplement(18%). The cell mixture was added to a Nucleocuvette™ along with, 1 μl of pre-warmed stock PMO (5mM) either undiluted (250 μM) or diluted 1:4 in filter sterilised water (50 μM). PMOs were pre-warmed for 5 min at 37°C. The Nucleocuvette™ strip was subsequently placed into the X unit of the Amaxa 4D-Nucleofector and pulsed with the predefined code optimised for dermal fibroblasts; CA-137. After electroporation cells were allowed to 'recover' for 10 min before the contents of each cuvette were diluted in 5%-FBS DMEM. The nucleofected cell mixture was divided between 4 wells in a 24 well plate. Two wells were seeded with 5×10^4 for RNA analysis and two coverslip-lined wells with 1×10^5 cells for immunofluorescence. Each well was made up to 500 μl with 5% FBS DMEM and incubated at 37°C for between 24 hours and 14 days as indicated. For incubation past three days, media was replaced with fresh 5% FBS DMEM as required.

Endo-Porter® (Gene Tools) was used to deliver select PMOs according to the manufacturer's instruction. Fibroblasts were seeded into a 24 well plate at a density of 8×10^4 cells per well and incubated for 24 hours before transfection. Culture medium was replaced with 500 μl fresh 10% FBS DMEM containing 3 μl of Endo-Porter®. One microlitre of stock PMO (5 mM) was added either undiluted (10 μM) or diluted 1:4 in filter sterilised water (2.5 μM) and the plate gently mixed. Cells were incubated for 72 hours at 37°C and 5% CO_2 .

Neon transfection

To compare the three chemistries particular 2'OMe-PS, PMO and TMO AOs were delivered into fibroblasts using the Neon Transfection System and 10 μl Kit following the manufacturer's protocol. In brief, cells were trypsinised, counted and washed with PBS, centrifuging for 2 min at 1,000 g between each step. Washed cells were resuspended in Resuspension Buffer R, with 3.15×10^5 cells in 10 μl of buffer per treatment. To a separate tube, 10 μl of cell mixture and AO were mixed before being drawn into a 10 μl Neon® tip using a Neon® Pipette. The pipette and tip were then placed into Neon® tube containing 3 ml of Electrolytic Buffer E and electroporated with a protocol optimised in-house for dermal fibroblasts consisting of 3 pulses at 1650 volts 10 milliseconds apart. Transfected cells were divided between a total of 5 wells. Two wells were seeded with 5×10^4 cells for RNA analysis, two wells with 1×10^5 cells for fibrillin-1 immunofluorescence staining and one well with 15,000 cells for paraspeckle protein immunofluorescence staining.

2.2.4 Cell harvesting and RNA extraction

Following the specified incubation period, transfected cells were harvested using MagMAX™ lysis binding solution. Total RNA was extracted with the MagMAX™ express-96 machine

(Applied Biosystems) and RNA isolation kit according to the manufacturer's protocol using a modified version of the program AM1830. Modifications include an additional 5 min of mixing during the lysis binding step and an extra 90 seconds for all washing steps. Samples were eluted into 42 µl of elution buffer and quantified using the NanoDrop™ 1000 Spectrophotometer (Thermo Fisher Scientific).

2.2.5 Polymerase chain reaction and gel electrophoresis

Target regions of the *FBNI* transcript were amplified via reverse transcription-polymerase chain reaction (RT-PCR) using the SuperScript™ III One-Step RT-PCR System with Platinum™ Taq DNA Polymerase as per the manufacturer's protocol. The components of each PCR reaction were as follows; 25 ng of the RNA template, 25 ng of each forward and reverse primer, along with provided 2x buffer and SuperScript™ III mixtures to a final volume of 12.5 µl. The *COLIA2*, exon 4 to 20, and *SMNI*, exon 4 to 8, gene transcripts were used as a housekeeping and control respectively. These transcripts were similarly amplified through RT-PCR with the following modifications. For the *COLIA2* amplicon, a lower 10 ng of each primer was used, while for *SMNI* transcript amplification, 50 ng of template RNA was used. The primers and thermocycling conditions for each gene are described in Table 2.4. Each primer is labelled according to the nomenclature set out in Figure 2.2.

A second control, *COL7A1* was amplified between exons 72 and 77 using a two-step process. Firstly, cDNA was synthesised using SuperScript™ IV First-Strand Synthesis System as per the manufacturer's protocol with 70 ng RNA as a template in a 10 µl reaction. With 35 ng of cDNA as a template, a second round of amplification was performed using TaKaRa LA Taq® DNA Polymerase, with an annealing temperature of 60°C for 34 cycles.

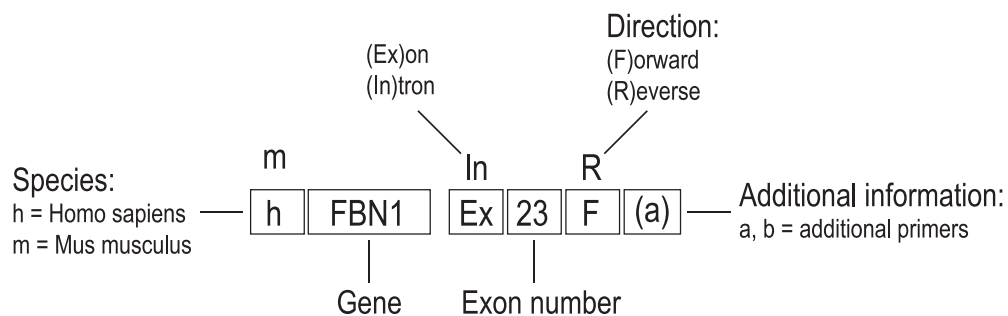


Figure 2.2: Primer nomenclature

Primer ID includes species, gene, target, primer direction and addition information as required

Table 2.4: List of primer sets.

The target, product sizes, primer name, sequence and thermocycling conditions of the primers used in this study. FL: full-length amplicons, Δ: amplicons lacking the target exon.

Target exon	Size (bases)	Primer	Sequence (5'-3')	Cycling conditions
SSIII one-step, RNA template				
15, 16	FL: 843 Δ15 720 Δ16 720	hFBN1 Ex13F hFBN1 Ex20R	GGATATCAGAGCACACTCAC GTAGATAAATCCCTTGGGGC	
22	FL: 969 Δ22 831	hFBN1 Ex19F hFBN1 Ex27R	TCAACTGGGAAAACTGCGT GAGGTCAGGAGATATGCGGC	
26, 27	FL: 628 Δ26 502 Δ27 499	hFBN1 Ex24F hFBN1 Ex28R	TGTTAAACACTAGGGGGTCAT ACTTCCCTCTGTGTTATGG	
31, 32	FL: 670 Δ31 544 Δ32 544	hFBN1 Ex29F hFBN1 Ex34R	CCGTTGCGTGAACCTCATAG CTTGACAGACAGCGGTAAG	
39	FL: 618 Δ39 549	hFBN1 Ex37F hFBN1 Ex42R	CACCTGATTTTGAACCTGAACC AGCACATCTTCTTGGTCATGT	55°C for 30 min
44, 45, 46, 47	FL 914 Δ44 788 Δ45 791 Δ46 788 Δ47 797 Δ45-47 548	hFBN1 Ex42F hFBN1 Ex49R	TGACAACCAGACCTGTGATGG GACTGTATCCAGGTGGGCAA	94°C for 2 min 94°C for 30 sec 55°C for 1 min 68°C for 1 min
47	FL 498 Δ47 381	hFBN1 Ex45F hFBN1 Ex49R	GCTTCACCTCCACAGGACAG GACTGTATCCAGGTGGGCAA	20 cycles
49, 52	FL 801 Δ49 681 Δ52 735	hFBN1 Ex47F hFBN1 Ex54R(a)	GGTTTCATCCTTTCTCACAAC AATCACATTCTTGCAGGTTC	
52	FL 860 Δ52 794	hFBN1 Ex47F hFBN1 Ex54R(b)	GGTTTCATCCTTTCTCACAAC TCACATGTCATCATTGGACC	

59	FL 830 Δ59 707	hFBN1 Ex56F hFBN1 Ex62R	GACCTGATGGAGAAGGCTGTG ATCAAGTGAGAATCCCCGCTG		
SMN exon 7	FL 404 Δ7 293	hSMN Ex4F hSMN Ex8R	AGGTCTCCTGGAAATAAATCAG TGGTGTCAATTTAGTGCTGCTCT	55°C for 30 min 94°C for 2 min 94°C for 30 sec 55°C for 1 min 68°C for 1 min	25 cycles
COL1A2 Housekeeping gene	FL 971	hCOL1A2 Ex4F hCOL1A2 Ex20R	GAGATAGAGGACCAGGTGGAG GTTACCGCTCTCTCCTTTGGA	55°C for 30 min 94°C for 2 min 94°C for 30 sec 55°C for 1 min 68°C for 1 min	18 cycles
AmpliTaqGold, gDNA template					
59	FL 952	hFBN1 In58F hFBN1 In59R	AGATGTGGAAGACAGTGGTTT TGATTGTCTGTGCTTTCCCTA	94°C for 6 min	
47	FL 186	hFBN1 Ex47F hFBN1 In47R	GGTTTCATCCTTTCTCACAAC GCACATTGTATTTGACAAGTCCC	94°C for 30 sec	30 cycles
52	FL 529	hFBN1 In51R hFBN1 Ex53R	ATCACAGATGCCCAAGGAGT TCGGGTTCTTTGCATTCGTC	55°C for 1 min	
32	FL 588	hFBN1 In31R hFBN1 In32R	GATTAAGTGGCCTGCTGCTT TATTCAATACACCTTTTCCCCC	72°C for 2 min	
Two steps, SSIV and TaKaRa					
COL7A1 exon 73	FL 521 Δ73 320	hCOL7A1 Ex72F hCOL7A1 Ex77R	AGATCGTGGAGACCTGGGATG CCTGTCTCCTTTGGGACCTTG	94°C for 6 min 94°C for 30 sec 60°C for 1 min 72°C for 1 min	34 cycles

Gel electrophoresis

After thermal cycling, the products of RT-PCR were mixed 4:1 (v:v) with gel-loading buffer and fractionated on 2% agarose gels in TAE buffer for approximately 90 minutes at 100 volts. In the first and last lanes, 2 µl of 100 bp DNA ladder was loaded to indicate product sizes. To detect the products, gels were immersed in RedSafe™ Nucleic Acid Staining Solution for 10 min under constant agitation, followed by washing in water for 30-60 minutes. Gels images were captured using the Fusion capture advance FX7 software on a Vilber Lourmat Fusion FX system (Vilber, Collégien, France). Bright artefacts were removed using the capture software, with an artefact correction radius of two pixels and a threshold of 1000. Images were cropped using Adobe Photoshop CC and analysed using ImageJ software.¹⁵⁶

2.2.6 Amplicon identity and mutation confirmation

Amplicon identity was confirmed using an isolation method called bandstab¹⁵⁷ and Sanger sequencing. Agarose gel electrophoresis and staining were performed as described in section 2.2.5, however, before imaging, gels were visualised using a blue-light transilluminator. A sample of each band of interest was collected by stabbing the gel with a P200 pipette tip, without any visible carryover agarose. The pipette tip was transferred immediately into a tube with a pre-prepared PCR mix containing, 50 ng of each forward and reverse primers, 5 nM dNTPs and 25 mM MgCl₂, 10x buffer and AmpliTaq Gold DNA Polymerase made to a total volume of 50 µl with sterile filtered water. Primers and thermocycling conditions are described in Table 2.4. Amplicons were fractionated on 2% agarose gel to confirm isolation and purity of the targeted product.

For mutation confirmation at the genomic level; genomic DNA was extracted from cell pellets using a PureLink™ genomic DNA mini kit following the manufacturer's protocol. After extraction, the *FBNI* region of interest was amplified using AmpliTaq Gold™ DNA polymerase and appropriate primers (Table 2.4) with 50 ng of gDNA as template. For confirmation at the cDNA level, cDNA was derived from patient RNA using RT-PCR as described in section 2.2.5. For analysing splicing mutations, the full-length and skipped transcript products were isolated through bandstab.

Amplicons were purified using Diffinity RapidTips® (Sigma-Aldrich) as per the manufacturer's instructions. Purified samples were mixed with the appropriate primer and submitted to the Australian Genome Research Facility (AGRF, Perth Australia) for Sanger sequencing. Sequencing results were analysed using Chromas version 2.6.6 and SnapGene® Viewer 5.1 software.

2.2.7 Immunofluorescent staining analysis

Cell culture and fixation

For fibrillin-1 staining, nucleofected and Neon transfected fibroblasts were seeded onto 13 mm No.1 round uncoated glass coverslip (ProSciTech, QLD, Australia) in 100 μ l of 5% FCS DMEM at a density of 1×10^5 cells per coverslip. Cells were incubated at 37°C for 30 minutes to allow cells to adhere to the coverslip before an additional 400 μ l of 5% FCS DMEM was added. The cells were then incubated for a further 24 hours to 14 days, with media replaced every 3-4 days as necessary.

For paraspeckle protein staining of Lipofectamine 3000 transfected cells, approximately 15,000 cells were dotted onto coverslips in 'colonies'. Cells were allowed to adhere for 30 minutes before adding growth media and incubating for 24 hours before transfection. Post transfection cells were incubated for a further 24 hours. For paraspeckle protein staining of Neon transfected cells, post-transfection 15,000 cells were seeded in colonies and similarly left to adhere before adding 400 μ l of 5% FCS DMEM and incubating for 24 hours.

After the incubation period, all coverslips were washed once with cold 1x PBS and fixed in ice-cold acetone-methanol (1:1) for 4 min on ice. Samples were stored at -80°C in slide sleeves until required.

Fibrillin-1 immunofluorescence staining

As required, coverslips were thawed to room temperature and maintained at room temperature unless stated otherwise. Coverslips were re-hydrated with 1x PBS before incubation with 10x blocking buffer (1x PBS + 10% Goat serum) for 30 min. Anti-fibrillin-1 primary antibody was applied at a dilution of 1:100 in 1x blocking buffer (1x PBS + 1% Goat serum) and coverslips were incubated at 4°C overnight (~16 hours). Following primary antibody incubation, coverslips were washed in 1x PBS three times for 5 min each and incubated for 1 hour in goat-anti-mouse Alexa Fluor 568 secondary antibody diluted to 1:400 in 1x blocking buffer. Coverslips were washed four times for 5 min each, with Hoechst 33342 (1:160) added to the second to last wash. Finally, coverslips were mounted with ProLong™ Gold antifade reagent, allowed to dry in the dark for 1 hour and then stored at 4°C.

Paraspeckle protein Immunofluorescence staining

Coverslips were thawed and maintained at room temperature, unless stated otherwise. After rehydration with 1x PBS, coverslips were washed with 1% Triton X-100 PBST for 5 min followed by two 5 min washes with PBS to remove excess Triton X-100. Coverslips were incubated for 1 h with primary antibody diluted in 0.05% Tween-20 PBST to 1:1,500 or 1:1,000 for PSPC-

1/NONO and SFPQ antibodies, respectively. Coverslips were washed three times for 5 min each with 0.2% Triton X-100 PBST before incubation for 1 hour with appropriate secondary antibody diluted to 1:400 in 0.05% Tween-20 PBST. Coverslips were washed with 0.2% Triton X-100 PBST three times for 5 min each, followed by incubation with Hoechst (1:160) for 3 min. Coverslips were washed with PBS a final time before mounting with ProLong™ Gold antifade reagent. All details of antibodies and nuclei stain are provided in Table 2.5

Imaging and Post-imaging modifications:

Imaging was performed using two microscopes; a Nikon 80i microscope using NIS-Elements Advanced Research software, and an Echo Revolve microscope with built-in software. Images were taken with either a 20x or 40 x lens. Texas red and FITC filters were used to capture fibrillin-1 and paraspeckle proteins, respectively. Hoechst was visualised using UV-2A (Nikon) or DAPI (Echo) filters. All conditions were maintained between images within an experiment.

Brightness and contrast of individual channel images were altered on the whole image and were altered equally for each image using Adobe Photoshop CC. Channels were then merged and the merged image cropped from original 1280px by 1024px size. A scale bar of 20 μm was added using ImageJ software.¹⁵⁶

Table 2.5: List of antibodies, details and dilutions

Antibody	Host	Clonality/ Conjugate	Supplier	Cat #	Lot #	Dilution	Incubation
Primary Antibodies							
Anti-fibrillin-1	Mouse	Monoclonal, Clone 26	Merck Millipore	mAb2502	2859140 2910144	1:100	4°C, 16 hr
Anti-SFPQ	Rabbit	Polyclonal	Abcam	ab38148	GR314817-1	1:1000	25°C, 1 hr
Anti-PSPC-1/NONO	Mouse		Gift from Prof. Archa Fox UWA, Australia			1:1500	25°C, 1 hr
Secondary Antibodies							
anti-Mouse IgG	Goat	Alexa Fluor 568	Thermo Fisher Scientific	A-11004	1613919	1:400	25°C, 1 hr
anti-Mouse IgG	Goat	Alexa Fluor 488	Thermo Fisher Scientific	A-11001	1890503A	1:400	25°C, 1 hr
anti-Rabbit IgG	Goat	Alexa Fluor 488	Thermo Fisher Scientific	A-11008	790311	1:400	25°C, 1 hr
Nuclei stain							
Hoechst 33342			Sigma-Aldrich	14533		1:160	25°C, 5 min

Chapter 3
Proof-of-concept: Antisense Oligonucleotide-
mediated Skipping of Fibrillin-1 Exon 52

The following is a modified version of the submitted article:

Cale JM, Greer K, Fletcher S, Wilton SD (submitted 10/02/2021) Proof-of-concept: Antisense oligonucleotide-mediated skipping of fibrillin-1 exon 52.

Author Contributions:

Conceptualization, J.C. and S.D.W.; methodology, J.C. and K.G.; formal analysis, J.C.; investigation, J.C. and K.G.; writing—original draft preparation, J.C.; writing—review and editing, J.C, K.G., S.F. and S.D.W.; visualization, J.C.; supervision, S.F., S.D.W.; funding acquisition, S.D.W. All authors have read and agreed to the final version of the manuscript.

3.1 Introduction

Marfan syndrome (MFS, MIM [154700](#)) is one of the most common dominantly inherited connective tissue diseases, affecting an estimated 2-3 in 10,000 individuals,^{27,28} in a family of disorders called the type-1 fibrillinopathies.²⁶ Marfan syndrome is characterised by extreme height with disproportionate limb and digit length in comparison to the torso, coupled with a myriad of other skeletal, ocular, skin and cardiovascular abnormalities.³⁴ However, it is the progressive growth of the aorta often eventuating into aortic dissection and rupture that is the most common cause of death.³⁵

Marfan syndrome was linked in the early 1990s to mutations in the, then recently discovered,¹¹ fibrillin-1 gene (*FBNI*).^{1,158} Since then over 2800 disease-causing mutations have been reported.² The fibrillin-1 gene encodes a large 350 kDa glycoprotein of the same name that is secreted from the cell and deposited into the extracellular matrix (ECM).¹¹ In a healthy individual, fibrillin-1 monomers aggregate into multimer units within the first few hours after secretion.¹⁷ Fibrillin-1 multimers form the backbone of microfibrils¹¹ that are essential in the majority of connective tissues and to which many microfibril associated proteins bind.¹⁵⁹ It is in the microfibril form that fibrillin-1 exerts its structural and regulatory roles, acting as a backbone of microfibrils,¹³ maintaining the stability of elastic fibres,¹⁴ and regulating the bioavailability of signalling proteins such as transforming growth factor-beta (TGF- β).^{12,16}

In an MFS patient, the disease-causing *FBNI* mutation results in a lack of functional microfibrils, in turn leading to instability of the ECM that is further compounded by the dysregulation of TGF- β .^{13,72} The loss of functional microfibrils leads to an increase in bioavailable TGF- β that activates a signalling cascade resulting in, among other outcomes, an increase in matrix metalloproteinase expression.¹⁶ Matrix metalloproteinases degrade fibrillin-1 and other matrix proteins leading to further destabilisation of the ECM.^{16,160} The initial loss of functional microfibrils is theorised to depend on the type of mutation. In general, missense mutations, that do not affect a conserved cysteine, as well as splicing mutations are thought to be dominant negative. Such mutations result in the production of a dominant aberrant monomer that disrupts the assembly of the wild-type protein into microfibrils.⁶⁸ In contrast, the majority of nonsense and frameshifting mutations are associated with haploinsufficiency.^{31,69} This haploinsufficiency is the result of transcript instability that leads to degradation and thus a reduction in fibrillin-1 expression.¹⁶¹ A small subgroup of nonsense and frameshift mutations that affect the C-terminal region can produce stable transcripts that are translated into protein rather than being degraded.^{52,66} Such mutations have been associated with intracellular retention of fibrillin-1, the outcome of which is a similar lack of microfibrils in the ECM.^{66,69}

The most common type of mutations are missense mutations that result in the disruption of a cysteine residue.^{2,3} The fibrillin-1 protein has several repeated domains including 47 epidermal growth factor (EGF)-like domains; 43 of which are involved in calcium-binding (cbEFG-like), seven TGF- β binding protein-like (TB) domains and two hybrid domains.^{20,21} Each of these domains are cysteine-rich with 6-8 conserved cysteine residues that play a critical role in the folding and stability of the fibrillin-1 protein.^{20,24} Mutations affecting a conserved cysteine have been shown to either increase the susceptibility of fibrillin-1 to proteolysis^{15,23} or disrupt the folding and secretion of fibrillin-1 leading to intracellular retention.²⁵ The outcome of either scenario is a similar decreased microfibril stability and abundance.

Following the discovery that mutations in fibrillin-1 result in TGF- β dysregulation, a research area emerged focussing on the antagonism of TGF- β as a therapeutic strategy.^{79,83} However, no breakthroughs have yet been made in the field and treatment of MFS patients remains heavily focused on symptom management. The current standard of care includes surgical correction of scoliosis, ectopia lentis, pectus deformities and aortic dilatation, as well as pain management and the use of β -adrenergic receptor blockers³³ or angiotensin II receptor type 1 blockers^{79,80} that slow the progressive aortic dilation and reduce the associated complications.^{27,33} Here we propose that personalised medicines using antisense oligonucleotides (AO) to alter *FBNI* exon selection during the splicing process, may be an appropriate therapeutic approach for Marfan syndrome.

Antisense oligonucleotides are short sequences, generally between 15 to 30 bases in length, that are single-stranded analogues of nucleic acids. Antisense oligonucleotides are designed to be complementary to the region of interest binding to the target RNA or DNA through Watson-Crick base pairing. When bound to the target sequence, AOs can work through two main mechanisms; recruiting RNase-H to cleave the target leading to degradation^{108,109} or physically blocking the binding of regulatory factor or machinery of the transcription,¹¹¹ translation¹¹² or splicing^{107,162} processes. Several studies have outlined the potential and efficiency of AOs in the treatment of genetic diseases. Several notable examples of which; Eteplirsen,^{123,140} Nusinersen^{145,163} and more recently Golodirsen¹⁴² and Viltolarsen¹⁶⁴ have now been approved by the United States Food and drug authority (FDA). All four drugs are a class of AO commonly referred to as splice switching. Splice switching AOs function by blocking the splicing machinery or regulatory features, altering the normal splicing process.

Splicing is an essential process for all multi-exon genes; removing the non-coding introns and re-joining the coding exons, before translation. The splicing process is, therefore, tightly regulated by several *cis*- and *trans*-acting elements. The majority of multi-exon genes, however, also undergo a process called alternative splicing.⁸⁹ Alternative splicing allows the production of multiple transcripts, and thus proteins, from a single gene, significantly increasing genetic complexity and diversity. To maintain the precise removal of introns, as well as supporting

alternative splicing, the regulation of these processes is multi-layered and complex while maintaining a level of flexibility in the definition of an exon.

This flexibility in exon selection is reliant on a balance of positive and negative splicing regulators that determine if a region bounded by canonical splice sites is to be defined as exonic or intronic in a tissue, developmental or environmental specific manner. The presence, or absence, of sufficient regulatory motifs determines if the spliceosome will recognise a region as exonic, ultimately determining if the region will be included in the mature transcript. Taking advantage of the inherent flexibility of exon definition, Eteplirsen, Nusinersen, Golodirsen and Viltolarsen all confer therapeutic value by altering exon selection. Eteplirsen, Golodirsen and Viltolarsen are designed to restore the reading frame of dystrophin mRNA in patients with amenable mutations by inducing the exclusion of exon 51^{123,144} and exon 53,^{143,165} respectively. Conversely Nusinersen is designed to induce the inclusion of *SMN2* exon 7, restoring the expression of a functional full-length transcript.¹⁴⁵ These opposing applications are achieved by targeting different regulatory elements involved in the splicing process.

To induce exon exclusion, AOs are commonly targeted to motifs involved in exon recognition and processing, such as the acceptor and donor splice sites, as well as hotspots for splicing enhancers either in the intron (ISE) or exon (ESE). Targeting enhancer sites can block the binding of positive splicing factors, thus decreasing the definition and recognition of an exon sufficiently to result in its exclusion.^{103,104} In contrast, targeting exonic splicing silencer (ESS) or intronic splicing silencer (ISS) sequences can inhibit the binding of negative splicing factors, increasing exon recognition leading to inclusion.^{104,139}

The affinity, specificity, efficiency, stability and tolerance of an AO can be increased by modifying the compounds chemical structure. There are two widely used chemistries utilised in this study. First of which has 2'-O-methyl (2'OMe) ribose ring modifications with a negatively charged phosphorothioate (PS) backbone. The resulting 2'OMe-PS compounds are robust RNase-H independent AOs that are nuclease resistant and relatively cost-effective to synthesise. The second chemistry is the phosphorodiamidate morpholino oligomer (PMO) that completely replaces the ribose sugar moiety with a morpholino ring and has phosphorodiamidate linkages.¹²⁰ The PMO chemistry is RNase-H independent, and has a neutral charge that does not interact with proteins, greatly reducing the possibility of off-target effects.^{118,166} While the PMO chemistry is both more technically challenging and costly to synthesise than 2'OMe-PS AOs, PMOs are generally recognised as both safe and effective in a clinical setting, making it a promising chemistry for drug development.^{123,124}

As described previously, fibrillin-1 monomers are secreted from the cell and rapidly aggregated into multimer units to form the backbone of fibrillin-1 microfibrils.¹⁷ Mutations in *FBN1* disrupt the formation of microfibrils, ultimately leading to a disease phenotype; either

Marfan syndrome or another type-1 fibrillinopathy. Therefore, we propose that removal of a mutation harbouring exon from all *FBNI* transcripts during the splicing process could result in the production of fibrillin-1 proteins that are able to form functional microfibrils restoring ECM stability. To assess the viability of this hypothesis, we addressed three preliminary questions using *FBNI* exon 52 as a model. (1) Can an exon be specifically removed from *FBNI* pre-mRNA using antisense oligonucleotides, (2) Can sufficient exon skipping be achieved, and (3) can the internally truncated fibrillin-1 protein form microfibrils.

3.2 Results

3.2.1 The *FBNI* transcript and antisense oligonucleotide design

The fibrillin-1 transcript ([LRG 778t1](#)) contains 11,695 bases separated into 66 exons, 65 of which encode the 350 kDa fibrillin-1 protein (Figure 3.1.a). Exon 52 of *FBNI* encodes a total of 22 amino acids and makes up a portion of the sixth, of seven, TB domain. Over 20 disease-causing mutations have been reported to affect exon 52, the majority of which result, or are predicted to result, in aberrant exon 52 splicing.^{2,3} To excise exon 52, along with the flanking introns during the splicing process, five AOs were designed across exon 52 targeting the acceptor, and donor splice sites as well as ESE and ISE sites predicted using the webtool SpliceAid¹⁵³ (Figure 3.1.c). SpliceAid studies the exonic and intronic sequence of interest and determines associated silencer and enhancer sites. Each site is given a score of 1 to 10 which indicates the strength of the site with the value closest to 10 being the strongest ESE sites

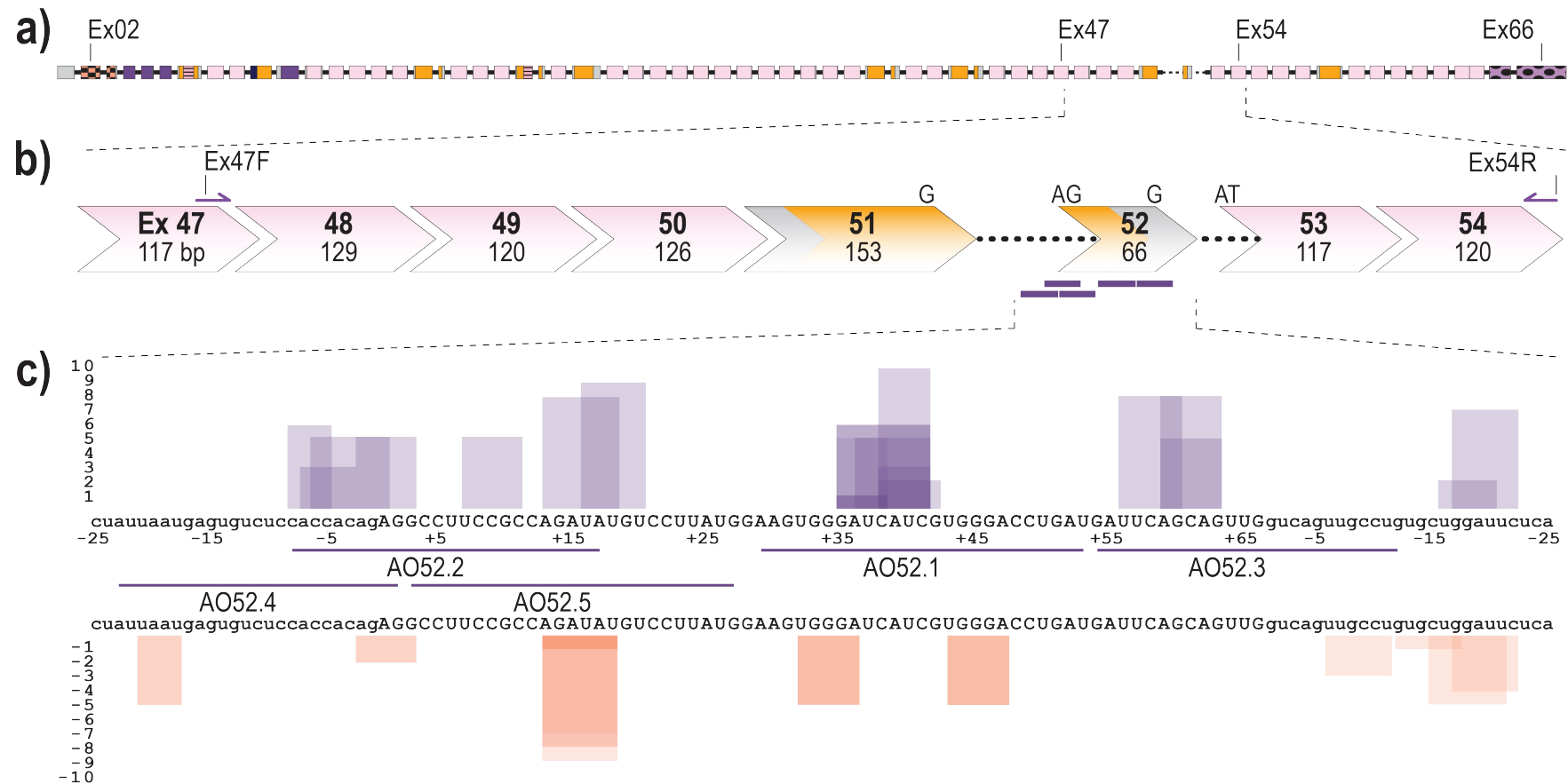


Figure 3.1: Schematic of *FBN1* pre-mRNA highlighting the region between exons 47 and 54 as well as AO binding sites

a) Full fibrillin-1 pre-mRNA transcript with each box representing an exon. Colours indicate the domain that the exon encodes. The solid black line represents introns (not to scale) b) Highlighting the region between exons 47 forward and 54 reverse primers and antisense oligonucleotide binding sites (purple bars). Chevron sides indicate exons bounded by partial codons. Pink and yellow fill indicate regions encoding cbEGF-like and TB domains, respectively. The black dotted line indicates partial introns 51 and 52. c) Antisense oligonucleotide binding sites and the regulatory motifs they target predicted using spliceAid.¹⁵³ Each box represents a predicted enhancer (purple) or silencer (orange) site. The height of the box represents the strength of the site with 1 being the weakest and 10 being the strongest. Exonic and intronic sequences are shown in upper- and lower-case respectively

3.2.2 Evaluation of AOs to induce exon 52 skipping from *FBN1* transcripts

Initial AO screening was performed using AOs composed of 2'OMe-PS molecules. An unrelated control AO that does not anneal to any transcript was included in all transfections as a sham treatment to observe any chemistry or delivery related effects on cell health and transcript abundance. A complete list of AOs can be found in Table 3.1.

Table 3.1: Sequences and binding co-ordinates of control and *FBN1* exon 52 AOs

The name, ID, sequence and chemistry of AOs designed to induce *FBN1* exon 52 exclusion. Two control sequences were used to reveal any chemistry-related effects. AO nomenclature described in Figure 3.5. The AOs targeting exons 52 were designed by Mr Kane Greer (unpublished, 2017).

Nomenclature (FBN1 H...)	Name	Sequence (5'-3')	Chemistry
52A(+29+53)N	AO52.1n	AUC AGG UCC CAC GAU GAU CCC ACU U ATC AGG TCC CAC GAT GAT CCC ACT T	2'OMe-PS PMO
52A(+29+53)M	AO52.1m	AUC AGG UCC CAC AAU GAU CCC ACU U	2'OMe-PS
52A(-08+17)	AO52.2	UAU CUG GCG GAA GGC CUC UGU GGU G	2'OMe-PS
52D(+13-12)	AO52.3	CAG GCA ACU GAC CAA CUG CUG AAU C	2'OMe-PS
52A(-23+02)	AO52.4	CUC UGU GGU GGA GAC ACU CAU UAA U	2'OMe-PS
52A(+03+27)	AO52.5	CAU AAG GAC AUA UCU GGC GGA AGG C	2'OMe-PS
Unrelated control	Ctrl	GGA UGU CCU GAG UCU AGA CCC UCC G	2'OMe-PS
GeneTools Control	GTC	CCT CTT ACC TCA GTT ACA ATT TAT A	PMO

All 2'OMe-PS AOs were transfected into fibroblasts, derived from a healthy control subject, at three concentrations (200 nM, 100nM and 50 nM) and incubated for 24 hours before collection for RNA extraction and RT-PCR analysis to assess exon skipping efficiencies. The 24-hour transfection incubation period was chosen after a time course of 24, 48 and 72 hours revealed negligible changes in skipping efficiency over time (data not shown). However, treated cells, in particular those treated with the higher concentration, were observed to change in morphology and begin to die after 48 hours (data not shown).

Analysis of PCR amplicons revealed the presence of two transcript products in several samples; the expected full-length (FL) product between exon 47 forward and exon 54 reverse primers, as well as a smaller product corresponding to the expected product of exon 52 skipping ($\Delta 52$)(Figure 3.2.a). The identity of the amplicons was confirmed by band purification and Sanger sequencing, confirming the precise removal of all 66 bases of exon 52 (Figure 3.2.b and c).

The most efficient exon 52 skipping was induced by AO52.1ⁿ, with 41% of transcripts lacking exon 52 after transfection at 200 nM (Figure 3.2.a). However, three other sequences; AO52.1^m, AO52.3 and AO52.5 were also relatively efficient, inducing up to 40%, 37% and 22% skipping respectively (Figure 3.2.a). The remaining two sequences did not induce any measurable exon 52 skipping. The sequences, AO52.1ⁿ and AO52.1^m differ by a single base, with each being an exact complementary pair for the wild-type and a known Marfan syndrome patient cell line,

respectively. This AO was designed in the hopes of understanding the mechanism behind the mutation that is known to cause mis-splicing of exon 52. The one base-pair mismatch did not greatly reduce the efficiency of AO52.1^m in healthy control cells.

Exon skipping efficiency was dose dependent with the most efficient skipping at a transfection concentration of 200 nM. There was negligible cell death evident for any of the three concentrations tested. A higher concentration of 400 nM was tested for selected samples in an attempt to further increase skipping efficiency. However, the increase in concentration did not translate into increased efficiency and instead induced up to 80% cell death (data not shown).

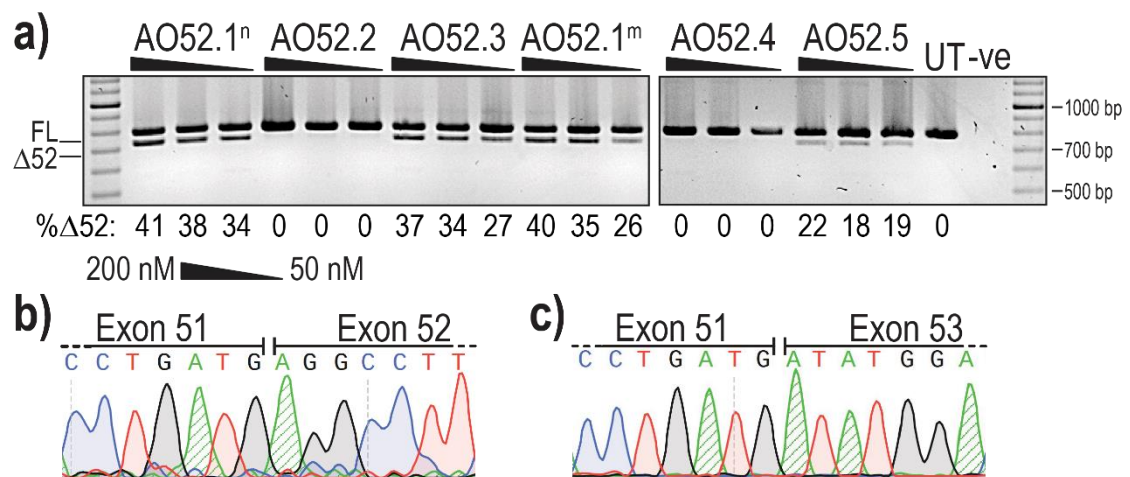


Figure 3.2: Evaluation of AOs designed to induce *FBNI* exon 52 skipping.

a) Screening of 2'OMe-PS AOs targeting exon 52. Healthy control fibroblasts were transfected with AOs as lipoplexes at three concentrations, 200, 100 and 50 nM. The values below each gel image indicate the percentage of exon 52 skipped ($\Delta 52$) transcripts in each sample. Ctrl: an unrelated sequence used as a sham treatment, UT: untreated control, -ve: RT-PCR negative control. 100bp molecular marker used for size reference. b) Sanger sequencing analysis showing the junction between exons 51 and 52 in full-length transcripts (FL, 859bp); c) Sanger sequencing analysis showing the junction between exon 51 and 53 exon 52-skipped transcripts ($\Delta 52$, 793bp).

Following initial AO screening, removal of exon 52 was deemed an appropriate option. In an attempt to further enhance exon exclusion, two AOs targeting *FBNI* exon 52 were combined into cocktails and evaluated. This method has previously been shown to boost skipping efficiency through synergy between the two AOs.¹⁶⁷ All AO cocktails reported were co-transfected into healthy control fibroblast at equimolar ratios, with total transfection concentrations of 200 nM, 100 nM and 50 nM. Six of the eight cocktails tested, induced between 23% and 42% exon 52 skipping at 200 nM (Figure 3.3). However, the efficiency was suggestive of an additive or baseline effect, similar to that achieved with a single AO. The combination of AO2.1ⁿ with AO52.2 or AO52.3 was antagonistic resulting in no measurable exon skipping (Figure 3.3). No synergistic cocktails were identified therefore AO52.1ⁿ was chosen as the most promising candidate and the sequence was synthesised as a PMO for further analysis (Table 3.1).

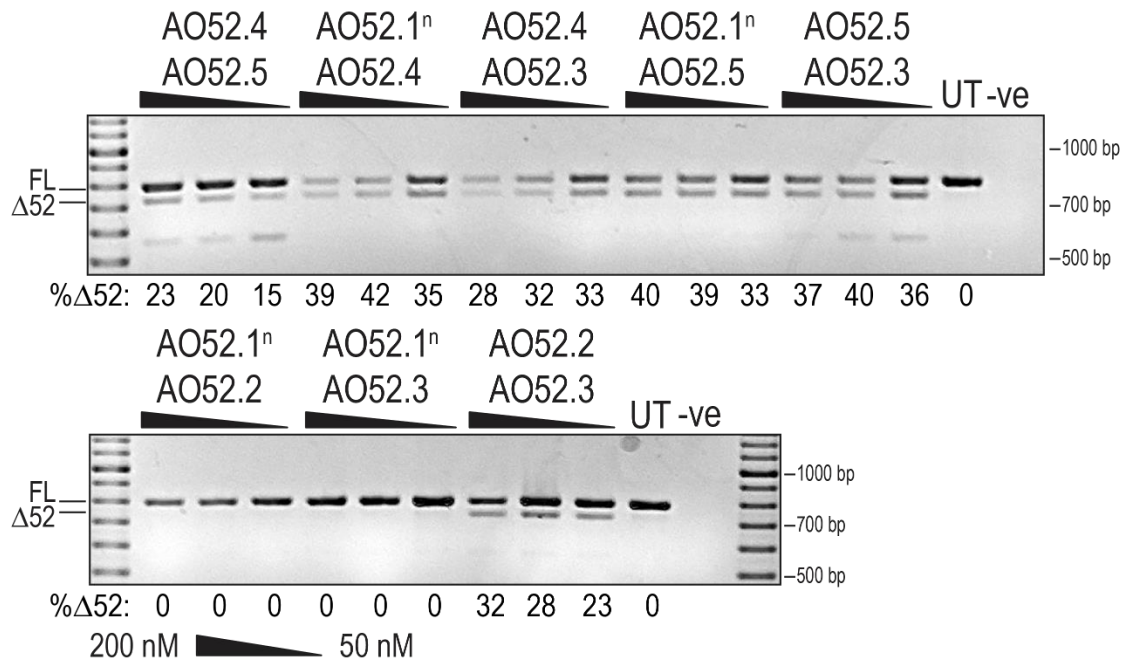


Figure 3.3: Evaluation of AO cocktails designed to induce *FBN1* exon 52 skipping.

Healthy control fibroblasts were transfected with AOs at three concentrations, 200, 100 and 50 nM. The values below each gel image indicate the percentage of exon 52 skipped ($\Delta 52$) transcripts in each sample. Ctrl: an unrelated sequence used as a sham treatment, UT: untreated control, ve: RT-PCR negative control. 100 bp molecular marker used for size reference.

3.2.3 PMO52 induces efficient exon 52 skipping and an increase in fibrillin-1 immunofluorescent staining.

To both confirm the efficiency of the AO52.1ⁿ sequence as a PMO, and to assess the effect of exon 52 skipping on fibrillin-1 microfibril formation, PMO52 was transfected into healthy control fibroblasts. An electroporation-based transfection method, Nucleofection, was used to deliver PMO52 into control cells at two concentrations; 250 μ M and 50 μ M, as calculated in a 20 μ l cuvette. Transfected cells were plated either directly into 24 well plates or onto coverslips and incubated for 72 hours before cells were collected for RNA analysis and coverslips fixed for immunofluorescent staining.

Representative results of healthy control cells treated with PMO52 are presented in Figure 3.4.a. These representative RT-PCR results reflect exon 52 removal from approximately 100% of transcripts, with no measurable FL product remaining. The lower AO concentration was observed to induce approximately 50% skipping, with no endogenous exon 52 skipping observed in either the control or untreated samples (Figure 3.4.a). Analysis of RT-PCR amplicons across four replicates revealed relatively consistent dose-dependent exon 52 skipping. On average $\Delta 52$ transcripts constituted 91% of total *FBN1* transcripts from cells transfected at the higher concentration and 55% at the lower concentration (Figure 3.4.b). The lowest skipping efficiency at the highest concentration was 74%; in the same experiment, the lower concentration maintained the average 55% skipping efficiency (Figure 3.4.b).

Fibrillin-1 protein was detected through immunofluorescent staining using a fibrillin-1 specific primary antibody and a fluorescently tagged secondary. Staining of the untreated sample revealed the long-thin extracellular fibre-like formations expected of fibrillin-1 (Figure 3.4.c.iii). Notably, the morphology of fibres in the sample with more than 90% skipping is comparable to those seen in the untreated healthy control (Figure 3.4.c.i and iii). The abundance of fibrillin-1 staining, as well as the abundance of fibre-like formations is, however, noticeably reduced in the 250 μ M treated samples. In contrast to the fibre formation in both untreated and high concentration of PMO52, healthy control cells treated with 50 μ M of PMO52, present with a complete loss of fibrillin-1 fibres and an overall reduction in fibrillin-1 staining (Figure 3.4.c.ii).

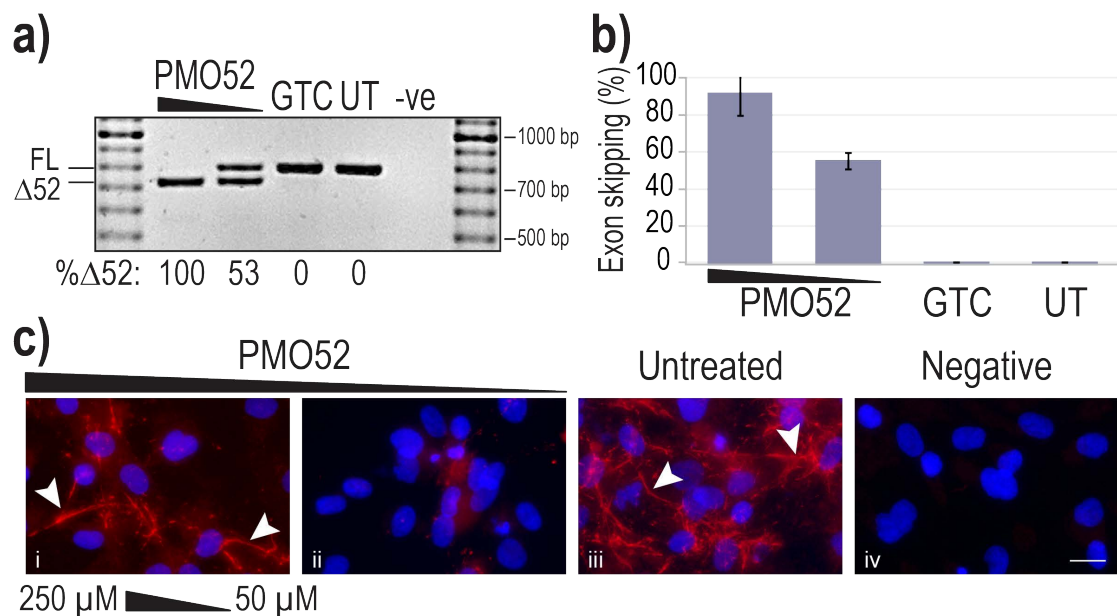


Figure 3.4: Efficiency and effect of PMO52

Healthy control fibroblasts were harvested for protein and RNA analysis, 72 h after Nucleofection with PMO52 at concentrations of 250 μ M and 50 μ M; calculated in the 20 μ l nucleofection cuvette. a) Agarose gel fractionation of *FBN1* exons 47 to 54 amplicons showing full-length (FL, 859bp) and exon 52-skipped ($\Delta 52$, 793bp) transcripts. The values below the gel image indicate the percentage of $\Delta 52$ transcripts. GTC: Gene Tools control PMO used as a sham treatment, UT: Untreated control, -ve: RT-PCR negative control, 100bp molecular marker used as a size reference. The gels were cropped for presentation. b) The percentage of full-length transcripts across four biological replicates (means plus error bars. Error bars = standard deviation, n = 4). c) Fibrillin-1 protein analysed via immunofluorescent staining. Merged fluorescence images of Hoechst staining of the nucleus (blue) and fibrillin-1 (red) with 'healthy' fibre-like morphology of fibrillin-1 indicated by white arrowheads. Negative: No primary antibody added, to control for non-specific binding of the secondary antibody. Untreated: no PMO added. Scale bar = 20 μ m.

3.3 Discussion

Although Marfan syndrome is well established as an inherited connective tissue disorder caused by mutations in the fibrillin-1 gene, the exact mechanism of pathogenesis has not been fully resolved. Current understanding suggests that the pathogenesis is dependent on the mutation type with an overarching basis that a lack of functional fibrillin-1 microfibrils leads to TGF- β dysregulation, further compounding ECM destabilisation.^{16,71} Therefore, we propose that removal

of a mutation-associated exon from all *FBNI* transcripts could result in the production of internally truncated fibrillin-1 proteins that retain some function and are able to form microfibrils. We addressed this hypothesis by designing antisense oligonucleotides to induce exon 52 exclusion from unaffected *FBNI* pre-mRNA. We suggest that many fibrillin-1 gene lesions will be amenable to the removal of the affected exon for two main reasons. Firstly, fibrillin-1 is highly repetitive suggesting the possibility of functional redundancy. Secondly, excluding exons 2, 3, 64, 65 and 66, the majority of fibrillin-1 exons are in-frame, and therefore, can be removed without disrupting the reading frame.

Here, we describe evidence for the efficient removal of *FBNI* exon 52. Of the five 2'OMe-PS AOs tested three were found to induce exon 52 skipping. Earlier dystrophin screening studies similarly found that 2 out of 3 AOs induced some skipping, albeit at different efficiencies¹⁶⁷ Our data also shows that skipping of exon 52 is not only possible but is even more efficient and consistent when using PMOs. Immunofluorescent staining of fibrillin-1 in treated cells supports the hypothesis that fibrillin-1^{Δ52} proteins can interact to form multimers. We observed fibre formation, mirroring that of the untreated control cells, when more than 90% exon 52 skipping was induced. We also established that inducing approximately 50% exon 52 skipping results in a complete loss of fibrillin-1 fibre staining in healthy control fibroblasts mimicking the disease-like state caused by splicing mutations. Together, these results demonstrate proof-of-concept that the internally truncated fibrillin-1^{Δ52} proteins produced through efficient exon 52 skipping are able to form multimers.

Of particular interest, is the total loss of microfibril formation caused by inducing a mixture of wild-type and *FBNI*^{Δ52} transcripts that results from sub-optimal levels of the PMO. This finding not only supports the dominant-negative pathogenic model; demonstrating the inability of a heterogeneous population of fibrillin-1 proteins to form microfibrils, but also has relevance to mapping of amenable *FBNI* exons that could be targeted in a splice intervention therapy. The elimination of fibrillin-1 fibres with 50% exon skipping and subsequent re-appearance of fibrillin-1 fibres with increased skipping efficiency could prove to be an invaluable tool in optimisation of fibrillin-1 AO sequences as well as identification of target exons. Importantly, being able to induce a disease-like state would allow the use of healthy control cells, rather than specific patient cells, for the identification of exons that when removed do not affect the expression or function of fibrillin-1.

We predict that the AOs reported here can manipulate *FBNI* splicing such that, at lower skipping efficiencies disease characteristics can be induced in healthy control cells and upon increased efficiency, sufficient skipping can be induced to reduce the key phenotype of MFS. This prediction is based on the dominant-negative model that suggests that in the presence of two protein isoforms, the aberrant protein disrupts the formation of microfibrils by the wild-type

protein⁶⁸ It is unknown exactly what ratio of wildtype to aberrant proteins would negate the dominant negative effects. However, the results presented here suggest that this tolerable threshold may be approximately 95%. We demonstrate that fibrillin-1 fibres can be formed when exon 52 skipping is sufficient, likely >90% skipping, such that more than 95% of total multimers that are formed would be of the fibrillin-1^{Δ52}-fibrillin-1^{Δ52} structure. We also note, however, that mutations resulting in haploinsufficiency lead to disease. Therefore, we believe that the abundance of microfibrils has to be maintained, as a minimum, above that observed in haploinsufficiency patients.^{31,161}

While we demonstrated efficient and consistent exon skipping using PMO52, the concentrations used are relatively high, when compared to similar studies targeting other genes.^{167,168} One of the possible explanations for the high concentration required is the abundance of fibrillin-1 transcripts. Fibrillin-1 RNA is expressed in the vast majority of cell types and is maintained at relatively high levels throughout the body.¹⁶⁹ We noted the efficient PCR amplification of *FBNI* transcripts; requiring 20 or fewer rounds of amplification coupled with the need for very low template concentrations (25 ng). While the *in vitro* PMO transfection concentrations used seem relatively high, we noticed no changes in morphology or health of cell cultures up to four days post-transfection with PMO52. The PMO chemistry is generally considered to be safe with no off-target effects nor toxicity.¹²³⁻¹²⁵ Nevertheless, while the PMO chemistry may be safe and a higher concentration required due to the level of fibrillin-1 expression, there are still several ways in which the efficiency of an AO can be improved, including optimisation of AO delivery, sequence, length and chemistry. Further optimisation could allow for the use of a significantly lower dosage that in turn would not only reduce the possibility of off-target effects or toxicity but also lower the cost of treatment.

The fibrillin-1 protein produced by excising exon 52 is predicted to be internally truncated, fibrillin-1^{Δ52}, and lacking the last seven amino acids of the sixth TB domain. This isoform has only been reported in the context of exon 52 mutations, where it is known to act in a dominant negative manner against the wild-type protein and result in a severe lack of functional microfibrils.^{151,170} Liu et al.¹⁷⁰ also reported that an exon 52 splicing mutation leads to reduced fibrillin-1 synthesis, less than 50% of that observed in healthy controls, while the mutant mRNA levels remain unchanged, suggesting that the fibrillin-1^{Δ52} proteins are unstable. Liu et al.¹⁷⁰ suggests this instability may result from the partial deletion of a TB domain that leads to misfolding of the fibrillin-1 protein increasing its susceptibility to proteolysis. If this is the case then attempts to induce exon skipping of other exons encoding partial TB domains; 10, 11, 17, 18, 38, 39, 42, 43 and 51, would likely face the same issue. It is possible that removal of the two exons encoding the TB domain as a pair could solve this problem. However, we show that the fibrillin1^{Δ52} proteins studied here are able to be synthesised, secreted from the cell and form fibre-

like structures. Nevertheless, the synthesis, deposition and function of fibrillin-1^{Δ52}, especially in the absence of wild-type fibrillin-1, needs to be investigated further.

Here we illustrate that when fibrillin-1^{Δ52} is the predominant product it is able to be both synthesised and secreted from the cell, with no evidence of intracellular staining. We also demonstrate that fibrillin-1^{Δ52} proteins can form fibres; provided that *FBNI*^{Δ52} transcripts make up more than 90% of total *FBNI* transcripts. These results suggest that the fibrillin-1^{Δ52} protein is functional, although further protein analysis is required to assess if the fibres formed can interact with the microfibril associated proteins with which fibrillin-1 naturally interacts. The ability of fibrillin-1^{Δ52} proteins to sequester TGF-β also needs to be assessed. If removal of exon 52 disrupts the regulation of TGF-β, then regardless of the high skipping efficiency and fibre formation that is observed, symptoms such as aortic growth would continue to progress with no benefit from this treatment.

As previously noted, our results support the hypothesis that fibrillin-1^{Δ52} can form fibres. However, while the morphology of fibres is superficially similar to that of the untreated, healthy control, their abundance is reduced. The reduction of abundance could be the result of the experimental design and protocols. For example, Nucleofection is known to cause cell stress reducing fibrillin-1 expression, or the transfection incubation time could be insufficient to allow more efficient formation of microfibrils after treatment. However, it is likely that, as reported by Liu et al.,¹⁷⁰ fibrillin-1^{Δ52} synthesis is reduced in comparison to the wild-type. Western blotting analysis of intracellular and extracellular fibrillin-1 was attempted, however, due to poor signal and resolution in samples from healthy control fibroblasts we were unable to confirm any changes in fibrillin-1 abundance. Further optimisation of the Western blot protocol to produce reliable results is required before the effect of *FBNI* exon skipping on the abundance of fibrillin-1 can be assessed. While restoring microfibril abundance and function to a 'normal' state would be ideal, this may not be possible. We believe that any increase in functional microfibrils could provide a therapeutic benefit by reducing disease progression and severity.

As discussed earlier, the current standard of care for individuals living with MFS relies heavily on invasive surgical interventions and the lifelong use of medicines such as β-adrenergic receptor blockades that slow the progression of aortic dilation.^{33,76,78} These interventions have proven lifesaving, as well as life-extending.^{35,75} However, the burden of MFS on quality of life, and the economic stress, for both patients and their families, remains substantial.^{171,172} In more recent years major efforts have been made to discover and develop therapeutics for MFS.^{37,78,79,83} Research has focused on slowing aortic growth as well as a continued improvement upon current treatment strategies for the main symptoms of MFS. With FDA approval of AO therapeutics to restore gene function in spinal muscular atrophy¹⁴⁵ and Duchenne muscular dystrophy,^{123,144} we

suggest that antisense oligonucleotide-mediated splice switching as described here could be an appropriate direction for the development of therapies for Marfan syndrome.

In conclusion, this study assessed the ability of a suite of AOs to induce targeted exon 52 skipping from full-length *FBNI* mRNA transcripts expressed in healthy control fibroblasts. The most efficient sequence, and the consequences of splice modification, was further evaluated in healthy control fibroblasts. We showed *in vitro*, that AO52.1ⁿ, AO52.1^m and AO52.3 as well as PMO52 induced dose-dependent exon 52 skipping. Encouragingly the presence of more than 90% of one transcript type; wild-type or *FBNI*^{Δ52}, corresponded with the formation of fibrillin-1 fibres. In contrast, a mixed transcript pool resulted with the complete loss of fibrillin-1 fibres, mimicking the disease-like state.

While this study is a preliminary, *in vitro* investigation, our candidate PMO consistently induces efficient exon 52 exclusion while maintaining fibrillin-1^{Δ52} fibre formation. With increasing numbers of AO therapeutics being approved for clinical use, our results suggest that PMO52 may be an attractive therapeutic option for the treatment of Marfan syndrome caused by mutations in fibrillin-1 exon 52. This study provides proof-of-concept and a foundation for the further development of antisense oligonucleotide therapies for Marfan syndrome.

3.4 Materials and methods

3.4.1 Design and synthesis of antisense oligonucleotides.

Antisense oligonucleotides were designed to target splicing regulatory motifs at the exon-intron junctions as well as exonic splicing enhancer sequences predicted using the spliceAID web tool.¹⁵³ AO sequences were also analysed using NCBI nucleotide BLAST¹⁷³ to identify any possible off-target annealing. Antisense oligonucleotides with 2'OMe-PS chemistry were purchased from TriLink biotechnologies (Maravai LifeSciences, San Diego, CA, USA), and PMOs were purchased from GeneTools LLC (Philomath, OR, USA). Two unrelated sequences, one for each chemistry, were used as sham treatments. These controls allow for the observation of any sequence-independent chemistry-related effects. The nomenclature of AOs is based on that described in Mann et al.¹⁵⁵ and provides information on the gene, exon, annealing co-ordinates and species (Figure 3.5). A full list of AOs used in this study are provided in Table 3.1.

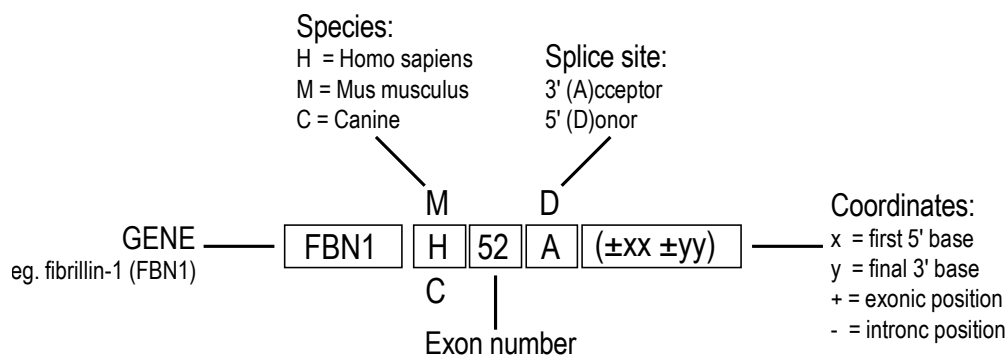


Figure 3.5: Nomenclature of antisense oligonucleotides

The name of each AO is unique and includes information on the gene, specific, target exon, splice site and sequence co-ordinates. Figure adapted from Mann et al. ¹⁵⁵

3.4.2 Cell culture and transfection

Healthy control fibroblasts were originally sourced from a dermal biopsy derived from a healthy volunteer with informed consent. The use of human cells for this research was approved by the Murdoch University Human Ethics Committee, approval numbers 2013_156 and The University of Western Australia Human Research Ethics Committee; approval number RA4/1/2295. Fibroblasts were maintained in Dulbecco's Modified Essential Medium (DMEM, Gibco; Life Technologies, Melbourne, Australia) supplemented with 10% foetal bovine serum (FBS, Scientifix, Cheltenham, Australia) and incubated at 37°C with 5% CO₂.

Antisense oligonucleotides (2'OMe-PS chemistry) used for target site screening were transfected into healthy control fibroblasts using Lipofectamine 3000 (Life Technologies, VIC, Australia). Transfections were prepared by incubating the AO with 3 µl of Lipofectamine 3000, at room temperature in 50 µl of Opti-MEM (Gibco; Thermo Fisher Scientific, VIC, Australia), according to manufacturer's protocol. The transfection mixture was then diluted to the desired AO concentration in a final volume of 1 ml and applied to cells. Transfected cells were incubated for 24 hrs before collection.

The PMO was delivered using the 4D-Nucleofector™ and P3 Nucleofection kits (Lonza, VIC, Australia). One microliter of stock PMO (5 mM), either undiluted (250 µM) or diluted 1:4 in sterilised water (50 µM), was added into a cuvette along with 300,000 fibroblasts resuspended in 19 µl of pre-warmed transfection solution. The mixture of fibroblasts and PMO was subsequently nucleofected using the pulse code, CA 137, previously optimised in our laboratory for dermal fibroblasts. Nucleofected fibroblasts were maintained in DMEM supplemented with 5% FBS before collection after 3 or 4 days.

3.4.3 RNA extraction and RT-PCR analysis

Total RNA was extracted using MagMax™ nucleic acid isolation kits (ThermoFisher Scientific, Melbourne, Australia) as per the manufacturer's protocol. Total RNA concentration and purity were determined using a Nanodrop 1000 spectrophotometer (ThermoFisher Scientific). Transcripts were amplified using one-step SuperScript® III reverse transcriptase with 25ng of total RNA as a template. To observe exon 52 skipping, *FBN1* transcripts were amplified using exon 47 Forward (5'-GGTTTCATCCTTTCTCACAAC-3') and exon 54 Reverse (5'-TCACATGTCATCATTGGACC-3') primers (Integrated DNA Technologies, IDT, NSW, Australia). The cycling conditions were as follows; 55°C for 30 min, 94°C for 2 min followed by 20 cycles of 94°C for 30 sec, 55°C for 30 sec and 68°C for 1min. The PCR amplicons were fractionated on 2% agarose gels in Tris-Acetate-EDTA buffer. Images were analysed using ImageJ (version 1.8.0_112) imaging software (NIH, Bethesda, MD, USA)¹⁵⁶ to determine the relative density of amplicons.

3.4.4 Immunofluorescence

Immediately after Nucleofection, 100,000 fibroblasts were seeded into each well of a 24-well plate lined with a 13 mm No.1 round uncoated glass coverslip. Cells were incubated for 72 hours before being fixed in ice-cold acetone: methanol (1:1, v:v) and allowed to air dry. Fixed cells were washed once with PBS to rehydrate before blocking with 10% goat serum in PBS for 1 hour at room temperature. The primary antibody, Anti-fibrillin-1 antibody clone 26 (Merck Millipore, Sydney, Australia), was applied at a dilution of 1:100 in 1% goat serum-PBS and incubated overnight at 4°C. Secondary antibody; AlexaFluor568 anti-mouse IgG (Thermo Fisher Scientific, VIC, Australia) was applied, 1:400, for 1 hour at room temperature, and co-stained with Hoechst 33342 (Sigma-Aldrich) for nuclei detection (1 mg/mL diluted, 1:125). Coverslips were mounted using ProLong™ Gold antifade mountant (Thermo Fisher Scientific, VIC, Australia). Fibrillin-1 was detected using a Nikon 80i microscope with NIS-Elements software (Nikon, Australia). The brightness and contrast of individual channel images were altered equally for each image, then merged. The merged image was cropped from the original 1280 x 1024 pixel image using Adobe Photoshop CC. A 20 µm scale bar was added using ImageJ software.¹⁵⁶

Chapter 4
Multiple Mutations One Drug

4.1 Introduction

4.1.1 The complexity of the type 1 fibrillinopathies

The type-1 fibrillinopathies are a complex and diverse family of diseases that can be caused by many types of mutations affecting the fibrillin-1 gene (*FBNI*). Numerous features characteristic of the type-1 fibrillinopathies hinder diagnosis and the development of therapeutics, including (a) highly variable prevalence from 2-3 in 10,000 for Marfan syndrome (MFS) and less than 1 in 1,000,000 for Stiff skin syndrome (SSKS), Geleophysic dysplasia 2 (GPHYSD2) and Marfan lipodystrophy syndrome (MFLS); (b) over 2800² unique mutations; (c) a high rate (25-30%³) of *de novo* mutations; (d) phenotypic overlap between the type-1 fibrillinopathies and other diseases and (e) extensive intra- and inter-familial phenotypic variability. Examples of this complexity and the impact on diagnosis and therapy development are outlined below.

Asymmetric Marfan syndrome

Before the association of Marfan syndrome with fibrillin-1 mutations, Burgio et al.¹⁷⁴ and Godfrey et al.¹⁷⁵ described a case of asymmetric Marfan syndrome resulting from a postzygotic mutation. Only one half of the patient's body was affected, resulting in a unique case in which the patient's left-hand side was 4 cm longer than the right before the age of seven years old.¹⁷⁵ Not only did this case provide insight into the exact symptoms of Marfan syndrome, it also enabled Godfrey et al.¹⁷⁵ to observe the lack of microfibril formation on the left-hand side, signifying the importance of fibrillin-1 fibre formation in Marfan syndrome.

Phenotypic and genotypic overlap

One major hurdle in the development of cost-effective and efficient diagnostic tests for the type-1 fibrillinopathies, is the overlap in phenotypes between the different fibrillinopathies as well as with other diseases. The type-1 fibrillinopathies form a spectrum of severity from mild disorders that affect a single organ system, such as Ectopia lentis syndrome, to severe phenotypes affecting the entire body, as seen in MFS. However, across the whole spectrum, each disease shares phenotypic similarities. Ectopia lentis, for example, is characteristic of Ectopia lentis syndrome, MFS and MFLS, while short stature, is common to Weill-Marchesani Syndrome 2, GPHYSD2 and acromicric dysplasia (ACMID).

The overlap in phenotypes is further complicated by genotypic overlap whereby several *FBNI* mutations are reported to result in different disease phenotypes in various individuals. Examples of such overlap are ACMID and GPHYSD2. While clinically distinct, these two diseases share the majority of phenotypic characteristics such as; short stature, short fingers and toes, joint stiffness and skin thickening. A lack of cardiac involvement in acromicric dysplasia is one of the

only features that distinguished these conditions. While both diseases are incredibly rare, two mutations; p.Tyr1699Cys and p.Ala1728Thr have been attributed with causing both phenotypes in different individuals.⁵⁷

Both phenotypic and genotypic overlap pose significant hurdles in the diagnosis of the type-1 fibrillinopathies. However, this overlap could prove useful in therapy development. Due to the overlap in genotype, and phenotype, therapies designed to treat the cause of disease, *FBNI* mutations, could potentially apply to all type-1 fibrillinopathies.

Recessive Marfan syndrome

Marfan syndrome is primarily considered an autosomal dominant disease caused by heterozygous mutations in the fibrillin-1 gene. However, there are a small number of cases in which inheritance is recessive, with individuals homozygous for the mutation exhibiting the MFS phenotype. In these cases, relatives that are heterozygous for the mutation or have no mutation are unaffected. Such cases are highlighted in Hilhorst-Hofstee et al.³², Khan et al.¹⁷⁶ and de Vries et al.³¹ Supposing that such instances are representative of a true recessive mode of inheritance, this suggests that some *FBNI* mutations result in monomers capable of forming microfibrils with wild-type monomers, but incapable of forming microfibrils with other mutant monomers. This opposes the dominant-negative pathogenesis model and suggests that there is some other mechanism at play.

Interestingly some ‘recessive’ mutations manifest as dominantly inherited in other individuals or families, indicating the involvement of additional unknown factors. Overwater et al.¹⁷⁷ reports two unrelated families with an autosomal dominant inheritance of a c.1453C>T, p.Arg485Cys *FBNI* mutation. The same mutation was previously reported by De Vries et al.³¹, who describes a family with an affected homozygous individual and unaffected heterozygous relatives. Overwater et al.¹⁷⁷ suggests that the age of patients at the time of clinical assessment, as well as clinical variability may account for the lack of clinical phenotype observed in heterozygous individuals. Aubart et al.¹⁷⁸ explored possible modifier genes that could explain the lack of disease phenotype, including other extracellular matrix proteins and several matrix metalloproteinases. However, the study found no conclusive evidence of such associations and further research into the field is still required. On the other hand, Aoyama et al.⁶⁹ advocates that the effect of the mutation on the synthesis and deposition of fibrillin-1 in the extracellular matrix is the reason we observe so much phenotypic variability.


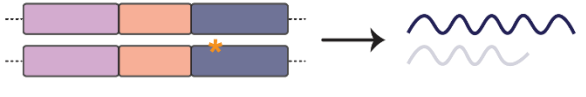
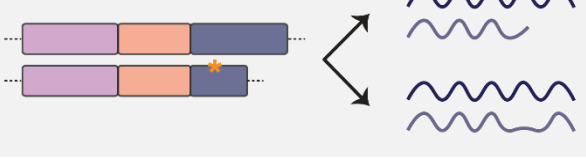
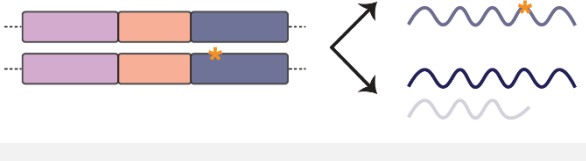

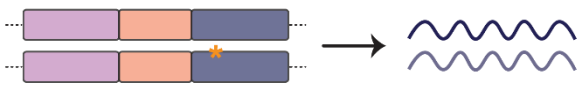
4.1.2 Mutation classification and pathogenesis

Fibrillin-1 proteins are known to assemble into multimer units immediately after secretion from the cell, forming the backbone of microfibrils.^{14,179} Microfibrils are essential in the majority of connective tissues, and it is in the microfibril form that fibrillin-1 plays a crucial part in elastic fibre formation and stability,^{14,15} while also regulating signalling proteins such as transforming growth factor-beta (TGF- β).^{180,181} The dysregulation of TGF- β , as a result of insufficient functional microfibrils, is now considered the leading factor in the pathogenesis of Marfan syndrome.^{16,71,74}

The cause and severity of the reduction in microfibrils has been linked with the type of *FBNI* mutation and its effect on the synthesis, secretion and function of the resulting fibrillin-1 proteins. Aoyama et al.⁶⁹ proposed five groups of *FBNI* mutations according to the levels of fibrillin-1 synthesis and deposition as compared to those in healthy controls. These groups include mutations that result in (I) reduced synthesis and deposition, (II) reduced synthesis and severely reduced deposition, (III) intermediate synthesis and mildly reduced deposition, (IV) intermediate synthesis and severely reduced deposition and (V) a small group with normal synthesis and deposition.⁶⁹ These groups are summarised in Table 4.1.

Table 4.1: *FBN1* mutation groups according to fibrillin-1 synthesis and deposition.

The majority of *FBN1* mutations can be classified into one of five groups. These groups describe the relationship between pathogenesis, mutation outcome and the observed synthesis and deposition of fibrillin-1 protein. Adapted from Aoyama et al.⁶⁹

Group	Synthesis	Deposition	Pathogenesis	Mutation outcome
Unaffected	100%	100%		 Normal fibrillin-1 monomer Normal fibrillin-1 monomer
I	<70%	≥35%	Haploinsufficiency	 Normal fibrillin-1 monomer Truncation or no protein produced
II	<70%	<35%	Dominant negative	 Normal fibrillin-1 monomer C-terminal truncation Normal fibrillin-1 monomer Internal truncation
III	≥70%	35-70%	Loss of function or degradation	 Normal fibrillin-1 monomer Normal fibrillin-1 monomer with abnormal function Normal fibrillin-1 monomer No protein produced
IV	≥70%	<35%	Dominant negative	 Normal fibrillin-1 monomer Abnormal monomer
V	≥70%	≥70%	Loss of function	 Normal fibrillin-1 monomer Non-functional monomer

Group I mutations, and some group III mutations, are predicted to result in fibrillin-1 haploinsufficiency.⁶⁹ As such, mutations in these groups are often nonsense, frameshift or out-of-frame splicing mutations that result in either no protein production from the affected allele or an unstable protein that is degraded.¹⁸² A small subset of premature termination codon (PTC) mutations, usually affecting the C-terminal, are associated with average fibrillin-1 synthesis and reduced deposition due to intracellular retention.⁶⁶ The remainder of type III mutations result in stable fibrillin-1 monomers that are capable of forming microfibrils but are either non-functional or have an abnormal function.⁶⁹

A large proportion of *FBNI* mutations result in abnormal fibrillin-1 monomers that interfere with the assembly of normal monomers. Such mutations fall into either group II or IV and are referred to as dominant negative.⁶⁹ Type II mutations result in a reduction of both fibrillin-1 synthesis and deposition and have been associated with frameshift, nonsense, splicing and missense mutations.^{61,69,170} Type IV mutations are most commonly missense, deletion and splicing mutations that do not affect the reading frame resulting in stable but abnormal monomers.^{25,69,182}

The mechanism behind group V mutations, which do not affect fibrillin-1 synthesis or deposition, is not fully understood. However, we theorise that such mutations may be loss-of-function. That is the mutation-associated fibrillin-1 monomers can be synthesised and assembled into microfibrils, but these microfibrils are non-functional or unable to interact with microfibril-associated proteins.

4.1.3 Aims and rationale

Due to the many characteristics described above; clinical and molecular diagnosis, symptom management, and therapy development for the type-1 fibrillinopathies has been difficult and slowly evolving. We hypothesise that personalised medicines utilising antisense oligonucleotides (AO) designed to target particular sets of mutations may be the most appropriate therapeutic approach to reduce the severity of *FBNI* mutations. We propose the use of AOs, as they present a highly customisable and specific platform capable of intervening in the splicing process to achieve the desired exon exclusion or inclusion. Previously, we demonstrated proof-of-concept, showing that exon 52 could be efficiently removed from the *FBNI* mRNA and that when removed, from 90% of transcripts, the encoded proteins could form the characteristic fibrillin-1 fibrils. Here, we extend this proof-of-concept to patient cell models as well as an additional *FBNI* exon.

Of the four patient cell lines used in this study, two are reported to harbour mutations affecting exon 52. Exon 52 is one of the smallest exons in *FBNI*; with only 66 bases and is associated with over 20 disease-causing mutations. The majority of mutations in exon 52 either directly affect the canonical splice sites or alter splicing indirectly, resulting in the in-frame removal of exon 52

during the splicing process. Since exon 52 can be removed without disrupting the reading frame and the majority of mutations in this exon are associated with exon exclusion, we proposed two hypotheses. Firstly, enhancing definition of the exon sufficiently to override the silencing effect of a mutation could result in the inclusion of exon 52 in affected transcripts, restoring all fibrillin-1 proteins to their healthy, functional form. Or as shown previously, the removal of exon 52 from all transcripts, encoded by both the healthy and disease-causing alleles, can result in the production of internally truncated but identical fibrillin-1 proteins from all transcripts allowing them to form functional microfibrils, thus reducing disease severity.

The remaining two patient cell lines harbour mutations affecting exon 59. Similar to exon 52, *FBNI* exon 59 is in-frame and linked to 22 unique disease-causing variants. Exon 59 is larger than exon 52 at 123 bases, and encodes one of the 43 calcium-binding epidermal growth factor (cbEGF)-like domains that make up the majority of the fibrillin-1 protein. We hypothesise that removal of an amenable but potentially dispensable exon from all transcripts will result in functional microfibrils regardless of the original mutation type. Therefore, we propose that all mutations affecting an exon can be overcome with the same AO, given that efficient exon skipping is induced.

We rationalise that the removal of an amenable mutation-associated exon will result in one of the following scenarios;

Missense mutations

- Exclusion of the exon from both affected and unaffected transcripts.
 - Removal of aberrant cysteines allowing for correct disulphide bond arrangement.
 - Restoration of fibrillin-1 monomer homogeneity.

Mutations resulting in exon skipping

- Exclusion of the exon from unaffected transcripts.
 - Restoration of fibrillin-1 monomer homogeneity.

OR

- Retention of the exon in the disease-causing transcript.
 - Restoration of healthy, functional fibrillin-1 monomers.

Nonsense and frameshift mutations

- Exclusion of the exon from both the disease-causing and healthy transcripts.
 - Removal of PTC and restoration of the reading frame.
 - Restoration of the C-terminal region allowing secretion from the cell.
 - Restoration of fibrillin-1 monomer homogeneity.

4.2 Confirming mutations in patient cells

A total of five cell lines were used in this chapter. The use of human cells for this research was approved by the Murdoch University Human Ethics Committee; approval numbers 2013_156 and 2017_101 and The University of Western Australia Human Research Ethics Committee; approval number RA4/1/2295. Healthy control fibroblasts were cultured from a dermal biopsy of a healthy volunteer taken after informed consent.

The following cell lines were obtained from the NIGMS Human Genetic Cell Repository at the Coriell Institute for Medical Research: GM21941, GM21952, GM21937 and GM21992. The mutation profile of each patient cell line was confirmed using Sanger sequencing (Figure 4.1.a). Mutation nomenclature was determined with respect to the *FBN1* gene Locus Reference Genomic sequence transcript 1 ([LRG_778t1](#)) in which the start codon is in the second of 66 exons.

The GM21941 cell line, hereafter referred to as MFS^{Δ52}, was reported to be heterozygous for the synonymous change, c.6354C>T that changes codon 2118 from AUC to AUU, both of which encode isoleucine. However, Liu et al.¹⁵¹ also identified that this mutation results in skipping of exon 52 that is in-frame. It was later noted that this mutation results in reduction of fibrillin-1 synthesis (41%) and a severe reduction in fibrillin-1 deposition (5%) compared to that in healthy controls, placing the mutation into group II.^{69,170} Both the c.6354C>T mutation and the resulting exon 52 skipping; r.6314_6379del, were confirmed using Sanger sequencing (Figure 4.1.a). *In silico* analysis of the healthy and mutation-harboring sequences using the web tools spliceAid¹⁵³ and SpliceAid2¹⁵⁴ revealed that the c.6354C>T mutation alters the balance of predicted splicing enhancer (ESE) and silencer (ESS) elements within exon 52. The mutation disrupts six predicted ESE sites ranging in strength from two to ten whilst also forming three predicted ESS sites (Figure 4.1.b).

The GM21952 (MFS^{C2111R}) patient cell line was reported to carry a missense mutation, c.6331T>C, predicted to result in p.Cys2111Arg, disrupting one of the highly conserved cysteine residues of the sixth TGF-β binding protein-like (TB) domain. This mutation was confirmed by sequencing both the gDNA and cDNA (Figure 4.1.a).

The GM21992 (MFS^{R2414*}) cell line was reported to harbour a c.7240C>T mutation that resulted in the creation of a PTC, p.Arg2414*.⁶¹ This mutation was confirmed by gDNA sequencing (Figure 4.1.a). However, the mutant transcript was undetectable by cDNA sequencing (Figure 4.1.a), suggesting the mutant transcripts are subjected to very efficient nonsense-mediated decay (NMD). This is supported by the findings of Schrijver et al.⁶¹ who categorised this mutation as group II, reporting reduced fibrillin-1 synthesis (41%) and deposition (21%) in patient cells compared to those from a healthy control subject.

Finally, the GM21937 (MFS^{Δ59}) cell line were confirmed to carry the splice site mutation, c.7205-2A>G, reported by Liu et al.¹⁸³ (Figure 4.1.a) This mutation alters the conserved AG canonical acceptor splice site of exon 59 to GG and is confirmed to result in skipping of exon 59 that is in-frame, generating the r.7205_7330del transcript (Figure 4.1.a). Liu et al.¹⁸³ reported that this mutation results in a mild reduction of fibrillin-1 synthesis, yielding 92% of the protein present in the control, however, fibrillin-1 deposition is severely reduced to only 14%, making this a group IV mutation.

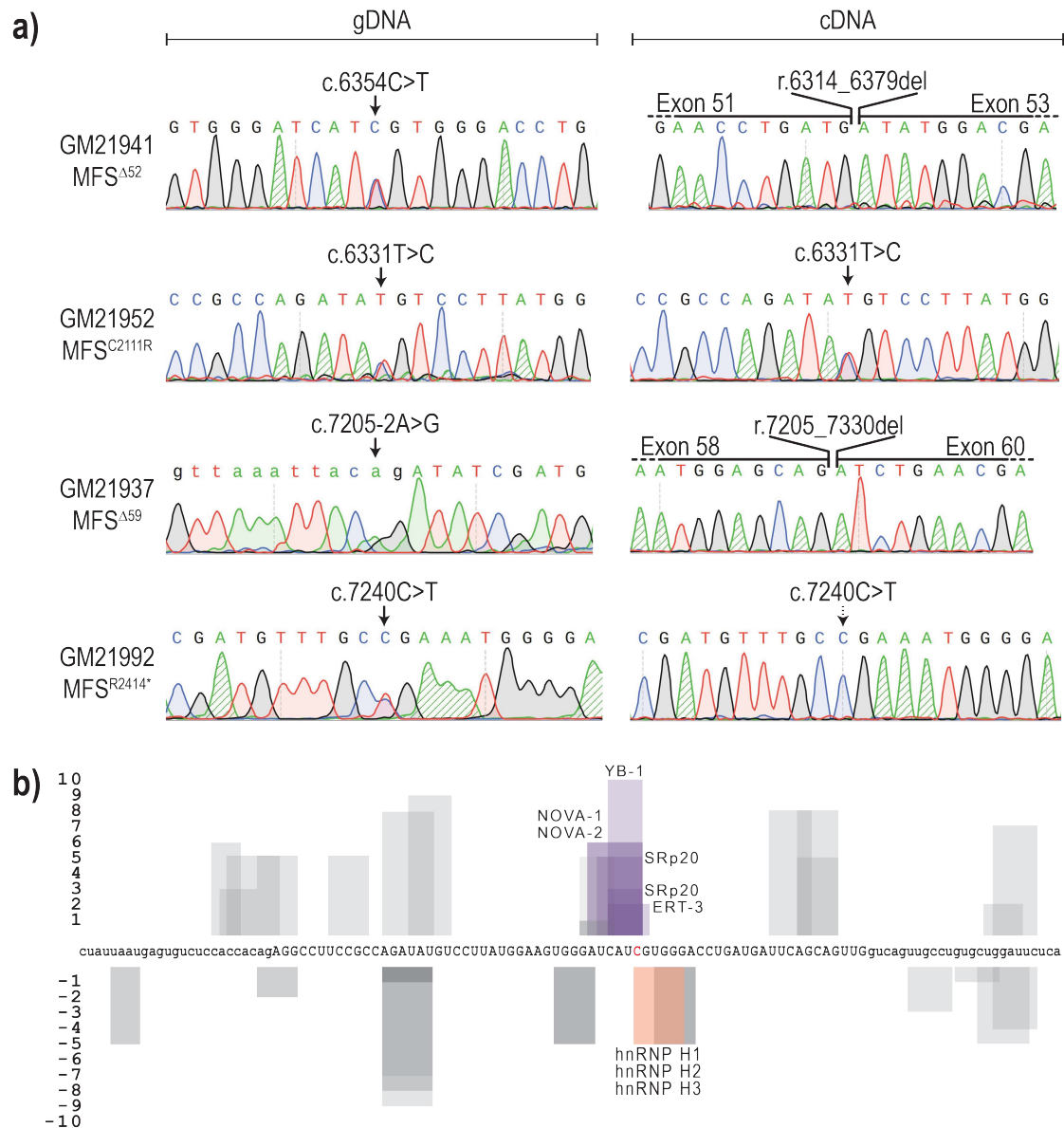


Figure 4.1 Confirmation of patient cell line mutations

a) The reported disease-causing mutation for each patient cell line was confirmed via Sanger sequencing using gDNA, or cDNA derived from fibroblast RNA, as a template. b) *In silico* analysis of *FBN1* exon 52 ESE and ESS sequences showing those that differ between the wild-type (purple) and MFS^{Δ52} mutation (orange) sequence. Those in grey are shared between the two sequences. ESE and ESS sites predicted by, and diagram adapted from spliceAid¹⁵³ and SpliceAid 2.¹⁵⁴

4.3 AO design and synthesis

The first generation of 2'OMe-PS AO sequences designed to induce exon 52 exclusion or promote exon 52 inclusion were designed by Mr Kane Greer (unpublished, 2017; Table 4.2). Several AO sequences were similarly designed by the author to induce exon 59 skipping, targeting both splicing regulatory motifs at the exon-intron junctions as well as additional regulatory sequences within the body of the exon. Sequences designed to mediate exon exclusion AOs were targeted to exon splice enhancers while exon inclusion were targeted toward intronic splice silencers predicted using both SpliceAid¹⁵³ and SpliceAid 2¹⁵⁴. Two sequences unrelated to *FBN1*, one for each chemistry, were used as sham treatments. These controls allow for the observation of any sequence-independent chemistry-related effects. The AOs used in this chapter are listed in Table 4.2.

Table 4.2: Antisense oligonucleotide sequences used in this study

The name, ID, sequence and chemistry of AOs designed to target *FBN1* exons 52 and 59. Two control sequences were also used to reveal any chemistry-related effects. AO nomenclature described in Chapter 2, Figure 2.1. The AOs targeting exon 52 were designed by Mr Kane Greer (Unpublished, 2017).

AO name (FBN1 H...)	ID	Sequence (5'-3')	Chemistry
Exon 52 exclusion			
52A(+29+53) ^M	AO52.1 ^m	AUC AGG UCC CAC AAU GAU CCC ACU U	2'OMe-PS
52A(+29+53) ^N	AO52.1 ⁿ , Pos	AUC AGG UCC CAC GAU GAU CCC ACU U	2'OMe-PS
52A(+29+53) ^N	PMO52	ATC AGG TCC CAC GAT GAT CCC ACT T	PMO
52A(-08+17)	AO52.2	UAU CUG GCG GAA GGC CUC UGU GGU G	2'OMe-PS
52D(+13-12)	AO52.3	CAG GCA ACU GAC CAA CUG CUG AAU C	2'OMe-PS
52A(-23+02)	AO52.4	CUC UGU GGU GGA GAC ACU CAU UAA U	2'OMe-PS
52A(+03+27)	AO52.5	CAU AAG GAC AUA UCU GGC GGA AGG C	2'OMe-PS
Exon 52 inclusion			
52A(-181-157)	AOi51.1	CCC UAA GAU GUU GUG UCU ACU CCU U	2'OMe-PS
52A(-130-106)	AOi51.2	AAU GAU GGA AAA AAC AAG CCC AGA A	2'OMe-PS
52A(-44-20)	AOi51.3	UAA UAG AUA GAA CAA UAG CAA UUC A	2'OMe-PS
52D(-01-25)	AOi52.1	UGA GAA UCC AGC ACA GGC AAC UGA C	2'OMe-PS
52D(-46-74)	AOi52.2	AAA AUA AGA AUA ACU AGA GAA GAA GCA GA	2'OMe-PS
52D(-98-122)	AOi52.3	AAU GAA GGG ACA AAA AAG UAG CAC U	2'OMe-PS
Exon 59 Exclusion			
59A(-21+04)	AO59.1	AUA UCU GUA AUU UAA CAA AUA UAA A	2'OMe-PS
59A(+41+65)	AO59.2	UCC UCU GUC AUU GAC ACA UUC CCC A	2'OMe-PS
59A(+41+65)	PMO59	TCC TCT GTC ATT GAC ACA TTC CCC A	PMO
59A(+86+110)	AO59.3	AGU UAU AUC UGG AGU GUA CCC AGU U	2'OMe-PS
59A(+36+60)	AO59.2+5	UGU CAU UGA CAC AUU CCC CAU UUC G	2'OMe-PS
59A(+46+70)	AO59.2-5	UAU GAU CCU CUG UCA UUG ACA CAU U	2'OMe-PS
Controls			
Unrelated control	Ctrl	GGA UGU CCU GAG UCU AGA CCC UCC G	2'OMe-PS
GeneTools control	GTC	CCT CTT ACC TCA GTT ACA ATT TAT A	PMO

4.4 AO-mediated selection of *FBN1* exon 52

4.4.1 Assessment of AO-mediated inclusion of exon 52

A total of six 2'OMe-PS AOs were designed to promote exon 52 inclusion, targeting silencer sequences within flanking introns 51 and 52 (Figure 4.2.a). These AOs were transfected into the MFS^{Δ52} patient cell line. Three concentrations; 200 nM, 100 nM and 50 nM were tested, and transfected cells incubated at 37 °C for 24 hours. The proportion of full-length (FL) *FBN1* transcripts is noted below each gel lane in Figure 4.2. None of the six AOs induced clear exon inclusion, and no dose-response was evident, with each sample showing full-length product within 5% of the baseline of 57% in the untreated control. The positive control, AO52.1ⁿ, was previously determined to be the most efficient of the exon skipping AOs tested. When MFS^{Δ52} cells are treated with this positive control, Δ52 transcripts make up over 70% of total transcripts, indicating that the transfection efficiency is not compromised (Figure 4.2.b).

In an attempt to increase the efficiency of AO-mediated inclusion, each compound was tested in combination with another non-overlapping AO in a cocktail. Each AO was added to the cocktail in equimolar amounts, with total cocktail concentrations of 200 nM and 50 nM tested. Evaluation of the two-AO combinations did not reveal any synergistic effect, and no increase in exon 52 inclusion was evident (Figure 4.2.c).

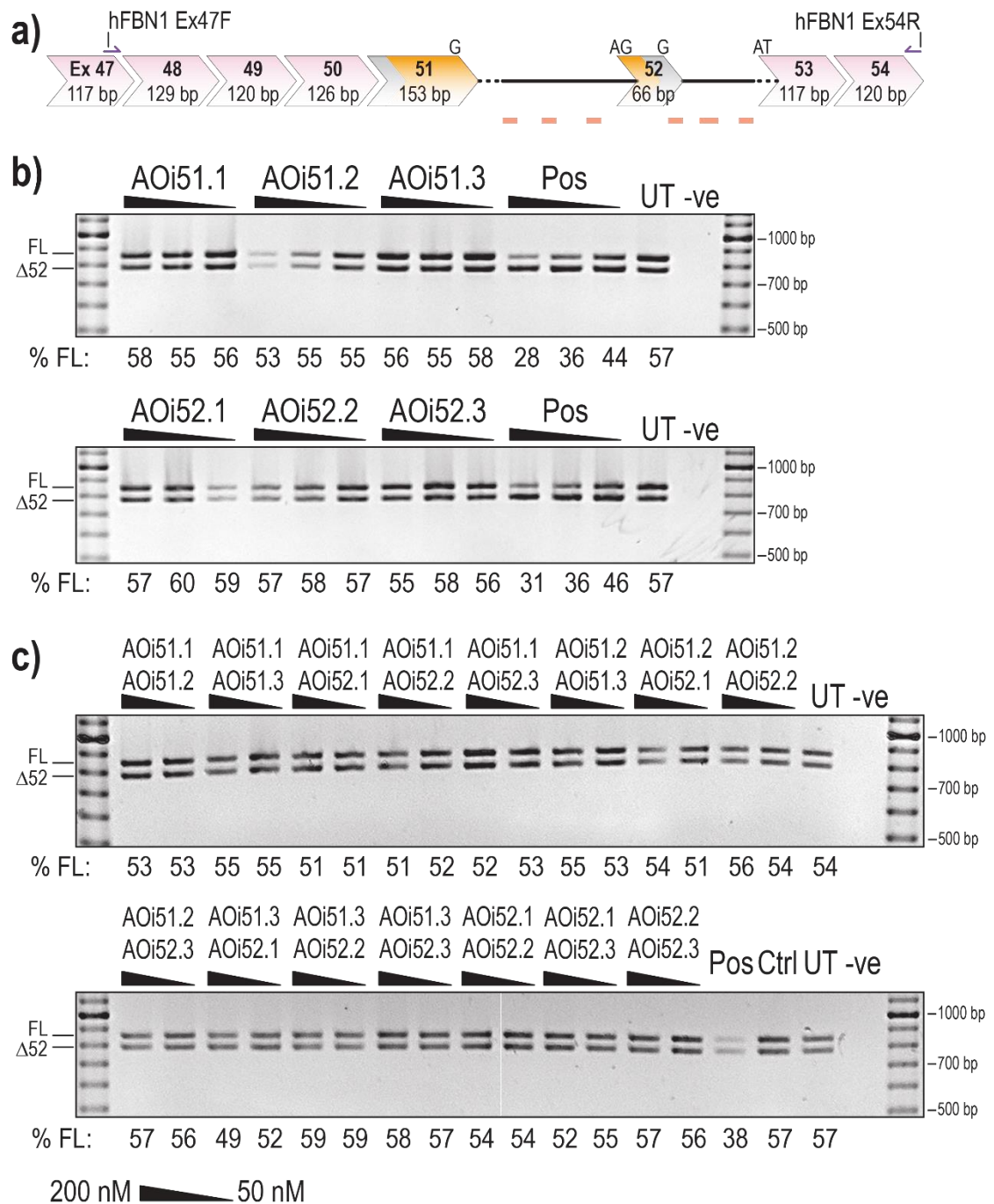


Figure 4.2: Evaluation of AO sequences designed to induce exon 52 inclusion

a) The region of *FBN1* between exons 47 and 54 and the location of the 2'OMe-PS AOs (Orange bars) are shown. RT-PCR amplicons from *MFS^{Δ52}* fibroblasts transfected with b) individual 2'OMe-PS AOs (200, 100 and 50 nM) and c) cocktails of two 2'OMe-PS AOs (200 and 50 nM). The proportion of full-length transcripts are noted under each gel lane. The optimal exon exclusion AO AO52-1ⁿ was used as a positive control (Pos) to assess transfection efficiency. Screening of 2'OMe-PS AOs targeting exon 52. Healthy control fibroblasts were transfected with AOs as lipoplexes at three concentrations, 200, 100 and 50 nM. Ctrl: an unrelated sequence used as a sham treatment, UT: untreated control, -ve: RT-PCR negative control. 100bp molecular marker used for size reference.

4.4.2 Assessment of AO-mediated exclusion of exon 52 in patient fibroblasts

The AOs designed to induce exon 52 exclusion described in the previous chapter were transfected into healthy control fibroblasts, as well as into the two MFS patient cell lines harbouring exon 52 mutations. In-line with the results of chapter 3, AO52.1ⁿ induced the most efficient exon 52 skipping in healthy control fibroblasts (Figure 4.3.a). Similarly, AO52.1ⁿ was the most efficient AO in the MFS^{C211R} cells inducing up to 49% exon 52 skipping (Figure 4.3.c). While not as effective in MFS^{Δ52} cells, that already have approximately 46% skipping, as a result of the synonymous mutation, AO52.1ⁿ remains the most efficient of the AOs tested, increasing Δ52 transcripts to ~58% (Figure 4.3.b).

In each cell line, AO52.3 was also a relatively effective candidate, albeit to a lesser extent than AO52.1ⁿ, with 30%, 53% and 41% exon 52 skipping at the highest concentration tested in healthy control, MFS^{Δ52} and MFS^{C211R} cell lines, respectively (Figure 4.3). The AO52.1^m sequence differs from AO52.1ⁿ by one base, with AO52.1^m complimentary to the c.6354C>T mutation sequence of MFS^{Δ52} cells. This AO was designed in the hope of taking advantage of the effect that the silent mutation has on exon selection, increasing the AO efficiency. However, AO52.1^m is less efficient than AO52.1ⁿ in the two cell lines tested; 22% exon skipping induced in the healthy control and 49% in the MFS^{Δ52} cells (Figure 4.3.a and b).

Cocktails of AOs were previously identified as either ineffective or antagonistic; therefore, the majority of cocktails were not re-tested. However, two cocktails were tested in MFS^{C211R} cells to identify any synergism derived from the use of the two most efficient AOs, AO52.1ⁿ and AO52.3, and AO52.5, which is ineffective, inducing no skipping. However, in both cases, AO52.5 negatively impacts on exon 52 skipping, resulting in lesser skipping than with AO52.1ⁿ and AO52.3 alone (Figure 4.3.c).

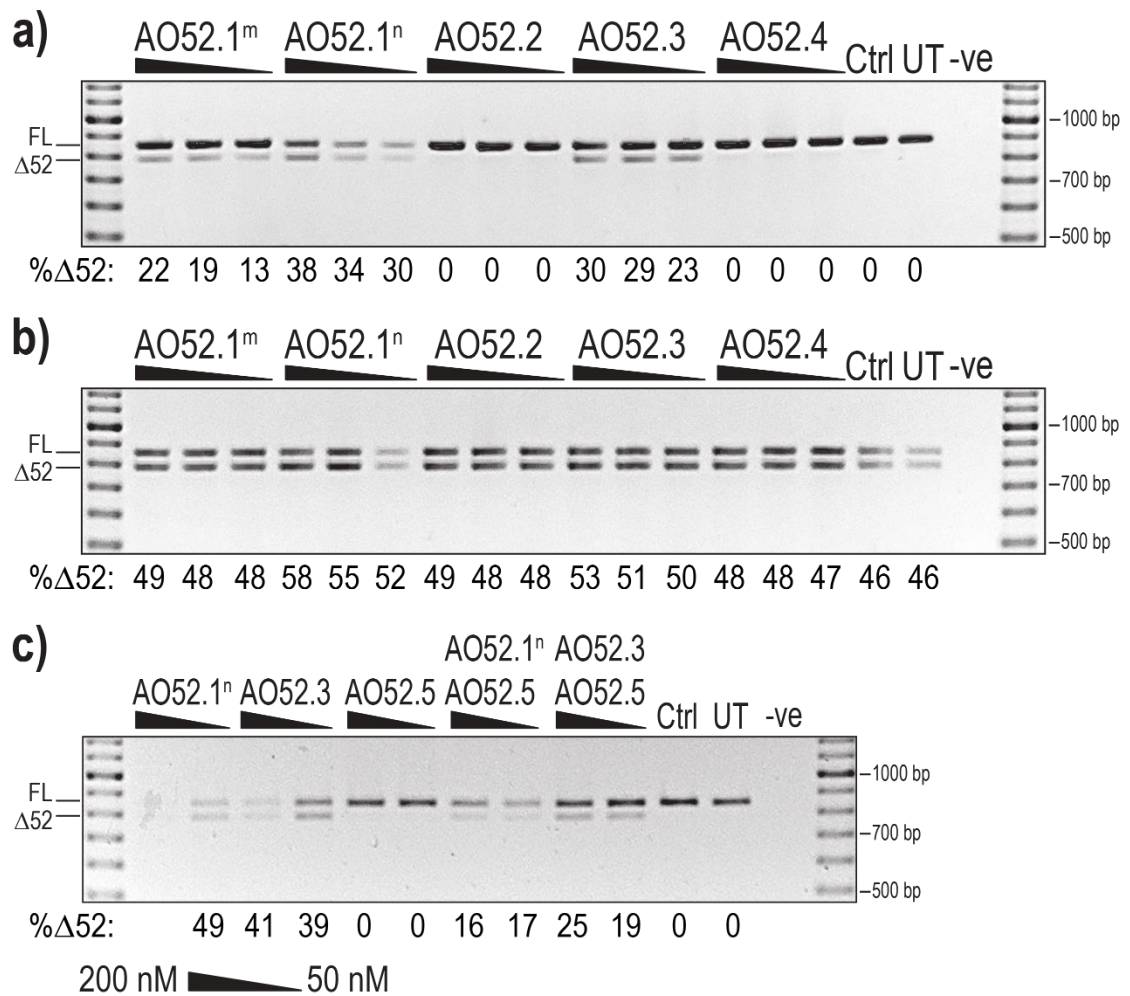


Figure 4.3: Evaluation of AOs designed to induce skipping of *FBN1* exon 52

RT-PCR amplicons generated from a) healthy control b) *MFS*^{Δ52} and c) *MFS*^{C2111R} fibroblasts transfected with 2'OMe-PS AOs at three (a, b); 200, 100, 50 nM or two (c); 200 and 50 nM, concentrations. The values below each gel image indicate the percentage of exon 52 skipped ($\Delta 52$) transcripts in each sample. Ctrl: an unrelated sequence used as a sham treatment, UT: untreated control, -ve: RT-PCR negative control. 100bp molecular marker used for size reference.

4.4.3 Optimisation of post-transfection incubation period.

To identify the optimal time point for assessing exon skipping efficiency, PMO52, the PMO version of the AO52.1ⁿ sequence, was nucleofected into healthy control fibroblasts that were then collected at multiple time points; 24, 48 and 72 hours as well as four and ten days after transfection. The efficiency of exon 52 skipping increased at every timepoint until four days post-transfection (Figure 4.4.a). Between four- and ten-days after transfection, cell health began to deteriorate, and treated cells began to die. The result of which was the regrowth of cells and a corresponding decrease in the skipping efficiency for both cell lines (Figure 4.4.a).

Previously, PMO52 resulted in the formation of fibrillin-1 fibres in healthy control cells when more than 90% skipping was induced; however, fibre abundance was reduced. The duration of incubation after transfection was proposed as a possible contributing factor. Therefore, the optimal length of time for fibrillin-1 fibres to form was also assessed using untreated healthy

control fibroblasts to define a baseline. Fibrillin-1 staining revealed fibre formation as early as 24 h; however, fibres at this time point were fragmented and in low abundance (Figure 4.4.b.i). After four days, long thin fibres were observed with a more continuous morphology and higher abundance, covering the majority of the coverslip in a uniform layer (Figure 4.4.b.ii). The intensity, length and abundance of fibres continued to increase at each, 7- 10- and 14-day, timepoint (Figure 4.4.b.iii-v). Taking both exon skipping efficiency and fibre formation dynamics into account, two timepoints; four- and ten-days, were used for remaining studies.

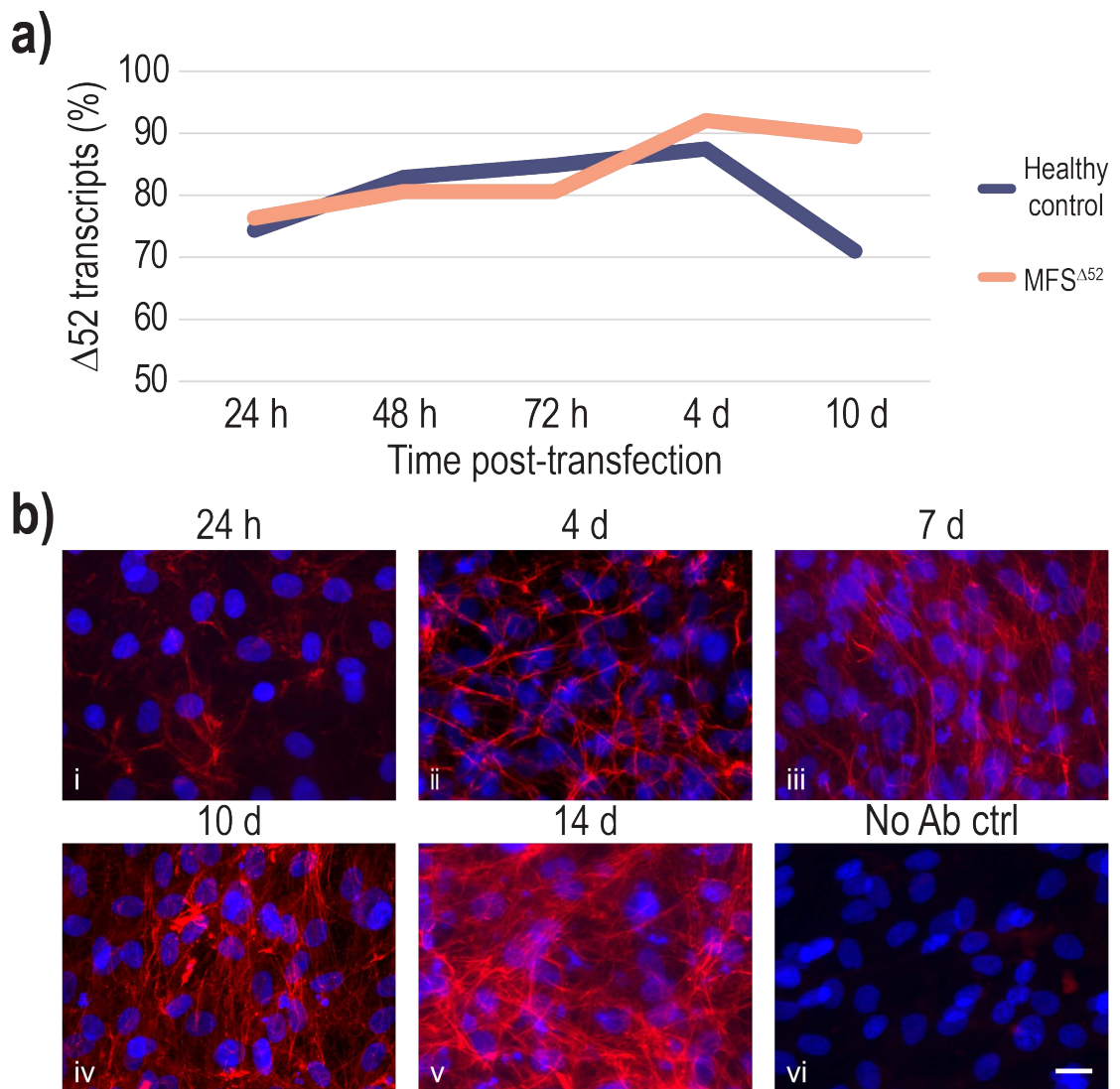


Figure 4.4: Exon 52 skipping efficiency and fibrillin-1 fibre formation post-transfection.

a) PMO52-mediated skipping induced at 250 μ M, calculated in a 20 μ l cuvette, in healthy control and MFS^{Δ52} fibroblasts; 24, 48 and 72 hours as well as 4 and 10 days after transfection. b) Immunofluorescent staining of fibrillin-1 (red) in healthy control fibroblasts after 24 hours, then 4, 7, 10 and 14 days. Counterstained with Hoechst (blue) for nuclei detection. No primary antibody control (No Ab ctrl) used to observe non-specific binding of the secondary and autofluorescence. Scale bar = 20 μ m

4.4.4 Evaluation of PMO52-mediated exon skipping and fibrillin-1 morphology

To assess PMO52-mediated exon 52 skipping and consequences on fibrillin-1 protein the AO was nucleofected into both MFS^{Δ52} and MFS^{C2111R} patient cell lines and healthy control fibroblasts. Two concentrations, 250 μM and 50 μM; calculated in the Nucleofection cuvette containing 300,000 cells in 20 μl of transfection reagent, were tested, and cells were incubated for four or ten days. After four days, Δ52 transcripts averaged 85%, 97% and 85% of total transcripts in healthy control, MFS^{Δ52} and MFS^{C2111R} fibroblasts, respectively (Figure 4.5). An apparent decrease in the average skipping efficiency, at a transfection concentration of 250 μM, was observed after incubation for ten days. Healthy control and MFS^{C2111R} fibroblasts, in particular, were the most affected by the longer incubation period with skipping efficiency reduced to 72% and 67%, respectively. However, a decrease in skipping efficiency from 97% to 91% was also observed in MFS^{Δ52} cells (Figure 4.5). We also noted variable cell death between experiments (data not shown) and a corresponding increase in the variability of skipping efficiency between biological replicates after ten days in comparison to four days (Figure 4.5).

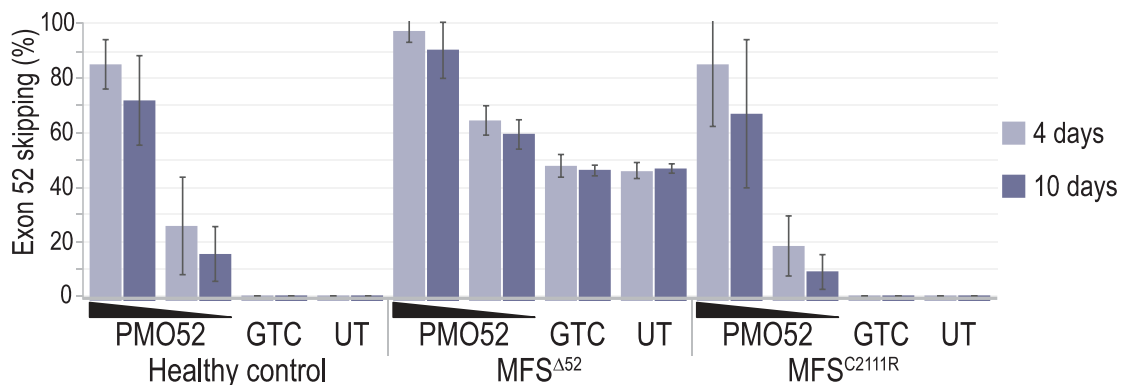


Figure 4.5: AO-mediated *FBN1* exon 52 skipping across three replicates.

Densitometric analysis of exon 52 skipping in fibroblasts from the healthy control, MFS^{Δ52} and MFS^{C2111R} patients after treatment with PMO52 at two concentrations; 250 μM and 50 μM, calculated in the 20 μl nucleofection cuvette volume, and collected after incubation for 4 or 10 days. Means plus error bars. Error bars = standard deviation, n = 3. GTC: Gene Tools control PMO used as a sham treatment, UT: untreated control.

Results of one of these replicate exon skipping experiments are shown in Figure 4.6; this replicate saw particularly efficient skipping in all three cell lines. Previously, the average skipping efficiency, over the three replicates, in both healthy control and MFS^{C2111R} cells was poorer than that observed in the MFS^{Δ52} cells that show a baseline skipping of approximately 50% (Figure 4.5). However, in this replicate, after treatment with 250 μM of PMO52, Δ52 transcripts made up 92% of total transcript product in both MFS^{Δ52} and healthy control fibroblasts, and 95% of transcripts in MFS^{C2111R} cells (Figure 4.6).

After transfection, cells were stained with an anti-fibrillin-1 antibody to identify the fibrillin-1 fibres. Immunofluorescent staining revealed the expected long thin fibres that form a lattice in

the untreated and GTC treated healthy control samples (Figure 4.6.b.xi, xii). These fibres were abundant, covering the majority of the field-of-view at any given location on the coverslip. In contrast, no fibrillin-1 fibres were observed in the untreated and GTC treated samples from either patient, with minimal fibrillin-1 staining in these samples overall (Figure 4.6.b.iii, iv, vii, viii).

The PMO52-mediated exon 52 skipping was dose dependant, with poorer skipping efficiency after transfection at a lower concentration. After treatment with 50 μM , $\Delta 52$ transcripts constituted 64%, 23% and 41% of the total transcript products from MFS $\Delta 52$, MFS $\text{C}^{2111\text{R}}$ and healthy control fibroblasts, respectively (Figure 4.6.a). Not surprisingly, the presence of both FL and $\Delta 52$ transcripts correlate with reduced fibrillin-1 staining in all three cell lines (Figure 4.6.b.ii, vi, x). This staining mirrors that of the untreated patient samples with no fibres and minimal fibrillin-1 staining overall (Figure 4.6.b).

The higher PMO52 concentration of 250 μM induces more than 90% exon 52 skipping in all three cell lines. The corresponding immunofluorescent staining, however, reveals a different story for each cell line. In healthy control cells, 92% skipping is associated with fibrillin-1 fibre formation (Figure 4.6.b.ix), mirroring that seen previously. However, in comparison to the fibres formed in the untreated healthy control sample, the fibres formed by healthy control cells transfected with 250 μM of PMO52 are fragmented and less abundant (Figure 4.6.b.ix, xii)

In the samples of MFS $\text{C}^{2111\text{R}}$ cells treated with 250 μM of PMO52, the corresponding immunostaining revealed an increase in fibrillin-1, compared to the untreated patient samples (Figure 4.6.b.v). However, minimal fibrillin-1 fibre formation is observed, and the staining instead appears to be sponge-like with no defined organisation. Sanger sequencing of the FL amplicons in the untreated, as well as 250 μM and 50 μM , treated MFS $\text{C}^{2111\text{R}}$ samples revealed no change in the ratio of healthy full-length (FL) and mutation-associated full-length (FL c.6331T>C) transcripts when exon 52 skipping was induced (Figure 4.6.c).

Encouragingly, in MFS $\Delta 52$ cells treated with the high concentration, fibrillin-1 fibres were present and have a continuous, non-frayed morphology comparable to those seen in the untreated healthy control cells (Figure 4.6.b.i). The fibres are also relatively abundant, filling the majority of the field-of-view; however, they are not as plentiful as those seen in the untreated healthy control, which form a multi-layer lattice (Figure 4.6.b.i, xii).

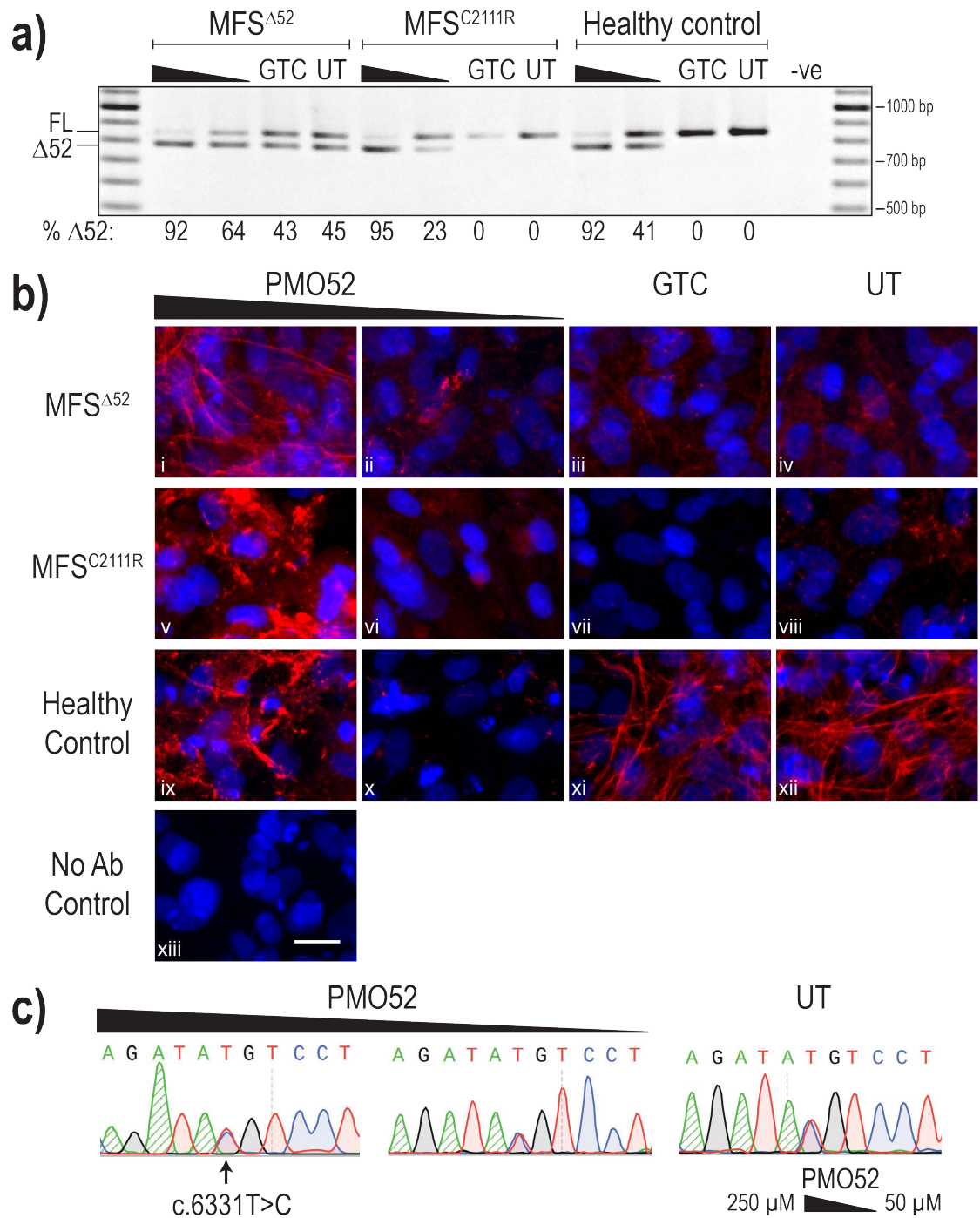


Figure 4.6: Evaluation of PMO52-mediated exon 52 skipping and fibrillin-1 morphology

Healthy control, MFS $\Delta 52$ and MFS^{C2111R} patient fibroblasts were transfected with PMO52, Gene Tools control PMO (GTC) or left untreated (UT). Two concentrations were tested; 250 μ M and 50 μ M, calculated in the 20 μ l nucleofection cuvette volume, and cells were collected after 4 days for a) RT-PCR analysis and b) Immunofluorescent staining. Cells were stained for Fibrillin-1 (red) and counterstained with Hoechst (blue) for nuclei detection. No Ab control: no primary antibody added. Scale bar = 20 μ m. The values below each gel image indicate the percentage of exon 52 skipped ($\Delta 52$) transcripts in each sample. -ve: RT-PCR negative control. 100bp molecular marker used for size reference. c) Sanger sequencing of the FL amplicons from MFS^{C2111R} cells showing the ratio of healthy full-length and full-length^{c.6331T>C} transcripts, with and without treatment. See Figure A2.1 for a larger version of part b.

4.5 Targeting Exon 59

4.5.1 Exon 59 exclusion screening and optimisation

In the same way that AOs targeting exon 52 were assessed, 2'OMe-PS AOs targeting exon 59 were screened in healthy control fibroblasts. Initial screening was performed using three AO sequences designed to target the exon 59 acceptor splice site as well as ESE sites predicted using the *in silico* tool spliceAid^{153,154} (Figure 4.7.c). Exon skipping efficiencies were determined by amplification of *FBNI* transcripts between exon 56 (forward) and exon 62 (reverse primers) (Figure 4.7.b). Additional sequences were then designed up-stream and down-stream of the most efficient AO target site identified in the first screen (Figure 4.7.c).

The original three AOs were transfected at two concentrations; 200 nM, and 50 nM into healthy control fibroblasts that were harvested 24 hours later for RNA extraction and RT-PCR to assess exon skipping. One of the three AOs, AO59.2, induced exon 59 skipping in a dose-independent manner; with 32% and 33% Δ 59 transcript products induced at 200 nM and 50 nM, respectively (Figure 4.8.a). The remaining two AOs did not induce measurable exon skipping. Sanger sequencing of the upper (FL) and lower (Δ 59) transcript products confirmed that they differ only by the loss of exon 59 in the Δ 59 transcript product (Figure 4.8.d and e).

An unrelated control AO sample (Ctrl) was included in all transfections as a sham treatment to reveal any chemistry-related effects on the growth and health of treated cells. However, an additional control, using the transfection reagent Lipofectamine 3000 (L3K) without any AO was also performed to reveal any changes in cell health as a result of the transfection process. Neither control induced any exon skipping, however, both controls caused a minor decrease in total RNA concentration compared to the untreated cells.

Two additional AO sequences were designed by micro-walking around the AO59.2 target site. This involved shifting the sequence five bases upstream (-5) or downstream (+5) from the original target while maintaining the 25-mer length. Neither of the micro-walked sequences was more efficient than the original AO59.2, both inducing less than 20% skipping of exon 59 (Figure 4.8.b).

Cocktails of two AOs together were also tested to identify any synergistic effects; however, while increasing efficiency marginally, this effect is additive at most and not sufficient to warrant the use of two AOs. Several cocktails, notably AO59.1 combined with AO59.2, resulted in substantial cell death, especially at a higher concentration (Figure 4.8.b).

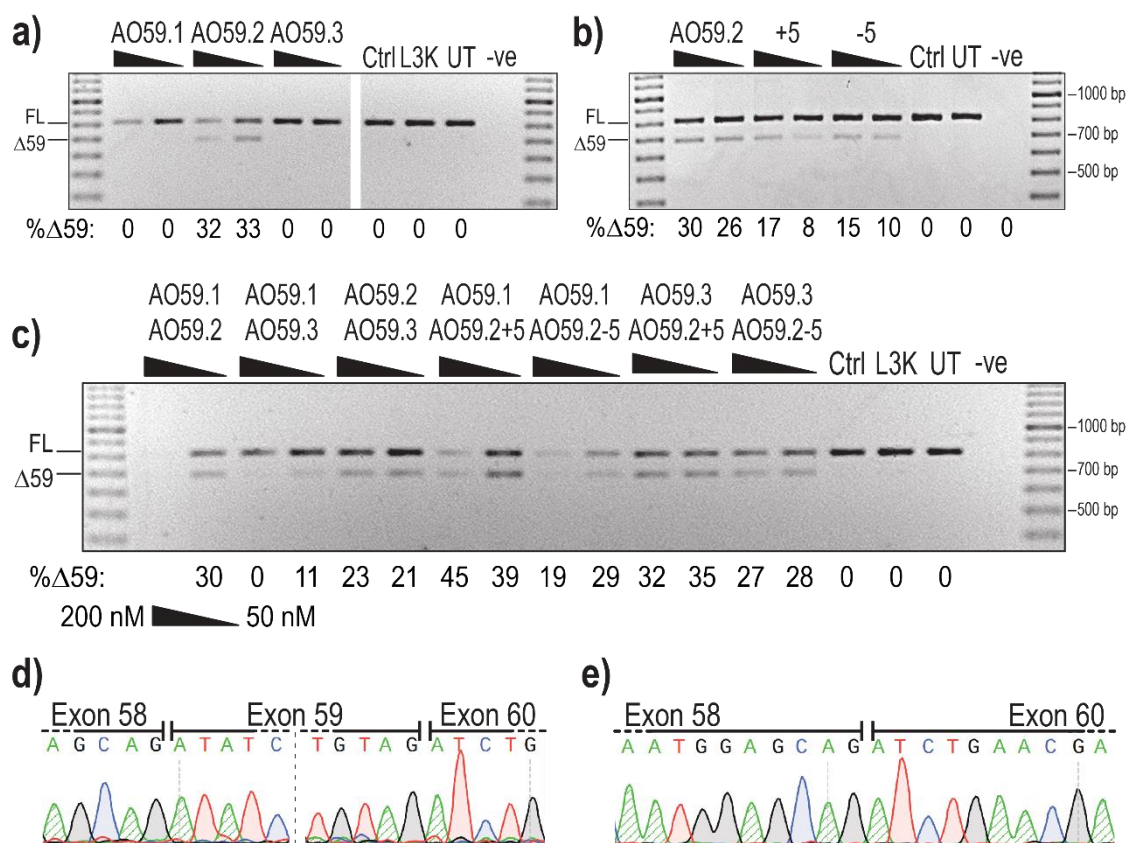


Figure 4.8: Evaluation of AO sequences targeting exon 59

Healthy control cells were transfected with a) individual AOs, b) micro-walked AOs or c) AO cocktails at 200 nM and 50 nM total AO concentrations. The values below each gel image indicate the percentage of exon 59 skipped ($\Delta 59$) transcripts in each sample. Ctrl: an unrelated sequence used as a sham treatment, L3K: transfection control with Lipofectamine 3000 reagent and no AO, UT: untreated control, -ve: RT-PCR negative control. 100bp molecular marker used for size reference. Sanger sequencing of the d) FL and e) $\Delta 59$ amplicons showing the exon junctions.

4.5.2 The effect of exon 59 skipping on fibrillin-1 morphology

The most promising 2'OMe-PS candidate sequence, AO59.2, was synthesised as a PMO, PMO59. The efficiency of PMO59 was assessed in healthy control and both $MFS^{\Delta 59}$ MFS^{R2424*} patient fibroblasts. Transfected cells were incubated for four and ten days then collected for RNA analysis and immunofluorescent staining with a fibrillin-1 specific antibody. Representative results from two independent replicates are presented in Figure 4.9.

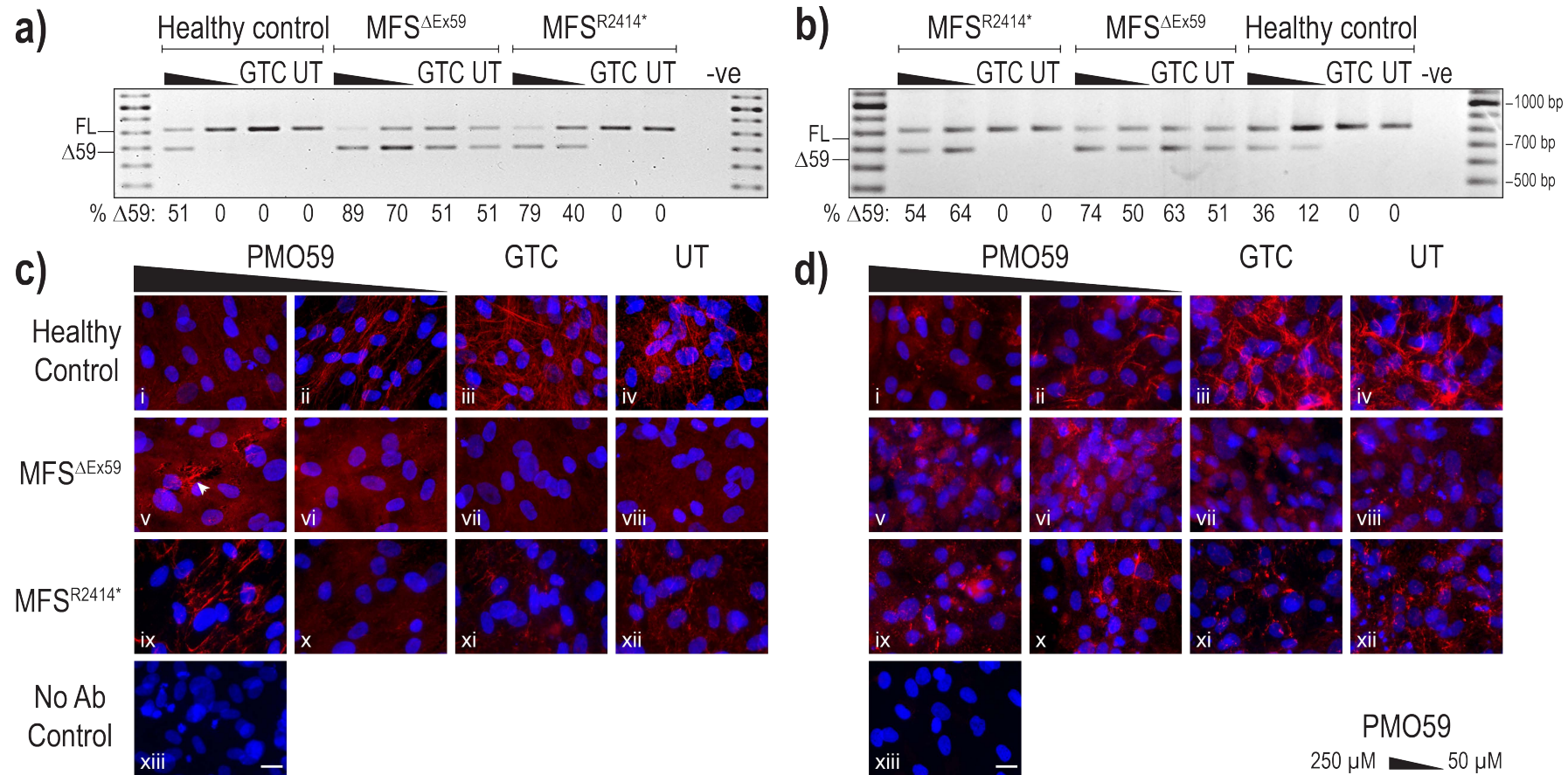


Figure 4.9: Evaluation of PMO59-mediated exon 59 skipping and fibrillin-1 morphology.

Healthy control, MFS Δ 59 and MFS^{R2414*} fibroblasts were nucleofected with PMO59 at 250 μ M, and 50 μ M; calculated in the 20 μ l nucleofection cuvette volume, in two replicate experiments. Total RNA was collected a) 10 days and b) 4 days after transfection to assess exon 59 skipping efficiency. The values below each gel image indicate the percentage of exon 59 skipped (Δ 59) transcripts in each sample. GTC: Gene Tools control PMO used as a sham treatment, UT: untreated control, -ve: RT-PCR negative control. 100bp molecular marker used for size reference. c) and d) show representative immunofluorescent images for replicates one and two after 10 and 4 days respectively. Transfected cells were stained for fibrillin-1 (red) and counterstained with Hoechst (blue) for detection of the nuclei. No Ab control: no primary antibody added, to control for non-specific binding of the secondary antibody. Scale bar = 20 μ m. See Figure A2.2 and Figure A2.3 for larger versions of part c and d respectively.

In the first replicate, the higher concentration of PMO59 induced relatively efficient exon 59 skipping in both MFS^{Δ59} (89%), and MFS^{R2414*} (79%) fibroblasts after ten days incubation (Figure 4.9.a). In contrast, PMO59 was less efficient in healthy control cells in which only 50% skipping was induced (Figure 4.9.a). In the second replicate, however, a high level of cell death, up to 30%, was evident in all samples, including the untreated cells (data not shown). Cell death led to the expansion of the remaining cells over the four- and ten-day incubation periods, diluting the effects of PMO59. The skipping efficiency was reduced in all three cell lines; 74% for MFS^{Δ59}, 64% for MFS^{R2414*} and 36% for healthy control fibroblasts at the highest concentration tested after four days (Figure 4.9.b). After the full 10-day incubation period, skipping efficiency had decreased further to 50%, 37% and 16% for MFS^{Δ59}, MFS^{R2414*} and healthy control fibroblasts, respectively (data not shown)

The difference in skipping efficiency between the two replicates was reflected in the corresponding fibrillin-1 immunofluorescent staining. In both replicates, untreated and GTC treated healthy control fibroblast samples present with abundant fibrillin-1 fibres throughout the coverslips (Figure 4.9.c.iii, iv and d.iii, iv). Similarly, the low concentration of PMO59 had little to no effect on fibre formation in the first replicate in which no skipping was induced (Figure 4.9.c.ii). However, yielding 12% skipping in replicate two correlated with a decrease in fibre abundance (Figure 4.9.d.ii).

In both replicates, untreated and GTC treated MFS^{R2414*} fibroblasts presented with thin fibres that, while covering approximately half of the coverslip, showed low staining intensity and were fragmented (Figure 4.9.c.xi, xii and d.xi, xii). In the first replicate, these fibres were entirely lost when the cells were treated with 50 μM of PMO59 that induced 40% skipping (Figure 4.9.c.x). Increasing the concentration of PMO59 to 250 μM resulted in 79% skipping and the formation of fibrillin-1 fibres (Figure 4.9.a and c.ix). The fibrillin-1 staining was robust with long thin fibres; however, as seen previously, the abundance of fibres is reduced in comparison to the untreated healthy control. The reduced skipping efficiency in replicate two correlated with no change in staining pattern, compared to the untreated samples (Figure 4.9.d.ix)

In the first replicate, untreated and GTC treated MFS^{Δ59} cells had minimal fibrillin-1 staining (Figure 4.9.c.vi, vii). In the second replicate, however, more cells remained on the coverslip, with an increase in fibrillin-1 staining. This staining was diffuse and likely intracellular, most often surrounding the nucleus (Figure 4.9.d.vi, vii).

The proportion of Δ59 transcripts induced in MFS^{Δ59} cells, which have 50% endogenous exon 59 skipping, was greater for every treatment group in both replicates than either MFS^{R2414*} or healthy control fibroblasts (Figure 4.9.a and b). In both replicates, treatment with either concentration of PMO59 increased the abundance of fibrillin-1 staining. However, this staining was sponge-like rather than fibre-like in morphology (Figure 4.9.c.v, vi and d.v, vi). Fibres were

infrequently observed in the 250 μ M treated cells in the first replicate; however, the fibres were frayed, fragmented and at very low abundance, an example of this staining is highlighted with a white arrow in Figure 4.9.c.v.

4.6 Discussion

We have previously shown proof-of-concept that an AO sequence can efficiently mediate skipping of *FBNI* exon 52, the result of which is the generation of apparently functional fibrillin-1 ^{Δ 52} fibres in healthy control cells. In this chapter, we aimed to extend this concept further, determining if; the same AO sequence is efficient in cell lines with different disease-causing mutations; different mutation types would respond in the same way and finally if the same concept of re-aligning fibrillin-1 monomers could be applied to exon 59.

Encouragingly the ‘most efficient’ AO targeting exon 52 showed consistent effects across the three cell lines tested, indicating that the AO sequence does not need to be customised for the different patients. Interestingly, this AO anneals across the synonymous mutation associated with exon skipping in the MFS ^{Δ 52} cell line.¹⁵¹ We determined that this mutation disrupts the balance of predicted silencer and enhancer sequences,¹⁵⁴ thus resulting in exon skipping. Identifying other silent or missense mutations that impact on splicing could help in designing AOs. The universal mutation database reports four synonymous mutations in amenable *FBNI* exons,³ all of which are predicted to alter the balance of ESE and ESS sequences (Figure A2.1).¹⁵⁴ AOs targeted to these regions could prove to be especially efficient.

While the sequence of the most effective AO for each cell line remained constant, the efficiency of exon skipping varied considerably between cell lines. This variability was particularly apparent when using the PMO chemistry and suggests that the required dose may need to be altered according to mutation type, with splicing mutations likely requiring a lower dose than missense mutations. That said, variability between experiments revealed that the PMO is capable of inducing efficient skipping in all three cell lines. The key implication is that the skipping efficiency needed to negate the dominant-negative effects of heterogeneous fibrillin-1 monomers is likely to be very high. Therefore, it is expected that a high PMO concentration will be required to ensure sufficient skipping regardless of the mutation type.

The effect of exon 52 skipping on fibrillin-1 fibres varied between mutation type. We note that skipping efficiency of more than 80% in MFS ^{Δ 52} cells results in the formation of fibrillin-1 fibres. However, the same skipping efficiency in the MFS^{C211R} cell line increases fibrillin-1 staining without restoring fibre formation. This poses two new questions, why are these fibrillin-1 monomers not forming fibres? And what fibrillin-1 abundance and morphology need to be induced for there to be a therapeutic effect? Addressing the former, we can speculate that the

presence of three different transcripts; *FBNI*, *FBNI*^{c.6331T>C} and *FBNI*^{Δ52} could affect either or both the synthesis and assembly of fibrillin-1^{Δ52} monomers. To possibly overcome this, after PMO treatment, the cells could be treated with an RNase-H-dependent AO targeted to exon 52. This would lead to degradation of both FL transcripts leaving only Δ52 monomers to form microfibrils without resulting in haploinsufficiency. Targeted transcript degradation has been reported several times with promising efficiency.¹¹³ The FDA approved drugs Vitravene¹⁴⁸ (discontinued) and Kynamro¹⁴⁹ are both examples of RNase-H-dependent AOs. However, both drugs have been associated with undesired side-effects^{148–150}; thus, any RNase-H AO targeting *FBNI* is more likely to be used as a research tool rather than a therapeutic one.

Antisense oligonucleotides targeted to exon 59 were, for the most part, relatively ineffective, although one sequence mediated relatively efficient exon 59 skipping. As a PMO this AO sequence exhibited variable efficiency not only between cell lines but between experiments. For the most part, this variability was associated with cell health rather than the efficiency of PMO itself; however, PMO59 was never as efficient as PMO52. Encouragingly, when sufficient skipping was induced in MFS^{R2414*} cells, the result was the formation of strong fibres, morphologically similar to untreated healthy controls. This provides proof that exon 59 is a potentially amenable target. However, the efficiency and reproducibility of PMO59 must be improved before the effects of exon 59 skipping can be fully assessed.

The variability in skipping efficiency between replicate one and two of the exon 59 skipping experiments illustrates the risk of inefficient skipping as this would most certainly lead to no benefit. As evidenced by the loss of the minimal endogenous fibres in MFS^{R2424*} cells, insufficient exon skipping could lead to a more severe phenotype than if left untreated. The major difference between these experiments was the level of cell death that ultimately resulted in cell proliferation, diluting the effects of the PMO. The safety of PMOs have been demonstrated in cells, mouse models and human clinical trials; PMOs themselves do not usually result in cell death or adverse effects. However, we have noticed that Nucleofection, the delivery method used here, is associated with some cell death, regardless of the AO sequence. Unfortunately, PMO delivery and efficiency both *in vitro* and *in vivo* in its current stage is somewhat unpredictable and limited. Intense efforts to enhance AO delivery to target organs and cells are underway and include; nanoparticles enclosing or decorated with the AO,^{184–186} cell penetrating peptides,^{134,187,188} lipids^{189,190} and nucleic acid aptamers.^{191,192} These advances are reviewed by Roberts et al.¹⁹³. A more efficient PMO delivery method would have been ideal for this study, however, in the meanwhile, further optimisation of the sequence including additional micro-walking, increased or decreased length and alternative chemistries could improve the efficiency of the AO.

The exon-skipping approach, when efficient skipping was achieved showed considerable promise. However, the requirement for extremely efficient skipping in order to restore transcript

homogeneity, is a major challenge. In a recent report, McNamara et al.¹⁹⁴ induced fibrillin-1 exon 30 skipping in a patient-derived iPSC cell line. While the group identified a cocktail of AOs that induced relatively efficient skipping in their model, they concluded that the proportion of skipping achieved was likely insufficient to alleviate the MFS phenotype.¹⁹⁴ The group used the 2'OMe-PS AO chemistry and reported comparable skipping efficiency to that achieved with 2'OMe-PS AOs in this study. The relative exon skipping efficiencies shown by 2'OMe-PS and PMO versions of the same sequence was discussed by Adams et al.¹⁶⁷ in relation to Duchenne muscular dystrophy, showing that effective 2'OMe-PS sequences most often translate into more efficient PMOs. It has since been revealed that not all AO sequences are more efficient as PMOs than their 2'OMe-PS counterparts.¹⁹⁵ However, here we observe that the PMO versions are not only more efficient but also tolerated at a higher concentration and are active for a more extended period of time. Therefore, we suggest that while 2'OMe-PS AOs provide a useful tool in the design and optimisation of therapeutic AOs, the PMO counterpart would be a more appropriate choice for further development.

Since the 1970s AOs have been moulded into a versatile and useful tool in the treatment of genetic diseases. To-date, eleven AO drugs have been approved by the FDA^{196,197} for the treatment of a range of conditions including cytomegalovirus associated retinitis¹⁴⁸, SMA¹⁴⁵, DMD^{143,144,198} and familial hypercholesterolemia¹⁴⁹. This includes one drug, Milasen, that was approved for the treatment of a single patient in an n=1 clinical trial¹⁹⁹ indicating an incredible and encouraging movement toward more personalised medicine. Here we hypothesised that identification of a single AO for each amenable *FBNI* exon could allow for the treatment of any patient with a mutation affecting that exon. We successfully identified AO sequences that mediate the skipping of *FBNI* exons 52 and 59. We also demonstrated in patient cells with two different mutation types that exon skipping can result in the formation of fibrillin-1 fibres.

While we showed that the same AO induced exon skipping in multiple cell lines, the efficiency of skipping varies. Additionally, our findings suggest that the tolerable threshold of truncated monomer abundance is different, depending on the type of mutation, demonstrating the importance of identifying the most efficient AO sequences. The development of AO therapies for Marfan syndrome is obviously still in its infancy, however with further studies building on the foundation outlined here, we may be able to develop targeted therapies for amenable *FBNI* mutations.

Chapter 5
Multi-exon Skipping Strategy

5.1 Fibrillin-1 mutation landscape

As previously discussed, the type-1 fibrillinopathies are caused by mutations in the large fibrillin-1 (*FBNI*) gene that encodes for the extracellular glycoprotein fibrillin-1. To-date over 2,800 unique mutations have been reported,^{2,3} the vast majority of which are private mutations, meaning they are unique to a single individual or family.^{2,3} the remaining 25% to 30% of *FBNI* mutations arise spontaneously with no prior family history.^{29,200}

Disease-causing mutations are spread across the entire *FBNI* sequence with no hotspots with a higher mutation density (Figure 5.1.a). The number of mutations in each exon is roughly correlated to exon size. Exon 64, for example, is associated with 3.5% of all mutations (Figure 5.1.a) but is also the largest coding exon contributing 2.7% of the total 8,613 bases of *FBNI* mRNA.

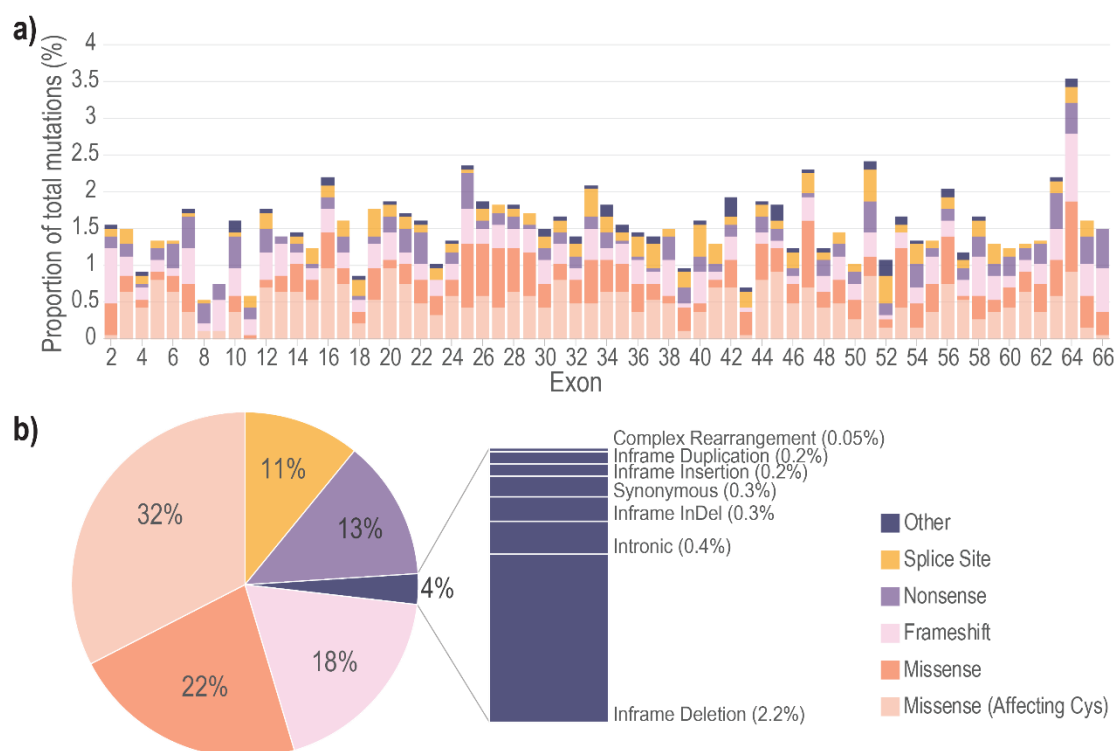


Figure 5.1: Distribution of *FBNI* mutations by exon and type

a) The frequency of mutation types by exon as a proportion of total mutations for that exon. b) distribution of mutations by type, the 'other' segment is highlighted in a bar graph to allow further resolution.

The roughly half (54%) of disease-causing variants affecting the fibrillin-1 gene are missense mutations, in particular, those resulting in the substitution of a conserved cysteine residue are very common; approximately 32% (Figure 5.1.b). Fibrillin-1 is cysteine-rich, made up of repeated domains, each containing between 6-8 conserved cysteine residues that form disulphide bonds in specific patterns.^{20,24} These bonds are essential for calcium-binding as well as the folding and stability of the fibrillin-1 protein.^{20,22} Mutations that either create or more commonly disrupt these

cysteine residues result in loss of calcium-binding and thus are associated with increased proteolysis of fibrillin-1.²³

While missense mutations are the most common, other mutation types have also been associated with Marfan syndrome. Nonsense and frameshifting mutations that lead to a premature termination codon (PTC) account for a further 31% of mutations (Figure 5.1.b). Such mutations often result in nonsense-mediated decay (NMD) and thus follow a haploinsufficiency pathogenic model.^{201,202} Other PTC mutations can ‘escape’ NMD resulting in the synthesis and secretion of truncated fibrillin-1 monomers incapable of forming functional microfibrils.²⁰² Lastly, some PTC mutations that affect the C-terminal result in the synthesis of a stable protein lacking a cleavage site essential for secretion from the cell and lead to intracellular retention.⁶⁶ Such mutations disrupt production of the protein-hormone Asprosin. Asprosin is cleaved from the C-terminal of the fibrillin-1 preproprotein post-translation, and its disruption leads to the rare type-1 fibrillinopathy known as Marfanoid lipodystrophy disorder.^{52,65}

It is estimated that up to 15%²⁰³ of all single nucleotide variants result in altered mRNA splicing, most commonly exon skipping, or the creation or activation of cryptic splice sites and retention of intronic sequences. In the HGMD database² (accessed November 17, 2020) splice site mutations; those directly affecting the splice sites or flanking sequences, account for 9% of total mutations across all genes and 11% of total mutations within *FBNI*. However, both figures are likely underestimates since the majority of mutations are identified through sequencing of genomic DNA. Therefore, any missense, nonsense and synonymous mutations, or deep-intronic mutations that affect splicing and exon selection would not be identified. A prime example of this is the synonymous mutation c.6354C>T, p.(Ile2118Ile) discussed in chapter 4, that disrupts the balance of the cis-acting regulatory silencer and enhancer sequences resulting in exon 52 skipping (r.6314_6379del).

5.1.1 Multi-exon skipping strategy

Thus far, we have discussed using AOs to mediate inclusion or exclusion of a single *FBNI* exon to treat dominant-negative mutations or restore the reading frame. The overarching hypothesis is that the production of identical fibrillin-1 monomers will allow for functional microfibrils to form, reducing the severity and progression of the Marfan phenotype. Both exclusion and inclusion of a disease associated-exon using antisense oligonucleotides (AO) have been applied to many different diseases with varying levels of efficacy, including Pompe disease,²⁰⁴ Duchenne muscular dystrophy (DMD),^{143,144} spinal muscular atrophy²⁰⁵ and spinocerebellar ataxia type 3.^{168,206} However, a now relatively well-established approach described for DMD is the removal of multiple exons simultaneously both *in vitro* and *in vivo*.^{207–}

An example of multi-exon skipping was described by Adkin et al.,²⁰⁷ who assessed the efficiency of double exon skipping involving *DMD* exonic regions 19-21 and 50-52. Fall et al.²¹¹ similarly assessed multi-exon skipping in *DMD* successfully excluding exons 19-25 using a cocktail of AOs. Both reports recognized that some exons are more challenging to skip than others, requiring a combination of two AOs for one exon, within the multi-exon skipping cocktail.²⁰⁷ A similar study by Yokota et al.²⁰⁸ demonstrated the efficacy of a multi-AO cocktail in inducing skipping of exons 6 and 8 flanking the exon 7 splice site mutation that causes golden retriever muscular dystrophy,²¹² resulting in triple-exon skipping.

Multi-exon skipping has three main advantages: (1) allowing restoration of the reading frame for mutations that require the removal of more than one exon; (2) enabling the treatment of greater number of patients with fewer drugs, potentially resulting in a more consistent patient response to treatment and (3) enabling the truncated protein to be more fully optimised to produce the most effective isoform. For *DMD* it is estimated that only 70% of deletion patients and 47% of nonsense mutation patients are amenable to single exon skipping, while over 90% of all patients are theoretically treatable with multi-exon skipping.²¹³

We propose that a multi-exon skipping approach could also be applied to *FBNI* to treat the type-1 fibrillinopathies. However, rather than to restore the reading frame, since most fibrillin-1 exons are in-frame, we suggest that the main advantage of a multi-exon skipping approach for *MFS* will be the potential to treat more patients with fewer compounds. This is particularly important since *MFS* is a rare disease with no mutation hotspots and many mutation types. Of the 66 exons of *FBNI* exons, 60 can be skipped without disrupting the reading-frame therefore, approximately 90% of all mutations are theoretically amenable to an exon-skipping strategy, assuming that the deleted exon does not completely compromise function. However, a different AO would be required for each exon, with each AO only effective against approximately 1.5% of mutations.

We hypothesised that efficient multi-exon skipping, much like single exon skipping, would result in identical internally truncated fibrillin-1 monomers capable of assembling into microfibrils. We also suggest that; if efficient, this multi-exon skipping approach could be used for any patient with a mutation in one of the targeted exons. We chose the region from exons 45 to 47 as our model as we had access to two patient cell lines, one with genomic deletion of exons 45, 46 and 47, and the second with a splice site mutation resulting in exon 47 skipping.

5.2 Confirmation of patient mutations

The use of human cells for this research was approved by the Murdoch University Human Ethics Committee; approval numbers 2013_156 and 2017_101 and The University of Western Australia Human Research Ethics Committee; approval number RA4/1/2295. Healthy control fibroblasts were cultured from a dermal biopsy of a healthy volunteer taken after informed consent.

The following cell lines were obtained from the NIGMS Human Genetic Cell Repository at the Coriell Institute for Medical Research: GM21934 and GM21940. Both patients have been previously characterised by Liu et al. in articles published in 1996¹⁸³ and 2001¹⁷⁰. Please note that mutation nomenclature was determined with respect to the *FBNI* gene Locus Reference Genomic sequence transcript 1 ([LRG_778t1](#)) in which the non-coding 5' exon is considered as exon 1, and the translation start codon is located in exon 2. Therefore, the exons under investigation will be referred to as exon 47 and exon region 45-47. The GM21934 cells hereafter referred to as MFS^{Δ47}, were originally reported to harbour a donor splice site mutation resulting in skipping of exon 46. The GM21940 (MFS^{Δ45-47}) cells were originally reported to have a genomic deletion of exons 44-46.

The patient cell line mutations were confirmed using Sanger sequencing. Genomic DNA was extracted from a MFS^{Δ47} fibroblast pellet, and the region of *FBNI* between exon 47 forward and intron 47 reverse primers was amplified using AmpliTaqGold polymerase. Fibrillin-1 cDNA, between exons 42 and 49, was derived from total RNA extracted from MFS^{Δ47} and MFS^{Δ45-47} fibroblasts.

5.2.1 Confirming the MFS^{Δ47} mutation

The MFS^{Δ47} fibroblasts were confirmed to harbour the reported c.5788+5G>A splice site mutation that results in exon 47 skipping using both gDNA (Figure 5.2.a) and cDNA as sequencing templates (Figure 5.2.b). This mutation was one of the first recurrent mutations to be described and has been reported over 30 times, making it the second most common *FBNI* mutation.^{3,183,214} However, during fractionation of amplicons between *FBNI* exons 42 and 49 a third product, larger than both the expected 797 bp exon skipping product (Δ47) and 914 bp full-length (FL) product, was identified (Figure 5.2.d). This band on the gel was initially thought to be a heteroduplex. However, the band was consistently present after RT-PCR at various annealing temperatures and after using a two-step PCR protocol with a single annealing and elongation step, a method used to reduce the presence of heteroduplexes (data not shown). Finally, with two additional primers between exons 45 and 49 and exons 45 and 50 the product band was identified

as approximately 20-50 bp larger than the expected full-length amplicon, constituting approximately 23% of the total transcripts and 45% of the non-full-length product (Figure 5.2.d).

Band purification and Sanger sequencing of the RT-PCR product revealed that the larger amplicon contains 33 bases of retained intron 47 (Figure 5.2.c). The insertion of 33 bases of intron 47 is in-frame and does not introduce any premature termination sites. The presence of a single 'A' peak at c.5788+5 in transcripts with the 33 bp insertion confirmed that this inclusion does not occur in the wildtype allele and that it results from the splice site mutation and lack of the donor splice site recognition (Figure 5.2.c). This insertion is predicted to introduce 11 additional amino acids, GCAKLCISKGN, into the beginning of the 29th cbEGF-like domain. Within these amino acids are two cysteines that likely disrupt the folding and stabilisation of fibrillin-1.

Further *in silico* investigation using the web-based tool, Human Splicing Finder 3.0²¹⁵ revealed that this insertion into the transcript terminates at a predicted alternative donor splice site sequence in intron 47 before continuing directly into exon 48. This alternative donor site is of average strength with a consensus score of 82%, while the natural donor site has a score of 88% that is reduced to 78% as a result of the c.5788+5 G>A mutation (Table A3.1). We suggest that in most mutant transcripts, the spliceosome bypasses the canonical splice sites of exon 47, due to loss of donor site recognition, utilising exon 46 donor and exon 48 acceptor sites and leading to exon 47 skipping (Figure 5.2.d). However, a small portion of affected transcripts undergo splicing of intron 46 correctly utilising the exon 46 donor and exon 47 acceptor sites. Then, during splicing of intron 47, the spliceosome uses a cryptic donor splice site 33 bases into intron 47 and the canonical exon 48 acceptor site. This proposed splicing is depicted in Figure 5.2.d. The c.5788+5G>A mutation has previously been associated with activation of cryptic splice sites,²¹⁴ however, this particular site has not been described.

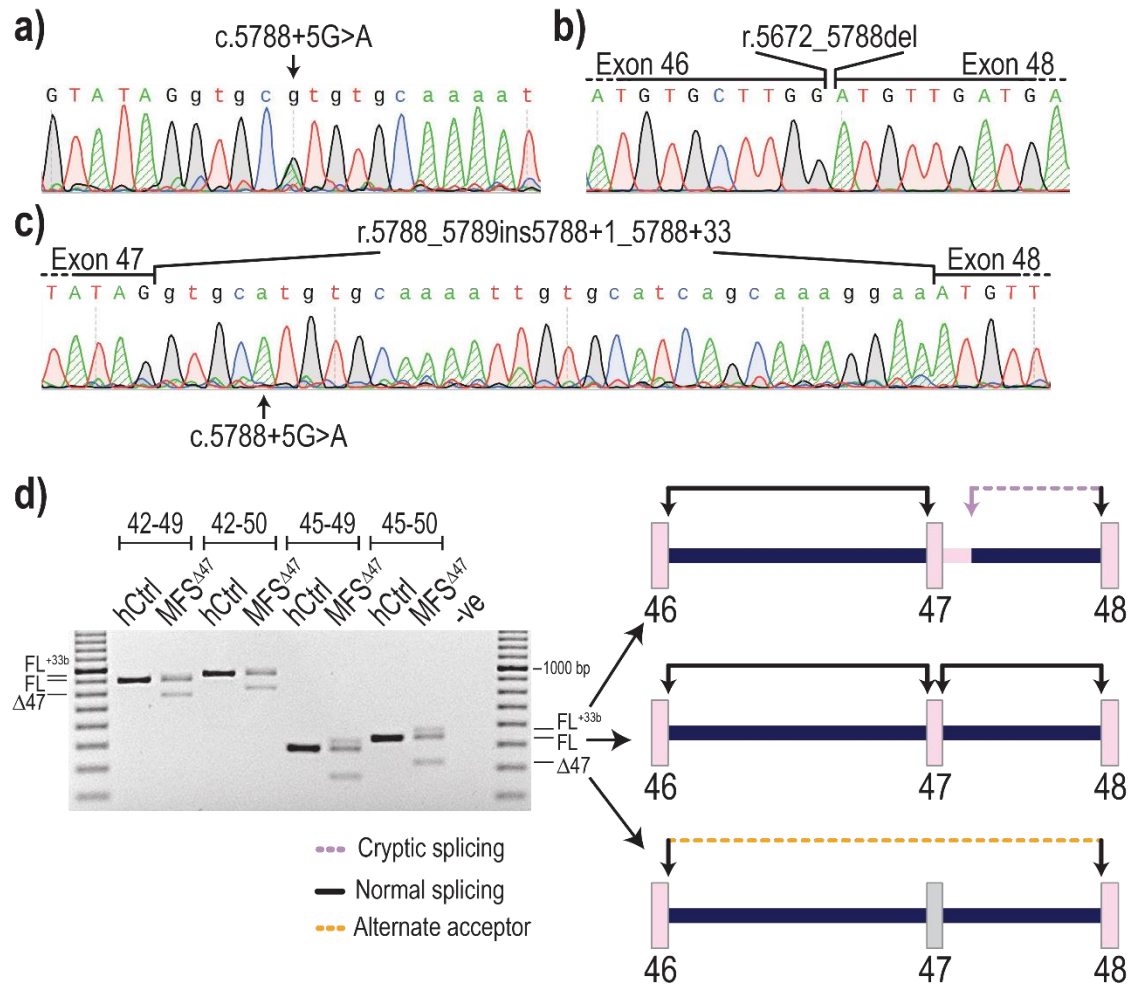


Figure 5.2: Mutation confirmation in MFS^{Δ47} fibroblasts

The reported disease-causing mutation harboured by MFS^{Δ47} patient fibroblasts was confirmed via Sanger sequencing using a) gDNA, and b) cDNA derived from fibroblast RNA, as a template. c) Analysis of Sanger sequencing results showing the retention of 33 bases of intron 47 that occurs as a secondary outcome of the splice site mutation. d) RT-PCR amplification of healthy control (hCtrl) and MFS^{Δ47} patient fibroblast RNA with four primer sets, showing the full-length (FL), exon 47 skipped ($\Delta 47$) and full-length plus 33 bases of retained intron 47 (FL^{+33b}) transcript products. 100 bp molecular marker used for size reference. A diagram showing the probable splice sites being utilised for each product is shown to the right.

5.2.2 Confirming the MFS^{Δ45-47} mutation

The mutation affecting MFS^{Δ45-47} cells was similarly confirmed at the cDNA level after Sanger sequencing; revealing the deletion of exons 45, 46 and 47 in their entirety (Figure 5.3.a). Liu et al.¹⁷⁰ reported that the breakpoints for this genomic deletion occurs within an ‘atattt’ pentamer at positions -282 to -278 of intron 44 and -325 to -321 of intron 47 (Figure 5.3.b). These breakpoints were not confirmed at the gDNA level. Loss of exons 45-47 in this patient is associated with a severe neonatal Marfan syndrome phenotype. This severe phenotype combined with the mutation being classified as type IV with 109% synthesis and only 13% deposition^{69,170} suggests an extreme dominant-negative effect resulting from this mutation.

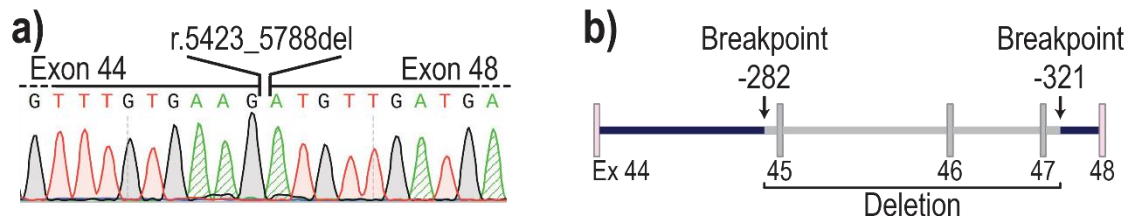


Figure 5.3: Mutation confirmation in MFS Δ 45-47 fibroblasts

a) Mutation confirmation for MFS Δ 45-47 cells at the cDNA/RNA level. b) schematic of the genomic deletion harboured by MFS Δ 45-47 cells reported by Liu et al.¹⁷⁰ showing the breakpoints in introns 44 and 47.

5.3 Antisense oligonucleotide design

The first panel of AOs were designed to target the acceptor and donor splice sites, as well as potential exonic splicing enhancers as predicted by SpliceAid.¹⁵³ Once an AO capable of inducing *FBNI* exon skipping in healthy control fibroblasts was identified, additional overlapping AOs were designed in an attempt to further increase the skipping efficiency. Two un-related AOs sequences, one for each chemistry, were included in cell transfections as sham treatments. All AO sequences used in this chapter are described in Table 5.1. Exon sequence maps showing the AO binding sites in relation to enhancer and silencer motifs predicted by SpliceAid¹⁵³ are presented in the supplementary Figure A3.1.

Table 5.1: List of antisense oligonucleotides used in Chapter 5

The name, ID, sequence, and chemistry of AOs designed to induce skipping of exons 45, 46 and 47. Two control sequences were also used to reveal any chemistry-related effects. AO nomenclature described in Chapter 2, Figure 2.1. The AOs targeting exons 45 and 46 were designed by Mr Kane Greer (unpublished, 2017).

AO name (FBN1 H...)	ID	Sequence (5'-3')	Chemistry
Exon 45			
45A(+15+39)	AO45.1	UGC GCU GGC ACA CUG GGC CGU UCU G	2'OMe-PS
45A(+15+39)	PMO45	TGC GCT GGC ACA CTG GGC CGT TCT G	PMO
45A(+49+73)	AO45.2	CGG UAG CUG CCU GCA GUG UUG AUG C	2'OMe-PS
45A(+87+111)	AO45.3	CUG UGG AGG UGA AGC GGU AGC CGG G	2'OMe-PS
45D(+21-04)	AO45.4	AUA CCA UUG CAC UGU CCU GUG GAG G	2'OMe-PS
Exon 46			
46A(-09+16)	AO46.1	UGA CAU UCA UUA CGA UCU GUA AAU A	2'OMe-PS
46A(+72+96)	AO46.2	UAA AAC CAG UGU GGC AAA GGC AAU A	2'OMe-PS
46D(+12-13)	AO46.3	AUU GCA UAC UUA CCC AAG CAC AUG G	2'OMe-PS
46D(+12-13)	PMO46	ATT GCA TAC TTA CCC AAG CAC ATG G	PMO
46A(-03+22)	AO46.4	AUU UCU UGA CAU UCA UUA CGA UCU G	2'OMe-PS
Exon 47			
47A(-03+20)	AO47.1	UCU UUC ACA UUC AUU UAU GUC UA	2'OMe-PS
47A(+58+77)	AO47.2	GCA GCG GCA GUU GAA GGA AC	2'OMe-PS
47A(+58+77)	PMO47	GCA GCG GCA GTT GAA GGA AC	PMO
47A(+83+102)	AO47.3	UGU GAG AAA GGA UGA AAC CA	2'OMe-PS
47D(+05-15)	AO47.4	AUU UUG CAC ACG CAC CUA UA	2'OMe-PS
47A(+44+68)	AO47.5	GUU GAA GGA ACC AAU UGU GUU CCG G	2'OMe-PS
47A(+69+93)	AO47.6	GGA UGA AAC CAU GAU UGC AGC GGC A	2'OMe-PS
47D(+24-01)	AO47.7	CCU AUA CAG UCA UUG UUG UGA GAA A	2'OMe-PS
47A(+56+80)	AO47.2-25mer	AUU GCA GCG GCA GUU GAA GGA ACC A	2'OMe-PS
47A(+53+82)	AO47.2-30mer	UGA UUG CAG CGG CAG UUG AAG GAA CCA AUU	2'OMe-PS
47A(+53+82)	PMO47-30mer	TGA TTG CAG CGG CAG TTG AAG GAA CCA ATT	PMO
Controls			
Unrelated control	Ctrl	GGA UGU CCU GAG UCU AGA CCC UCC G	2'OMe-PS
GeneTools control	GTC	CCT CTT ACC TCA GTT ACA ATT TAT A	PMO

5.4 Identifying candidate AOs for *FBN1* exons 45, 46 and 47

5.4.1 Exon 45 and 46

Three AOs were initially designed for each exon 45 and 46, covering the majority of the exons sequence. Each AO was transfected into healthy control fibroblasts at two concentrations; 200 nM and 50 nM. Cells were incubated for 24 hours before collection for RNA analysis to assess skipping efficiency. Of the three AOs tested for exon 45, only AO45.1 and AO45.2 induced any exon 45 skipping. However, the efficiency of exon removal was poor with only 3% and 9% Δ 45 transcripts for AO45.1 and AO45.2, respectively (Figure 5.4.a). Exon 46 AOs were similarly ineffective, with AO46.3 the most efficient inducing up to 10% skipping (Figure 5.4.b).

In an attempt to increase skipping efficiency, cocktails of two AOs together were tested. The cocktails of AO46.1 and AO46.3 induced substantially more exon skipping than either AO individually, up to 32% (Figure 5.4.b). However, none of the other exon 46 cocktails nor those for exon 45 were effective. One additional sequence, AO45.4 and AO46.4, were designed for each exon targeting the donor and acceptor site of exon 45 and 46, respectively. Neither of these additional AOs induced exon skipping (Figure 5.4.a and b). Despite their poor skipping ability AO45.1, AO45.2, AO46.1 and AO46.3 were deemed the most appropriate sequences to induce triple exon skipping.

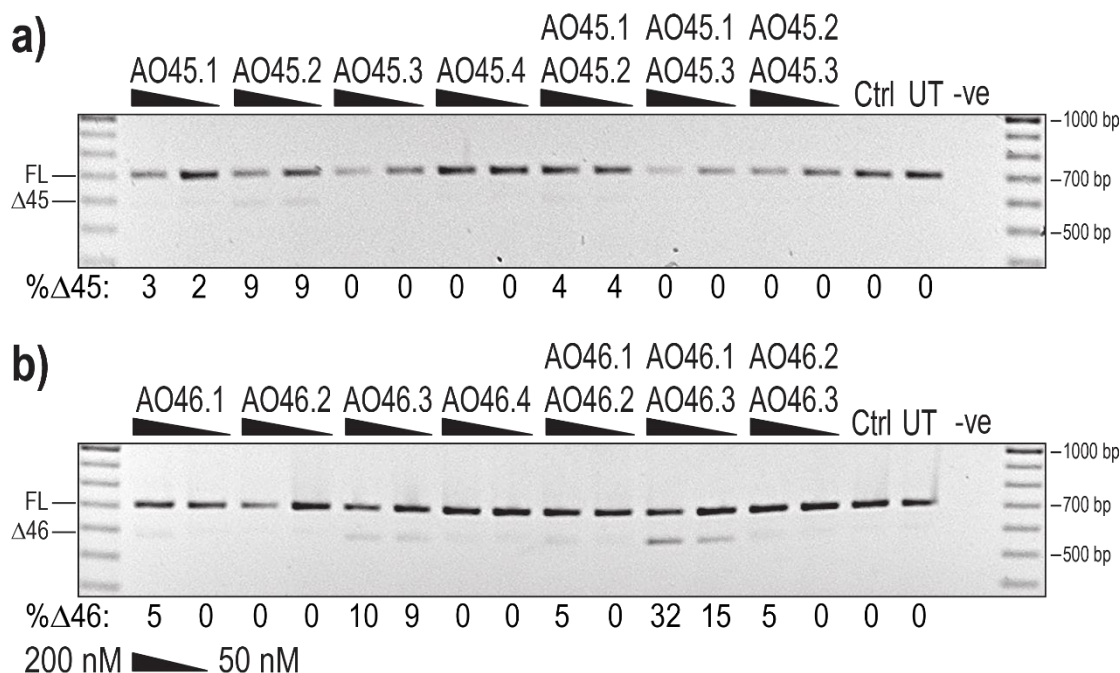


Figure 5.4: Evaluation of AOs designed to induce skipping of *FBN1* exon 45 and 46

Healthy control fibroblasts were transfected with 2'OMe-PS AOs targeted to a) exon 45 and b) exon 46. Two concentrations; 200 nM and 50 nM were tested, and treated cells were collected after 24 hours to assess skipping efficiency. The values below each gel image indicate the percentage of exon 45 (Δ 45) or 46 (Δ 46) skipped transcripts in each sample. Ctrl: an unrelated sequence used as a sham treatment, UT: untreated control, -ve: RT-PCR negative control. 100bp molecular marker used for size reference.

5.4.2 Exon 47

Four 2'OMe-PS AOs designed to induce exon 47 skipping were transfected into healthy control fibroblasts, and exon skipping was assessed after 24 hours. Three concentrations were tested: 200, 100 and 50 nM. Initial AO screening identified AO47.1, AO47.2 and AO47.3 as capable of inducing exon 47 skipping, albeit at different efficiencies (Figure 5.5.a). The most efficient AOs; AO47.2 and AO47.3, yielded 28% and 27% skipping at 200 nM, respectively (Figure 5.5.a). No measurable exon skipping was observed in samples treated with any concentration of AO47.4.

As previously undertaken, all non-overlapping combinations of two AO cocktails were tested to identify any synergistic effects. Every cocktail tested induced more than 30% skipping at the highest concentration tested, with the combination of AO47.3 and AO47.4 causing as much as 43% skipping (Figure 5.5.b). However, these skipping efficiencies were more suggestive of an additive effect, with each AO inducing approximately 20% skipping.

Two additional AOs, AO47.5 and AO47.6, were designed around the AO47.2 and AO47.3 target sites to further optimise the skipping efficiency. Due to the shorter 20-mer length of AO47.2, two longer versions, a 25-mer and 30-mer, were also designed, to ascertain if extending the AOs would increase exon skipping efficiency. Each of these additional AO sequences was transfected into healthy control fibroblasts at two concentrations: 200 nM and 50 nM. The AO47.5 and AO47.6 sequences induced 24% and 10% exon skipping, respectively, however, AO47.7 was not effective with no measurable skipping evident (Figure 5.5.c). The 25-mer and 30-mer versions of AO47.2 induced more than 40% skipping making them as efficient as the 20-mer (Figure 5.5.c). The AO47.2 and AO47.3 were selected for further study to induce triple-exon skipping. The AO47.2 sequence was also synthesised as a PMO for assessment in *MFS^{Δ47}* cells.

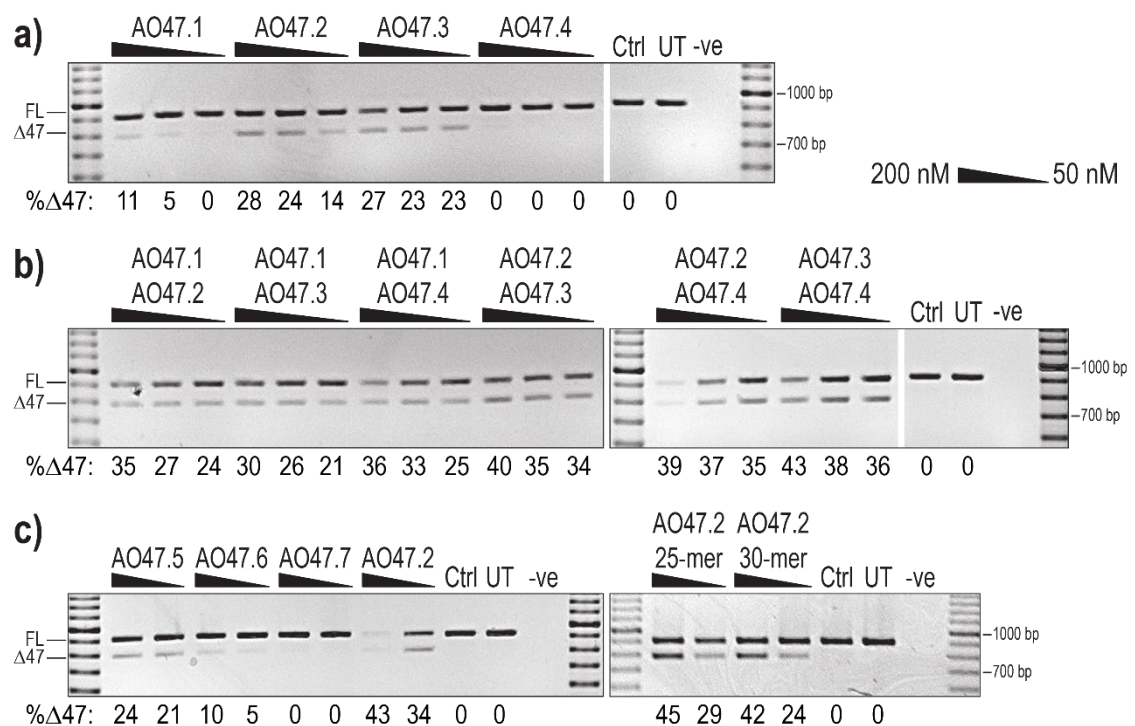


Figure 5.5: Evaluation of AOs designed to induce *FBN1* exon 47 skipping.

Exon 47 skipping efficiency in healthy control fibroblasts treated with a) individual 2'OMe-PS AOs, b) cocktails of two AOs or c) additional 2'OMe-PS AOs designed to improve upon the most efficient sequence by extending the length and micro-walking up-and down-stream of the original target site. Either three concentrations; 200 nM, 100 nM and 50 nM (a and b) or two concentrations; 200 nM and 50 nM (c) were tested, and all cells were collected for RNA analysis after 24 hours. The values below each gel image indicate the percentage of exon 47 skipped transcripts ($\Delta 45$) in each sample. Ctrl: an unrelated sequence used as a sham treatment, UT: untreated control, -ve: RT-PCR negative control. 100bp molecular marker used for size reference.

5.5 Evaluation of PMO47-mediated exon skipping

The screening of 2'OMe-PS AOs targeted to exon 47 identified AO47.2 as the most efficient, this sequence was synthesised as a PMO (PMO47) and nucleofected into healthy control and MFS^{Δ47} patient fibroblasts. The proportion of exon 47 skipped transcripts ($\Delta 47$) were assessed after four and ten days. In MFS^{Δ47} fibroblasts, the PMO47 sequence induced efficient exon 47 skipping averaging 92% after four days and 95% after ten days across two and three replicates, respectively (Figure 5.6). In healthy control fibroblast, where there is no endogenous skipping, exon 47 skipping efficiency was reduced, with an average of 75% and 62%, across three replicates, after four and ten days, respectively (Figure 5.6).

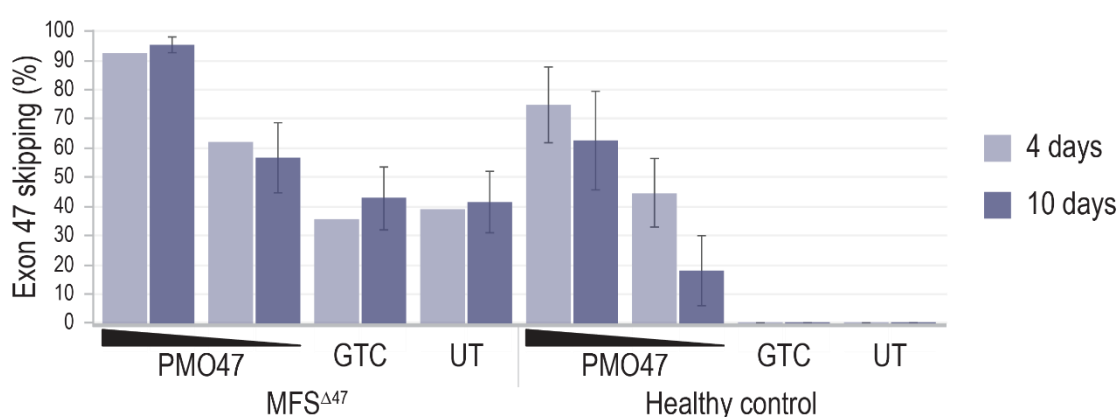


Figure 5.6: PMO47 mediated exon 47 skipping

Densitometric analysis over multiple replicates of MFS^{Δ47} patient and healthy control fibroblasts transfected with PMO47 at two concentrations; 250 μ M and 50 μ M, calculated in the 20 μ l nucleofection cuvette volume, and incubated for 4 or 10 days. Means plus error bars, error bars = standard deviation, n=3. For MFS^{Δ47} 4-day treatment groups n=2. GTC: Gene Tools control PMO used as a sham treatment, UT: untreated control.

The fibrillin-1 immunofluorescence results from one biological replicate collected after four days are displayed in Figure 5.7. Transfected fibroblasts were immunolabelled with an anti-fibrillin-1 antibody to reveal the morphology and abundance of fibrillin-1 fibres. Untreated healthy control and MFS^{Δ47} patient samples were found to exhibit similar fibrillin-1 abundance, however, MFS^{Δ47} patient fibroblasts have a stark lack of fibrillin-1 fibres (Figure 5.7.b.iv and viii). As seen previously, untreated healthy control fibroblasts have consistent long thin fibres that form a lattice and cover most of the coverslip (Figure 5.7.b.viii). In contrast, the MFS^{Δ47} patient fibroblasts show diffuse staining throughout the cells, suggesting intracellular retention and no evidence of microfibril formation (Figure 5.7.b.iv). In both cell lines, the morphology and abundance of fibrillin-1 are unchanged after treatment with the GTC sham control (Figure 5.7.b.iii and vii) indicating no chemistry-related effects.

Treatment with the lower concentration of PMO resulted in a similar mid-range exon skipping in both cell lines; 52% and 61% for healthy control and MFS^{Δ47} fibroblasts, respectively. The effect of the 50 μ M PMO47 treatment was also similar for both cell lines, with a substantial

decrease in fibrillin-1 abundance (Figure 5.7.b.ii and vi). In healthy control fibroblasts, the 50 μ M treatment eliminates fibrillin-1 fibre formations (Figure 5.7.b.ii).

When the PMO47 concentration was increased to 250 μ M, a corresponding increase in skipping efficiency was evident; 89% and 92% in healthy control and patient fibroblasts, respectively (Figure 5.7.a). Treatment with 250 μ M of PMO47 resulted in both an increase in fibrillin-1 abundance, compared to that in the 50 μ M treated cells, as well as the re-appearance of fibrillin-1 fibres (Figure 5.7.b.i and v). In the healthy control and patient fibroblasts treated with 250 μ M of PMO47, fibrillin-1 fibre morphology is similar to that seen when skipping exon 52 previously; with long and thin but occasionally fragmented fibres. These fibres are relatively abundant in both cell lines, covering more than 75% of any given field of view. One change in morphology from that seen when skipping exon 52 is additional sponge-like staining that is particularly noticeable in the treated healthy control sample (Figure 5.7.b.i). The sponge-like staining pattern could indicate intracellular retention or extracellular fibrillin-1 that has not correctly formed fibrils.

Of note is that treatment of MFS ^{Δ 47} cells with PMO47 appears to eliminate the additional 947 bp intron 47 inclusion transcript that occurs as a secondary effect of the c.5788+5G>A mutation (Figure 5.7.a). The 947 bp product could not be detected when isolating and amplifying the full-length product generated from the 250 μ M treated patient cell sample (data not shown). The elimination of this splicing pattern should limit any adverse effects that would result from multiple different fibrillin-1 transcripts.

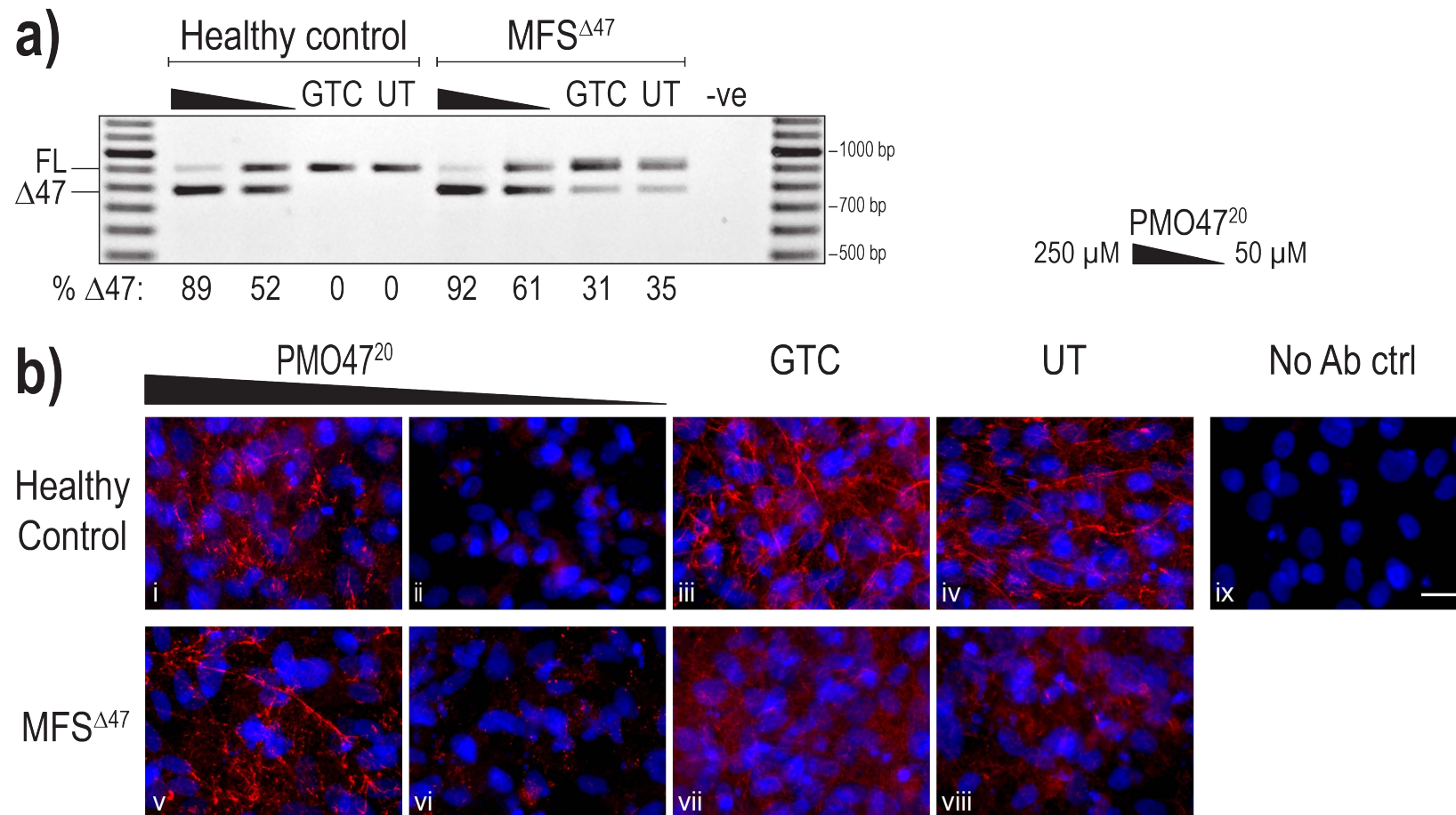


Figure 5.7: Evaluation of PMO47-mediated exon 47 skipping and fibrillin-1 morphology

Healthy control and $MFS^{\Delta 47}$ cells were nucleofected with PMO47, Gene Tool control PMO (GTC) or left untreated (UT) then collected after four days. Two concentrations were tested; 250 μM and 50 μM , calculated in the 20 μl nucleofection cuvette volume. a) RT-PCR amplicons between *FBN1* exons 42 and 49 showing full-length (FL; 914 bp) and exon 47 skipped ($\Delta 47$; 797 bp) transcript products. The values below the gel image indicate the percentage of $\Delta 47$ transcripts in each sample. -ve: RT-PCR negative control. 100bp molecular marker used for size reference. b) representative images of treated cells stained for fibrillin-1 (red) and counterstained with Hoechst (blue) for nuclei detection. No Ab control: no primary antibody added. Scale bar = 20 μm . See Figure A3.2 for a larger version of part b.

5.6 Triple-exon skipping

5.6.1 Identification of promising cocktails

Cocktails of AOs to skip exons 45, 46 and 47 simultaneously were assessed in healthy control and MFS^{Δ45-47} fibroblasts. These cocktails varied by AO as well as the number of AOs targeted to each exon. All multi-exon skipping cocktails are described in Table 5.2.

Table 5.2: Cocktails of 2'OMe-PS AOs designed to induce triple-exon skipping 2'OMe-PS AO cocktails. Each cocktail is a combination of AOs targeting exons 45, 46 and 47.

Cocktail ID	AO combination		
	Exon 45	Exon 46	Exon 47
Combined cocktails (5 AOs)			
CT-1	AO45.1 [45A(+15+39)] AO45.2 [45A(+49+73)]	AO46.1 [46A(-09+16)] AO46.3 [46D(+12-13)]	AO47.2 [47A(+58+77)]
CT-2	AO45.1 [45A(+15+39)] AO45.2 [45A(+49+73)]	AO46.1 [46A(-09+16)] AO46.3 [46D(+12-13)]	AO47.3 [47A(+83+102)]
CT-3	AO45.1 [45A(+15+39)] AO45.2 [45A(+49+73)]	AO46.2 [46A(+72+96)] AO46.3 [46D(+12-13)]	AO47.2 [47A(+58+77)]
CT-4	AO45.1 [45A(+15+39)] AO45.2 [45A(+49+73)]	AO46.2 [46A(+72+96)] AO46.3 [46D(+12-13)]	AO47.3 [47A(+83+102)]
Single AO per exon cocktails (3 AOs)			
CT-5	AO45.1 [45A(+15+39)]	AO46.1 [46A(-09+16)]	AO47.2 [47A(+58+77)]
CT-6	AO45.1 [45A(+15+39)]	AO46.1 [46A(-09+16)]	AO47.3 [47A(+83+102)]
CT-7	AO45.1 [45A(+15+39)]	AO46.3 [46D(+12-13)]	AO47.2 [47A(+58+77)]
CT-8	AO45.1 [45A(+15+39)]	AO46.3 [46D(+12-13)]	AO47.3 [47A(+83+102)]
Two-exon cocktails			
CT-9	AO45.1 [45A(+15+39)] AO45.2 [45A(+49+73)]		AO47.2 [47A(+58+77)]
CT-10	AO45.1 [45A(+15+39)] AO45.2 [45A(+49+73)]		AO47.3 [47A(+83+102)]
CT-11	AO45.1 [45A(+15+39)] AO45.3 [45A(+87+111)]		AO47.2 [47A(+58+77)]
CT-12	AO45.1 [45A(+15+39)] AO45.3 [45A(+87+111)]		AO47.3 [47A(+83+102)]

The first-generation cocktails consisted of two AOs targeting each of exons 45 and 46 that were challenging to skip, and a single AO targeting exon 47 that is more readily removed (Table 5.2). These cocktails did not induce any measurable triple exon skipping in healthy control fibroblasts, with the only skipping observed corresponding in size to single and double exon skipping (Figure 5.8.a). The identity of the exons being skipped could not be simply determined by gel fractionation due to their similar sizes; 123, 126 and 117 bases for exons 45, 46 and 47, respectively. The use of additional primer sets revealed that each exon was skipped at low levels, generating the intermediate sized amplicons (data not shown).

The same cocktails were tested in $MFS^{\Delta 45-47}$ patient cells. No intermediate products were detected; however, the intensity of the full-length band was reduced (Figure 5.8.b). While the ratio of $\Delta 45-47$ transcripts to the full-length product was increased, considering the lack of triple exon skipping in the healthy control cells, we suggest that the loss of full-length product is due to knockdown rather than skipping. This knockdown could be the result of intron retention, incomplete pre-mRNA processing or undesired skipping. However, further investigation found no evidence to suggest that either of the exons containing the primer annealing sites were skipped, nor was there any intron retention (data not shown). We also note a five-AO cocktail increases the level of cell death, despite using the same total AO concentration; 200 nM and 50 nM, as used for previous screening experiments.

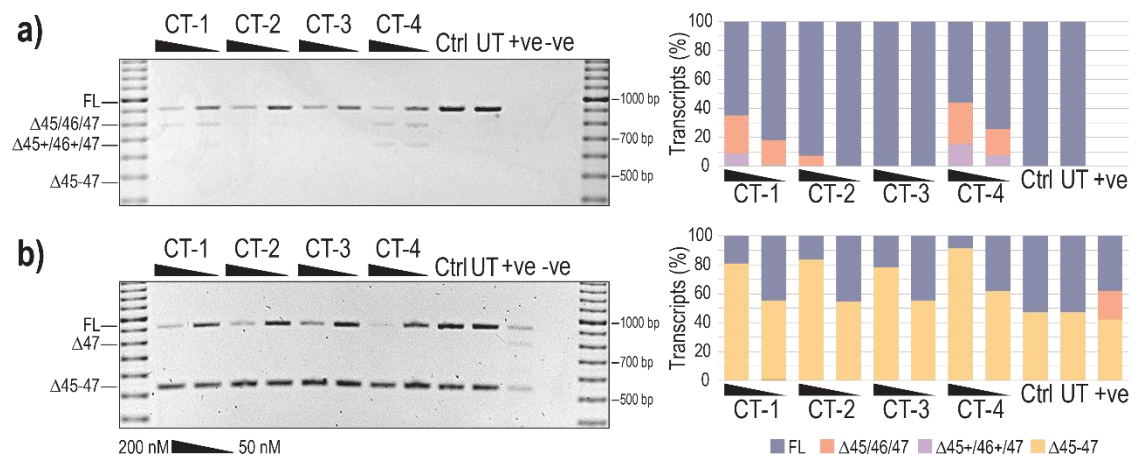


Figure 5.8: Evaluation of five-AO cocktails designed to induce exon 45-47 skipping.

RT-PCR results from a) healthy control and b) $MFS^{\Delta 45-47}$ patient fibroblasts treated with a cocktail of 2'OMe-PS AOs targeting exons 45, 46 and 47. Two concentrations, 200 nM and 50 nM, were tested, these are total cocktail concentrations and are made up of an equimolar ratio of each AO. The full-length (FL) transcript is 914 bp, the triple exon skipping ($\Delta 45-47$) transcript is 548 bp. Ctrl: an unrelated sequence used as a sham treatment, UT: untreated control, -ve: RT-PCR negative control. 100bp molecular marker used for size reference. The relative density of each band was determined using Image J and is displayed in the graph as the proportion of total transcript contributed by each isoform.

The second generation of cocktails attempted to streamline triple-exon skipping by reducing the number of AOs with only a single AO for each exon. These cocktails were more effective than the five-AO cocktails and resulted in less cell death. All single-AO per exon cocktails (Table 5.2) resulted in a ladderred splicing pattern, with full-length, single exon skipping, double exon skipping and triple exon skipping being induced (Figure 5.9.a). Both CT-7 and CT-8 induced the desired triple-exon skipping in healthy control cells (Figure 5.9.a).

Treatment with the second-generation cocktails resulted in a similar decrease in the intensity of the full-length product band without a proportionate increase in triple-exon or intermediate skipping products. The amplification of COL1A2 as a housekeeping gene transcript revealed that the relative amounts of PCR product in each well are similar (Figure 5.9.a and b). When the proportion of each transcript in patient samples was normalised against the AO control, the total amount of transcripts is noticeably reduced in the majority of treated samples (Figure 5.9.c).

Treatment of patient fibroblasts with any of the four cocktails, CT-5, CT-6, CT-7, or CT-8 resulted in an increase in the Δ 45-47 transcript product (Figure 5.9.a and c). However, in the healthy control cells, only CT-7 and CT-8 were shown to induce a robust amount of triple-exon skipping (Figure 5.9.a). In addition, the CT-7 formulation contains AO47.2 that was previously shown to be the most effective AO at inducing exon 47 skipping; therefore, CT-7 was chosen for further study. The exon 45 and 46 AO sequences, as well as the 30-mer version of AO47.2, were synthesised as PMOs.

We also tested four cocktails with two exon 45 AOs and one exon 47 AO, but no AO targeting exon 46 (Table 5.2). These were designed to determine if the exon 45-47 region could be skipped as a single unit by targeting only the flanking exons. This approach has been previously described for DMD where two AOs, one targeted to exon 45 and the other to exon 51 of the *DMD* gene, resulted in the skipping of the entire regions between the two exons.²⁰⁹ The cocktails in this study did not result in any triple exon skipping, although they did result in both single and double exon skipping (Figure 5.9.a and b).

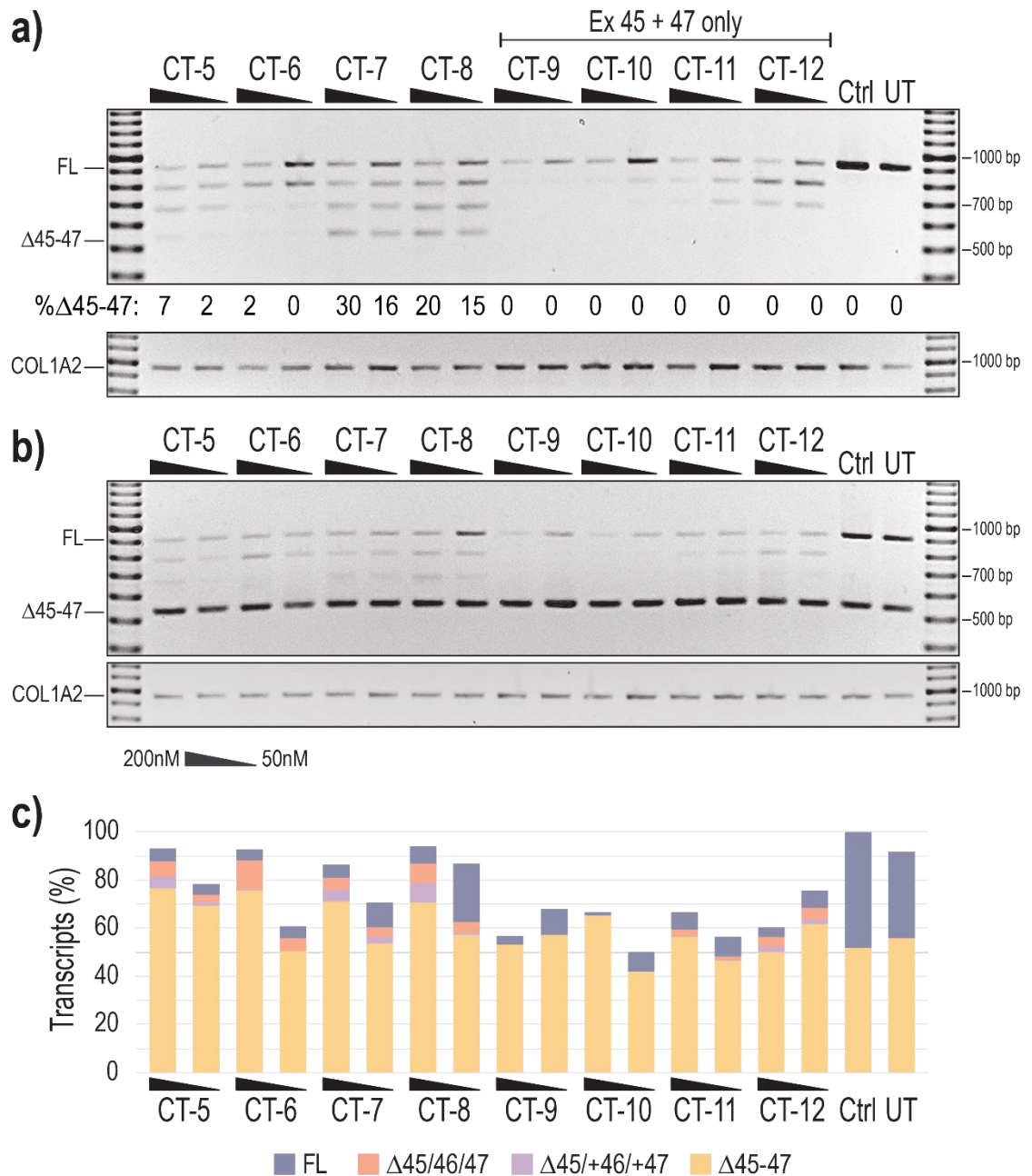


Figure 5.9: Evaluation of additional cocktails designed to induce exon 45-47 skipping.

Cocktails of AOs targeted to exon 45, 46 and 47, or 45 and 47 alone, were transfected into a) healthy control and b) $MFS^{\Delta 45-47}$ fibroblasts at two concentrations: 200n M and 50 nM. The Full-length (FL) transcript is 914 bp, the triple exon skipping ($\Delta 45-47$) transcript is 548 bp. The values below the first gel image indicate the percentage of $\Delta 45-47$ transcripts in each sample. Ctrl: an unrelated sequence used as a sham treatment, UT: untreated control, -ve: RT-PCR negative control. 100bp molecular marker used for size reference. c) The relative abundance of each isoform in, $MFS^{\Delta 45-47}$ fibroblasts, as a proportion of total transcripts normalised against the control sample.

5.6.2 Evaluation of PMO cocktails for triple exon skipping

We have shown that the relatively efficient 2'OMe-PS AO47-2 sequence translated into an efficient PMO. However, the 'best' sequences for exons 45 and 46 induced minimal exon skipping as 2'OMe-PS AOs. Therefore, it was unknown what effect the PMO chemistry would have on the efficiency of these sequences. Nevertheless, the AO sequences for exons 45 (AO45.1) and 46 (AO46.3), that were found to be most effective when used as a cocktail with AO47.2, were synthesized as PMOs. An additional sequence targeting exon 47; a 30-mer version was also synthesised as a PMO.

Optimisation of cocktail concentration

Cocktails of PMO45, PMO46 and either the original 20-mer PMO47²⁰ or longer 30-mer PMO47³⁰ (Table 5.3) were nucleofected into MFS^{Δ45-47} patient fibroblasts. The efficiency of triple exon skipping was determined after incubation for ten days. Originally cocktail concentrations of 250 μM and 50 μM were tested. These concentrations are calculated in the 20 μl cuvette of the nucleofector system and are the total PMO concentration made up of equimolar amounts of each AO. Neither concentration induced sufficient triple-exon skipping and the intermediate products were likely too abundant to be able to provide any potential benefit (Figure 5.10.a).

Table 5.3: Optimal triple-exon skipping cocktails.

Each cocktail is a combination of AOs targeting exons 45, 46 and 47.

Cocktail ID	AO combination		
	Exon 45	Exon 46	Exon 47
CT-7	AO45.1 [45A(+15+39)]	AO46.3 [46D(+12-13)]	AO47.2 [47A(+58+77)]
CT-7 ²⁰	PMO45 [45A(+15+39)]	PMO46 [46D(+12-13)]	PMO47 ²⁰ [47A(+58+77)]
CT-7 ³⁰	PMO45 [45A(+15+39)]	PMO46 [46D(+12-13)]	PMO47 ³⁰ [47A(+53+82)]

To identify the PMO concentration required to achieve sufficient skipping a concentration titration with two additional total cocktail concentrations; 720 μM and 150 μM, was performed. These results reveal that while there is no defined dose-response below 250 μM, the higher 750 μM concentration induces up to 78% triple-exon skipping (Figure 5.10.b). We also note that the cocktail is more efficient with PMO47³⁰ than with PMO47²⁰. The CT-7³⁰ formulation induces both more triple-exon skipping and less intermediate transcripts (Figure 5.10.b).

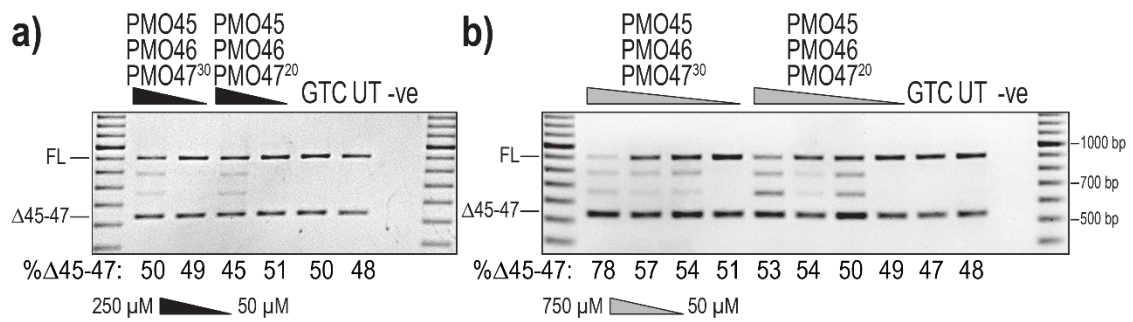


Figure 5.10: Optimisation of PMO concentration required to induce exon 45-47 skipping.

Two cocktails of PMOs targeting exons 45, 46 and 47 were nucleofected into MFS^{Δ45-47} patient fibroblasts at a total cocktail concentration of a) 250 μM and 50 μM or b) 750 μM, 250 μM, 150 μM and 50 μM. Concentrations are calculated in 20 μl transfection volume and are the total concentration of the cocktail containing equimolar amounts of each PMO. Treated cells were collected for RNA analysis after ten days. The full-length (FL) transcript is 914 bp, the triple exon skipping (Δ45-47) transcript is 548 bp. The values below each gel image indicate the percentage of exon 45 (Δ45) or 46 (Δ46) skipped transcripts in each sample. GTC: Gene Tools control PMO used as a sham treatment, UT: untreated control, -ve: RT-PCR negative control. 100bp molecular marker used for size reference.

Effect of triple-exon skipping on fibrillin1 fibre formation

Using the optimised cocktail; CT-7³⁰, and concentrations; 750 μM and 150 μM, both healthy control and MFS^{Δ45-47} patient fibroblasts were nucleofected then incubated for 4- or 10-days. Treated cells were collected for both RNA analysis and immunofluorescence staining, the results of which are shown in Figure 5.11.

As reported in previous chapters, exon skipping efficiency was reduced after ten days compared to the 4-day time point (Figure 5.11.a and b). The proportion of intermediate products, however, was greater after ten days. This increase in intermediate products could indicate that the single and double exon skipped transcripts are more readily produced or accumulate with time than the triple-exon skipped products. Another difference between the two time-points is the additional product present below the Δ45-47 transcript products at four days (Figure 5.11.a). This band was confirmed via Sanger sequencing to be lacking exons 45, 46, 47 and 48 (Δ45-48) in their entirety (Figure 5.11.a and d). The Δ45-48 transcript product is lost after ten days; this could mean that this product is either diluted by cell growth and lost due to low initial abundance, or susceptible to degradation.

Immunofluorescent staining of treated cells revealed the expected strong fibrillin-1 fibres in the untreated, and GTC treated healthy control cells (Figure 5.11.c.iii and iv). However, patient control samples presented with diffuse fibrillin-1 staining throughout the cells on the coverslip, with no fibre formation (Figure 5.11.c.vii and viii). In both healthy control and patient cells treated with either concentration of CT-7³⁰, a severe reduction in overall fibrillin-1 abundance was observed (Figure 5.11.c). This reduction was particularly noticeable in the 150 μM treated healthy control cells where no fibrillin-1 staining was observed (Figure 5.11.c.ii). The diffuse fibrillin-1

staining seen in the untreated patient cell line was also absent after PMO47 treatment (Figure 5.11.c.v and vi).

The treatment of either cell line with 750 μM of CT-7³⁰ resulted in the formation of fibrillin-1 aggregates. The morphology of these aggregates was dissimilar to fibrillin-1 fibres seen previously, with staining of low-intensity fibres linking ‘spots’ of high intensity (Figure 5.11.c.i, v and vi). The same staining pattern was observed in MFS Δ^{45-47} cells treated with 150 μM of CT-7³⁰, which is to be expected as they have a similar proportion of Δ^{45-47} transcripts; 78% and 77% for 750 μM and 150 μM respectively (Figure 5.11.a).

The efficiency of triple-exon skipping after four days; up to 78% (Figure 5.11.a), is lower than that achieved with PMO52 or PMO47, both of which result in the formation of fibrillin-1 fibres. This lower triple exon skipping efficiency, combined with intermediate skipping products, is likely why we see no fibrillin-1 fibre formation. We also note that while the triple-exon skipping is more efficient after 4-days, this time point is also associated with the presence of the Δ^{45-48} transcript product. The Δ^{45-48} transcripts account for up to 24%, and 18% of total transcripts in healthy control and MFS Δ^{45-47} fibroblasts respectively (Figure 5.11.a) and the resulting fibrillin-1 isoform; if synthesised, is likely to interact negatively with the other isoforms present.

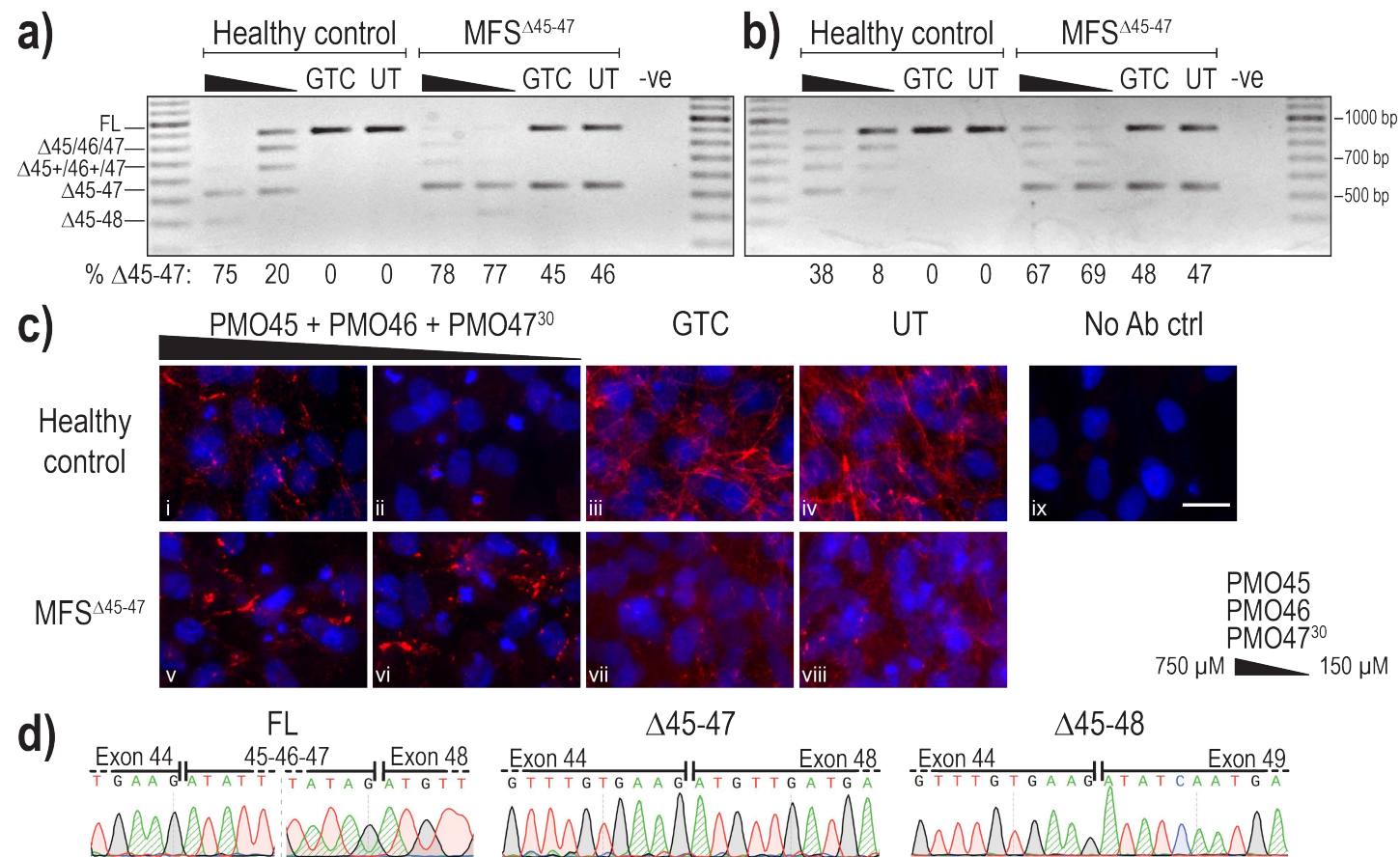


Figure 5.11: Evaluation of triple exon skipping mediated by a PMO cocktail.

Healthy control and MFS $\Delta45-47$ fibroblasts nucleofected with a cocktail of PMO45, PMO46 and PMO47³⁰, a Gene Tool control PMO (GTC) or left untreated (UT). Two concentrations were tested; 750 μ M and 150 μ M, calculated in the 20 μ l nucleofection cuvette volume. RT-PCR amplicons from cells collected a) 4 days and b) 10 days after transfection showing transcript products between *FBN1* exons 42 and 49. The values below each gel image indicate the percentage of $\Delta45-47$ transcripts in each sample. -ve: RT-PCR negative control. 100bp molecular marker used for size reference. c) Representative images of treated cells (4 days) stained for fibrillin-1 (red) and counterstained with Hoechst (blue) for nuclei detection. No Ab control: no primary antibody added. Scale bar = 20 μ m. See Figure A3.3 for a larger version of part c. d) Analysis of Sanger sequencing of the FL, $\Delta45-47$ and $\Delta45-48$ products confirming their identity.

5.7 Discussion

The application of AOs to alter exon selection to restore the reading frame, or re-establish homogeneity between fibrillin-1 proteins, has been discussed throughout this thesis. However, the focus has been on the removal of a single exon to overcome a mutation, in a personalised approach. This chapter explored the possibility of multi-exon skipping to increase the proportion of patients that would be amenable to a single therapeutic preparation. Here we report two strategies that could address mutations affecting exons 45, 46 and 47. The first, as previously described, is the more personalised approach of skipping each exon individually. The second strategy is to induce multi-exon skipping, the excision of all three exons simultaneously. If efficient triple exon skipping could be achieved and the resulting protein isoform was functional, this strategy would be amenable to 5% of total mutations; more than any single exon skipping approach.

This study had four key findings: (1) Fibrillin-1 exons 45 and 46 are challenging to skip; (2) Exon 47 is readily skipped, and its efficient removal results in the re-appearance of fibrillin-1 fibres; (3) While triple-exon skipping is possible, the current study was unable to demonstrate sufficient exon skipping in order to assess fibrillin-1 fibre formation and (4) A single mutation can result in multiple outcomes. While we show here that both single and triple-exon skipping are promising therapeutic strategies for MFS, there are many limitations to this study that in turn, limit the conclusions that can be made, including; inefficient skipping, imbalance in skipping efficiency, lack of synergistic AO effects, and unexpected exon skipping. These findings, limitations and future research directions are discussed in more detail below.

Imbalance in skipping efficiency

For the first time, we describe two *FBNI* exons that were not readily skipped with at least one of the initial AOs tested. Exons 45 and 46 proved extremely difficult to skip using 2'OMe-PS AOs, even when combined into two-AO cocktails. Calculation of the splice site scores for exons 45 and 46 revealed them to be average or above average for constitutive exons and of a similar strength to exon 47,²¹⁶ suggesting splice site strength is not the cause of the inefficient skipping observed here. However *in silico* analysis of the mRNA secondary structure of exon 45, 46 and 47 using the online tool, RNAfold.²¹⁷ shows the predicted effect of AO binding. The predicted structure of exon 45 mRNA is made up of hair-pin loops, to one of which PMO45 binds, indicating the AO must overcome strong secondary structures in order to anneal (Figure A3.4.a). The exon 46 mRNA has a similarly simple hair-pin loop structure (Figure A3.5.a). For both exons AO binding significantly alters the predicted structure leading to a more complex structure with additional hair-pin loops. We speculate that this altered secondary structure influences splicing

factor binding, limiting the efficacy of the AOs. Conversely binding of PMO47²⁰ does not appear to significantly alter the predicted exon 47 mRNA secondary structure (Figure A3.6)

An additional sequence was designed to target each exon, meaning almost the entire exon was assessed for AO target sites (Figure A3.1). However, no AO targeting either exon induced more than 10% skipping. Despite evaluating the majority of the exon sequence, the ‘optimal’ AO sequence was not identified. A strategy that evaluates the entire exon for all possible AO target sites would reveal the most efficient sequence. However, there are 149 possible 25-mers across exon 45 alone, adding 25 bases of flanking intron at the donor and acceptor sites, and considering limitation on resources make this approach unfeasible. Nevertheless, further optimisation of the sequences targeting exons 45 and 46 is undoubtedly required. Identification of a more efficient AO could both enable comparison between single and multi-exon skipping and increase multi-exon skipping efficiency. However, it needs to be noted that AO-mediated exclusion is not necessarily applicable to every one of the 60 in-frame *FBNI* exons and therefore the cost of investigation must be weighed against the benefits to determine practical targets.

Contrary to the minimal skipping efficiency of AOs targeting exons 45 and 46, exon 47 was much more readily skipped. Of the nine AOs tested in total, seven AOs induced exon skipping, albeit at different efficiencies. In particular, the AO47.2 and PMO47 sequence was found to induce extremely efficient exon 47 skipping in both healthy control and patient fibroblasts. Not only was the exon 47 skipping efficient but immunofluorescent staining of treated cells mirrored that seen when skipping exon 52. Fibrillin-1 fibre formation was lost entirely after approximately 50% skipping of exon 47 was induced, and then fibres were able to be formed when more than 80% exon skipping was induced. These results further support the concept that identical fibrillin-1 monomers can assemble into fibres despite being internally truncated.

The imbalance in skipping efficiency between the three exons is the likely cause of the intermediate transcript products we observe. One way Adams et al.¹⁶⁷ achieved greater multi-exon skipping was by altering the ratios of each AO in the cocktail, increasing or decreasing the amount of an AO depending on its ability to skip targeted exons. Changing the AO ratio resulted in fewer intermediate products with skipping of just one exon and a higher proportion of the desired transcript.¹⁶⁷ The same could be applied to the *FBNI* AOs discussed here. By increasing the ratio of PMO45 and PMO46 in relation to PMO47, the overall triple-exon skipping efficiency could be improved.

An additional question left unanswered by this study is; are different ratios of AOs required for different mutation types and mutations in each of the three exons? In both the healthy control and *MFS*^{Δ45-47} models used, each exon is present at equal levels in the endogenous transcript. However, treatment of *MFS*^{Δ47} may require a different ratio of exon 47 to exon 45 and 46 AOs to be effective, since only ~50% of the transcripts contain exon 47. If a different ratio is required,

the multi-exon skipping approach is unlikely to be an effective therapeutic strategy; therefore, these factors need to be fully explored.

Absence of AO synergy

Based upon earlier DMD exon skipping studies, some AO sequences are known to work synergistically when combined, while others work additively or even antagonistically.¹⁶⁷ However, it is unknown what characteristics of the AO influence this relationship. The PMO45, PMO46 and PMO47³⁰ sequences used here do not appear to have a synergistic relationship when combined into a cocktail. A high concentration of each AO is required to achieve relatively efficient skipping of its respective exon. The initial exon skipping attempt with the PMO cocktail at a total concentration of 250 μ M, which was effective for PMO47, PMO52 and PMO59, was inefficient when attempting to induce triple exon skipping. The AOs discussed here may lack synergy due to their individual inefficiencies, however, Adams et al.¹⁶⁷ reported that synergistic cocktails do not always result from the most efficient AOs and that two ineffective AOs can work synergistically. We speculate this is due to one AO binding and altering the mRNA secondary structure sufficiently to allow the second AO to bind to its target. However, it is also probable that AO synergy works differently when the AO sequences target different exons. As discussed previously, one of the most effective and achievable ways to increase AO efficiency and possibly synergy is optimising the sequences themselves or altering the ratios of each AO in the cocktail.

Apart from the clear requirement for extremely efficient exon skipping to create a homogenous population of fibrillin-1 proteins, increasing AO efficiency and synergy could allow for the use of lower cocktail concentrations. The high concentration of PMOs used in this study would lead to more expensive treatment and an increased risk of off-target and side effects. Currently approved AO therapies for DMD cost upward of \$US300,000 per year^{218,219} meaning every effort should be made to increase efficiency and decrease the cost of these drugs. A longer AO length decreases the likelihood of the AO being complimentary to a sequence other than its intended target and has been linked with increased activity,²²⁰ however, shorter AOs are more cost effective to synthesise. Here we demonstrated that the 30-mer version of PMO47 was more effective at mediating triple-exon skipping along with PMO45 and PMO46. However, the 20-mer PMO47 sequence was extremely efficient at inducing skipping of exon 47 alone. In circumstances where 20-mer and 30-mer AO sequences result in a similar exon skipping efficiency, other considerations such as cost, and ease of synthesis become more relevant.

Functionality of fibrillin-1 ^{Δ 45-47}

Fibrillin-1 exons 45, 46 and 47 all encode for cbEGF-like domains. The cbEGF-like domains bind to calcium, essential for fibrillin-1 stabilisation, tertiary structure, protein-protein interactions and protection against proteolysis.^{21,221,222} Calcium-binding relies on the structure of

a cbEGF-domain that in-turn is determined by the disulphide bonds formed between conserved cysteine residues within each domain.^{214,222} It is well established that heterozygous mutations affecting these domains; generally associated with disrupting domain structure and calcium-binding, cause MFS.^{2,3} However the function and stability of the fibrillin-1^{Δ45-47} isoform in the presence only of other fibrillin-1^{Δ45-47} monomers is unknown.

The results of this study are unable to demonstrate that the fibrillin-1^{Δ45-47} protein is functional. The skipping achieved was insufficient to result in only one fibrillin-1 isoform; thus, no fibre formation was observed. However, we did show that efficient removal of exon 47 does result in fibre formation, suggesting possible redundancy in the cbEGF-like domains. However, further functional analysis of the internally truncated proteins produced is required to determine if they can perform their other functions such as interaction with microfibril associated proteins and regulation of TGF-β.

Homozygous mutations could provide insight into the effect of 100% exon skipping. However, no homozygous deletions of this region, or any similar region, have been reported; therefore, the resulting phenotype is unknown if there is one. Of the ten reported homozygous *FBNI* mutations associated with MFS, none are deletion mutations.^{3,223} Two of the homozygous mutations reported affect the first base of an exon; c.6998A>C³ and c.7454A>T³² potentially altering pre-mRNA splicing. The c.6998A>C mutation was never studied at the cDNA level, so it is unknown if this mutation results in altered splicing. However, Hilhorst-Hofstee et al.³², confirmed that the c.7454A>T mutation did not result in aberrant mRNA splicing. The lack of homozygous deletions and splicing mutations could be explained by one of the following; they have yet to be identified due to low frequency of homozygous mutations, they are embryonic lethal, or they do not result in an MFS phenotype.

Unexpected exon 48 skipping

The majority of transcript products observed when efficiently inducing triple-exon skipping was the expected Δ45-47 product; however, an additional splicing product was also created. This transcript was confirmed to result from exon 45-48 skipping. The Δ45-48 transcript maintains the reading frame and is therefore capable of being translated into a protein. The presence of the Δ45-48 and Δ45-47 transcript products, along with traces of full-length, single-exon skipping and double exon skipping products means there are up to nine different transcripts generated. Each transcript could be translated into a different fibrillin-1 isoform, each interacting negatively with one another. The expected outcome of which is the absence of fibrillin-1 microfibril formation precisely as we observed.

One possible mechanism for this unexpected exon skipping is non-sequential intron removal. The supraspliceosome model outlined by Shefer et al.²²⁴ suggests that the supraspliceosome is

composed of four active spliceosomes connected by a single pre-mRNA, enabling the splicing of four introns simultaneously. However, intron removal is not necessarily in numerical order.²²⁴ Following this model the removal of introns 47 and, or 48 may occur prior to introns 45 or 46 and as a consequence exon 48 is removed along with the exon 45-47 region. The order of removal for the introns in the *FBNI* exon 45-48 region could be assessed using a method outlined by Kessler et al.²²⁵ and recreated by Ham et al.²²⁶. By determining the order of intron removal, we might reveal the mechanism behind the unexpected exclusion of exon 48 that we observe.

The skipping of exon 48 without being targeted by an AO is interesting as it mirrors a study described by Aartsma-Rus et al.²⁰⁹ in which a two AO cocktail was sufficient to induce skipping of a seven-exon region at very low levels; 45-51, in the *DMD* gene. We evaluated a similar strategy to induce the skipping of exons 45-47 with AOs targeting only exons 45 and 47. However, consistent with the *DMD* example this strategy was ineffective, resulting only in single and double exon skipping. This strategy may only apply to ready skippable exons or those AOs that naturally induce multi-exon skipping despite having only a single target. Therefore, skipping of the exon 45-47 region with only two AOs, considering the recalcitrant nature of exons 45 and 46 and poor triple-exon skipping with three AOs, is unlikely to be a viable strategy.

The ability to induce exon 48 skipping without a specific AO targeting the exon, suggests that exon 48 is potentially highly amenable to the splice-stitching strategy. Determining which of the PMOs in CT-7³⁰ leads to exon 48 exclusion could also prove useful. If occurring due to a single PMO, changing this AO sequence could abolish the quadruple-exon skipping effect decreasing the number of undesired transcripts. Alternatively increasing the proportion of exon 45-48 skipped transcripts could allow for the treatment of patients with mutations in any of these four exons. Reducing the number of AOs required in a cocktail could also allow for more manageable cocktail concentrations with more efficient skipping results. Major challenges for multi-exon skipping strategy will include safety testing and the requirement for approval of multiple sequences, especially when some AOs would not be necessary for some mutations. The multi-exon skipping strategy is very ambitious and may prove impracticable, especially for *FBNI*, however, testing our hypothesis led to the identification of a promising candidate for exon 47 and demonstrated that the concurrent skipping of multiple *FBNI* exons is possible.

Alternate mutation outcome

The mutation harboured by MFS^{A47}; c.5788+5G>A splicing mutation resulting exon 47 skipping, was one of the first recurrent mutations to be identified and reported in over 30 different cases making it the second most frequent mutation.^{2,3} In this study, we determined that the outcome of this splice site mutation, in this particular patient cell line, is twofold with the co-occurrence of the expected skipping of exon 47 as well as retention of exon 47, with a 33 base

insertion of intron 47 (*FBNI*^{+33b}). This insertion is in-frame and is predicted to result in eleven additional amino acids between the 28th and 29th cbEGF-like domains.

We suggest that this aberrant splicing results from activation of a predicted cryptic donor splice site within intron 47.²¹⁵ *In silico* analysis comparing the ‘strength’ of the natural, c.5788+5G>C and predicted cryptic donor sites showed that the mutation results in the expected decrease in consensus value of more than 10% signifying the sites disruption (Table A3.1).²¹⁵ Furthermore the ‘strength’ of the cryptic splice site (82%) confirms that it is likely able to be utilised as a donor splice site.²¹⁵ The same cryptic splicing and 33 base insertion has been described previously, however, was associated with a c.5788+1 mutation.²²⁷ This was the first, and largest, reported *FBNI* cryptic splicing event that results in a stable fibrillin-1 protein with additional amino acids.²²⁷ To our knowledge, there are no reports of co-existence of the *FBNI*^{Δ47} and *FBNI*^{+33b} transcripts nor the fibrillin-1 isoforms they encode.

The co-existence of these splicing products is predicted to further exacerbate the Marfan phenotype in this patient. Hutchinson et al.²²⁷ showed that the 33 base insertion leads to the delayed secretion of resulting fibrillin-1 isoform. The synthesis of the fibrillin-1 isoform encoded by the *FBNI*^{+33b} transcript is also mildly reduced; to 89% of the healthy control¹⁸³ together these findings suggest the mutation results in haploinsufficiency. However, in this patient the mutation is classified as group IV since it results in a severe reduction in fibrillin-1 deposition in the extracellular matrix; 11% of the healthy control.^{69,183} These findings combined demonstrate characteristics of both the haploinsufficiency and dominant negative pathogenesis models. Encouragingly PMO47 appears to target the cryptic splicing product with equal affinity as to the full-length. Thus, treatment of MFS^{Δ47} with PMO47 results in the complete elimination of the *FBNI*^{+33b} transcript products.

Conclusions

This chapter showed that triple-exon skipping can be achieved *in vitro*, albeit requiring a higher concentration than single exon skipping. Due to disruption by several undesired intermediate splicing products, we could not confirm if the fibrillin-1^{Δ45-47} isoform is capable of forming fibres. However, we did demonstrate that much like exon 52, skipping of exon 47 alone is both efficient and results in the formation of fibrillin-1 fibres in MFS^{Δ47} patient cells. While these results do not discount the multi-exon skipping strategy, they provide even more support for the single skipping approach. For MFS, multi-exon skipping is an ambitious strategy. Further optimisation to produce an ideal AO cocktail could allow for the treatment of many more mutations with fewer drugs making it a worthwhile path to pursue, however, this is not currently viable. Overall this chapter provides additional evidence for the applicability of antisense oligonucleotides in treating the type-1 fibrillinopathies.

Chapter 6
Alternative Targets and
Antisense Oligonucleotide Chemistries

6.1 Introduction

6.1.1 Fibrillin-1 structure and potential targets

In this thesis so far, we have discussed successful development of antisense oligonucleotides (AO) sequences targeting exons 47, 52, 59 and 45-47 of the fibrillin-1 gene (*FBNI*). However, the nature of this splice-switching strategy means that a different AO is required for each targeted exon. Assuming 100% effectiveness for all mutation types, which we acknowledge is unrealistic, the AOs described in previous chapters are effective against approximately 7.7% of all fibrillin-1 mutations. However, *FBNI* is a large gene spanning over 200Kb with an 8613 base coding sequence separated into 65 exons.⁶ Disease-causing mutations are found in all 65 exons and are distributed relatively evenly across the gene. Therefore, other amenable exons should be identified to develop a suite of optimal AO sequences.

To reiterate, the domain structure of fibrillin-1 is highly repetitive. Fibrillin-1 consists of a large number of cysteine-rich domains, including four epidermal growth factor-like (EGF-like) domains, 43 EGF-like domains with an additional calcium-binding motif (cbEGF-like), seven TGF- β binding protein-like (TB) domains and two hybrid-domains^{20,21} (Figure 6.1). While each domain's exact functions are unknown, the various domain types have been associated with different features of the fibrillin-1 protein.^{22,23,228}

The interaction of the cbEGF-like domains and calcium is essential for the stability of fibrillin-1 and protection from proteolysis.²³ Due to the abundance of cbEGF-like domains, most fibrillin-1 mutations occur in these domains, many of which directly affect their ability to bind to calcium.^{2,3} Thus far, all the exons targeted in this thesis; except exon 52, encode cbEGF-like domains. These exons were initially chosen due to the abundance of the cbEGF-like domain that indicates the possibility of functional overlap and thus redundancy. The skipping of these exons has been relatively efficient, and some formation of fibrillin-1 fibres has been observed. Therefore, we designed AOs to target additional cbEGF-like domains encoded by in-frame exons 15, 16, 26, 27, 31, 32, 44, and 49 (Figure 6.1).

The fibrillin-1 protein contains seven TB domains encoded by a total of 12 exons. Little is known about the exact function of the TB domain. However, they have been associated with the construction of the extracellular matrix and storage of latent TGF- β .²²⁸⁻²³⁰ These two functions are essential for the extracellular matrix's stability and, consequently mutations in these domains have been associated not only with Marfan syndrome, but also non-marfanoid type-1 fibrillinopathies such as acromicric dysplasia.^{3,57} We note that exon 52, which encodes the C-terminal portion of the 6th TB domain, is readily skipped and its efficient removal results in re-appearance of fibrillin-1 fibres in a patient cell line carrying a splicing mutation. To accomplish

similar outcomes elsewhere in the fibrillin-1 molecule, we designed AOs targeting exon 39 that makes up the C-terminal portion of the 4th TB domain (Figure 6.1).

Lastly, the third type of cysteine-rich motif is the hybrid domain. Fibrillin-1 consists of two hybrid-domains that share similarities with both the EGF-like and TB domains.²¹ The hybrid domains have been shown to play an integral role in fibrillin-1 folding and microfibril assembly.^{21,22} The effect of exon skipping of this target has not yet been described. Therefore, we designed AOs targeted to exon 22 that encodes the N-terminal portion of the second hybrid domain to investigate the outcome (Figure 6.1).

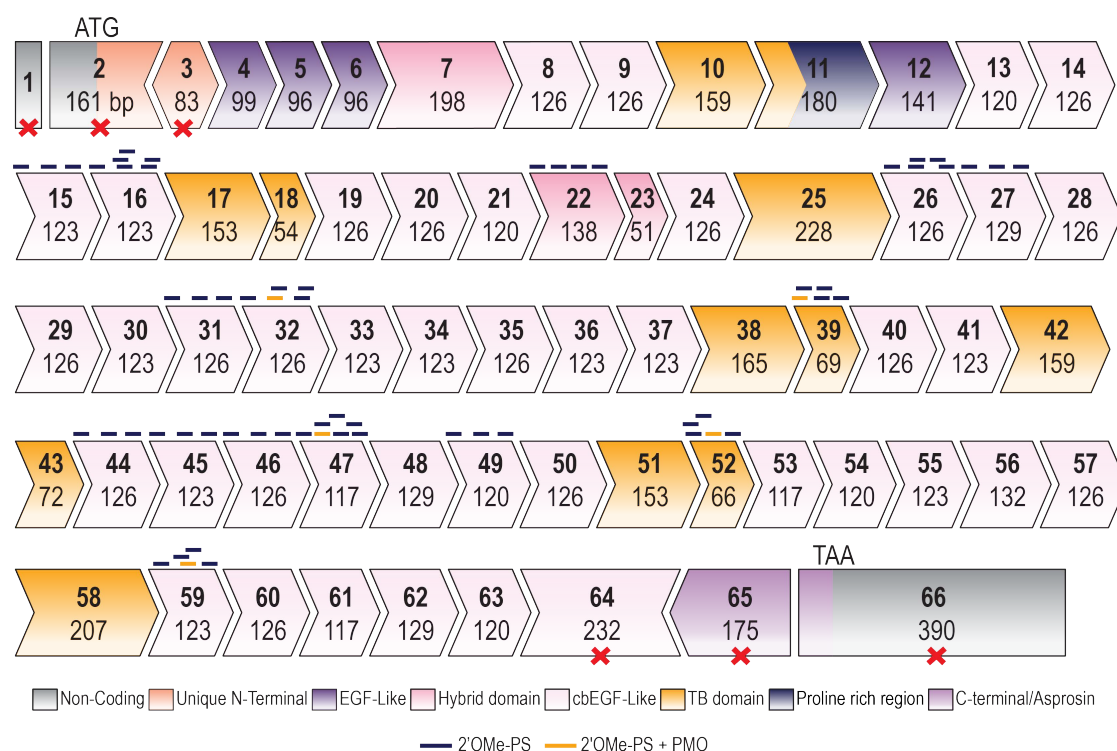


Figure 6.1: Fibrillin-1 gene map.

Each box indicates an exon with the exon number and exon length in bases shown inside. Chevron sides indicate exons bounded by partial codons. The domain encoded by each exon is indicated by coloured fill. Exons denoted by a red cross are not amenable to splice-switching strategies as their removal would disrupt the reading frame or contains the start codon or stop codon. Black bars indicate the approximate binding sites of AOs tested with the 2'OMe-PS chemistry, Yellow bars indicate those AO that were tested as both 2'OMe-PS and PMO.

6.1.2 Antisense oligonucleotide chemistries

Antisense oligonucleotides are versatile tools that can be utilised to manipulate gene expression in several ways, depending on the chemistry. RNase-H dependent chemistries are generally used to induce transcript degradation and the “classical” antisense down-regulation approach.^{108–110} However, this thesis focuses on RNase-H independent chemistries that can anneal to and physically block motifs in the target sequence to redirect splicing.¹¹³ This class of steric blocking AO can mediate exon inclusion¹⁰⁵ or exclusion,^{106,107} induce transcription inhibition¹¹¹ or inhibit translation.¹¹²

The 2'OMe-PS and PMO chemistries have been the focus of this thesis due to their respective advantages in the screening process and *in vivo* or clinical setting. The phosphorothioate (PS) backbone modification was introduced to overcome the high susceptibility of the phosphodiester backbone to nucleases, that generally resulted in AOs with a very short half-life.²³¹ The replacement of the non-bridging oxygen with sulphur to form the PS backbone confers greater stability to the AO, thereby increasing its half-life. The negative charge of the PS backbone allows for relatively efficient cellular uptake in a variety of cell type *in vitro*.²³² The PS backbone also increases AO affinity for serum proteins such as heparin, allowing the AO to be maintained in circulation for longer and delaying its removal by the liver.¹¹⁷ However, this protein binding and other off-target effects have been associated with increased toxicity.^{113,118}

The PS backbone modification can be used in combination with the 2'-*O*-methyl (2'OMe), modification to the sugar moiety, producing the 2'OMe-PS chemistry (Figure 6.2). This 2' modification engenders RNA properties and results in an increased affinity of the AO for the target and increased nuclease resistance, further extending the AO half-life. Another key feature is the inability of 2'-modified AOs to recruit and induce RNase-H activity.^{233,234} This RNase-H independence eliminates the applicability of the AO to RNase-H mediated RNA downregulation, but enhances their steric blockade applications.

The PMO chemistry is of particular interest for this study due to the high binding affinity,¹¹³ specificity,^{118,122} nuclease resistance¹²¹ and importantly, excellent safety profile.¹²³⁻¹²⁵ The PMO chemistry replaces the deoxyribose sugar and negatively charged backbone with morpholine rings, joined by phosphorodiamidate linkages (Figure 6.2).¹²⁰ The neutral charge of the PMO chemistry allows the AO to bind to RNA or DNA with higher specificity and affinity, while not recruiting RNase-H, thereby making these compounds excellent steric blockers. Due to these advantages, and their incredible stability, PMOs have been studied extensively in animal models and clinical trials, and are recognised as both safe and effective in a clinical setting.¹²³⁻¹²⁵ On the other hand, the neutral charge leads to decreased plasma half-life and inefficient cellular uptake.¹¹³ Nevertheless several PMO compounds have received accelerated approval for DMD.^{140,142,164} These PMOs are well tolerated, even at the relatively high doses used.^{144,235} In addition, among other strategies, PMOs can and have been conjugated with cell penetrating peptides that have proven very efficient at increasing the delivery of the PMO to target tissues.^{236,237} Clinical trials are currently underway for peptide conjugated PMO compounds for the treatment of DMD.^{238,239}

This chapter investigates a third more recently described chemistry called the Thiophosphoramidate Morpholino Oligomer (TMO). The TMO chemistry incorporates features of both the PMO and 2'OMe-PS chemistries to form a morpholino-PS hybrid (Figure 6.2). The use of a thiophosphoramidate backbone, rather than a phosphorodiamidate backbone, allows the oligomer to be more readily generated on conventional nucleic acid synthesisers, and enables the

incorporation of other chemical modifications such as 2'OMe, 2'-O-methoxyethyl.²⁴⁰ The morpholine ring rigidity results in high affinity for RNA and the combination of morpholino bases and phosphorothioate linkages results in excellent stability against nucleases. While the synthesis, stability and pharmacokinetics of this AO chemistry are now more established,²⁴⁰ the chemistry is still relatively new. Therefore, we aim to evaluate the efficiency of TMOs at inducing fibrillin-1 exon skipping and compare this chemistry to both the 2'OMe-PS and PMO chemistries used previously.

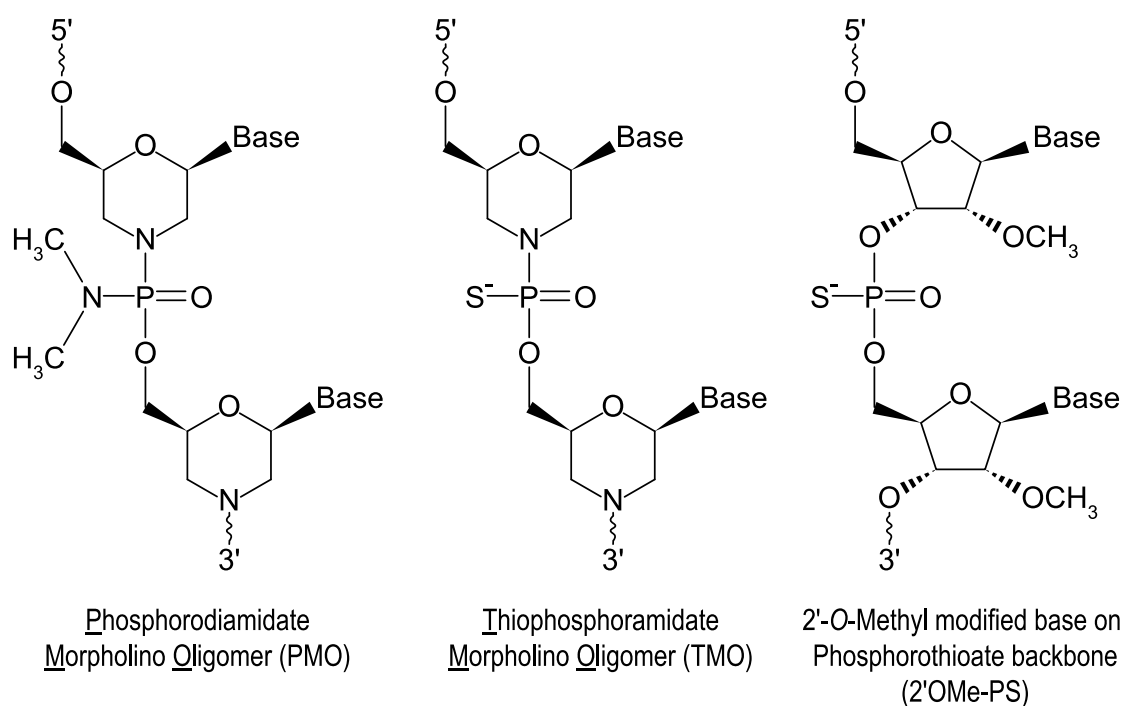


Figure 6.2: Chemical representation of PMO, TMO and 2'OMe-PS compounds

Figure modified from Langner et al.²⁴⁰ and Kole and Krieg²⁴¹

6.2 Additional *FBN1* targets

6.2.1 Antisense oligonucleotide design

To minimise screening costs, three AOs were designed for each targeted exon for the initial screen. In general, one AO was designed to cover each of the canonical splice sites and a third AO designed to target a region predicted to be rich in ESE sites. Upon the identification of strong exon skipping potential, further overlapping sequences were designed around the most efficient AO. As previously, two unrelated sequences were used as a sham control, one for each chemistry. These controls allow for the assessment of any sequence-independent chemistry-related effects. All AOs tested in this chapter are described in Table 6.1. Exon sequence maps showing the AO binding sites in relation to enhancer and silencer motifs predicted by SpliceAid¹⁵³ are presented in the supplementary Figure A4.1.

Table 6.1: List of antisense oligonucleotides used in Section 6.2

The target exon, name, ID, Sequence and chemistry of the AOs screened in Section 6.2. The AO nomenclature is outlined in Chapter 2, Figure 2.1. The AOs targeting exons 15, 27, 31, 44 and 49 were designed by Mr Kane Greer (unpublished, 2017).

AO name (FBN1 H...)	ID	Sequence (5'-3')	Chemistry
Exon 15			
15A(-15+10)	AO15.1	UCA UCC AUA UCU GAA AAU ACA AAA C	2'OMe-PS
15A(+41+65)	AO15.2	ACU GCC AUC UUC AUU GAU ACA CAU U	2'OMe-PS
15D(+12-13)	AO15.3	UUA UAG CAC GAA CCU UUG CAA UAA C	2'OMe-PS
Exon 16			
16A(-14+11)	AO16.1	CUC GUU AAU GUC UGU GGC AGA GAA A	2'OMe-PS
16A(+27+51)	AO16.2	UGA CGC AAC GCC CAU UCA UGC AGA U	2'OMe-PS
16D(+14-11)	AO16.3	UGU UUU CUU ACC AAC ACA CAC ACG G	2'OMe-PS
16A(+22+46)	AO16.2+5	CAA CGC CCA UUC AUG CAG AUC CCA G	2'OMe-PS
16A(+32+56)	AO16.2-5	AGU GUU GAC GCA ACG CCC AUU CAU G	2'OMe-PS
16D(+09-16)	AO16.3-5	CAU GAU GUU UUC UUA CCA ACA CAC A	2'OMe-PS
Exon 22			
22A(-13+12)	AO22.1	CCU UGA UGG UUU CUG CAG AGG AGG G	2'OMe-PS
22A(+45+69)	AO22.2	UGG CUC CAU UGA UGU UGA UCU CAC A	2'OMe-PS
22A(+84+108)	AO22.3	CAC GCA GCA CCG AGG GAG GAG CAG C	2'OMe-PS
22D(+16-09)	AO22.4	UUC UCU UAC CAA CUU GGC AUA GGG U	2'OMe-PS
Exon 26			
26A(-18+07)	AO26.1	UUG AUA UCU UCA AGA AUA AGA AAA U	2'OMe-PS
26A(+70+94)	AO26.2	AAG CCG CUG UCA CAC CUG CAC UUA A	2'OMe-PS
26D(+22-03)	AO26.3	GAC CUG UGC AGU UCC UUU CUU CAG A	2'OMe-PS
26A(+75+99)	AO26.2-5	GAG CAA AGC CGC UGU CAC ACC UGC A	2'OMe-PS
26A(+100+124)	AO26.3+5	GUG CAG UUC CUU UCU UCA GAA UCA A	2'OMe-PS
Exon 27			
27A(-25-01)	AO27.1	CUG CAC AAA AAC AGC AAG UGG CAG C	2'OMe-PS
27A(+38+62)	AO27.2	AGG GGU GUU CAC ACA CUG GCC UCU G	2'OMe-PS
27A(+105+129)	AO27.3	CCA UGC AGU UCU UCA UCA UCA UGA A	2'OMe-PS
Exon 31			
31A(-21+04)	AO31.1	AUG UCU GCA AAG AAU AAA ACC AAC A	2'OMe-PS
31A(+76+100)	AO31.2	GCC AUG AAU CCA UCA UAA CAC AAG C	2'OMe-PS
31D(+13-12)	AO31.3	UUC UUU GCU UAC CUA CAC AAG UCU U	2'OMe-PS
Exon 32			
32A(-13+12)	AO32.1	ACU CAU UGA CAU CUG UAA AAC AUA U	2'OMe-PS
32A(+47+71)	AO32.2	AAA UGA GCC UUU CGU GUU UUC ACA G	2'OMe-PS
32A(+47+71)	PMO32	AAA TGA GCC TTT CGT GTT TTC ACA G	PMO
32D(+14-11)	AO32.3	AAC AAA CAC ACC UGU ACA GCC AGU U	2'OMe-PS
32A(+42+66)	AO32.2+5	AGC CUU UCG UGU UUU CAC AGG UCC C	2'OMe-PS
32D(+09-16)	AO32.3-5	ACU UGA ACA AAC ACA CCU GUA CAG C	2'OMe-PS
32A(-08+17)	AO32.1-5	GUC ACA CUC AUU GAC AUC UGU AAA A	2'OMe-PS
32A(+52+76)	AO32.2-5	CAG AUA AAU GAG CCU UUC GUG UUU U	2'OMe-PS
32D(+19-06)	AO32.3+5	ACA CAC CUG UAC AGC CAG UUU UUC C	2'OMe-PS
Exon 39			
39A(-12+13)	AO39.1	AUU UUG UAC UCG GCU AUU GAA ACA A	2'OMe-PS
39A(-12+13)	PMO39	ATT TTG TAC TCG GCT ATT GAA ACA A	PMO
39A(+31+55)	AO39.2	GUG AUA GGA UUU GGU CGG AAA CCU U	2'OMe-PS
39D(+04-16)	AO39.3	AAG GAA ACA CAA UUA CCU UC	2'OMe-PS
39A(-07+18)	AO39.1-5	AAA GAA UUU UGU ACU CGG CUA UUG A	2'OMe-PS
39A(+36+60)	AO39.2-5	UAA CGG UGA UAG GAU UUG GUC GGA A	2'OMe-PS
39A(+13+37)	AO39.4	AAA CCU UCC CCU CCA GGA CAA AGA A	2'OMe-PS
39D(+16-09)	AO39.5	CAC AAU UAC CUU CCA AUA UAA CGG U	2'OMe-PS
Exon 44			
44A(+14+38)	AO44.1	UUC ACA GAC CCC UGG GAU CUC CCG G	2'OMe-PS
44A(+44+68)	AO44.2	GCU GCC AAC CAU GUU GAU ACA CAC U	2'OMe-PS

44D(+19-06)	AO44.3	ACU UAC CUU CAC AAA CCA ACA ACU U	2'OMe-PS
Exon 49			
49A(-13+12)	AO49.1	AUU CAU UGA UAU CUG CAA AGA AAA G	2'OMe-PS
49A(+19+43)	AO49.2	CCU GGU GCA CAU UUU CUG GGU UCU A	2'OMe-PS
49A(+83+107)	AO49.3	AUU UUG AAG ACU GUA UCC AGG UGG G	2'OMe-PS
Control AOs			
Unrelated Control	Ctrl	GGA UGU CCU GAG UCU AGA CCC UCC G	2'OMe-PS
GeneTools control	GTC	CCT CTT ACC TCA GTT ACA ATT TAT A	PMO

6.2.2 Screening of 2'OMe-PS AOs

Evaluation of the exon skipping activity of 2'OMe-PS AOs was performed in healthy control fibroblasts. Fibroblasts were transfected using Lipofectamine 3000 with two AO concentrations; 200 nM and 50 nM, and cells were collected 24 hours after addition of the 2'OMe-PS AOs. The results of this screening are shown in Figure 6.3. The RT-PCR results revealed that for five of the ten exons targeted (15, 16, 27, 31 and 49), a single AO was not sufficient to mediate exon skipping at the transfection concentrations used (Figure 6.3). Through the use of two AO cocktails, exons 15, 16 and 31 were able to be excised from the mature mRNA, albeit at a very low efficiency for both exons 15 (8%; Figure 6.3.a) and 31 (14%; Figure 6.3.f), and marginally more efficient for exon 16 (22%; Figure 6.3.b). Exons 27 and 49 could not be skipped with any of the single AOs or cocktails tested (Figure 6.3.e and j).

Conversely, skipping of exons 22, 32 and 39 was relatively efficient using either single AOs or cocktails. A total of four AOs targeting exon 22 were tested, two of which induced moderate levels of exon 22 skipping. The AO22.2 sequence was the most efficient, inducing up to 32% skipping (Figure 6.3.c). The lower AO concentration; 50 nM, induced more efficient exon skipping than the higher concentration, a phenomenon observed several times during our AO evaluation studies (Figure 6.3). The combination of AO22.2 with either AO22.1 or AO22.3 was counter-productive and inhibited exon 22 exclusion (Figure 6.3.c). The combination of AO22.4 and AO22.2 resulted in a marginal increase in skipping efficiency, increasing the proportion of skipped products to 36% (Figure 6.3.c).

For exons 32 and 39, all three 'first generation' AOs tested induced some level of exon skipping. The AOs targeting exon 39 were relatively efficient, with all three inducing more than 30% skipping (Figure 6.3.h). The AO32.2 and AO39.1 sequences were the most efficient inducing up to 36% and 43% skipping of their respective target exon (Figure 6.3.g and h). Combining any two exon 32 AOs into a cocktail was also effective resulting in either additive or synergistic levels of exon skipping. The cocktail of AO32.1 and AO32.2 that induce 7% and 36% skipping at 50 nM, respectively, induced an additive 50% exon 32 skipping after transfection at 100 nM (Figure 6.3.g). The combination of AO32.1 and AO32.3 that induced 7% and 11% exon skipping at 50 nM respectively, was synergistic, resulting in 42% skipping after transfection at 100 nM (Figure 6.3.g). Conversely, at the 400 nM transfection concentration, the effect of combining two AOs

targeting exon 39 into cocktails was not evident. All three cocktails targeting exon 39 resulted in similar skipping efficiencies to the individual AOs that were transfected at 200 nM (Figure 6.3.h). Furthermore, the lower total cocktail concentration of 100 nM resulted in a higher level of exon 39 skipping than 400 nM (Figure 6.3.h).

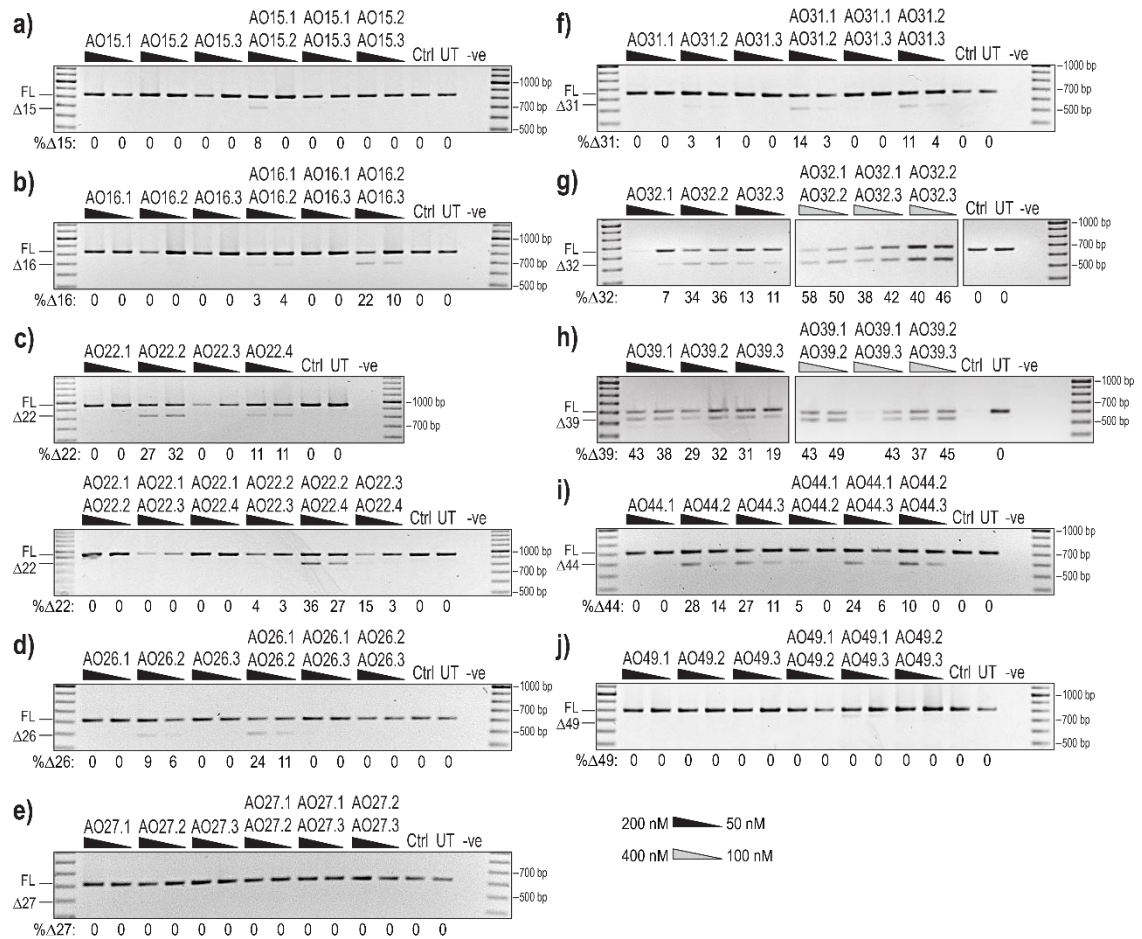


Figure 6.3: Evaluation of 2'OMe PS AOs targeting specific *FBN1* exons for removal.

AOs were transfected as lipoplexes at two concentrations, 200 and 50 nM, except for the exon 32 and exon 39 cocktails that were transfected at total AO concentrations of 400 nM and 100 nM. RT-PCR amplification was used to amplify the appropriate region of the fibrillin-1 mRNA and gel fractionation of products revealed the following transcripts (a) Ex 13-20 FL=843 bp, Δ 15=720bp, (b) Ex 13-20 FL=843 bp, Δ 16=720 bp, (c) Ex 19-27 FL=969 bp, Δ 22=831 bp, (d) Ex 24-28 FL=628 bp, Δ 26=502 bp, (e) Ex 24-28 FL=628 bp, Δ 27=499 bp, (f) Ex 29-34 FL=670 bp, Δ 31=544 bp, (g) Ex 29-34 FL=670 bp, Δ 32=544 bp, (h) Ex 37-42 FL=618 bp, Δ 39=549 bp, (i) Ex 42-48 FL=720 bp, Δ 44=594 bp, j) Ex 46-53 FL=812 bp, Δ 49=692 bp. The values below each gel image indicate the percentage of transcript from which the target exon has been skipped. Ctrl: an unrelated sequence used as a sham treatment, UT: untreated control, -ve: RT-PCR negative control. 100bp molecular marker used for size reference.

Micro-walking around the AO target site and additional sequence design

In an attempt to further optimise the efficiency of excising targeted exons, additional AOs were designed around the existing target sites. Micro-walking AO sequences, shifted up or downstream of an existing AO target site while maintaining the same AO length, are labelled as -5 or +5 indicating a sequence shifted five bases upstream (moved 5'), or downstream (moved 3') respectively.

Three additional AOs were designed to target exon 16 by micro-walking around AO16.2 and AO16.3. None of the additional, 'second generation' sequences induced any exon skipping, meaning that of six AOs targeting this exon, none were effective when used individually (Figure 6.4.a). Two additional AOs were designed to target exon 26, one shifted upstream of AO26.2 the other downstream of AO26.3, AO26.2-5 was much more efficient than the original AO26.2 inducing up to 26% exon skipping (Figure 6.4.b). Lastly, five additional AOs targeting exon 32 were designed by micro-walking around all three original AO target sites. Except for AO32.3-5, each of these AOs induced 32 skipping with equal or greater efficiency to the original. The AO32.1-5 and AO32.3+5 sequences were both more efficient than their respective original sequences (Figure 6.4.c). The sequences designed by micro-walking around AO32.2 induced similar skipping efficiencies, with 37%, 34% and 33% exon 32 skipping, respectively (Figure 6.4.c).

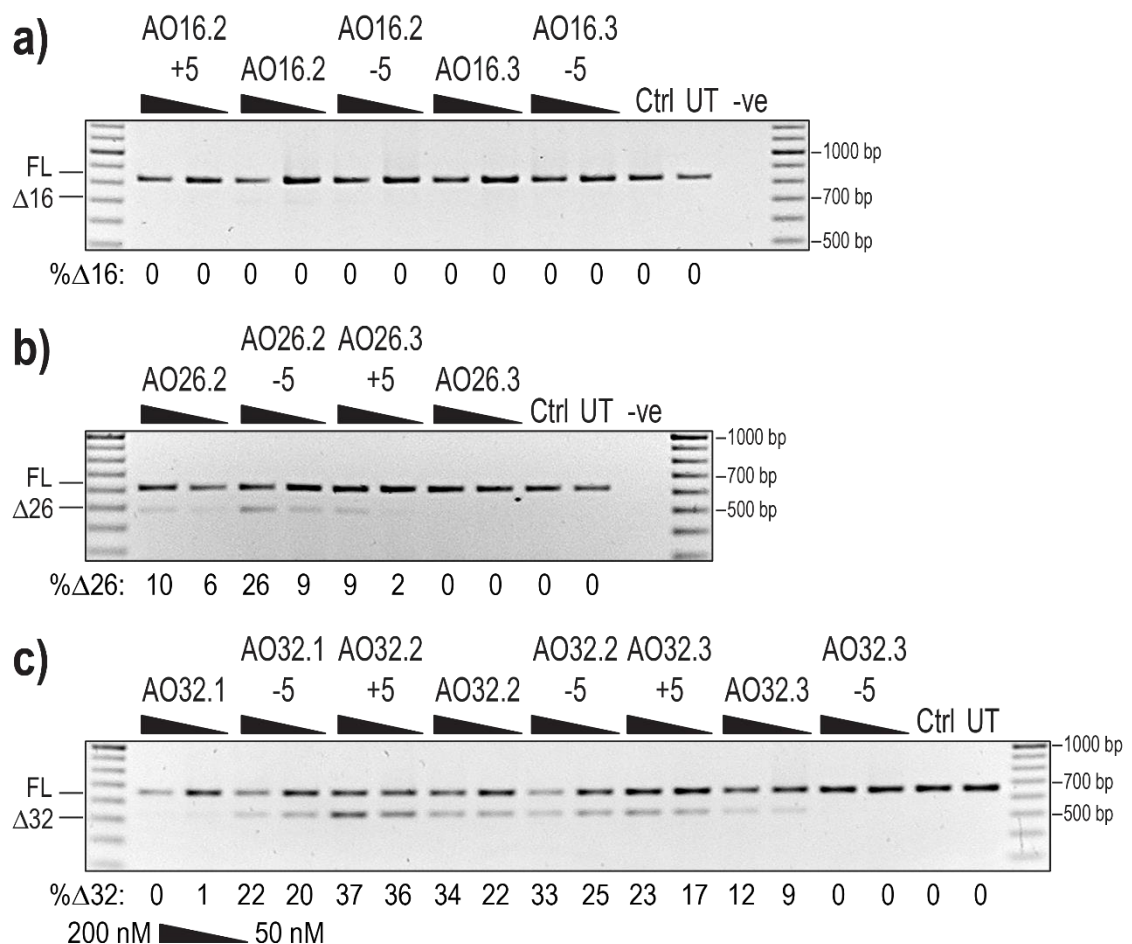


Figure 6.4: Evaluation of micro-walking AOs.

The micro-walking and original 2'OMe-PS AOs targeting exons a) 16, b) 26 and c) 32 were transfected into healthy control cells at two concentrations, 200 and 50 nM, and collected after 24 hours. RT-PCR amplification and gel fractionation revealed the following transcripts a) Ex 13-20 FL=843 bp, Δ 16=720 bp, b) Ex 24-28 FL=628 bp, Δ 26=502 bp and c) Ex 29-34 FL=670 bp, Δ 32=544 bp. The values below each gel image indicate the percentage of transcript from which the target exon has been skipped. Ctrl: an unrelated sequence used as a sham treatment, UT: untreated control, -ve: RT-PCR negative control. 100bp molecular marker used for size reference.

Overlapping cocktails

Generally, AO cocktails are created by combining non-overlapping AOs, limiting the number of potential combinations. However, here the skipping efficiency of cocktails created by combining two overlapping AOs, was investigated, allowing several additional cocktails to be tested. Overlapping-AO cocktails were tested for exon 16; for which skipping is challenging, and exon 32 that is readily skipped. The cocktails used in this section are outlined in Table 6.2, including an alignment of their respective sequences. Each AO overlaps with its cocktail partner by either 15 or 20 bases.

Table 6.2: Overlapping AO cocktails

The aligned sequences in each overlapping-AO cocktail, a dash indicates bases that do not overlap.

Nomenclature	ID	Aligned sequence
16A(+27+51)	AO16.2	UGACGCAACGCCCAUUCAUGCAGAU-----
16A(+22+46)	AO16.2+5	-----CAACGCCCAUUCAUGCAGAUCCCAG
16A(+27+51)	AO16.2	-----UGACGCAACGCCCAUUCAUGCAGAU
16A(+32+56)	AO16.2-5	AGUGUUGACGCAACGCCCAUUCAUG-----
16A(+22+46)	AO16.2+5	-----CAACGCCCAUUCAUGCAGAUCCCAG
16A(+32+56)	AO16.2-5	AGUGUUGACGCAACGCCCAUUCAUG-----
16D(+14-11)	AO16.3	-----UGUUUUCUUACCAACACACACACGG
16D(+09-16)	AO16.3-5	CAUGAUGUUUUCUUACCAACACACA-----
32A(-13+12)	AO32.1	-----ACUCAUUGACAUCUGUAAAACAUUAU
32A(-08+17)	AO32.1-5	GUCACACUCAUUGACAUCUGUAAAA-----
32A(+42+66)	AO32.2+5	-----AGCCUUUCGUGUUUUCACAGGUCCC
32A(+47+71)	AO32.2	AAAUGAGCCUUUCGUGUUUUCACAG-----
32A(+47+71)	AO32.2	-----AAAUGAGCCUUUCGUGUUUUCACAG
32A(+52+76)	AO32.2-5	CAGAUAAAUGAGCCUUUCGUGUUUU-----
32A(+42+66)	AO32.2+5	-----AGCCUUUCGUGUUUUCACAGGUCCC
32A(+52+76)	AO32.2-5	CAGAUAAAUGAGCCUUUCGUGUUUU-----
32D(+19-06)	AO32.3+5	-----ACACACCUGUACAGCCAGUUUUUCC
32D(+14-11)	AO32.3	AACAAACACACCUGUACAGCCAGUU-----
32D(+14-11)	AO32.3	-----AACAAACACACCUGUACAGCCAGUU
32D(+09-16)	AO32.3-5	ACUUGAACAAACACACCUGUACAGC-----
32D(+19-06)	AO32.3+5	-----ACACACCUGUACAGCCAGUUUUUCC
32D(+09-16)	AO32.3-5	ACUUGAACAAACACACCUGUACAGC-----

All the overlapping-AO cocktails targeting exon 16 were essentially ineffective. Two of the four cocktails resulted in traces of exon 16 skipping, with only 2-3% skipping achieved (Figure 6.5.a). More efficient skipping was achieved with the non-overlapping combination of AO16.2 and AO16.3 that induced up to 22% exon skipping (Figure 6.3.b). Conversely, cocktails of overlapping AOs targeting exon 32 induced relatively efficient exon skipping (Figure 6.5.b). While the overlapping exon 32 cocktails did induce strong skipping, the efficiency was generally lower than that of either the AOs alone or the non-overlapping cocktails. Side by side comparison

of skipping efficiency of each AO individually, and their combination in a cocktail revealed that the majority of overlapping cocktails are less efficient than at least one of the single AOs (Figure 6.5.c). We also observed that even when the combination induced more efficient skipping, it was usually only a marginal improvement and not a cumulative effect of the two AOs. The exception to this was the combination of AO32.1 and AO32.1-5 that resulted in up to 50% skipping (Figure 6.5.b) despite the inefficiency of both AOs individually; 7% and 22% skipping respectively. Other cocktails, such as the combination of AO32.2 and AO32.2-5, were less effective than each AO individually demonstrating antagonism (Figure 6.5.b and c).

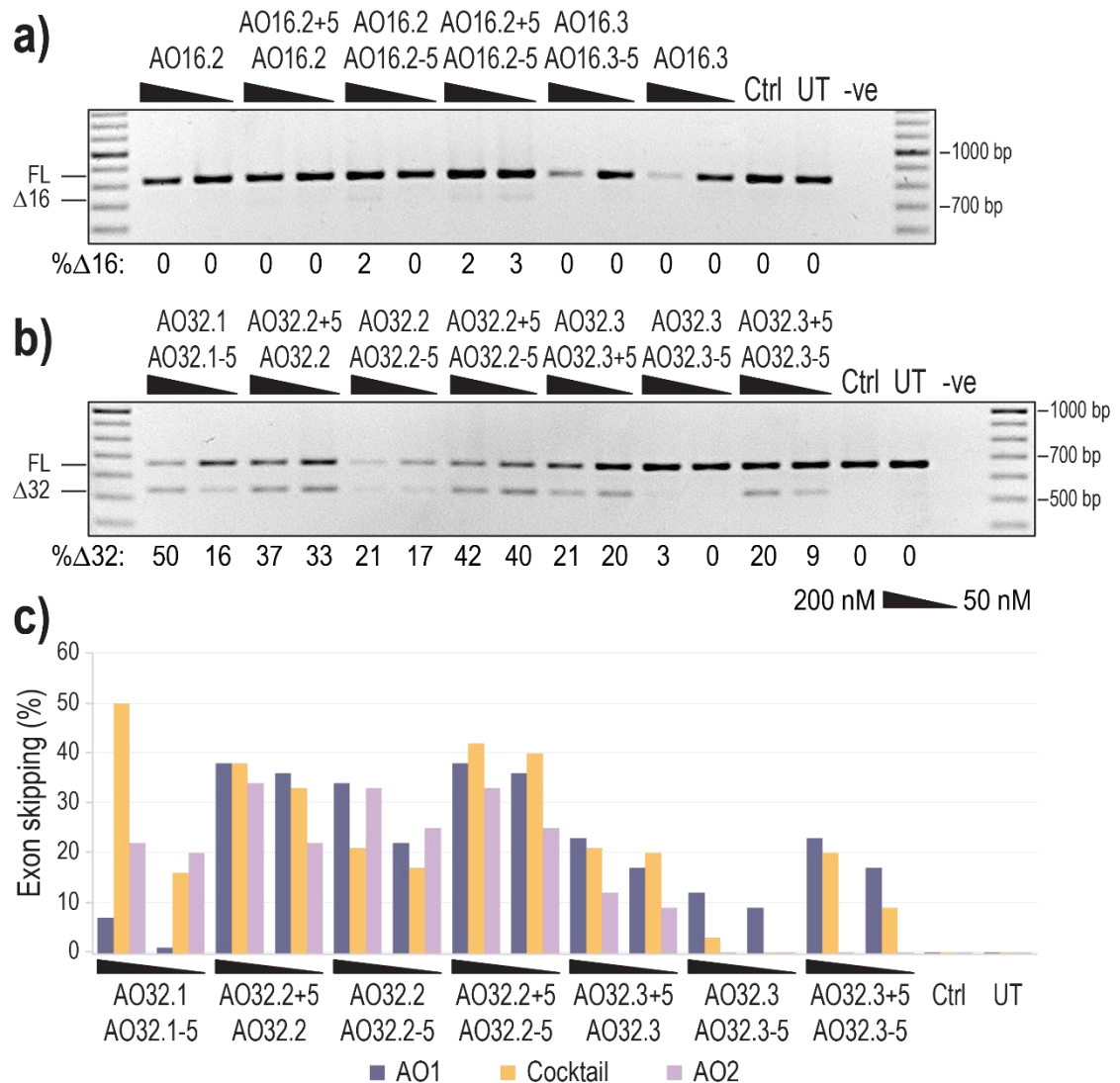


Figure 6.5: Evaluation of overlapping-AO cocktails targeting *FBN1* exon 16 and 32

Healthy control fibroblasts were transfected with cocktails consisting of two overlapping AOs for exons a) 16 and b) 32. The skipping efficiency was assessed after 24 hours. The values below each gel image indicate the percentage of exon 16 ($\Delta 16$) or 32 ($\Delta 32$) skipped transcripts in each sample. Ctrl: an unrelated sequence used as a sham treatment, UT: untreated control, -ve: RT-PCR negative control. 100bp molecular marker used for size reference. c) Comparison of AO sequences targeting exon 32 showing the skipping efficiency of the first AO in the cocktail (AO1) in purple, the overlapping-AO cocktail in yellow and the second AO in the cocktail (AO2) in pink.

6.2.3 Promising sequences

The most promising AO sequences targeting exon 32 (AO32.2) and exon 39 (AO32.1) were synthesised as PMOs. The efficiencies of PMO32 and PMO39 were assessed in healthy control and patient cells. Two Marfan syndrome patient cell lines were obtained from the NIGMS Human Genetic Cell Repository at the Coriell Institute for Medical Research: GM21936 and GM21932. The GM21936 (MFS^{Δ32}) cell line was reported by Liu et al.¹⁸³ to harbour a heterozygous acceptor splice site mutation; c.3839-1G>A, resulting in skipping of exon 32. The GM21932 (MFS^{C1589F}) cell line was reported to harbour a c.4766G>T missense mutation predicted to result in substitution of a cysteine residue for phenylalanine; p.(C1589F) in exon 39.²⁴² The mutations harboured by both patients were confirmed via Sanger sequencing using amplicons generated from cDNA derived from total RNA or gDNA as sequencing templates (Figure 6.6.a)

Initially, PMO32 was transfected into healthy control and MFS^{Δ32} cells using Nucleofection and incubated for 72 hours. The proportion of skipping, while relatively efficient, up to 62% in healthy control and 72% in MFS^{Δ32} fibroblasts (Figure 6.6.b), was deemed insufficient to rescue the phenotype. Therefore, two additional delivery methods were tested to determine if they would allow for more efficient PMO delivery and therefore improved exon skipping efficiency. Lipofectamine 3000 was used in the same manner as 2'OMe-PS AO transfection (Chapter 2, section 2.2.3). However, the delivery of PMO32 with Lipofectamine 3000 was ineffective, resulting in only 14% skipping in healthy control cells at the highest concentration; 5 μM in 1 ml transfection volume (Figure 6.6.c). The second transfection reagent used, Endo-Porter, is designed by Gene Tools for the delivery of PMOs.¹²⁹ Endo-Porter was tested in only patient fibroblasts due to minimal available reagent. Approximately 12% additional skipping was achieved with Endo-Porter, increasing the proportion of Δ32 transcripts from the endogenous 48%, resulting from the splice site mutation, to 60%, with PMO32 at 10 μM (Figure 6.6.d).

Healthy control and MFS^{C1589F} cells were similarly transfected with PMO39 using both Nucleofection and Lipofectamine 3000 (Figure 6.6.e and f). Nucleofection again proved more effective than Lipofectamine 3000. However, the 49% and 54% exon 39 skipping induced in healthy control and MFS^{C1589F} cells, respectively (Figure 6.6.e) using Nucleofection is again insufficient to provide any therapeutic benefit, based on our current hypothesis. Delivery of PMO39 using Lipofectamine 3000 was similarly less efficient than Nucleofection, inducing up to 16% and 22% skipping in healthy control and MFS^{C1589F} cells, respectively (Figure 6.6.f).

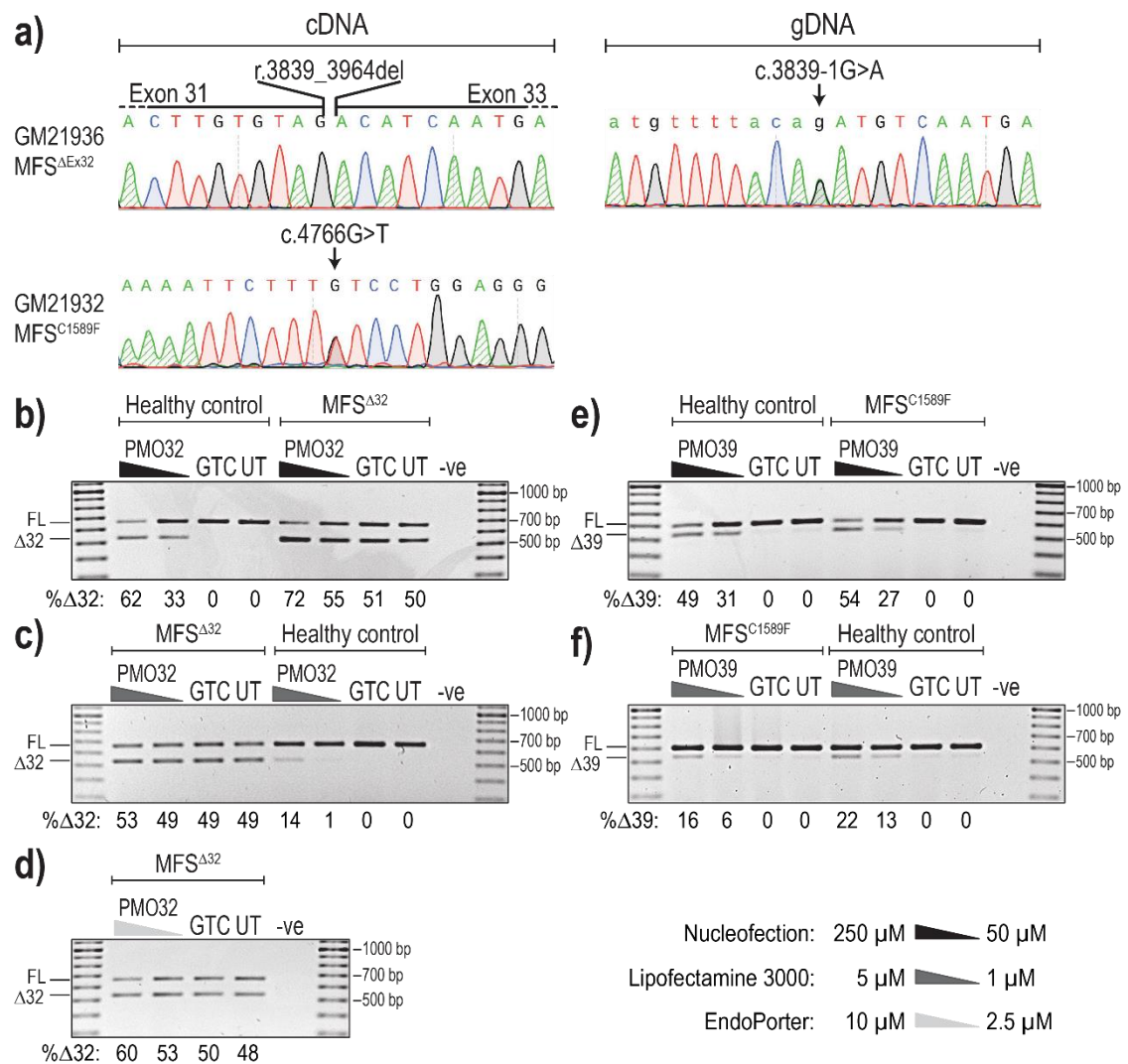


Figure 6.6: Evaluation of PMO32 and PMO39 in healthy control and MFS patient fibroblasts

a) Sanger sequencing results confirming mutations harboured by MFS^{Δ32} and MFS^{C1589F} patient fibroblasts. Healthy control and MFS^{Δ32} fibroblasts were transfected with PMO32 using b) Nucleofection, c) Lipofectamine 3000 and d) Endo-Porter. Healthy control and MFS^{C1589F} fibroblasts were transfected with PMO39 using e) Nucleofection and f) Lipofectamine 3000. The concentrations used were calculated in the transfection volume: 250 μM and 50 μM in 20 μl volume for Nucleofection, 5 μM and 1 μM in 1 ml volume for Lipofectamine 3000 and 10 μM and 2.5 μM in 500 μl volume for Endo-Porter. All transfected cells were collected after 72 hours. The values below each gel image indicate the percentage of exon 32 (Δ32) or 39 (Δ39) skipped transcripts in each sample. GTC: Gene Tools control PMO used as a sham treatment, UT: untreated control, -ve: RT-PCR negative control. 100bp molecular marker used for size reference.

6.3 Alternative AO chemistry

While there are many potential target exons within *FBN1*, many have proven to be very challenging to skip from the mature mRNA. However, only two chemistries; 2'OMe-PS and PMOs have been discussed. During the course of this project a third chemistry, the thiophosphoramidate morpholino oligomer (TMO), became available for evaluation. In collaboration with Distinguished Professor Marvin Caruthers (University of Colorado Boulder, USA), two 20-mer versions of the best performing exon 52 AO were synthesised as TMOs. One limitation in using the TMO chemistry is length, and only 20-mer AOs were available initially.

The 20-mer AOs were designed by removing five bases from either the 5' (52-1) or 3' (52-2) end of the original AO52.2 sequence. To ensure comparability, the same 20-mer AO sequences were also synthesised as both PMO and 2'OMe-PS chemistries. The details of these AOs, along with the control sequences used, are outlined in Table 6.3.

Table 6.3: Optimal exon 52 AO identified in the original screen and details of 20-mer versions used in chemistry comparison experiments.

The target gene and exon, AO name, ID, sequence and chemistry of AOs used in this section. The AO nomenclature is outlined in Chapter 2, Figure 2.1.

AO name	ID	Sequences(5'-3')									Chemistry
FBN1 H52A(+29+53)N	AO52.2	AUC	AGG	UCC	CAC	GAU	GAU	CCC	ACU	U	2'OMe-PS
	PMO52	ATC	AGG	TCC	CAC	GAT	GAT	CCC	ACT	T	PMO
FBN1 H52A(+29+48)	52-1		G	UCC	CAC	GAU	GAU	CCC	ACU	U	2'OMe-PS
			G	TCC	CAC	GAT	GAT	CCC	ACT	U	TMO
			G	TCC	CAC	GAT	GAT	CCC	ACT	T	PMO
FBN1 H52A(+34+53)	52-2	AUC	AGG	UCC	CAC	GAU	GAU	CC			2'OMe-PS
		ATC	AGG	TCC	CAC	GAT	GAT	CC			TMO
		ATC	AGG	TCC	CAC	GAT	GAT	CC			PMO
Control AOs											
SMN2 H7A(+13+32)	SMN-7	CAC	CUU	CCU	UCU	UUU	UGA	UU			2'OMe-PS
		CAC	CTT	CCT	TCT	TTT	TGA	TU			TMO
		CAC	CTT	CCT	TCT	TTT	TGA	TT			PMO
COL7A1 H73A(+21+40)	COL-73	CGC	CCU	UCA	GCC	CGC	GUU	CU			2'OMe-PS
		CGC	CCT	TCA	GCC	CGC	GTT	CU			TMO
		CGC	CCT	TCA	GCC	CGC	GTT	CT			PMO
Control AO1	Ctrl AO1	ATG	TCC	TGA	GTC	TAG	ACC	CU			TMO
GeneTools control-20mer	Ctrl	U	CUU	ACC	UCA	GUU	ACA	AUU	U		2'OMe-PS
		T	CTT	ACC	TCA	GTT	ACA	ATT	U		TMO
GeneTools control	Ctrl	CCT	CTT	ACC	TCA	GTT	ACA	ATT	TAT	A	PMO

6.3.1 Delivery method optimisation

To determine the most appropriate delivery method for TMOs, healthy control cells were transfected with both TMO sequences either un-complexed or as Lipofectamine 3000 lipoplexes. Transfected cells were collected 24 hours after transfection and analysed for exon 52 skipping. No skipping was evident in cells transfected without a transfection reagent (Figure 6.7). Conversely, delivery of TMO52-1 and TMO52-2 using Lipofectamine 3000 resulted in up to 71% and 69% skipping respectively, demonstrating the efficacy of the TMOs when using the Lipofectamine 3000 transfection reagent (Figure 6.7). An unexpected product was also identified in control AO1 treated cells (Figure 6.7), purification and Sanger sequences of this product identified it as $\Delta 52$ (data not shown). This finding was consistent across multiple replicates indicating contamination of the control sequence with either TMO52-1 or TMO52-2, and therefore this control AO preparation was not used for further experiments. The control was replaced by a 20-mer TMO version of the standard Gene tools control sequence used for PMO studies (Table 6.3). This same control sequence was also synthesised as the 2'OMe-PS chemistry (Table 6.3)

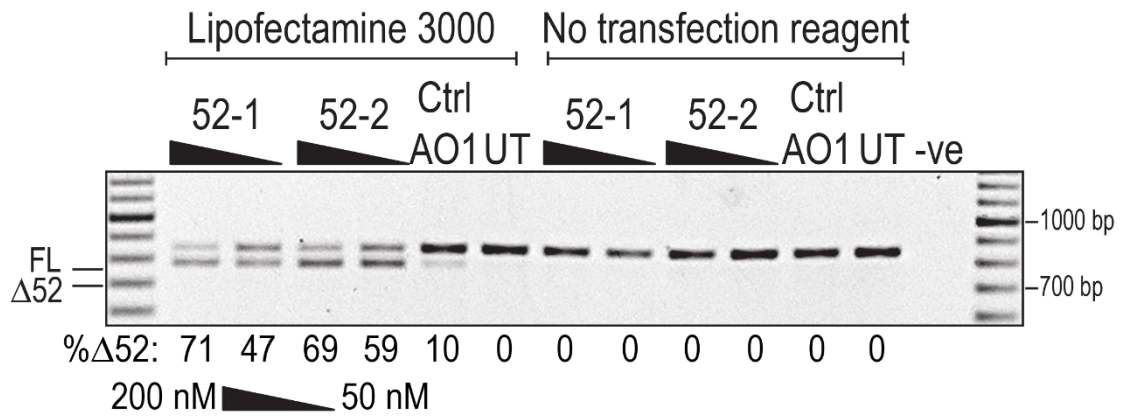


Figure 6.7: Optimisation of TMO delivery in healthy control fibroblasts.

The TMO52-1 and TMO52-2 sequences were delivered into healthy control fibroblasts using either Lipofectamine 3000 or without a transfection reagent. Two concentrations; 200 nM and 50 nM were used, and cells were collected after 24 hours. The values below the gel image indicate the percentage of exon 52 (Δ 52) skipped transcripts in each sample. Ctrl AO1: an unrelated sequence used as a sham treatment, UT: untreated control, -ve: RT-PCR negative control. 100bp molecular marker used for size reference.

6.3.2 Comparison between TMO and 2'OMe-PS AOs

To compare the TMO and 2'OMe-PS chemistries, healthy control fibroblasts were transfected with AOs composed of both chemistries over a range of concentrations from 200 nM to 5 nM. All four AOs induced relatively efficient exon 52 skipping, with the 20-mer 2'OMe-PS AOs inducing similarly efficient exon skipping to the original 25-mer AO. The 2'OMe-PS 52-1 sequence was slightly more efficient, inducing up to 44% skipping compared to the 38% by 2'OMe-PS 52-2 (Figure 6.8.b). Both TMO versions were more efficient than the 2'OMe-PS counterparts, with approximately 20% more skipping when using a TMO compared to the 2'OMe-PS AO (Figure 6.8). Both TMO sequences induced similar levels of exon 52 skipping, with 60% of transcript missing exon 52 after transfection at 200 nM (Figure 6.8.a). The TMOs induced a similar skipping efficiency at 10 nM as the 2'OMe-PS sequences did at 100 nM to 200 nM (Figure 6.8).

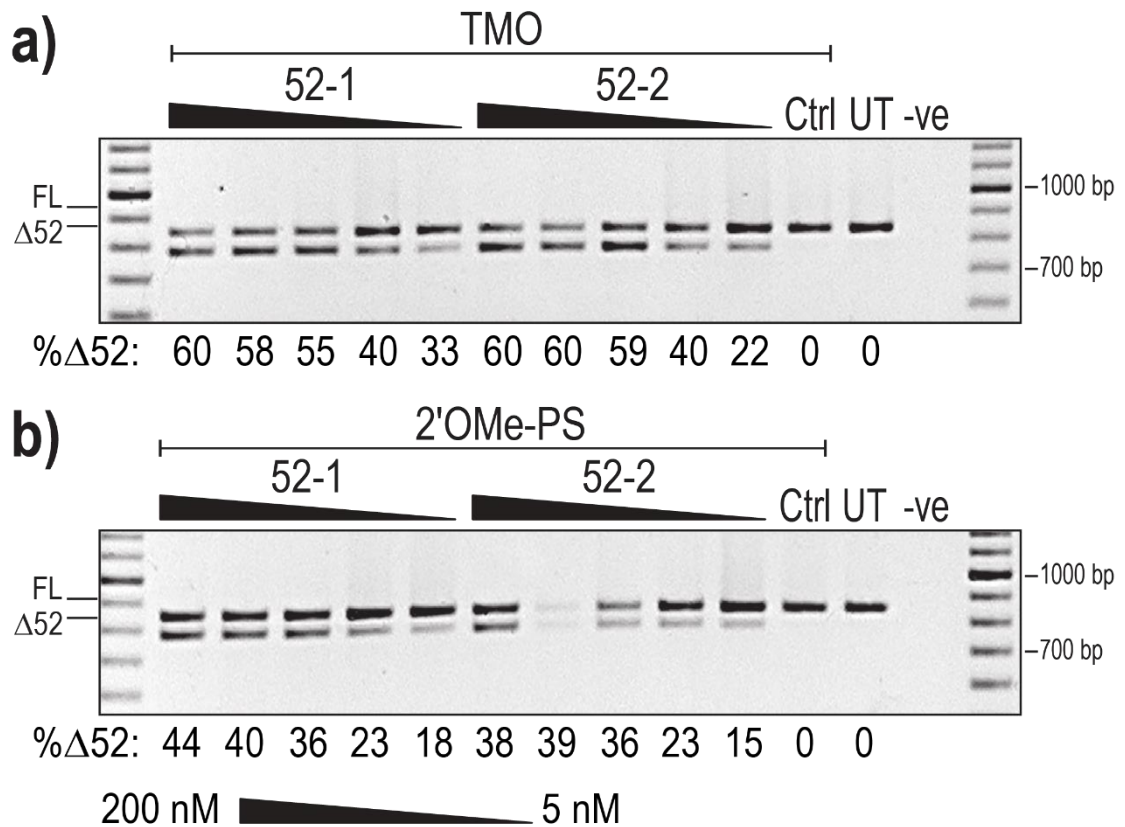


Figure 6.8: Comparison of exon 52 skipping efficiency of 2'OMe-PS and TMO chemistries

Healthy control cells were transfected, using Lipofectamine 3000, with a) TMO and b) 2'OMe-PS AOs. Cells were transfected at a range of concentrations; 200 nM, 100 nM, 50 nM, 10 nM and 5 nM, and were collected for RNA analysis after 24 hours. The values below each gel image indicate the percentage of exon 52 ($\Delta 52$) skipped transcripts in each sample. Ctrl: an unrelated sequence used as a sham treatment, UT: untreated control, -ve: RT-PCR negative control. 100bp molecular marker used for size reference.

Assessing off-target effects of 2'OMe-PS and TMO chemistries

It is now well established that the phosphorothioate (PS) backbone interacts with and sequesters paraspeckle and other nuclear proteins, limiting their availability for normal cellular functions and leading to toxicity.^{243,244} However, the effect of the TMO chemistry on nuclear proteins is unknown. Therefore, the localisation of the paraspeckle protein non-POU domain-containing octamer-binding protein (NONO) was assessed after treatment with either 2'OMe-PS AOs or TMOs of the same sequence. Before transfection, 15,000 healthy control fibroblasts were seeded onto coverslips in colonies. All AOs were transfected at 100 nM using Lipofectamine 3000 and left for 24 hours. Coverslips were fixed and subsequently immunolabelled using a NONO primary antibody (a gift from Prof. Archa Fox) and counterstained with Hoechst for nuclei detection.

A minimum of 250 cells were counted for each treatment group, and each cell was categorised as having one of the following staining patterns. (1) normal; diffuse staining throughout the nucleus with minimal spots of high intensity, this was considered normal since it was observed in all untreated cells, (2) foci; multiple high-intensity aggregates within the nucleus, with minimal

diffuse staining, (3) filaments; elongated aggregates within the nucleus, with minimal diffuse staining (4) cytoplasmic; multiple high-intensity aggregates within the cytoplasm, with diffuse nuclei staining. Representative images of NONO and Hoechst staining in each treatment group are shown in Figure 6.9.b. The percentage of cells showing aberrant NONO staining following AO treatment is shown in Figure 6.9.c. The skipping efficiency in transfected cells was also assessed to ensure cells had been successfully transfected (Figure 6.9.a)

Immunofluorescent staining of NONO revealed that all 2'OMe-PS sequences, including the control AO, altered NONO staining (Figure 6.9.b). Both punctate foci and filament aggregates were observed, with foci forming more frequently (Figure 6.9.b and c). In particular, the 2'OMe-PS 52-2 sequence caused aggregates in more than 50% of cells. The staining in TMO treated cells was for the most part consistent with untreated cells, with diffuse NONO staining throughout the nucleus and occasional spots of higher staining intensity (Figure 6.9.b and c). The TMO 52-1 and SMN-7 sequences did not induce any abnormal NONO staining (Figure 6.9.c). However, TMO 52-2 resulted in foci in approximately 5% of cells (Figure 6.9.c). Cytoplasmic aggregates were observed to form in cells treated with the TMO control AO and TMO COL-73 (Figure 6.9.b and c). However, the TMO COL-73 sequence did not result in any exon skipping in this experiment (Figure 6.9.b and c) where previously the sequence was found to induce approximately 50% skipping of the target exon in *COL7A1* transcripts (Data not shown, Kristin Ham unpublished).

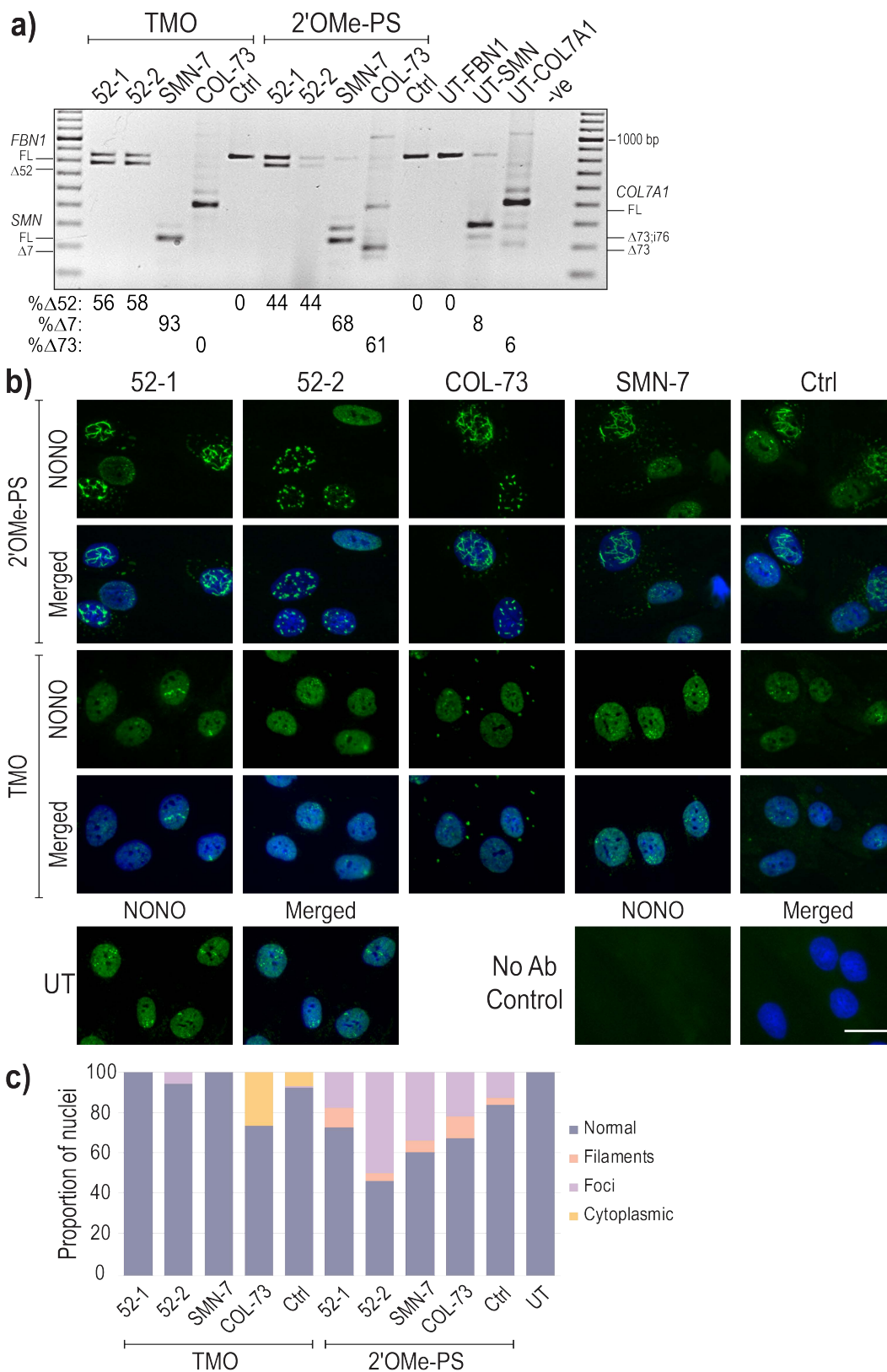


Figure 6.9: Evaluation of skipping efficiency and NONO immunofluorescence staining after transfection with TMO and 2'OMe-PS AOs.

Healthy control fibroblasts were transfected, using Lipofectamine 3000, with 100 nM of TMO or 2'OMe-PS AOs. a) RT-PCR amplicons from cells collected 24 hours after transfection showing transcripts between *FBN1* exons 42 and 49, *SMN* exons 4 and 8 and *COL7A1* exons 72 and 77. b) representative images of treated cells stained for NONO (green), and nuclei (blue). The upper and lower panels of each set of immunofluorescence images show the NONO and merged images, respectively. No Ab control: no primary antibody added. Scale bar = 20 μ m. See Figure A4.2 for a larger version of part b. c) Percentage of healthy control fibroblasts showing disrupted NONO staining.

6.3.3 TMO, 2'OMe-PS and PMO chemistry comparison

Lastly, all three chemistries, 2'OMe-PS, PMO and TMO, were compared. In order to use the same concentration for each of the AO chemistries in the most cost-effective way, a different delivery method called Neon transfection was used. Similar to Nucleofection, Neon transfection uses electroporation to deliver the AO into cells, however the transfection volume for the Neon protocol is only 10 μ l allowing the use of less reagent. Two concentrations were tested; 20 μ M and 5 μ M, as calculated in the 10 μ l tip, which are equivalent amounts of AO as used for 200 nM and 50 nM 2'OMe-PS screening experiments. Transfected cells were left for both 24 hours and 10 days.

After 24 hours, relatively efficient exon skipping was achieved with all three chemistries, where both the 52-1 and 52-2 sequences induced similar levels of targeted exon skipping. However, the 52-1 sequence was marginally more efficient across the board, inducing up to 79%, 68% and 81% exon 52 skipping as TMO, 2'OMe-PS and PMO chemistries respectively after 24 hours (Figure 6.10.a). The skipping efficiency using the 2'OMe-PS AOs was slightly more efficient than seen previously with this chemistry with both sequences inducing more than 60% skipping after 24 hours at both concentrations tested after Neon transfection.

At the 24-hour time-point, the PMO sequences induced the most efficient skipping (Figure 6.10.a). However, after 10 days, the proportion of Δ 52 transcripts was reduced both in cells treated with PMOs and in cells treated with the 2'OMe-PS AOs (Figure 6.10.b). Cell death was observed in treated samples from both chemistries, and cells had begun to regrow in PMO samples (data not shown). Conversely, the TMO treated cells had an increased proportion of skipping after the 10-day incubation. The TMO 52-1 and TMO 52-2 sequences induced up to 92% and 84% exon skipping, respectively (Figure 6.10.b). The 10-day time point also revealed a greater difference in efficiency between the 52-1 and 52-2 sequences, with 52-1 consistently inducing more skipping across all three chemistries (Figure 6.10.b).

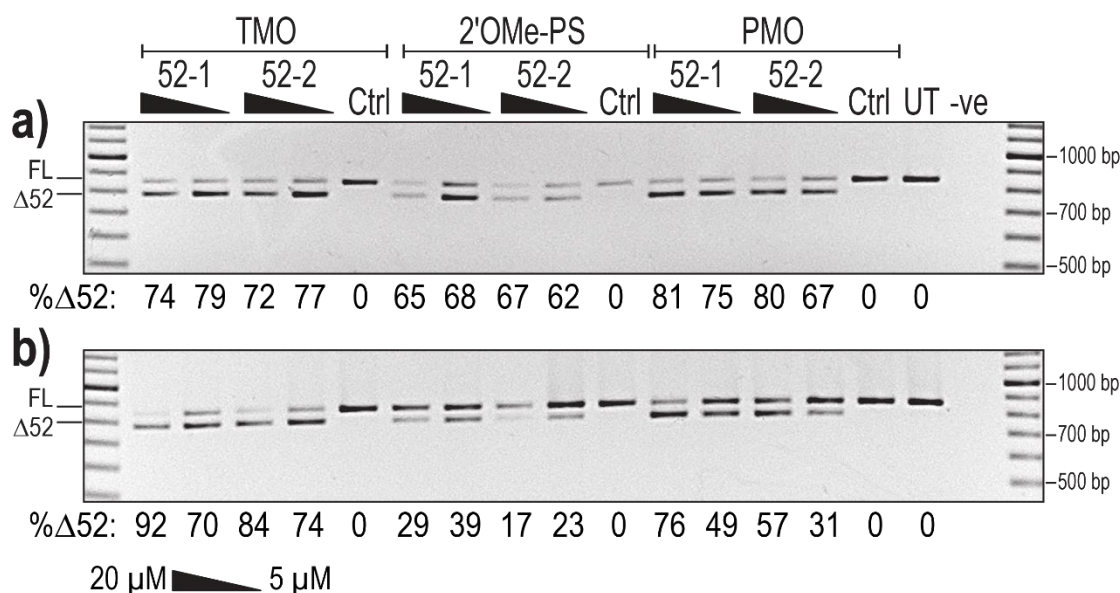


Figure 6.10: Evaluation of two AO sequences targeting *FBN1* exon 52 as the 2'OMe-PS, TMO and PMO chemistries.

Healthy control cells were Neon transfected with the indicated AO or left untreated (UT) before collection after a) 24 hours or b) 10 days. Two concentrations were used; 20 μ M and 10 μ M, calculated in the 10 μ l Neon transfection volume. The proportion of skipped product (Δ 52) is shown below each lane. Ctrl: an unrelated sequence used as a sham treatment, UT: untreated control, -ve: RT-PCR negative control. 100bp molecular marker used for size reference.

Fibrillin-1 fibre morphology and abundance after AO treatment

The TMO, 2'OMe-PS and PMO sequences were again Neon transfected into healthy control fibroblasts, as well as the two patient cell lines; MFS Δ 52 and MFS^{C2111R}, described in chapter 4. Despite the lower exon skipping efficiency known to result from transfection of both 2'OMe-PS and PMO sequences after 10 days, this time point was chosen to perform fibrillin-1 protein staining.

This repeated experiment revealed robust skipping, with the TMO sequences inducing 88% and 81% skipping (Figure 6.11) compared with 92% and 84% seen previously (Figure 6.10.b). Similar skipping efficiency to that achieved in healthy control cells was seen in both patient cell lines (Figure 6.10.b and c), with the TMO sequences again the most efficient across all three cell lines. The TMO52-1 sequence, in particular, induced the most efficient skipping in both healthy control (88%) and MFS Δ 52 (99%) cells (Figure 6.11.a and b). However, in MFS^{C2111R} patient cells, the TMO52-2 sequence was slightly more efficient, inducing up to 89% exon 52 skipping (Figure 6.11.c). Cell death was evident in all samples treated with PMO or 2'OMe-PS AOs, with the cell death particularly apparent in MFS^{C2111R} cells treated with the two 2'OMe-PS AOs, resulting in dropout of the RT-PCR in these samples (Figure 6.11.c)

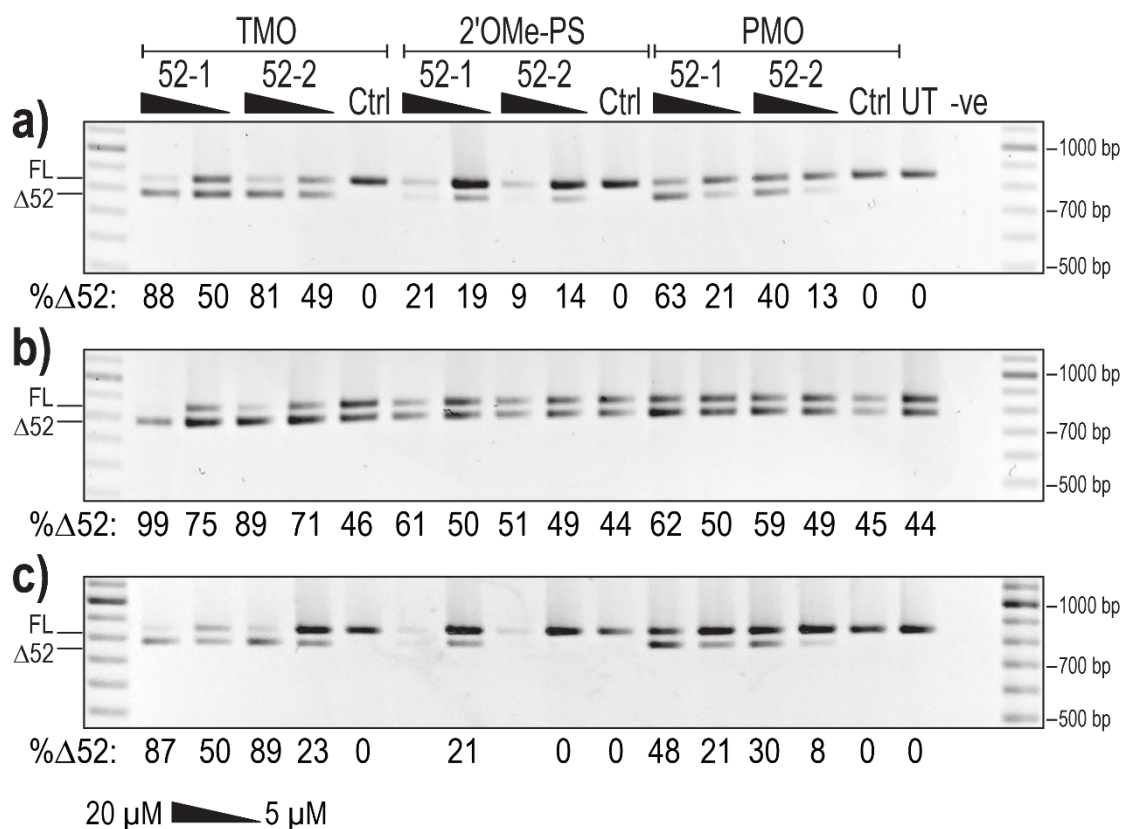


Figure 6.11: Comparison of AO chemistry efficacy in control and MFS patient fibroblasts.

The TMO, 2'OMe-PS and PMO sequences were Neon transfected into a) Healthy control, b) MFS^{Δ52} and c) MFS^{C211R} fibroblasts. Two concentrations were tested; 20 μM and 5 μM, calculated in the 10 μl Neon transfection volume, and cells were incubated for 10 days prior to collection. The proportion of skipped product (Δ52) is shown below each lane. Ctrl: an unrelated sequence used as a sham treatment, UT: untreated control, -ve: RT-PCR negative control. 100bp molecular marker used for size reference.

A portion of Neon transfected cells were seeded onto coverslips and incubated for 10 days. These coverslips were immunolabelled for fibrillin-1 and counterstained with Hoechst for nuclei detection. Representative immunofluorescent images are displayed in Figure 6.12.

Healthy control fibroblasts

Untreated healthy control cells present with strong, unfragmented fibrillin-1 fibres across the entire coverslip (Figure 6.12.a.xvi). Similarly, control cells treated with any one of the three control AOs exhibit intense fibre staining (Figure 6.12.a.xiii, xiv, xv). The fibre morphology, and fibrillin-1 staining overall was lost in healthy control cells treated with the lower concentration of either TMO that induces approximately 50% skipping (Figure 6.12.a.iv, x). Increased TMO concentration, and skipping efficiency resulted in a restoration of fibrillin-1 staining and the presence of fibres (Figure 6.12.a.i, vii). However, the morphology of these fibres was fragmented, and their abundance was reduced, compared to the untreated healthy control.

The opposite staining pattern is observed in healthy control cells treated with 2'OMe-PS AOs. Cells treated with the lower concentration of either 2'OMe-PS AO; both of which induce less than

15% skipping, present with fibres. However, these fibres have a similar low abundance and fragmented morphology to those seen in 20 μ M TMO treated cells (Figure 6.12.a.v, xi). Healthy control cells treated with the higher concentration of 2'OMe-PS AOs have no fibre formations. The cell density was also greatly reduced, consistent with the high level of cell death observed (Figure 6.12.a.ii, viii). The 2'OMe-PS control sequence resulted in higher cell viability than either AO targeting *FBNI*, despite being used at the same 20 μ M concentration.

The lower exon skipping efficiency induced by the PMO sequences in this experiment (Figure 6.11.a); compared to that previously seen at 24 hours or 4 days, corresponds with the lack of fibre formation observed. Treatment of healthy control cells with either concentration of PMO5-1 or 20 μ M PMO52-2 resulted in the complete loss of fibres, mimicking the disease-like state (Figure 6.12.a.iii, vi, ix). Cells treated with 5 μ M of PMO52-2, which induced only 13% skipping, present with highly fragmented fibrillin-1 fibres (Figure 6.12.a.xii)

Patient fibroblasts

Samples from untreated MFS ^{Δ 52} and MFS^{C211R} cell lines present with a distinct lack of extruded fibrillin-1 fibres. Although untreated MFS ^{Δ 52} cells have minimal fibrillin-1 staining overall (Figure 6.12.b.xvi), untreated MFS^{C211R} cells have some diffuse fibrillin-1 staining seen throughout the monolayer culture (Figure 6.12.c.xvi). The fibrillin-1 staining pattern remains unchanged in both cell lines after treatment with any of the control sequences. We also observed very little change in the fibrillin-1 staining pattern of MFS^{C211R} cells in any of the treatment groups, including when efficient; 87% and 89%, skipping was induced with TMO52-1 and TMO52-2 respectively (Figure 6.12.c). The only noticeable divergence in fibrillin-1 staining is in the 20 μ M 2'OMe-PS treatment group in which widespread cell death led to very few cells remaining on the coverslip and thus minimal fibrillin-1 staining (Figure 6.12.c.ii, viii).

Similarly, treatment of MFS ^{Δ 52} cells with 2'OMe-PS and PMO AOs had minimal effect on the fibrillin-1 staining pattern. The 2'OMe-PS AOs also cause a extensive MFS ^{Δ 52} cell death, especially at the higher AO concentration tested, leading to minimal fibrillin-1 staining (Figure 6.12.b). Treatment of MFS ^{Δ 52} cells with 20 μ M of PMO52-1; which induces 62% skipping, increased diffuse fibrillin-1 staining; however, no fibres were observed (Figure 6.12.b.iii). Conversely, treatment of MFS ^{Δ 52} cells with 20 μ M of either TMO 52-1 or 52-2 resulted in the formation of fibrillin-1 fibres (Figure 6.12.b.i, vii). These fibres are of high staining intensity and have a similar unfragmented morphology to those seen in the untreated healthy control cells. However, the fibres are less abundant, covering approximately half of any given field of view. Fibrillin-1 fibres were also observed in the 5 μ M TMO52-1 and TMO52-2 treated cells where 75% and 71% skipping was induced respectively (Figure 6.12.b.iv, x). However, the fibres were highly fragmented, infrequent and isolated; not forming the lattice seen in untreated healthy control fibroblasts.

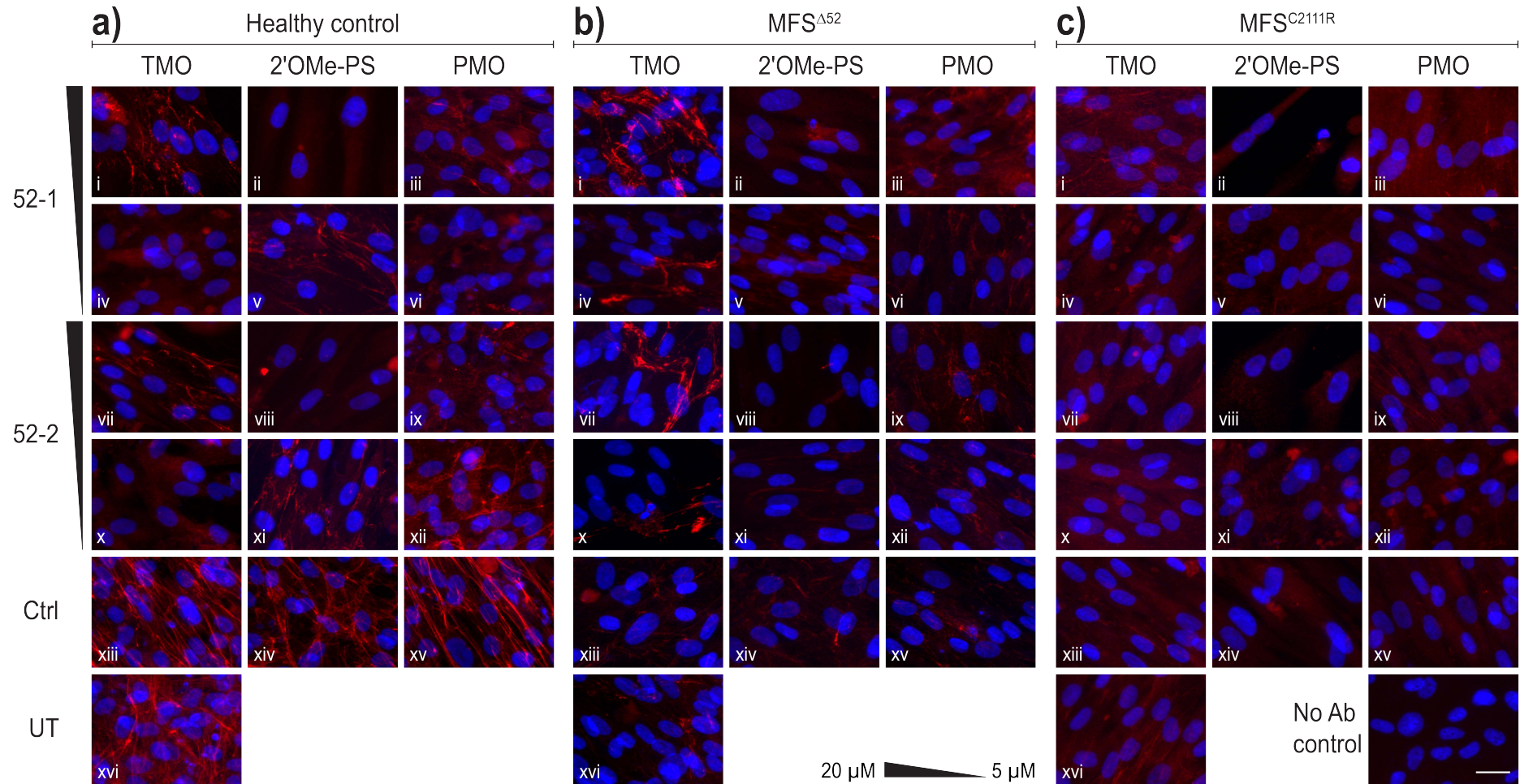


Figure 6.12: Fibrillin-1 morphology and abundance after transfection with TMOs, 2'OMe-PS AOs or PMOs

Representative immunofluorescent images of a) healthy control, b) MFS^{Δ52} and c) MFS^{C2111R} fibroblasts Neon transfected with TMOs, 2'OMe-PS AOs or PMOs and collected after 10 days. Two concentrations 20 μM and 5 μM; calculated in a 10 μl transfection volume, were tested. Treated cells were immunolabelled for fibrillin-1 (red) and nuclei (blue). Ctrl: an unrelated sequence used as a sham treatment, UT: untreated control, No Ab control: no primary antibody added. Scale bar = 20 μm. See Figure A4.3, Figure A4.4 and Figure A4.5 for larger versions of part a, b and c respectively.

Comparing the effects of AO chemistries on paraspeckle proteins

The 2'OMe-PS sequences were previously shown to result in aggregates of the nuclear protein, NONO, while all of the TMO sequences tested resulted in very few visible aggregates. This experiment was repeated to assess the effect of the PMO chemistry on a paraspeckle protein. Healthy control cells were Neon transfected with 10 μ M of each AO or left untreated and seeded onto coverslips in colonies. Coverslips were fixed after a 24-hour incubation and immunolabelled for the paraspeckle protein Splicing Factor Proline and Glutamine Rich (SFPQ) that normally co-localises with NONO. The staining pattern of SFPQ was categorised as normal, foci, filaments or cytoplasmic. A minimum of 300 cells per treatment group were counted and categorised. The proportion of nuclei within each category are displayed in Figure 6.13.

The 2'OMe-PS sequences resulted in a large proportion of nuclei with abnormal SFPQ staining. Of the 2'OMe-PS treated cells with abnormal SFPQ staining, the majority have foci, with the 52-2 sequence transfection resulting in foci in 42% of cells (Figure 6.13). While foci were most common in the 2'OMe-PS treated samples, only a small proportion (<1%) of cells treated with any of the PMOs or TMO52-2 also showed foci after staining for SFPQ (Figure 6.13). The number of samples showing cytoplasmic aggregates was greater in this experiment than that described in Section 6.3.2. Abnormal SFPQ localisation and distribution occurred in all treatment groups, although with very different severity and pattern of staining. The cytoplasmic aggregates were most common in the 2'OMe-PS treated samples and were occasionally an extension of foci, with a single cell able to present with both morphologies. Except for TMO52-2, all other AOs resulted in less than 1% of cells with cytoplasmic aggregates (Figure 6.13). The TMO52-2 sequence resulted in cytoplasmic aggregates in 1.9% of cells (Figure 6.13). Untreated cells were completely free of abnormal staining; however, they were not subjected to the Neon electroporation process.

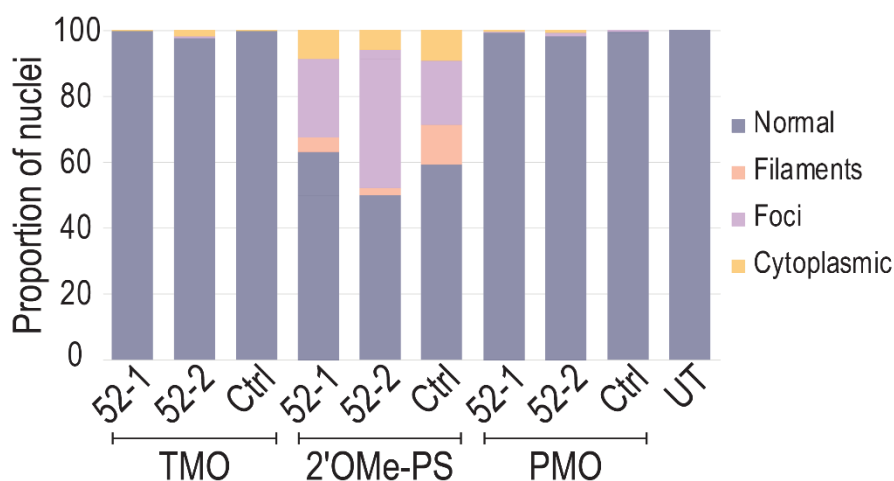


Figure 6.13: SFPQ staining in fibroblasts after treatment with TMO, 2'OMe-PS AOs or PMOs

Percentage of healthy control fibroblasts showing disrupted SFPQ staining 24 hours after transfection with 10 μ M of TMO, 2'OMe-PS AOs or PMOs. A minimum of 300 cells were counted, and the staining of SFPQ aggregates was assessed as being either normal, foci, filaments or forming cytoplasmic foci. Ctrl: an unrelated sequence used as a sham treatment, UT: untreated control.

6.4 Discussion

Thus far we have demonstrated AO-mediated skipping of *FBNI* exons 52, 59, 47 and the exon region from 45-47 and that this splicing is relatively efficient, especially when using the PMO chemistry. However, the basis of a splice-switching therapy for MFS patients means that each exon region requires a different therapeutic compound. In theory 60 of the 66 fibrillin-1 exons can be skipped individually, without disrupting the reading frame, presenting numerous potential therapeutic targets. Therefore, the first aim of this chapter was to identify and evaluate AOs targeted to additional fibrillin-1 exons. The second aim here was to assess the efficiency and applicability of a third AO chemistry that is a hybrid chemistry between 2'OMe-PS, which can be efficiently delivered but result in some non-antisense off-target effects, and the extremely safe PMO chemistry that is hampered by poor cellular uptake.

Additional AO screening

Through screening of 2'OMe-PS AOs, we clearly demonstrated that not all *FBNI* exons are readily skipped. We screened AOs against an additional ten fibrillin-1 exons and found that half of the exons could not be skipped using any of the initial three AO sequences designed. Adams et al.¹⁶⁷ reported that approximately 2 out of 3 of AOs tested induced dystrophin exon skipping, although with very different efficiencies. Here, we found that a lower 36 of the total 69 sequences tested (52%) induced some skipping of the target exon (Table A4.1). Screening of additional AO sequences targeting these exons could reveal that targeting a particular set of ESE or splice sites would prove effective.

We wrote a simple python script that generates a list of all possible oligomers of a chosen length across the target exon (Figure A4.6). When used in conjunction with a tool for splicing regulator prediction such as SpliceAid^{153,154} or Human Splicing Finder,²¹⁵ this script provides a relatively efficient way to design and name AOs. However, AO synthesis costs and the costs of screening multiple AO sequences means that it is not feasible to test every possible sequence for every exon, especially if AO length is also varied. For example, for the five ‘difficult to skip’ exons presented here there are over 750 possible 25-mer AO sequences, given 25 bases of flanking intron is included in the targeting.

For the majority of these difficult-to-skip or recalcitrant exons, we found that the use of a two AO cocktail enabled the exon to be removed from a portion of transcripts. However, for exons 27 and 49 neither single nor two-AO cocktails induced any exon skipping. One explanation for the lack of skipping could be that all three AOs targeting exon 27 bind to ESE sites rather than completely covering either the acceptor or donor splice sites. These sequences were chosen as they targeted regions with multiple predicted ESE sites (Figure A4.1). Similarly, none of the AOs targeting exon 49 bind to the donor splice site. Therefore, it is possible that the sequences themselves are not targeting the optimal motifs. Thus, testing additional sequence that cover these splice sites could lead to the identification of an effective AO. However, of all the AOs tested thus far those targeting the ESEs have most successfully induced exon skipping, with 68% of all ESE-targeting AOs having some effect on exon selection (Table A4.2). For those AOs targeting the donor splice site, only 44% result in skipping, this is further reduced to 33% for AOs targeting the acceptor splice site (Table A4.2)

Adams et al.¹⁶⁷ reported that when testing AO cocktails against the recalcitrant exons in the dystrophin gene transcript, AO cocktails that were clearly synergistic were not necessarily composed of those AOs targeting the splice sites nor was efficient skipping associated with the number of ESE sites targeted. Here, we found that for those exons where single AOs were ineffective, but a two AO cocktail induced some exon skipping, the combination of an AO targeting one of the splice sites and a region of ESEs were those that induced skipping. In none of these cases did the combination of AOs targeting both the acceptor and donor sites induce any exon skipping, and in only one case did two AOs solely targeting ESE sites induce exon skipping. This finding further suggests the importance of assessing AO sequences targeting the splice sites of *FBN1* exons 27 and 49.

Other factors that could limit the splice-switching potential of AO sequences include pre-mRNA secondary structure and splice site ‘strength’. The secondary structure of pre-mRNA has been shown to play a crucial role in both the splicing process²⁴⁵ and AO binding, with certain secondary structures limiting the binding affinity of an AO to its target.²⁴⁶ We also speculate that synergistic cocktails rely on one AO changing the secondary pre-mRNA structure allowing the

second AO to bind and block splicing. Therefore, further investigation of the pre-mRNA secondary structure of exons 27 and 49, could reveal optimal sequences to target to increase the strength of AO binding. Alternatively, it is possible that exons 27 and 49; which encode cbEGF-like domains, are essential in some way to the function or stability of fibrillin-1 and therefore their selection during splicing is more tightly regulated. The splice site scores for exon 27 and 49 are relatively 'strong' with consensus values for the donor of both exons and acceptor of exon 49 greater than average for constitutive exons (Table A4.3). While splice site scores are only a predicted measurement of the likelihood of the splicing machinery recognising the splice site, the relatively 'strong' splice site scores for exon/introns around exon 27 and 49 could impact AO efficacy.

While exons 15, 16, 26, 31, and 44 were extremely difficult to skip and required two-AO cocktails, the skipping of exon 22, 32 and 39 was relatively efficient using both single AOs and when using cocktails. This led to the identification of promising sequences for each exon 32 and exon 39. Interestingly the combination of two overlapping AOs targeting exon 32 resulted in a synergistic effect. We speculate that this occurs, due to AO binding being a dynamic, rather than static process, in which the AO might anneal to the target mRNA at the 5' end, release and then anneal again from the 3'-end or centre. This 'breathing' effect could allow for the partial binding of the first AO to facilitate changes to the mRNA structure that enhances the binding of the second AO, allowing both sequences to be active. The synergy observed here between two overlapping AOs indicates that overlapping-AO cocktails should not be discounted during the screening process.

The *FBNI* exons we have targeted for exon skipping, mainly encode the cbEGF-like domains that make up 43 of the 55 cysteine-rich motifs, as described in the previous chapters. However, skipping of a hybrid domain had not been attempted. The hybrid domains share similarities with both the EGF-like and TB domains and have been shown to play an integral role in fibrillin-1 folding and microfibril assembly.^{21,22} This could suggest that the encoded domain is critical and therefore this exon is unsuitable for exon skipping. However, we note that skipping of exon 22 that encodes part of the second hybrid-domain, is quite efficient using 2'OMe-PS AOs. Further assessment of the AOs targeting exon 22 as PMOs or TMOs, could reveal either an optimal target or the creation of a non-functional fibrillin-1 protein, unable to assemble into microfibrils. Either outcome would provide further evidence toward the identification of amenable *FBNI* exon skipping targets.

The correlation in splice-switching efficacy between 2'OMe-PS and PMO compounds of the same sequence is well established for DMD both *in vitro*¹⁶⁷ and in mouse models.²⁴⁷ This correlation shows that the PMO version of an AO sequence is generally at least, if not more efficient than its 2'OMe-PS counterpart. This correlation is expected because the neutral backbone

of the PMO chemistry prevents electrostatic repulsion by the negatively charged RNA or DNA, enabling these oligomers to bind to their targets with much higher specificity and affinity.¹¹³ However, other reports have shown that an efficient 2'OMe-PS sequence does not always translate into an effective PMO.^{195,248} These reports also suggest that some differences in efficiency are sequence and exon-specific rather than due to the different chemistries.^{195,248} We have similarly identified examples of poor translation between chemistries, in some cases conceivably the result of poor synthesis or quality rather than the AO sequence. Such issues are extremely expensive to investigate and bring forth the dilemma of re-synthesis or re-design.

In chapters 3, 4 and 5, we reported that the PMO version of an AO sequence usually induces a higher proportion of skipped products than the 2'OMe-PS version. However, here we show that PMO32 and PMO39 are not as efficient as might be expected. Two very different delivery methods and transfection concentrations make a direct comparison between the two chemistries impossible. We also observed a larger proportion of skipped products when using the PMO than the 2'OMe-PS AO. However, PMO32 and PMO39 are much less efficient than PMO52, PMO59 or PMO47 when used at the same concentration, despite the 2'OMe-PS AO equivalents of all five sequences inducing similar skipping efficiencies. These findings suggest that the PMO32 and PMO39 sequences are not as efficient as expected from the 2'OMe-PS AO screening.

Considering factors such as sequence length, base composition and self-complementarity, the only apparent separation between the design of the PMOs targeting exons 32 and 39 and those targeting exons 47, 52 and 59 was their GC content. Both PMO32 and PMO39 have lower GC content, 40% and 32%, respectively, than PMO47 (60%), PMO42 (52%) or PMO59 (48%). *In silico* analysis of the *FBNI* exon 32 and 39 mRNA secondary structure showed that PMO32 (Figure A4.7) and PMO39 (Figure A4.8) both target tight hair-pin loop structures. These AOs must therefore overcome tight secondary structures in order to anneal to the respective targets. However, neither the GC content nor the annealing site's secondary structure is specific to the PMO chemistry. Consequently, the cause of the lower than expected PMO efficiency is unknown. Further investigation to assess the quality and purity of the batch of PMO used, would indicate if poor synthesis is at fault.

The level of exon skipping induced by PMO32 and PMO39, while relatively good under some circumstances were insufficient for the purposes of this study where transcript homogeneity is vital. We speculated that the lower exon skipping efficiency was related to poor delivery of the PMO and therefore, we tested two additional delivery methods, Lipofectamine 3000 and Endo-Porter. It is generally considered that Lipofectamine 3000 transfection is applicable only to the delivery of negatively charged compounds; however, Aung-Htut et al.¹³¹ demonstrate that Lipofectamine 3000 can, in some instances, result in robust delivery of PMOs. On the other hand, Endo-Porter was designed by Gene Tools specifically for the delivery of PMOs.¹²⁹ Despite the

efficacy of these delivery methods in different situations, neither technique resulted in more efficient exon skipping than Nucleofection. We discovered very late in the project that the recently acquired Neon transfection system is incredibly efficient at delivering not only PMOs, but also TMO and 2'OMe-PS sequences. However, the Neon transfection system was not used to deliver the PMO32 and PMO39 sequences. Delivery of these PMOs using Neon transfection could allow for sufficient exon skipping to assess the effects of exon removal on the fibrillin-1 protein structure and function. However, we also believe that the sequences themselves should be further optimised to ensure the most efficient skipping, regardless of the delivery method.

Alternative chemistry

While there are many possible target exons within the fibrillin-1 gene, we have shown during the screening process that many are not readily skipped from the mature mRNA. We also showed that an efficient 2'OMe-PS AO sequence identified during screening does not always translate into a more efficient PMO. However, previously we had only tested two AO chemistries despite the many available options. We tested a third chemistry, the TMO, that shares similarities with both PMO and 2'OMe-PS chemistries. The TMO chemistry proved to be very efficient at inducing exon 52 skipping, more so than any 2'OMe-PS tested, and at 10 days after transfection more so than the PMO chemistry.

We found that the TMO and PMO sequences tested were consistently more efficient than their 2'OMe-PS counterparts. The TMO sequences were more effective at inducing target exon skipping after transfection using both Lipofectamine 3000 and the Neon transfection system. Since the 2'OMe-PS AOs can be delivered using the same systems as the TMOs the difference in efficiency is unlikely to be related to poor delivery of the 2'OMe-PS AOs. We also demonstrate that the 2'OMe-PS sequences result in marked cell death, especially after 10 days. Cell death was also observed in PMO treated cells; however, the remaining cells were observed to continue proliferating, which would have resulted in the dilution of PMO in treated cells. Similar levels of cell death were seen previously when using the Nucleofection transfection system, but this was thought to be associated with the stress of the Nucleofection process and the use of a relatively high PMO concentration. However, here a much lower concentration was used, and cell death was still evident.

Further investigation to determine the cause of lowered cell viability after PMO transfection could allow for modification to the transfection protocol to improve cell survival. Interestingly the TMO chemistry resulted in minimal cell death, even after 10 days and was more effective than both PMO and 2'OMe-PS sequences at this time-point. Extension of this incubation period could reveal the residence time of the TMO chemistry in cells and possibly better reflect the quality of the extruded fibrillin-1. Such experiments would be essential prior to embarking on *in vivo* work, which requires a more defined timeline and outcome measures.

Since TMOs carry a negatively charged backbone, these AOs can be efficiently delivered using Lipofectamine 3000, similar to 2'OMe-PS and other negatively charged AOs. The use of cationic liposome preparations could not be applied to deliver PMO32 and PMO39, prompting the evaluation of a second electroporation-based method, the Neon transfection system. We found Neon transfection to be extremely efficient, achieving similar exon skipping efficiencies to Nucleofection in the same number of cells, while using 12.5 times less of the total PMO amount required for Nucleofection. Employing the Neon transfection method for further studies should allow for sufficient and reproducible exon skipping mediated by additional sequences. Furthermore, this would enable additional fibrillin-1 functional assays to be performed, evaluating if exon skipping allows for not only the formation of fibrillin-1 fibres but also the formation of functional fibrillin-1 microfibrils.

The PS backbone is known to interact with and sequester numerous nuclear proteins, including paraspeckle proteins, forming nuclear and cytoplasmic aggregates that can disrupt normal cellular function.^{113,243,244} The exact effect of nuclear protein aggregates on cell biology is not clearly defined. However, these aggregates are of particular importance as the majority of the proteins involved are RNA-binding proteins,^{249,250} and are involved in cellular processes such as regulation of transcription, transport, splicing and ribosomal RNA processing.^{249,250} Therefore, the aggregates observed could be expected to disrupt the nuclear structure and compromise global cellular functions, such as gene expression and splicing, ultimately leading to apoptosis.^{243,244}

We observed disrupted staining of both NONO and SFPQ in cells treated with 2'OMe-PS AOs. We also confirmed that the disruption of paraspeckle protein staining was not delivery-method specific, with very similar results arising from both Lipofectamine 3000 and Neon transfection systems. In contrast, the NONO and SFPQ staining in TMO and PMO treated cells was, for the most part, consistent with untreated cells. The absence of abnormal staining in PMO treated cells is consistent with the report by Flynn et al.²⁴⁴ who similarly observed extensive disruption of paraspeckle protein staining with 2'OMe-PS AOs and normal staining in PMO treated cells using several different delivery methods. We note that while the vast majority of cells retained their normal staining pattern, cytoplasmic foci formed in all of the Neon transfected samples, indicating cellular stress resulting from the Neon transfection process. This is further supported by the lack of abnormal staining in the untreated cells that were not subjected to the Neon transfection process. The minimal disruption of staining in TMO treated cells despite sharing some similarity with the 2'OMe-PS chemistry further supports the safety profile and tolerability of the TMO chemistry. These findings support the use of TMOs and PMOs, over 2'OMe-PS AOs for further pre-clinical investigation of splice switching AOs for *FBNI*.

Immunofluorescent staining of fibrillin-1 in cells treated with each of the three chemistries revealed a similar story, as seen in chapters 3 and 4 of this thesis. Skipping efficiencies that result

in a mixture of fibrillin-1 transcripts and thus proteins, result in the complete loss of fibrillin-1 staining in healthy control cells and maintenance of no fibrillin-1 fibre staining in MFS^{Δ52} cells and MFS^{C211R} patient cells. This was consistent across all three chemistries. In contrast, fibrillin-1 fibres formed in healthy control and MFS^{Δ52} cells after transfection with the TMO sequences that resulted in more than 80% exon skipping. However, as seen previously, even extremely efficient exon skipping is insufficient to result in fibrillin-1 fibre formation in the MFS^{C211R} cells. The exact cause of this remains elusive, as previously hypothesised the presence of a small amount of each of the *FBNI* and *FBNI*^{c.6331T>C} transcripts could be causing this lack of fibrillin-1 fibre formation.

Interestingly due to both extremely efficient exon skipping (>80%) in some cases and poor exon skipping (<20%) in others, we observed fibre formation when the proportion of either FL or Δ52 transcripts was above a certain threshold. This threshold was particularly noticeable in healthy control fibroblasts treated with the lower concentration of either 2'OMe-PS sequence when the low level of exon 52 skipping (<20%) resulted in a very similar fibrillin-1 fibre morphology and abundance as seen when inducing greater than 80% exon 52 skipping. Therefore, for exon 52, this threshold appears to be approximately 80-85%. Unfortunately, the skipping efficiencies of the 2'OMe-PS and PMO AOs were insufficient to overcome this threshold and thus, no fibrillin-fibre formation was observed. We propose that additional research with additional time-points identifying each chemistry's optimal incubation time could reveal that all three chemistries result in a similar staining pattern when inducing sufficient exon skipping.

While Eteplirsan and Golodirsan have been found to have positive impacts on clinical endpoints,^{144,251} they need only result in the expression of trace amounts of dystrophin to be beneficial in the treatment of DMD.^{252,253} However, for an AO to be of therapeutic value for MFS, it must consistently and robustly induce sufficient exon skipping to result in a homogenous population of fibrillin-1 monomers. Therefore, the variable and insufficient exon skipping observed here pose a significant barrier, especially when moving forward into *in vivo* studies where AO delivery is a major limiting factor, particularly since AOs tend to accumulate in the liver and kidney.^{254,255}

Of several efforts that have been made to enhance the delivery of AOs to the target tissue, one promising method is the conjugation of the AO with a cell-penetrating peptide.^{134,187,188} Cell-penetrating peptides are typically short peptide fragments derived from naturally occurring protein translocation motifs¹⁹³ that can greatly improve the delivery of AOs. Peptide-PMO (PPMO) conjugates designed to treat DMD have demonstrated efficacy in mouse models of DMD;^{236,237} however, some arginine-rich cell-penetrating peptides result in toxicity at high doses.^{132,133} Nevertheless, a clinical trial is currently underway for the PPMO SRP-5051 (Sarepta Therapeutics), targeting DMD patients amenable to exon 51 skipping ([NCT04004065](https://clinicaltrials.gov/ct2/show/study/NCT04004065)). Sarepta

therapeutics released an announcement in July 2020 that SRP-5051 shows improved tissue exposure, exon skipping, and dystrophin production at a lower dose than Eteplirsen, with no negative renal findings.²⁵⁶ The clinical trial is ongoing to date. The application of peptide conjugated PMOs and possibly TMOs is particularly relevant to this project, where AO-mediated exon skipping must be consistent and robust to facilitate a homogenous population of fibrillin-1 monomers.

In the previous chapters of this thesis, we described promising AO sequences that can mediate the exclusion of *FBNI* exons 47, 52 and 59 and lead to the formation of fibrillin-1 fibres under certain conditions. This chapter focused on screening AO sequences targeting additional fibrillin-1 exons to identify a suite of AOs with therapeutic potential. We found that not all *FBNI* exons are readily skipped and that there is significantly more work that can be done to optimise this therapeutic strategy further. We also investigated the efficacy of a third chemistry. We found that the TMOs tested were more efficient than their 2'OMe-PS counterparts and at 10 days, more so than the PMO equivalents. We also demonstrate that both the PMO and TMO chemistries result in minimal disruption of the paraspeckle proteins NONO and SFPQ, further demonstrating their safety and supporting their use in further therapy development. The use of antisense oligonucleotides is rapidly evolving, and we believe that the research presented here shows the great advantage and promise of antisense therapies for the type-1 fibrillinopathies.

Chapter 7
Final Discussion and Conclusions

7.1 Current knowledge and splice-switching strategies

Marfan syndrome (MFS) is a dominantly inherited connective tissue disorder characterised by progressive skeletal, ocular and cardiovascular abnormalities.³⁴ The MFS phenotype varies drastically both between and within affected families, leading to a spectrum of severity.⁴ In the most severe form; neonatal MFS, patients begin showing symptoms as neonates and have a life expectancy of fewer than 24 months.⁴⁹ However, for the majority of patients, life expectancy is approximately 70 years.⁷⁵ This life expectancy is more than 30 years longer than that estimated in the 1970s, primarily due to advances in surgical intervention and symptom management.^{35,75,257} However, despite these advancements, a diagnosis of MFS still places a considerable burden on the livelihood and quality of life of those affected,^{28,171,258} and there are currently no therapeutic options that address the primary aetiology of the disease.

Marfan syndrome is caused by mutations in the fibrillin-1 gene (*FBNI*),¹ with over 2800 unique disease-causing mutations reported that are spread throughout the *FBNI* sequence.^{2,3} Immediately after translation and secretion the fibrillin-1 protein, encoded by 65 of the 66 *FBNI* exons, the fibrillin-1 monomers aggregate to form the backbone of microfibrils to which other microfibril associated proteins bind.^{11,13,17} Fibrillin-1 is expressed in most connective tissues and has both structural¹¹ and regulatory roles.¹² An essential function of fibrillin-1 is the regulation of transforming growth factor-beta (TGF- β) bioavailability, and thus its activity through sequestration and regulated release.^{12,16} This regulation is critical to maintaining extracellular matrix stability; dysregulation due to loss of functional fibrillin-1 microfibrils is one of the keystones of the MFS pathogenesis.^{16,71,72} The way in which *FBNI* mutations result in loss of functional microfibrils is dependent on the mutation type. Broadly speaking, mutations can result in haploinsufficiency,^{31,161} dominant-negative interaction,⁶⁸ increased susceptibility to proteolysis,^{15,23} intracellular retention^{25,52,66} or loss of function.⁶⁹

The approvals of the splice-switching antisense oligonucleotide (AO) drugs Eteplirsen,¹⁴⁰ and Nusinersen¹⁶³ by the United States Food and Drug Administration (FDA) in late 2016 led to the conception that splice-switching strategies could be applied to address fibrillin-1 mutations. We hypothesised that removing an amenable mutation-associated exon from all *FBNI* transcripts would result in internally truncated but identical fibrillin-1 monomers, capable of forming microfibrils regardless of the original mutation type.

We hypothesised that the removal of an amenable exon would result in one of the following scenarios. For missense mutations, removing the mutation-associated exon from affected and unaffected transcripts would eliminate the aberrant sequence and restore homogeneity between fibrillin-1 monomers. For splice-site and in-frame deletion mutations, excluding the mutation-

associated exon(s) from the remaining unaffected transcripts would also restore the domain periodicity and monomer homogeneity. Alternatively, enhancing exon selection could negate the effects of splicing mutations and lead to exon inclusion, restoring monomers to the full-length state. Lastly, for nonsense and intra-exonic frame-shifting insertion or deletion mutations, excluding the mutation-associated exon from the affected transcripts would restore the reading frame, rescuing transcript functionality. The mutation-associated exon would also need to be removed from the unaffected transcripts to maintain monomer homogeneity. For each of these scenarios, we hypothesised that the internally truncated proteins produced would be capable of forming microfibrils, given a sufficiently homogenous monomer population.

7.2 Main findings and study limitations

The main focus of this thesis was the development of a suite of antisense oligonucleotides applicable for therapeutic applications in MFS. We developed AOs to mediate the exclusion of the target exon from the *FBNI* pre-mRNA and assessed efficacy in healthy control and patient-derived cells. We also assessed the effects of exon skipping on microfibril formation through immunofluorescent staining of fibrillin-1.

7.2.1 Proof-of-concept

As an initial proof-of-concept for this project 2'OMe-PS AOs targeting *FBNI* exon 52 were assessed in healthy control fibroblasts where they were shown to induce exon 52 exclusion. A promising AO sequence was then evaluated as a Phosphorodiamidate morpholino oligomer (PMO) in healthy control fibroblasts, the result of which was an encouraging increase in induced products missing exon 52 in a strong dose-dependent manner. These titration experiments were invaluable, allowing us to observe the formation of healthy fibres with 0% exon skipping, loss of fibrillin-1 fibres with 50% skipping and subsequent re-appearance of fibrillin-1 fibres with greater than 80% skipping. This finding provided the initial evidence that AOs can mediate exclusion of a *FBNI* exon leading to the formation of fibrillin-1 fibres.

The dose-response observed in healthy control cells further supports the dominant-negative pathogenic model; demonstrating the inability of a heterogenous population of fibrillin-1 proteins to form microfibrils. However, this finding also has relevance to mapping potentially amenable *FBNI* exons that could be targeted with splice-switching therapies. Importantly, being able to induce a disease-like state would allow for the use of healthy control cells, rather than specific patient cells, to identify exons that when removed do not disrupt the expression or function of fibrillin-1. This would be especially applicable to mutations that result in the loss of an exon as the target of the AO sequence in such cases is the healthy exon rather than the mutation-harboured exon.

After demonstrating initial proof-of-concept, we further extended the research question, asking whether the same AO sequence is efficient in multiple cell lines with different mutations? And are all mutation types affecting the targeted exon amenable to this splice-switching strategy? Further assessment of the PMO52 sequence in fibroblasts from two patients with exon 52 mutations revealed that the most effective AO sequences were optimal in all cell lines tested. However, the effect of exon skipping in the two patient cell lines in response to PMO52 treatment differed. The MFS^{Δ52} cell line, with a heterozygous synonymous mutation that resulted in exon 52 skipping, responded in much the same way as the healthy control cells, with no fibre formation at 50% exon skipping and re-appearance of fibres with more than 80% skipping. However, in the MFS^{C211R} fibroblasts carrying a missense mutation, no fibres were formed even when 95% exon skipping was induced. This finding highlights the necessity for extremely efficient exon skipping. We suggest the lack of fibres is due to the presence of both wild-type and mutant full-length proteins that impedes the ability of the fibrillin-1^{Δ52} monomers to aggregate. However, further investigation, such as removing all full-length transcripts using RNase-H mediated cleavage, will reveal if this is truly the case. Conversely, some *FBNI* missense mutations may result in a negative gain of function or dominant negative effect and hence may not be amenable to this splice-switching strategy.

Extending the concept further, we endeavoured to identify effective AOs targeting other *FBNI* exons. Screening of additional 2'OMe-PS AOs revealed promising candidate sequences targeting exons 32, 39, 47 and 59. However, for the most part, the PMO equivalents for these sequences induced insufficient exon skipping to meet the high demand required for transcript and therefore protein homogeneity. The PMO targeting exon 47 was the exception to this, inducing extremely efficient skipping in healthy control and MFS^{Δ47} patient fibroblasts. The resulting fibrillin-1 staining pattern mirrored that observed after exon 52 skipping. That is, strong fibres in the untreated healthy control, total lack of fibres with ~50% skipping and subsequent re-appearance of extracellular fibrillin-1 fibres, albeit at a lower abundance, correlated with greater than 80% skipping. This finding further supported our hypothesis and cemented the idea that splicing mutations are particularly responsive to this treatment strategy.

Conversely, the levels of exon skipping induced by PMO32 and PMO39 were insufficient to overcome the dominant-negative interaction between differing fibrillin-1 monomers. We speculated that a more effective delivery method could increase exon skipping levels *in vitro*; however, neither Lipofectamine 3000 nor Endo-Porter enhanced exon 32 or 39 skipping. It is likely that with further optimisation of the AO sequences, chemistry and delivery method, more efficient exon skipping could be achieved. For example, as shown in chapter 6, the TMO chemistry is very effective and Neon transfection is incredibly efficient. Assessment of AO sequences targeting exons 32, 39 and 59 using the TMO chemistry and Neon transfection could allow for sufficient skipping to evaluate function of the resulting fibrillin-1 isoforms.

Inconsistent exon skipping across multiple experiments proved to be a major limitation when assessing the efficacy of PMO59. In one replicate, PMO59 induced sufficient skipping (79%) in the MFS2414* patient cell line to induce some extruded fibrillin-1 fibres; although at a relatively low abundance. However, a second replicate saw a large decrease in exon skipping efficiency and a resulting lack of fibrillin-1 fibres. Further repeats of this experiment are required to gain a robust, and reproducible, understanding of the effects of exon 59 skipping in this patient cell line. Furthermore, it would appear that the threshold for ‘sufficient’ exon skipping that results in fibrillin-1 fibre formation, may be mutation or cell-line specific. Evidence for this is that more than 80% skipping of *FBNI* exon 47 or 52 was associated with fibre formation; however, 89% skipping of exon 59 resulted in only an increase in diffuse fibrillin-1 staining with minimal fibre formation in the MFS^{Δ59} patient cell line. However, inconsistent skipping efficiencies across experimental replicates made it impossible to accurately ascertain the abundance and morphology of the fibrillin-1 isoforms created. Determining and rectifying the cause of varying skipping efficiencies; most likely resulting from experimental design rather than the PMO itself, would allow for a more accurate measure of the effects of exon 59 skipping.

7.2.2 Recalcitrant *FBNI* exons

Further screening to identify additional *FBNI* exons amenable to exon skipping revealed that 4 of the 15 exons targeted could not be excluded from the transcript using any of the AOs designed initially. For a further three exons, a single AO induced less than 10% skipping. In contrast, previous studies investigating skipping of dystrophin exons found that 77 of 79 exons could be excised, and 2 out of 3 AOs induced some skipping, albeit at different efficiencies.¹⁶⁷ However, only 36 out of the 69 *FBNI* AO sequences tested here induced any exon skipping.

Development of AOs that successfully target these recalcitrant *FBNI* exons may be as simple as screening additional sequences. On the other hand, modification to the AO chemistry could result in more efficient skipping. A recent report identified that the addition of locked nucleic acid bases to produce LNA/2'OMe-PS mixmers resulted in more effective AOs.²⁵⁹ However, the cost of this improved skipping was the activation of cryptic splicing and other unwanted effects.²⁵⁹ Therefore, while mixmer AOs could reveal an effective sequence that could be further optimised, the balance between benefit and risk of such AOs would need to be evaluated prior to further development. Alternatively, we have shown that the TMO chemistry is extremely efficient at mediating exon 52 skipping. Assessment of TMO sequences for recalcitrant exons could yield a promising sequence that could then be further optimised and developed. Lastly, there is a strong likelihood that certain *FBNI* exons are not amenable to AO-mediated exon exclusion. Low skipping efficiency could be an indicator of necessity or particularly strong exon definition, and therefore exclusion of the exon could have negative impact on the function of fibrillin-1.

The use of AO cocktails to enhance antisense intervention has been reported several times^{167,260,261} and can greatly increase the level of exon skipping that is achieved compared to when using a single AO. We speculate that synergistic cocktails rely on one of the AOs altering the secondary structure, allowing the second AO to bind and block splicing. This theory could explain why the combination of two effective AOs can be antagonistic, as one may prevent the other from binding. The sequence features that result in these differing relationships has not been resolved and most likely will differ between targets. Here, we identified that the majority of cocktails evaluated resulted in similar skipping efficiencies expected from the two AOs individually. However, some synergistic cocktails were identified, most consisted of one AO targeting a splice site and the other AO targeting a region enriched for predicted ESEs. However, the number of AOs tested for each exon was limited, generally three, and therefore further investigation exploring a large number of AOs could reveal a more robust trend and aid in the design of optimal splice switching AOs.

7.2.3 Multi-exon skipping

As an alternative strategy to single exon skipping, we attempted to induce skipping of three consecutive exons simultaneously. Supported by the successful pre-clinical application of multi-exon skipping for DMD,^{262–264} the rationale is that effective multi-exon skipping would increase the number of individuals that could be treated with a single therapeutic preparation. The treatment of a greater number of patients with fewer therapies would prove particularly useful for MFS as *FBNI* mutations are spread throughout the gene with no mutation hotspots. On average, each single-exon skipping AO preparation could only be applied to 1.5% of all *FBNI* mutations.

The region from exon 45 to 47 was chosen as a model for multi exon skipping due to the availability of a patient cell line with genomic deletion of exons 45-47 (MFS^{Δ45-47}). Despite low skipping efficiencies achieved when screening 2'OMe-PS AOs targeting exons 45 and 46, the combination of PMO45, PMO46 and PMO47 induced triple-exon skipping in the majority of *FBNI* transcripts. Unfortunately, to induce such 'efficient' skipping, an extremely high total PMO cocktail concentration was required. The tolerability of this PMO concentration, and how it would translate to *in vivo* studies, has not been explicitly reported. However, the high the concentration is likely to be a major limiting factor in the further development of multi-exon skipping strategies for MFS. Especially since the higher the concentration required, the higher the cost of treatment and risk of toxicity.

A second limitation we identified was the unexpected exclusion of exon 48 along with exons 45, 46 and 47. Non-specific or unexpected AO-mediated exon exclusion has been reported for other genes.^{226,265} However, this was the first time we observed non-specific skipping in *FBNI* transcripts. The reason why exon 48 is also skipped has not been fully explored; however, binding of the AOs to nearby exons likely disrupts the motifs influencing exon 48 selection, resulting in

its exclusion. The fact that exon 48 seems to be readily excluded indicates that it may be a prime target for future therapy development. In addition, if efficient exon 45-48 skipping could be achieved, and the resulting protein was functional, such a preparation could be applied as a therapy to an even larger number of patients. Nevertheless, while we demonstrate that multi-exon skipping is possible for *FBNI*, it is not currently viable, at least for the *FBNI* exon 45-47 region. Furthermore, while the multi-exon skipping strategy would be exceptionally useful if successful, multicomponent drugs can be less favourable, especially if some components of the drug are not always required. Therefore, at this point, further research into this strategy for Marfan syndrome will likely be out of scientific curiosity; for example, to determine if other regions of *FBNI* are more readily removed.

7.2.4 Alternative chemistry

The final focus of this research project was the evaluation of the exon skipping induced by the newly developed TMO chemistry. The TMO combines properties of both 2'OMe-PS and PMO chemistries to form a morpholino-PS hybrid.²⁴⁰ The combination results in high affinity for RNA and excellent stability against nucleases.²⁴⁰ We identified that AO sequences targeting *FBNI* exon 52 were more efficient when applied as the TMO chemistry than as the 2'OMe-PS chemistry, regardless of the delivery method or duration of incubation. The TMOs and PMOs demonstrated similar exon skipping efficiencies 24 hours after transfection. After ten days, the PMO resulted in a loss of cell viability; subsequent cell proliferation then diluted the PMOs effects. In contrast, the TMO continued to show increased exon skipping over the ten-day period. One of the major advantages of the TMO chemistry is the ease of synthesis, compared to PMOs, that does not require specialised equipment other than a conventional nucleic acid synthesiser.²⁴⁰ The thiophosphoramidate backbone of the TMO chemistry also enables the incorporation of other chemical modifications allowing further customisation of the oligo.²⁴⁰ Therefore, the equal, or possibly greater, skipping efficiency of the TMO chemistry combined with its ease of synthesis provides strong support for its further evaluation and addition to the repertoire of chemistries routinely used in studies developing antisense therapeutics.

A second, unexpected outcome of the TMO evaluation process was the acquisition of the Neon® Transfection System (Life technologies, Thermo Fisher Scientific) and consequent efficient transfection of TMOs. The Neon system was initially evaluated as it requires a lower transfection volume and thus requires less reagent. We found this method to be incredibly efficient at delivering not only TMOs, but also PMOs and 2'OMe-PS AOs. One of the major advantages being the use of 12.5 times less PMO than required when using the 4D-Nucleofector™ (Lonza). Reassessment of the PMO AOs described throughout this thesis, using the Neon transfection system could result in sufficient skipping to accurately and reproducibly assess the effects of exon skipping on the function of the fibrillin-1 isoforms produced. It is important to note, however,

that while efficient *in vitro* delivery may provide proof-of-concept and efforts to enhance AO delivery to target organs and cells are underway^{184,188,190,191} *in vivo* delivery still faces significant challenges that must be overcome.^{132,193}

One of the main drawbacks of the 2'OMe-PS AOs that we have reported is their propensity to cause cell death and impact on cellular functions.²⁴⁴ This cell death limits the concentration and incubation period that can be tested, consequently limiting the exon skipping. We reported interaction between the PS backbone and paraspeckle and other nuclear proteins, leading to sequestration and the formation of nuclear and cytoplasmic aggregates, ultimately leading to apoptosis.^{113,243,244} Flynn et al.²⁴⁴ reported that PMO sequences do not induce the formation of aggregates. However, the effect of the TMO chemistry on paraspeckle proteins was unknown at that time. We demonstrate that while the 2'OMe-PS AOs caused aggregates in a large proportion of cells, the paraspeckle protein staining in TMO and PMO treated cells was, for the most part, consistent with untreated cells.

Antisense oligonucleotides with a PS-backbone have a varied history in the clinic. While some trials are on-going,¹⁹⁷ the Drisapersen DMD studies were suspended after failing to meet primary and secondary endpoints, while also associated with life threatening side effects including injection site reactions, renal effects and thrombocytopenia.²⁶⁶⁻²⁶⁸ The hepatotoxicity observed may, in-part, be the result of off-target hybridization, however, the exact cause of the injection site reactions remains unknown.²⁶⁹ Some groups have reported evidence suggesting the toxicity is mediated at least in part by the non-specific interaction of nuclear proteins with the PS backbone.^{243,244,270} Therefore, while further assessment of TMOs is certainly required to assess their tolerability and safety *in vivo*, the minimal disruption of SFPQ or NONO localisation in TMO-treated cells, despite the TMO sharing similarities with the 2'OMe-PS chemistry, provides promising evidence for the TMO chemistry's safety and tolerability. These findings further support use of the TMO and PMO chemistries, over 2'OMe-PS AOs, when further developing AO for potentially therapeutic applications.

7.3 Unanswered questions and future challenges

This study has shown proof-of-concept for the potential therapeutic benefit of AO mediated splice-switching to restore the homogeneity of fibrillin-1 monomers, at least for some mutations. However, this study has several limitations and questions left unanswered for which further investigation is required.

7.3.1 The function of the fibrillin-1 isoforms created

The primary finding of this study was the re-appearance of extracellular fibrillin-1 fibres in certain cell lines after more than 80% skipping was induced. This result demonstrated that the

fibrillin-1^{Δ47}, fibrillin-1^{Δ52} and fibrillin-1^{Δ59} proteins could form fibre-like aggregates in the near-absence of wild-type fibrillin-1 monomers. However, we were not in the position to further explore the function of the fibrillin-1 isoforms produced. To be of therapeutic value, the proteins produced must be capable of forming the microfibril backbone, interacting with microfibril associated proteins and regulating proteins such as TGF-β. Methods to evaluate particular functions of fibrillin-1 have been described,^{23,230,271,272} however, such functional analysis was outside of the scope of this thesis.

Each domain type in fibrillin-1 is associated with particular functions, however, the specific functions of each domain and the possibility of functional redundancy have not been fully explored. With the current knowledge of the fibrillin-1 domain types, we can begin to make assumptions about the effects of exon exclusion and indicate what particular function(s) the removal of the domain could disrupt. For example, the majority of exons we targeted encode for cbEGF-Like domains that bind to calcium. Most mutations affecting these domains disrupt calcium-binding, leading to proteolysis²³ or disruption of fibrillin-1 secondary or tertiary structure and microfibril assembly.^{25,183,273} We hypothesised that removal of the entire exon encoding these domains will negate the altered domain structure. Therefore, assessing the calcium-binding capacity and proteolysis of fibrillin-1 isoforms lacking these domains would be essential.

Similarly, targeting exons 39 and 52 lead to the partial removal of TB domains, while skipping of exon 22 leads to the partial removal of a hybrid domain. Homozygous mutations that result in skipping or in-frame deletion of these exons have not been reported; therefore, the function and stability of the fibrillin-1 isoforms lacking these partial domains are unknown. The hybrid domains are reported to play an integral role in fibrillin-1 folding and microfibril assembly.^{21,22} Therefore, changes in microfibril morphology, and bead-to-bead periodicity between wild-type and AO-induced isoforms could be revealed using electron microscopy.^{272,274} Less is known about the function of the TB domains, however, they are involved in extracellular matrix construction and storage of latent TGF-β.²²⁸⁻²³⁰ The importance of these domains could mean that a fibrillin-1 isoform lacking one domain may be non-functional. Therefore, the ability of the AO-induced fibrillin-1 isoforms to regulate TGF-β also needs to be assessed.

Another key finding to be addressed by further research is the overall decrease in fibrillin-1 staining abundance we observe when inducing exon skipping. We were unable to resolve the cause or effect of this loss of fibres. Attempts to isolate and visualise intracellular and extracellular fibrillin-1 via western blotting were inconsistent with poor fibrillin-1 detection in healthy control samples. This meant that possible changes in the abundance of fibrillin-1; that could explain loss of fibre formation, were unable to be assessed. One possible explanation is that the extruded fibrillin-1 fibrils are too unlike the normal protein and are degraded. Nevertheless, we know that fibrillin-1 haploinsufficiency leads to the MFS phenotype. Therefore, further investigation should

be performed to determine 1) the cause of reduced fibrillin-1 expression, 2) the amount of fibrillin-1 fibres required to reduce the MFS phenotype and 3) a way to increase the expression of the fibrillin-1 isoforms being produced. To better understand the function of the fibrillin-1 isoforms induced *in vivo* models would be required.

7.3.2 Fibroblast and animal models in therapy development

Fibroblasts derived from skin biopsies are a common model for *in vitro* studies because they are readily obtainable compared to many other cell types. Fibrillin-1 is expressed throughout the body, including dermal fibroblasts¹⁶⁹ making them a viable cell model for our initial investigations. However, Aubert et al.¹⁶¹ demonstrated that several different mechanisms, including fibrillin-1 expression, are involved in determining the severity of MFS symptoms, and that these mechanisms differ between organ, tissue and cell types. Therefore, while a fibroblasts model may be sufficient for initial screening and proof-of-concept, further investigation of splice-switching therapies should include assessment across multiple cell and tissue types.

Animal models, in particular mouse models, have greatly advanced our understanding of diseases, their mechanisms and enable pre-clinical assessment of therapeutic preparations.^{275–277} There are multiple mouse models available in which mutations have been generated in the mouse *Fbn1*. These mouse models have been reviewed by Sakai et al.²⁷⁸ and Rurali et al.²⁷⁵ Some of the phenotypes of Marfan syndrome were successfully recapitulated, and different models demonstrate the effects of hypomorphic, missense and in-frame deletion mutations. Of particular interest to this study are mouse models with in-frame deletions, as they could provide insight into exon skipping. The $mg\Delta^{loxPneo}$ has an in-frame deletion of *Fbn1* exons 19-24.²⁷⁹ In a heterozygous state $mg\Delta^{loxPneo}$ display a MFS phenotype while homozygous animals die 4-8 days after birth.²⁷⁹ This finding appears to conflict with our current hypothesis, however, quantification of the *Fbn1* mRNA levels revealed 47% expression of the wild-type protein.²⁷⁹ Therefore, this model is demonstrating a haploinsufficiency pathogenic mechanism.

Two other mouse models arise from *Fbn1* in-frame deletions of exon 7²⁸⁰ and exons 9-11,¹⁸⁰ however, in both cases, heterozygous and homozygous animals live long lives. Unfortunately, none of the currently available mouse models accurately demonstrate the effect of splice site mutations or the effects of exon skipping in a heterozygous or homozygous state. Due to the exon-specific nature of splice-switching AOs, a different mouse model would be required for each exon. Consequently, this is where the ability to create a disease-like state in normal cells through skipping the target exon in 50% of transcripts could prove useful in the initial testing of promising candidates.

While mouse models are, at this stage, unavoidable in pre-clinical assessment of potential therapies, the clinical relevance of splice-switching AOs in mouse models has limitations. Animal

models are often unable to fully recapitulate the human condition.^{281,282} An example of this is the mdx mouse in which a null allele due to stop codon results in no major phenotype despite disrupted dystrophin expression.^{283,284} Another major limitation is that the splicing machinery and regulatory sequences differ between species. Therefore, splicing outcomes in a mouse model do not always translate into those in human cells and vice versa. We previously reported a human-mouse comparison for dystrophin AO target sites showing that approximately 1/3 transferred coordinates, 1/3 had minor correlation and 1/3 worked in one species and not the other.²⁶⁰

The domain organisation of fibrillin-1 is conserved through evolution from jellyfish through to humans.^{285,286} However, regulatory motifs likely differ between the mouse and human sequences due to variability in the splicing factors themselves. Additionally, the mRNA secondary structure will vary between species, due to variation in the sequence and interaction with RNA binding proteins, resulting in an altered splicing pattern.²⁴⁵ Both factors are likely to alter the efficacy of specific AO sequences. Another consideration is that while fibrillin-1 is the predominant form in cells derived from a human adult skin biopsy, in mice *in vivo* there are two, and in humans, three, fibrillin genes and associated proteins.⁵ Since fibrillin-2 and to an extent fibrillin-3, would be involved in microfibril formation *in vivo*,^{5,18} it would be interesting to determine how this affects the efficacy, and specificity of the *FBNI* targeting AOs. It is possible that a pre-existing microfibril matrix could enhance the positive effects we observe as a result of exon skipping (L Sakai, 2021, personal communication 14 June). Conversely, other factors such as non-specific binding to the similar *FBN2* and *FBN3* gene transcripts could result in undesired splicing or sequester the AOs from their intended *FBNI* target. Such factors should be considered when moving forward into *in vivo* studies.

Alignment of the optimal AO sequences for exons 47, 52 and 59 with mouse *Fbn1* demonstrates both the sequence similarity and the narrow margin for variation. The AO sequences targeting *FBNI* exons 47 and 59 differ from the mouse sequence by three bases (Table 7.1). The exon 52 AO sequence differs by only two bases between mouse and human (Table 7.1). Interestingly, one of these two bases corresponds to the synonymous c.6354C>T mutation identified in the MFS^{Δ52} patient¹⁵¹ that results in exon 52 skipping by disrupting the balance between ESE and ESS motifs. The presence of a 'C' rather than a 'T' at this position without resulting in exon 52 skipping further indicates that the splicing motifs of the mouse *Fbn1* differ from those of the human gene. Mitrpant et al.²⁶⁰ reported a similar finding where two overlapping AO sequences designed to induce exon 53 skipping in mouse *dystrophin* resulted in cryptic splicing, however, no cryptic splicing was observed when targeting the same co-ordinates in the human *dystrophin* transcript. Nevertheless, animal models are currently the best available option for the pre-clinical evaluation of AOs. Therefore, the AOs tested here should follow this development pipeline. However, the limitations of these models should be taken into consideration when interpreting the results.

Table 7.1: Alignment of the optimal AOs targeting *FBN1* exons 47, 52 and 59 with the mouse *Fbn1*

AO47.2 / PMO47	
Human	G T T C C T T C A A C T G C C G C T G C
	* * *
Mouse	G C T C C T T C A A C T G T C G C T G T
AO52.1 ⁿ / PMO52	
Human	A A G T G G G A T C A T C G T G G G A C C T G A T
	* *
Mouse	A A G T G G G A T C A T T G T G G G C C C T G A T
AO59.2 / PMO59	
Human	T G G G G A A T G T G T C A A T G A C A G A G G A
	* * *
Mouse	T G G G G A G T G T G T C A A C G A C A G A G G G

7.3.3 Clinical trials for rare diseases

Another major challenge to the future of AO therapies for MFS and other rare diseases is the current clinical trial format that is less conducive to the development and assessment of personalised medicines. Some of the main limitations being small patient numbers, extensive phenotypic variation between patients, uncertain endpoints as well as varying ages and degree of disease progression. The ethical dilemma of treating an individual with a known disease outcome with a placebo drug should also be considered, especially when involving children. The FDA has now granted accelerated approval for three antisense drugs for DMD.^{140,142,164} However, before the approval of Eteplirsen in late 2016,^{140,144} concerns were raised over its efficacy, in particular, due to the small number of patients in the trial (12) and the lack of a placebo cohort. The rarity of such genetic disorders combined with the personalised nature of splice-switching therapies limits the number of patients able to participate in clinical trials. Therefore, clinical trials need to be adapted to overcome these limitations and additional clinical trial formats developed for rare diseases for which n-of-1, or similarly low participant numbers, are likely to be required.

To compensate for the small patient numbers robust surrogate outcome measures and biomarkers are used. For DMD, among a suite of other ambulation-based outcome measures,²⁸⁷ changes in muscle dystrophin is quantified and used to verify the efficacy of the treatment under evaluation.²⁸⁸ Evaluation of therapeutics for DMD also relies heavily on the well-established genotype:phenotype correlations between Duchenne- and Becker- muscular dystrophy that provides unequivocal evidence that some internally truncated dystrophin isoforms are functional.^{289–291} The known natural history of DMD could also aid in drug evaluation by acting as a ‘placebo-like’ comparison-point when assessing outcome measures.^{292,293} However many of these strategies would be less applicable to drug evaluation for MFS. Quantification of fibrillin-1 alone would be insufficient to determine if the protein is forming microfibrils and performing its other regulatory roles, making quantification an inaccurate outcome measure. Similarly, the variability in phenotype within and between MFS families^{30,273,294} hinders the ability to establish an unequivocal disease trajectory to use as a comparison point. While mild Marfan phenotypes

have been reported,^{295,296} the genotype-phenotype correlations are not as well established as they are for Duchenne- and Becker- muscular dystrophy. However other measures can be used, one of the most common biomarkers for MFS is serum levels of transforming growth factor- β (TGF- β).²⁹⁷ High levels of TGF- β in serum is correlated with faster aortic root growth and therefore changes in TGF- β levels has substantial prognostic value.²⁹⁷ For clinical trials evaluating Irbesartan, a drug aimed at decreasing dilatation of the aorta in MFS patients, the rate of aortic root dilatation was assessed as the primary endpoint.²⁹⁸ Identification of additional measures for more of the MFS phenotype could further increase the strength of such drug evaluation.

Another limitation in the clinical evaluation of many splice-switching therapies is the inability to assess the safety and tolerability of the drug in healthy volunteers. We have clearly demonstrated that less than 80% skipping in healthy control cells results in a disease-like loss of fibrillin-1 fibres. We also show that even with 80% skipping, the abundance of fibres can be greatly reduced. Therefore, assessment of *FBNI* AOs in individuals without MFS would likely result in deleterious effects. We suggest that while the safety of each AO chemistry needs to be evaluated in a clinical setting, the safety of individual AO sequences should be assessed in pre-clinical animal studies and patient cell-derived models.

The way in which safety studies are undertaken regarding dose escalation and selection of the maximum tolerated dose should also be considered. One class of phase 1 trial designs widely used is known as up-and-down designs that assess dose escalation and de-escalation based on prespecified algorithms.²⁹⁹⁻³⁰¹ One of the most well-known is the 3 + 3 design in which cohorts of three patients are sequentially enrolled, with each cohort receiving an increasingly high dose.^{299,300} However, for splice-switching therapies, the required dose and possible associated adverse events of one patient will not necessarily be consistent across all patients, especially when considering the extreme phenotypic variability of Marfan syndrome.^{30,273,294} A possible way to address this could be personalised dose-escalation. In this approach, following an initial dose, if the drug is well-tolerated, the dose is incrementally increased while monitoring adverse events until a change in specified biomarkers is observed. We believe that a more personalised approach to design, development and clinical evaluation of AO-mediated exon skipping therapies for the type-1 fibrillinopathies will be the most appropriate.

7.4 Final remarks and conclusions

This primary focus of this thesis was developing a suite of AOs that efficiently and specifically excise targeted exons from the *FBNI* pre-mRNA, thereby restoring fibrillin-1 microfibril assembly. Although this study is a preliminary, *in vitro* investigation, we demonstrate several novel findings. (1) Our candidate PMOs for exons 47, 52 and 59 induce efficient exclusion of the target exons. (2) Demonstrating proof-of-concept; more than 80% skipping of these exons can

result in fibrillin-1 fibre formation in healthy control and some of the patient fibroblasts. (3) Of particular significance, we demonstrate that in healthy control cells inducing approximately 50% skipping results in a disease-like loss of fibrillin-1 staining. This finding supports the dominant-negative model and indicates that healthy control cells could be used in place of specific patient samples for preliminary studies.

Throughout this thesis, we have demonstrated strong exon skipping across multiple *FBNI* exons. However, we also found that not all *FBNI* exons are as readily excluded signifying the extensive work that remains in developing this therapeutic strategy further. Lastly, we report on the more recently developed TMO chemistry. The TMO chemistry showed promising efficiency and tolerability *in vitro*; therefore, we believe it will become commonplace alongside PMOs in the development of Antisense therapies. While the requirement for extremely efficient exon skipping was one of the most significant limitations to this study, several other challenges and new questions were raised. Other factors that will need to be considered for future studies include the functionality of the fibrillin-1 isoforms produced, the effect of lowered fibrillin-1 abundance, the relatively high AO concentrations used, and inconsistency between experiments.

Advancements made to the management and surgical correction of MFS symptoms have significantly increased patients' life expectancy over the last 4-5 decades.^{35,75,257} However, therapies targeting the cause of disease could provide significant clinical benefit to patients; therefore, our search into AO-mediated therapies continues. The strategy presented here could be extended to several other genetic disorders with similar mechanisms, including the other type-1 fibrillinopathies. With the recent success of splice-switching AO therapies, namely the approval of Nusinersen,¹⁶³ Eteplirsen,¹⁴⁰ Golodirsen¹⁴² and Viltolarsen,¹⁶⁴ the number of clinically available antisense drugs has grown, and numerous pre-clinical and clinical trials are on-going. The use of antisense oligonucleotides is rapidly evolving, and we believe that the research presented here shows the great advantage and promise of antisense therapies for the type-1 fibrillinopathies.

Appendices

Appendix 1 Chapter 2 supplementary data

Fibrillin-1 antisense oligonucleotides

Table A1.1: A full list of antisense oligonucleotides used in this study.

The name, ID, GC content, length, chemistry and designer for each AO used in this study. The AO nomenclature is outlined in Chapter 2, Figure 2.1.

KG: Mr Kane Greer , JC: Ms Jessica Cale.

AO Name (FBN1 H...)	ID	Sequence (5'-3')	Length (bases)	Chemistry	Designed by
15A(-15+10)	AO15.1	UCA UCC AUA UCU GAA AAU ACA AAA C	25	2'OMe-PS	KG
15A(+41+65)	AO15.2	ACU GCC AUC UUC AUU GAU ACA CAU U	25	2'OMe-PS	KG
15D(+12-13)	AO15.3	UUA UAG CAC GAA CCU UUG CAA UAA C	25	2'OMe-PS	KG
16A(-14+11)	AO16.1	CUC GUU AAU GUC UGU GGC AGA GAA A	25	2'OMe-PS	JC
16A(+27+51)	AO16.2	UGA CGC AAC GCC CAU UCA UGC AGA U	25	2'OMe-PS	JC
16D(+14-11)	AO16.3	UGU UUU CUU ACC AAC ACA CAC ACG G	25	2'OMe-PS	JC
16A(+22+46)	AO16.2+5	CAA CGC CCA UUC AUG CAG AUC CCA G	25	2'OMe-PS	JC
16A(+32+56)	AO16.2-5	AGU GUU GAC GCA ACG CCC AUU CAU G	25	2'OMe-PS	JC
16D(+09-16)	AO16.3-5	CAU GAU GUU UUC UUA CCA ACA CAC A	25	2'OMe-PS	JC
22A(-13+12)	AO22.1	CCU UGA UGG UUU CUG CAG AGG AGG G	25	2'OMe-PS	JC
22A(+45+69)	AO22.2	UGG CUC CAU UGA UGU UGA UCU CAC A	25	2'OMe-PS	JC
22A(+84+108)	AO22.3	CAC GCA GCA CCG AGG GAG GAG CAG C	25	2'OMe-PS	JC
22D(+16-09)	AO22.4	UUC UCU UAC CAA CUU GGC AUA GGG U	25	2'OMe-PS	JC
26A(-18+07)	AO26.1	UUG AUA UCU UCA AGA AUA AGA AAA U	25	2'OMe-PS	JC
26A(+70+94)	AO26.2	AAG CCG CUG UCA CAC CUG CAC UUA A	25	2'OMe-PS	JC
26D(+22-03)	AO26.3	GAC CUG UGC AGU UCC UUU CUU CAG A	25	2'OMe-PS	JC
26A(+75+99)	AO26.2-5	GAG CAA AGC CGC UGU CAC ACC UGC A	25	2'OMe-PS	JC
26A(+100+124)	AO26.3+5	GUG CAG UUC CUU UCU UCA GAA UCA A	25	2'OMe-PS	JC
27A(-25-01)	AO27.1	CUG CAC AAA AAC AGC AAG UGG CAG C	25	2'OMe-PS	KG
27A(+38+62)	AO27.2	AGG GGU GUU CAC ACA CUG GCC UCU G	25	2'OMe-PS	KG
27A(+105+129)	AO27.3	CCA UGC AGU UCU UCA UCA UCA UGA A	25	2'OMe-PS	KG
31A(-21+04)	AO31.1	AUG UCU GCA AAG AAU AAA ACC AAC A	25	2'OMe-PS	KG

AO Name (FBN1 H...)	ID	Sequence (5'-3')	Length (bases)	Chemistry	Designed by
31A(+76+100)	AO31.2	GCC AUG AAU CCA UCA UAA CAC AAG C	25	2'OMe-PS	KG
31D(+13-12)	AO31.3	UUC UUU GCU UAC CUA CAC AAG UCU U	25	2'OMe-PS	KG
32A(-13+12)	AO32.1	ACU CAU UGA CAU CUG UAA AAC AUA U	25	2'OMe-PS	JC
32A(+47+71)	AO32.2 PMO32	AAA UGA GCC UUU CGU GUU UUC ACA G	25	2'OMe-PS PMO	JC
32D(+14-11)	AO32.3	AAC AAA CAC ACC UGU ACA GCC AGU U	25	2'OMe-PS	JC
32A(-08+17)	AO32.1-5	GUC ACA CUC AUU GAC AUC UGU AAA A	25	2'OMe-PS	JC
32A(+42+66)	AO32.2+5	AGC CUU UCG UGU UUU CAC AGG UCC C	25	2'OMe-PS	JC
32A(+52+76)	AO32.2-5	CAG AUA AAU GAG CCU UUC GUG UUU U	25	2'OMe-PS	JC
32D(+19-06)	AO32.3+5	ACA CAC CUG UAC AGC CAG UUU UUC C	25	2'OMe-PS	JC
32D(+09-16)	AO32.3-5	ACU UGA ACA AAC ACA CCU GUA CAG C	25	2'OMe-PS	JC
39A(-12+13)	AO39.1 PMO39	AUU UUG UAC UCG GCU AUU GAA ACA A	25	2'OMe-PS PMO	JC
39A(+31+55)	AO39.2	GUG AUA GGA UUU GGU CGG AAA CCU U	25	2'OMe-PS	JC
39D(+04-16)	AO39.3	AAG GAA ACA CAA UUA CCU UC	20	2'OMe-PS	JC
44A(+14+38)	AO44.1	UUC ACA GAC CCC UGG GAU CUC CCG G	25	2'OMe-PS	KG
44A(+44+68)	AO44.2	GCU GCC AAC CAU GUU GAU ACA CAC U	25	2'OMe-PS	KG
44D(+19-06)	AO44.3	ACU UAC CUU CAC AAA CCA ACA ACU U	25	2'OMe-PS	KG
45A(+15+39)	AO45.1	UGC GCU GGC ACA CUG GGC CGU UCU G	25	2'OMe-PS	KG
45A(+49+73)	AO45.2	CGG UAG CUG CCU GCA GUG UUG AUG C	25	2'OMe-PS	KG
45A(+87+111)	AO45.3	CUG UGG AGG UGA AGC GGU AGC CGG G	25	2'OMe-PS	KG
45D(+21-04)	AO45.4	AUA CCA UUG CAC UGU CCU GUG GAG G	25	2'OMe-PS	JC
46A(-09+16)	AO46.1	UGA CAU UCA UUA CGA UCU GUA AAU A	25	2'OMe-PS	KG
46A(+72+96)	AO46.2	UAA AAC CAG UGU GGC AAA GGC AAU A	25	2'OMe-PS	KG
46D(+12-13)	AO46.3	AUU GCA UAC UUA CCC AAG CAC AUG G	25	2'OMe-PS	KG
46A(-03+22)	AO46.4	AUU UCU UGA CAU UCA UUA CGA UCU G	25	2'OMe-PS	JC
47A(-03+20)	AO47.1	UCU UUC ACA UUC AUU UAU GUC UA	23	2'OMe-PS	JC
47A(+58+77)	AO47.2 PMO47 ²⁰	GCA GCG GCA GUU GAA GGA AC	20	2'OMe-PS PMO	JC
47A(+83+102)	AO47.3	UGU GAG AAA GGA UGA AAC CA	20	2'OMe-PS	JC
47D(+05-15)	AO47.4	AUU UUG CAC ACG CAC CUA UA	20	2'OMe-PS	JC
47A(+44+68)	AO47.5	GUU GAA GGA ACC AAU UGU GUU CCG G	25	2'OMe-PS	JC
47A(+69+93)	AO47.6	GGA UGA AAC CAU GAU UGC AGC GGC A	25	2'OMe-PS	JC

AO Name (FBN1 H...)	ID	Sequence (5'-3')	Length (bases)	Chemistry	Designed by
47D(+24-01)	AO47.7	CCU AUA CAG UCA UUG UUG UGA GAA A	25	2'OMe-PS	JC
47A(+56+80)	AO47.2-25mer	AUU GCA GCG GCA GUU GAA GGA ACC A	25	2'OMe-PS	JC
47A(+53+82)	AO47.2-30mer PMO47 ³⁰	UGA UUG CAG CGG CAG UUG AAG GAA CCA AUU	30	2'OMe-PS PMO	JC
49A(-13+12)	AO49.1	AUU CAU UGA UAU CUG CAA AGA AAA G	25	2'OMe-PS	KG
49A(+19+43)	AO49.2	CCU GGU GCA CAU UUU CUG GGU UCU A	25	2'OMe-PS	KG
49A(+83+107)	AO49.3	AUU UUG AAG ACU GUA UCC AGG UGG G	25	2'OMe-PS	KG
52A(+29+53)M	AO52.1 ^m	AUC AGG UCC CAC AAU GAU CCC ACU U	25	2'OMe-PS	KG
52A(+29+53)N	AO52.1 ⁿ PMO52	AUC AGG UCC CAC GAU GAU CCC ACU U	25	2'OMe-PS PMO	KG
52A(+29+48)N	2'OMe-PS 52-1			2'OMe-PS	
	PMO 52-1	GTC CCA CGA TGA TCC CAC TU	20	PMO	KG
	TMO 52-1			TMO	
52A(+34+53)N	2'OMe-PS 52-2			2'OMe-PS	
	PMO 52-2	ATC AGG TCC CAC GAT GAT CC	20	PMO	KG
	TMO 52-2			TMO	
52A(-08+17)	AO52.2	UAU CUG GCG GAA GGC CUC UGU GGU G	25	2'OMe-PS	KG
52D(+13-12)	AO52.3	CAG GCA ACU GAC CAA CUG CUG AAU C	25	2'OMe-PS	KG
52A(-23+02)	AO52.4	CUC UGU GGU GGA GAC ACU CAU UAA U	25	2'OMe-PS	KG
52A(+03+27)	AO52.5	CAU AAG GAC AUA UCU GGC GGA AGG C	25	2'OMe-PS	KG
59A(-21+04)	AO59.1	AUA UCU GUA AUU UAA CAA AUA UAA A	25	2'OMe-PS	JC
59A(+41+65)	AO59.2	UCC UCU GUC AUU GAC ACA UUC CCC A	25	2'OMe-PS	JC
	PMO59			PMO	
59A(+86+110)	AO59.3	AGU UAU AUC UGG AGU GUA CCC AGU U	25	2'OMe-PS	JC
59A(+36+60)	AO59.2+5	UGU CAU UGA CAC AUU CCC CAU UUC G	25	2'OMe-PS	JC
59A(+46+70)	AO59.2-5	UAU GAU CCU CUG UCA UUG ACA CAU U	25	2'OMe-PS	JC
Exon 52 inclusion					
52A(-181-157)	AOi51.1	CCC UAA GAU GUU GUG UCU ACU CCU U	25	2'OMe-PS	KG
52A(-130-106)	AOi51.2	AAU GAU GGA AAA AAC AAG CCC AGA A	25	2'OMe-PS	KG
52A(-44-20)	AOi51.3	UAA UAG AUA GAA CAA UAG CAA UUC A	25	2'OMe-PS	KG
52D(-01-25)	AOi52.1	UGA GAA UCC AGC ACA GGC AAC UGA C	25	2'OMe-PS	KG
52D(-46-74)	AOi52.2	AAA AUA AGA AUA ACU AGA GAA GAA GCA GA	29	2'OMe-PS	KG

AO Name (FBN1 H...)	ID	Sequence (5'-3')	Length (bases)	Chemistry	Designed by
52D(-98-122)	AOi52.3	AAU GAA GGG ACA AAA AAG UAG CAC U	25	2'OMe-PS	KG
Control AOs					
Unrelated Control	Ctrl	GGA UGU CCU GAG UCU AGA CCC UCC G	25	2'OMe-PS	
Control AO 1	Ctrl AO1	ATG TCC TGA GTC TAG ACC CU	20	TMO	
GeneTools control	GTC	CCT CTT ACC TCA GTT ACA ATT TAT A	25	PMO	
Modified GeneTools control	mGTC	TCT TAC CTC AGT TAC AAT TU	20	2'OMe-PS / TMO	
SMN H7A(+13+32)	SMN-7	CAC CTT CCT TCT TTT TGA TU	20	2'OMe-PS / TMO	
COL7A1 H73A(+21+40)	COL-73	CGC CCT TCA GCC CGC GTT CU	20	2'OMe-PS / TMO	

Patient cell lines

Table A1.2: Details of all Marfan syndrome patient cell lines used in this study.

All patient cells were obtained from the NIGMS Human Genetic Cell Repository at the Coriell Institute for Medical Research. Mutations were previously reported by the indicated reference. All mutations were confirmed via Sanger sequencing. F: female, M: male, cMFS: classic Marfan syndrome, nMFS: Neonatal Marfan syndrome. Type refers to the five groups outlined by Aoyama et al.⁶⁹ with S and D representing synthesis and deposition of fibrillin-1, respectively, as a proportion of that observed in a healthy control.

Coriell ID	ID	Sex/Age	Diagnosis	Exon	Variant in DNA/RNA	Predicted Protein change	Mutation type	Type	Reference
GM21936	MFS ^{ΔE32}	F	nMFS	32	c.3839-1G>A r.3839_3964del	p.(?) <i>In-frame loss of Exon 32</i>	Splice site	Type IV S:114% D:7%	Liu et al. ¹⁸³
GM21932	MFS ^{C1589F}	M/25	cMFS	39	c.4766G>T	p.(Cys1589Phe)	Missense, Cysteine substitution		Tynan et al. ²⁴²
GM21940	MFS ^{Δ45-47}	F	nMFS	45-47	c.(5424+1_5423-1)_(5789+1_5788-1)del r.5423_5788del	p.(?)	Genomic deletion	Type IV S:109% D:13%	Liu et al. ¹⁷⁰
GM21934	MFS ^{Δ47}	M	cMFS	47	c.5788+5G>A r.[5672_5788del, 5788_5789ins5788+1_5788+33]	p.(?) <i>In-frame loss of Exon 47 + 33bp insertion of intron 47</i>	Splice site	Type IV S:89% D:11%	Liu et al. ¹⁸³
GM21941	MFS ^{Δ52}	F	cMFS	52	c.6354C>T r.6314_6379del	p.(?) <i>In-frame loss of Exon 52</i>	Synonymous, Splicing	Type II S:41% D:5%	Liu et al. ¹⁵¹
GM21952	MFS ^{C2111R}	M	cMFS	52	c.6331T>C	p.(Cys2111Arg)	Missense, Cysteine substitution		Körkkö et al. ³⁰²
GM21992	MFS ^{R2414*}	F/22	Severe MFS	59	c.7240C>T	p.(Arg2414*)	Nonsense	Type II S:41% D:21%	Schrijver et al. ⁶¹
GM21937	MFS ^{Δ59}	M	cMFS	59	c.7205-2A>G r.7205_7330del	p.(?) <i>In-frame loss of Exon 59</i>	Splice site	Type IV S:88% D:16%	Liu et al. ¹⁸³

Appendix 2 Chapter 4 supplementary data

Enlarged immunofluorescence images

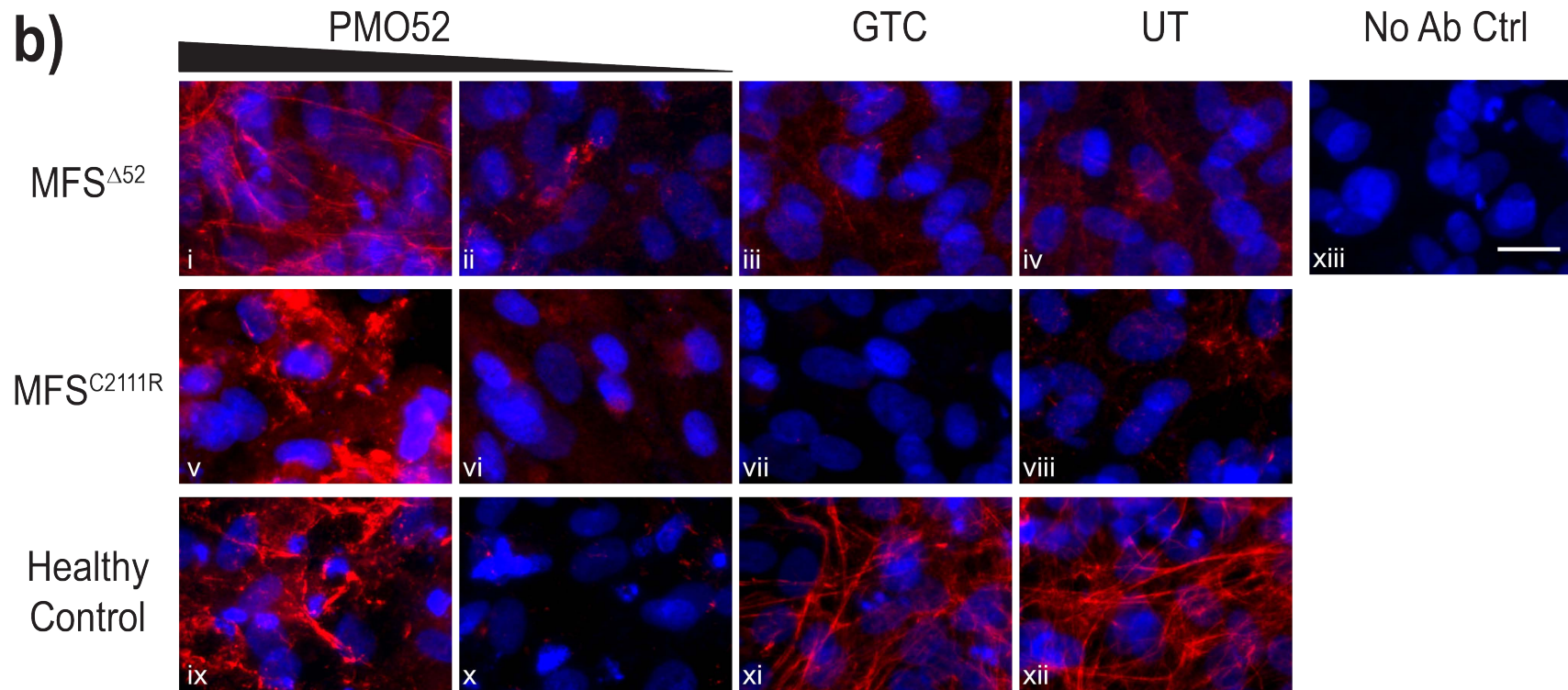


Figure A2.1: Enlarged immunofluorescence staining images from Figure 4.6

Healthy control, MFS^{Δ52} and MFS^{C2111R} patient fibroblasts were transfected with PMO52, Gene Tools control PMO (GTC) or left untreated (UT). Two concentrations were tested; 250 μM and 50 μM, calculated in the 20 μl nucleofection cuvette volume, and cells were collected after 4 days. Cells were stained for Fibrillin-1 (red) and counterstained with Hoechst (blue) for nuclei detection. No Ab control: no primary antibody added. Scale bar = 20 μm.

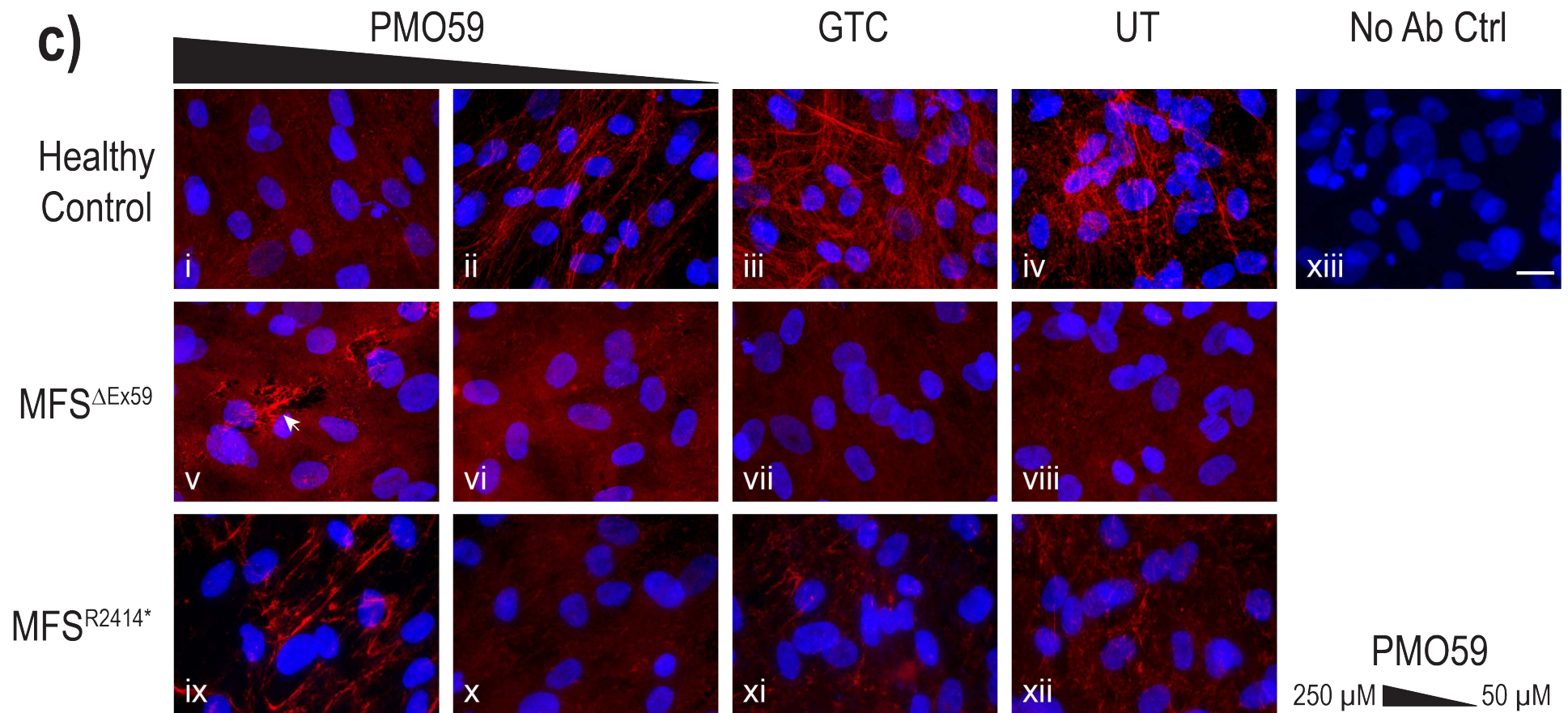


Figure A2.2: Enlarged immunofluorescence staining images from Figure 4.9 part c.

Healthy control, MFS^{Δ59} and MFS^{R2414*} fibroblasts were nucleofected with PMO59 at 250 μM, and 50 μM; calculated in the 20 μl nucleofection cuvette volume, in two replicate experiments and cells were collected after 10 days. GTC: Gene Tools control PMO used as a sham treatment, UT: untreated control. Transfected cells were stained for fibrillin-1 (red) and counterstained with Hoechst (blue) for detection of the nuclei. No Ab control: no primary antibody added. Scale bar = 20 μm.

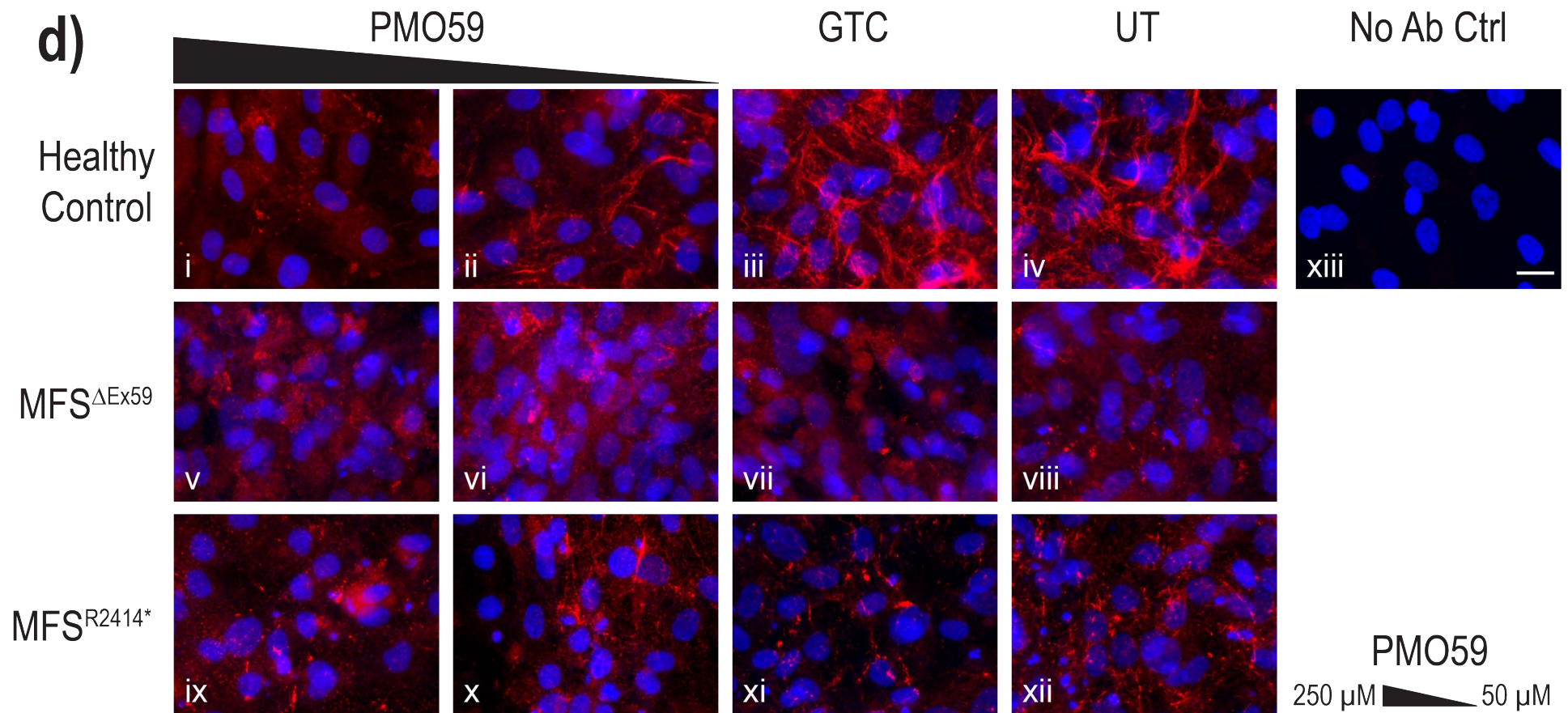


Figure A2.3: Enlarged immunofluorescence staining images from Figure 4.9 part d.

Healthy control, MFS^{Δ59} and MFS^{R2414*} fibroblasts were nucleofected with PMO59 at 250 μM, and 50 μM; calculated in the 20 μl nucleofection cuvette volume, in two replicate experiments and cells were collected after 4 days. GTC: Gene Tools control PMO used as a sham treatment, UT: untreated control. Transfected cells were stained for fibrillin-1 (red) and counterstained with Hoechst (blue) for detection of the nuclei. No Ab control: no primary antibody added. Scale bar = 20 μm.

Synonymous mutations affecting *FBN1*

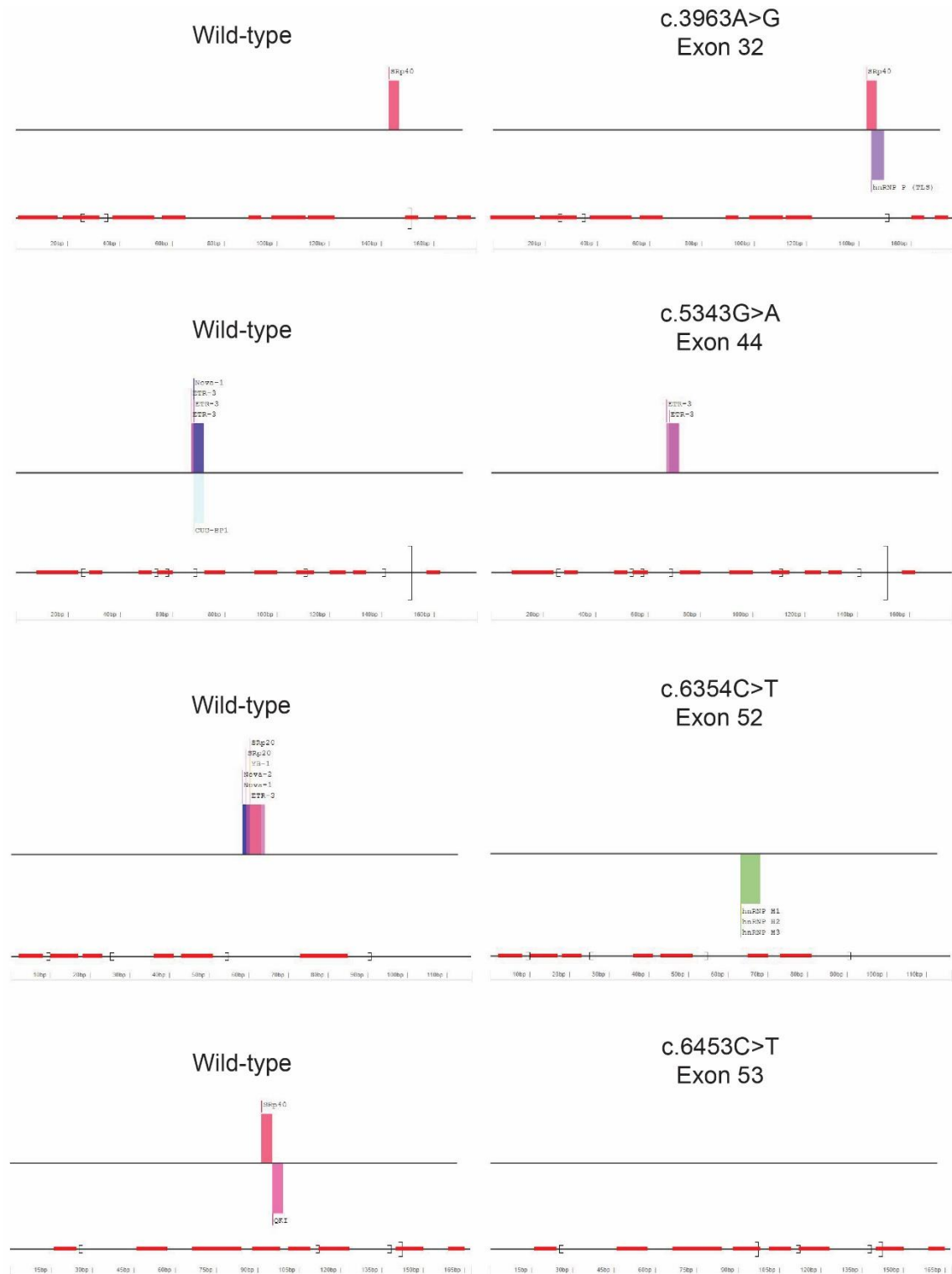


Figure A2.4: Enhancer and silencer motifs that are predicted to be altered by synonymous *FBN1* mutations.

SpliceAid 2¹⁵⁴ reports of predicted ESE (above line) and ESS (below line) motifs that differ between the normal *FBN1* sequence and corresponding sequence harbouring a known synonymous mutation. Only those sites that differ between the two sequences are shown.

Enlarged immunofluorescence images

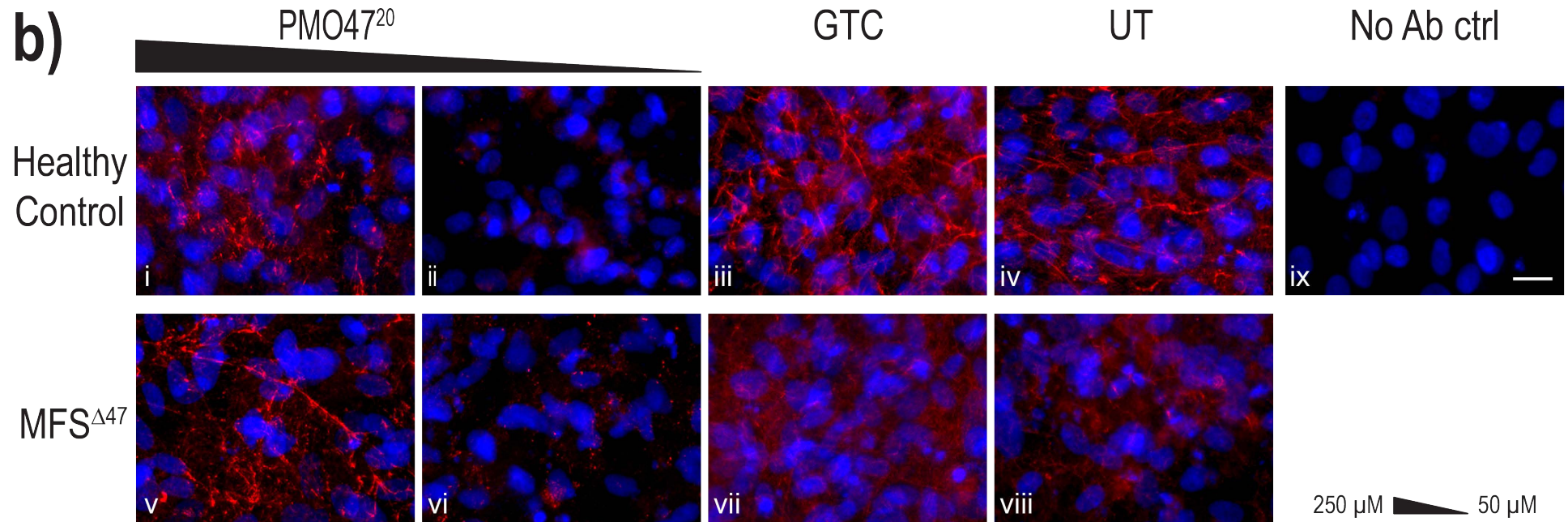


Figure A3.2: Enlarged immunofluorescence staining images from Figure 5.7

Healthy control and MFS^{Δ47} cells were nucleofected with PMO47, Gene Tool control PMO (GTC) or left untreated (UT) then collected after four days. Two concentrations were tested; 250 μM and 50 μM, calculated in the 20 μl nucleofection cuvette volume. Cells were stained for Fibrillin-1 (red) and counterstained with Hoechst (blue) for nuclei detection. No Ab control: no primary antibody added. Scale bar = 20 μm.

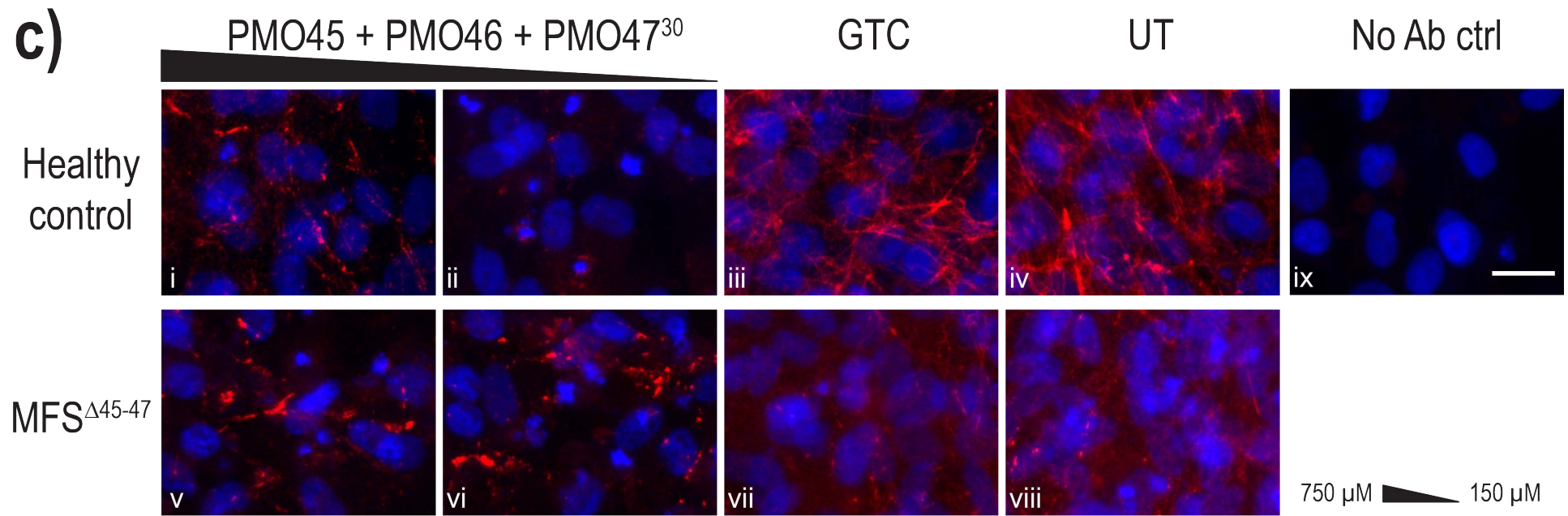


Figure A3.3: Enlarged immunofluorescence staining images from Figure 5.11

Healthy control and MFS^{Δ45-47} fibroblasts nucleofected with a cocktail of PMO45, PMO46 and PMO47³⁰, a Gene Tool control PMO (GTC) or left untreated (UT) and collected after 4 days. Two concentrations were tested; 750 μM and 150 μM, calculated in the 20 μl nucleofection cuvette volume. Cells were stained for Fibrillin-1 (red) and counterstained with Hoechst (blue) for nuclei detection. No Ab control: no primary antibody added. Scale bar = 20 μm.

In silico analysis of the mRNA secondary structure of FBN1 exon 45, 46 and 47 using RNAfold

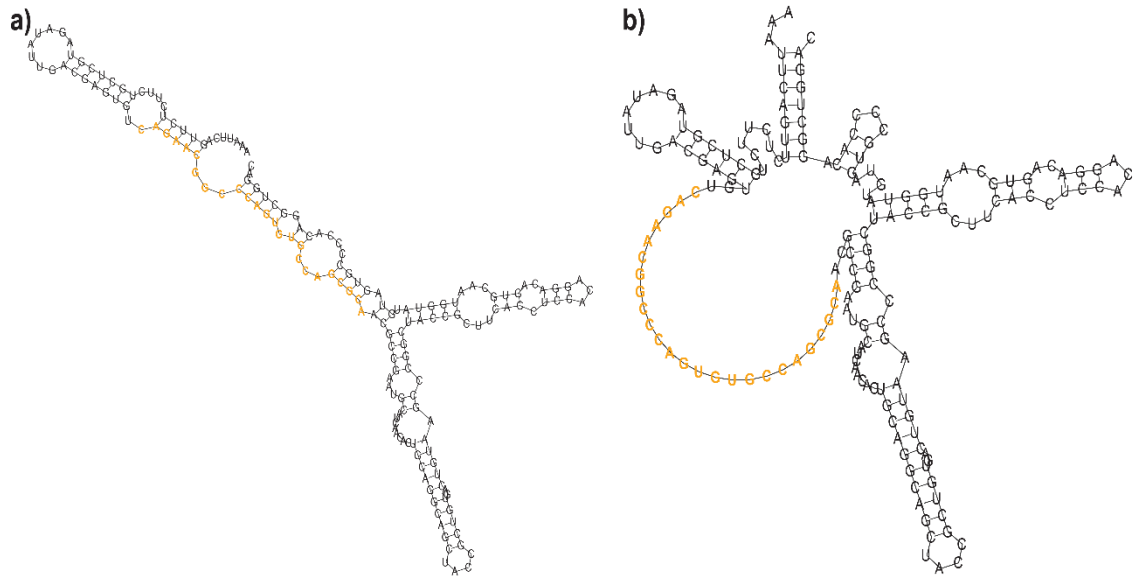


Figure A3.4: In silico prediction of the *FBN1* exon 45 mRNA secondary structure using the RNAfold web server²¹⁷

a) the *FBN1* exon 45 sequence without AO annealing, and b) the *FBN1* exon 45 sequence following PMO45 binding. Bases targeted by PMO45 are highlighted in yellow

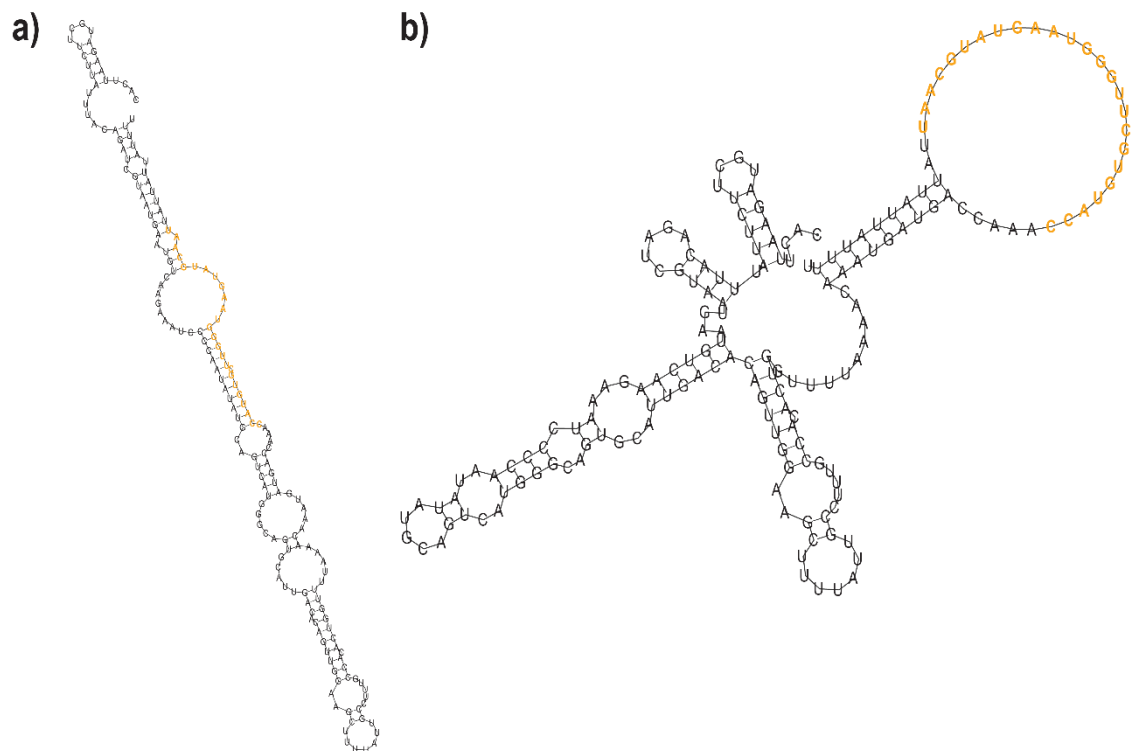


Figure A3.5: In silico prediction of the *FBN1* exon 46 mRNA secondary structure using the RNAfold web server.²¹⁷

a) the *FBN1* exon 46 sequence without AO annealing, and b) the *FBN1* exon 46 sequence following PMO46 binding. Bases targeted by PMO46 are highlighted in yellow

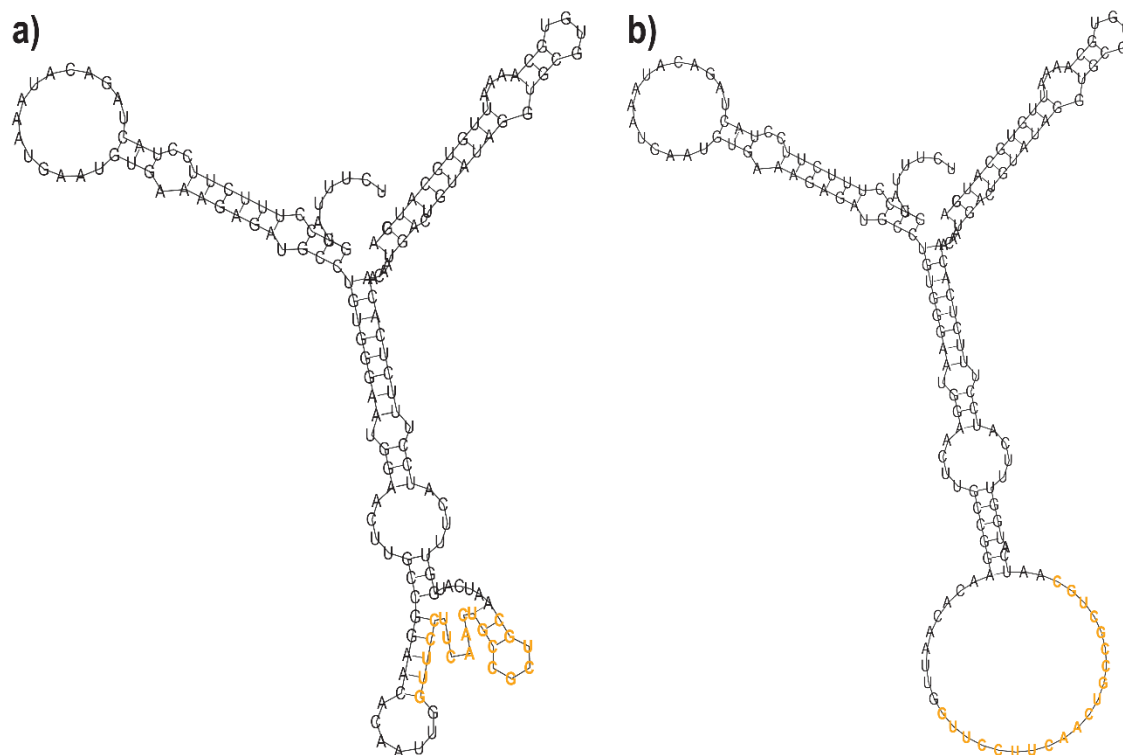


Figure A3.6: In silico prediction of the *FBN1* exon 47 mRNA secondary structure using the RNAfold web server²¹⁷

a) the *FBN1* exon 47 sequence without AO annealing, and b) the *FBN1* exon 47 sequence following PMO47²⁰ binding. Bases targeted by PMO47²⁰ are highlighted in yellow

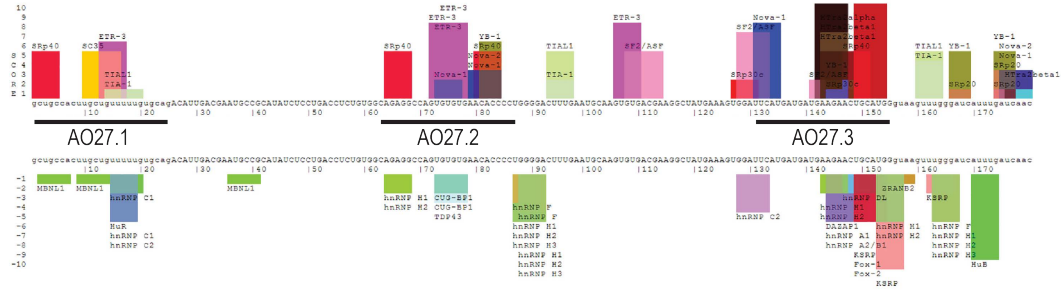
Splice site scores of FBN1 exon 47

Table A3.1: Donor splice site scores of human *FBN1* exon 47

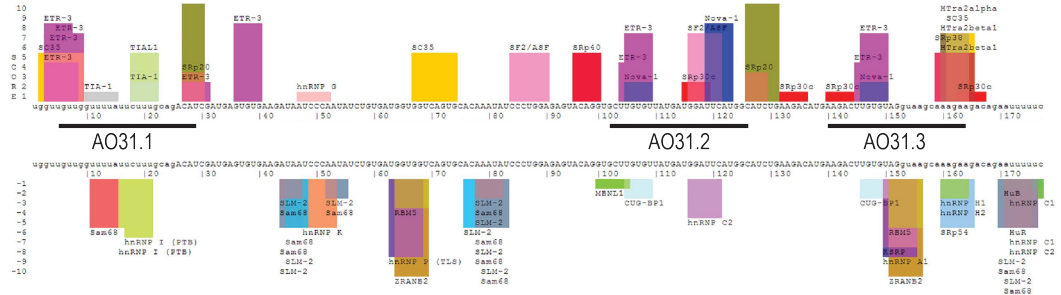
The splice site score of the natural donor, donor created through the c.5788+5G>A mutation and a predicted cryptic donor calculated by Human Splicing Finder 3.0.²¹⁵

Splice site	Splice site	Consensus value (0-100)
Natural donor	TAGgtgcgt	87.93
c.5788+5G>A donor	TAGgtgcat	78.36
Cryptic donor	GAAgtcagt	82.64

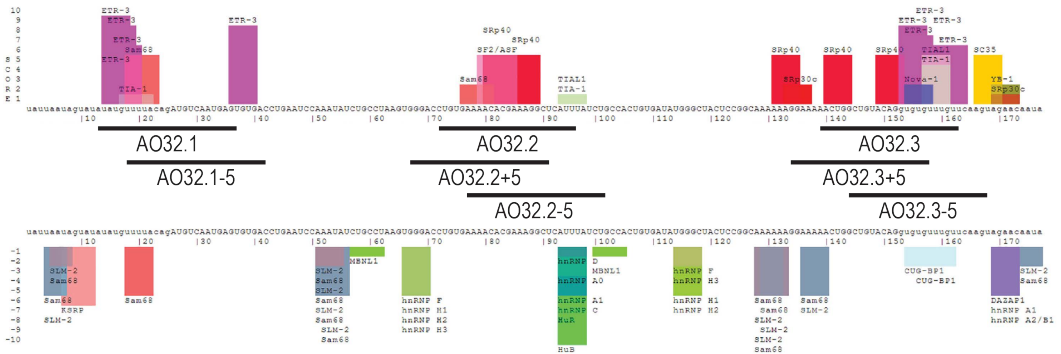
e) Exon 27



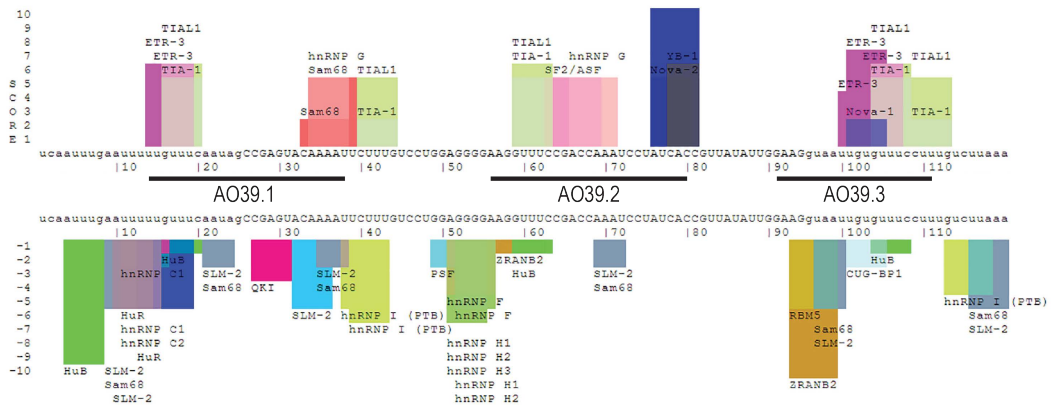
f) Exon 31



g) Exon 32



h) Exon 39



Enlarged immunofluorescence images

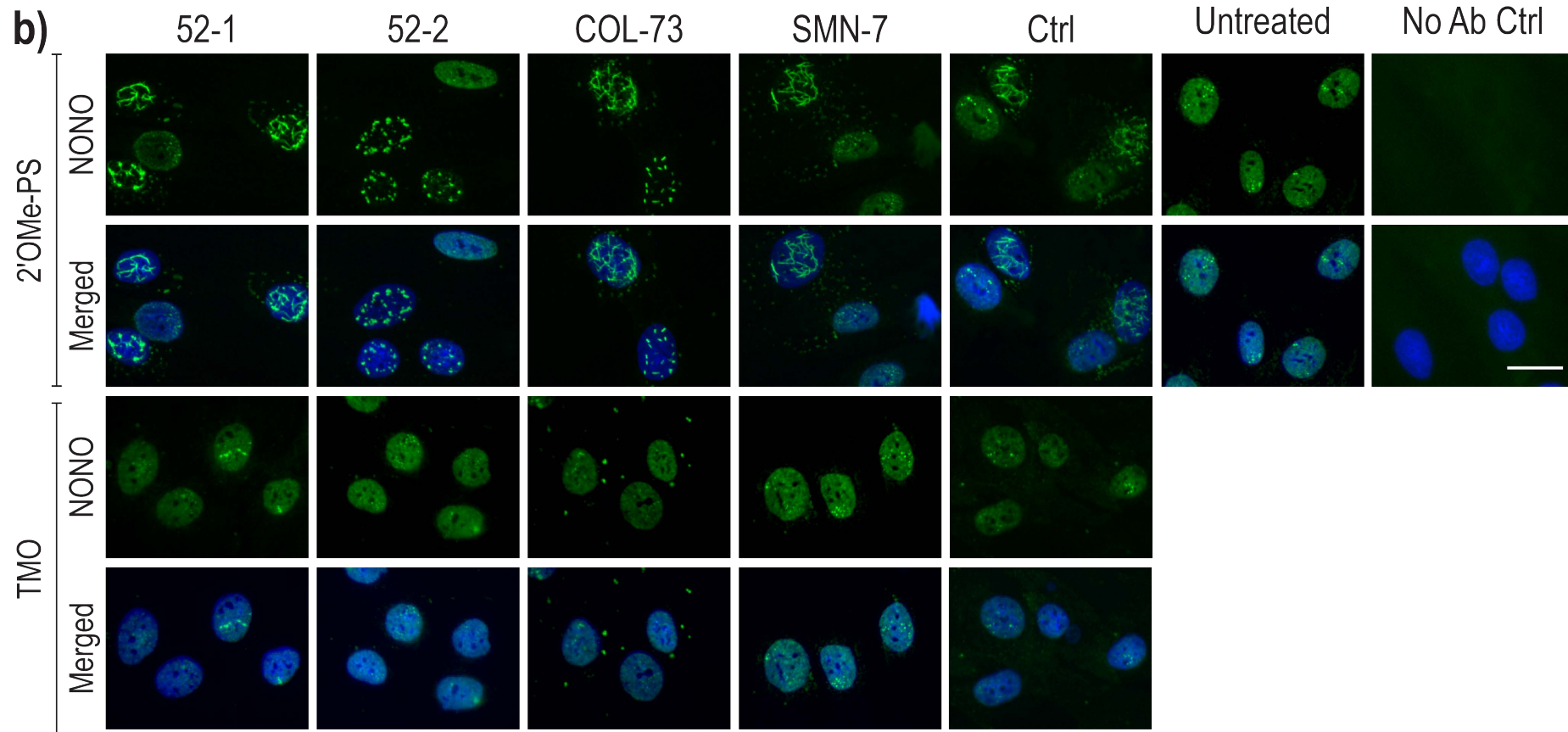


Figure A4.2: Enlarged immunofluorescence staining images from Figure 6.9

Healthy control fibroblasts were transfected, using Lipofectamine 3000, with 100 nM of TMO or 2'OMe PS AOs and collected after 24 hours. Treated cells were stained for NONO (green) and counterstained with Hoechst (blue) for nuclei detection. The upper and lower panels of each set of immunofluorescence images show the NONO and merged images, respectively. No Ab control: no primary antibody added. Scale bar = 20 μ m.

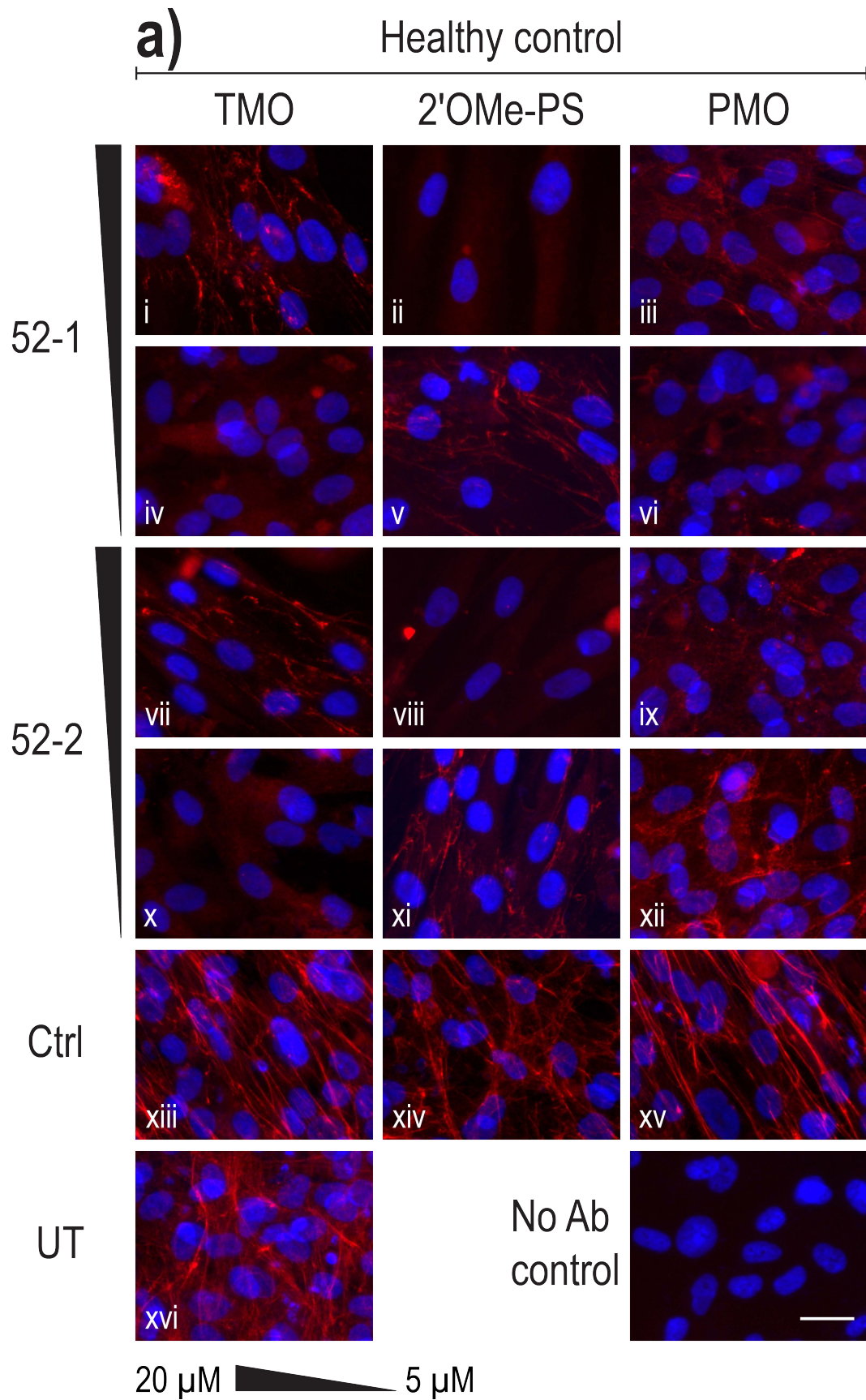


Figure A4.3: Enlarged immunofluorescence staining images from Figure 6.12 part a.

Healthy control fibroblasts were Neon transfected with TMO, 2'OMe PS or PMO AOs and collected after 10 days. Two concentrations 20 μM and 5 μM; calculated in a 10 μl transfection volume, were tested. Cells were stained for Fibrillin-1 (red) and counterstained with Hoechst (blue) for nuclei detection. No Ab control: no primary antibody added. Scale bar = 20 μm.

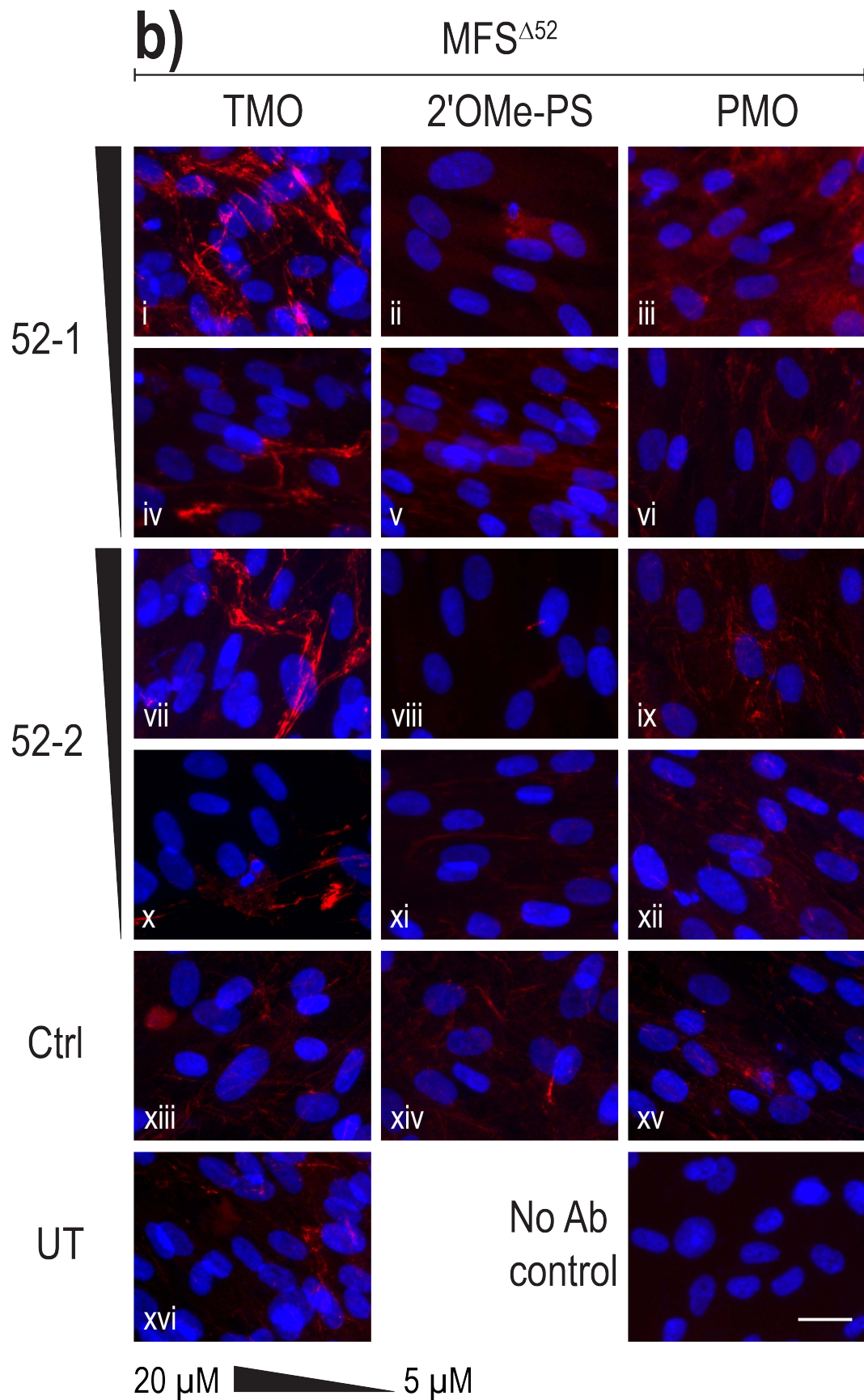


Figure A4.4: Enlarged immunofluorescence staining images from Figure 6.12 part b.

MFS^{Δ52} fibroblasts were Neon transfected with TMO, 2'OMe PS or PMO AOs and collected after 10 days. Two concentrations 20 μM and 5 μM; calculated in a 10 μl transfection volume, were tested. Cells were stained for Fibrillin-1 (red) and counterstained with Hoechst (blue) for nuclei detection. No Ab control: no primary antibody added. Scale bar = 20 μm.

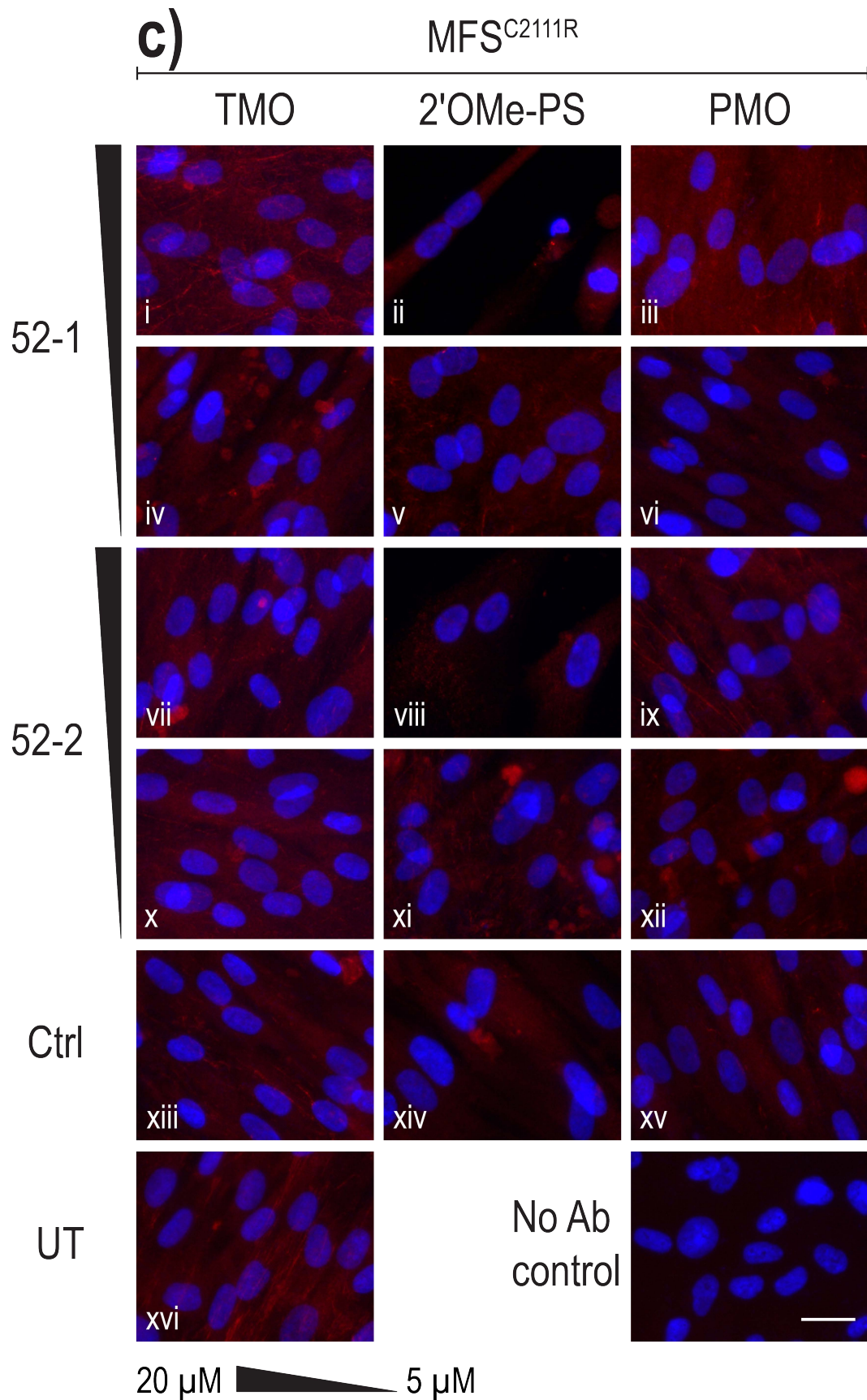


Figure A4.5: Enlarged immunofluorescence staining images from Figure 6.12 part c.

MFS^{C2111R} fibroblasts were Neon transfected with TMO, 2'OMe PS or PMO AOs and collected after 10 days. Two concentrations 20 μM and 5 μM; calculated in a 10 μl transfection volume, were tested. Cells were stained for Fibrillin-1 (red) and counterstained with Hoechst (blue) for nuclei detection. No Ab control: no primary antibody added. Scale bar = 20 μm.

Details of 2'OMe-PS AO sequences screened

Table A4.1: The skipping efficiencies of 2'OMe-PS AOs assessed in this thesis

The name, ID, GC content, binding site, designer, and highest proportion of skipping induced for each of the 2'OMe-PS AOs that were assessed. The proportion of skipping is in healthy control cells transfected at either 200 nM or 50 nM using Lipofectamine 3000. Site indicates if the AO anneals over the canonical acceptor or donor splice site or solely binds to a region containing exonic splicing enhancer (ESE) motifs. The AO nomenclature is outlined in Chapter 2, Figure 2.1. KG: Mr Kane Greer , JC: Ms Jessica Cale.

AO name (FBN1 H...)	ID	GC (%)	Site	Skipping (%)	Designed by
15A(-15+10)	AO15.1	28%	Acceptor	0%	KG
15A(+41+65)	AO15.2	36%	ESE	0%	KG
15D(+12-13)	AO15.3	36%	Donor	0%	KG
16A(-14+11)	AO16.1	44%	Acceptor	0%	JC
16A(+27+51)	AO16.2	52%	ESE	0%	JC
16D(+14-11)	AO16.3	44%	Donor	0%	JC
16A(+22+46)	AO16.2+5	56%	ESE	0%	JC
16A(+32+56)	AO16.2-5	52%	ESE	0%	JC
16D(+09-16)	AO16.3-5	36%	Donor	0%	JC
22A(-13+12)	AO22.1	56%	Acceptor	0%	JC
22A(+45+69)	AO22.2	44%	ESE	32%	JC
22A(+84+108)	AO22.3	72%	ESE	0%	JC
22D(+16-09)	AO22.4	44%	Donor	11%	JC
26A(-18+07)	AO26.1	20%	Acceptor	0%	JC
26A(+70+94)	AO26.2	52%	ESE	9%	JC
26D(+22-03)	AO26.3	48%	Donor	0%	JC
26A(+75+99)	AO26.2-5	60%	ESE	26%	JC
26A(+100+124)	AO26.3+5	40%	ESE	9%	JC
27A(-25-01)	AO27.1	52%	Acceptor	0%	KG
27A(+38+62)	AO27.2	60%	ESE	0%	KG
27A(+105+129)	AO27.3	40%	ESE	0%	KG
31A(-21+04)	AO31.1	32%	Acceptor	0%	KG
31A(+76+100)	AO31.2	44%	ESE	3%	KG
31D(+13-12)	AO31.3	36%	Donor	0%	KG
32A(-13+12)	AO32.1	28%	Acceptor	7%	JC
32A(+47+71)	AO32.2	40%	ESE	36%	JC
32D(+14-11)	AO32.3	44%	Donor	13%	JC
32A(-08+17)	AO32.1-5	36%	Acceptor	22%	JC
32A(+42+66)	AO32.2+5	52%	ESE	37%	JC
32A(+52+76)	AO32.2-5	36%	ESE	33%	JC
32D(+19-06)	AO32.3+5	48%	Donor	23%	JC
32D(+09-16)	AO32.3-5	44%	Donor	0%	JC
39A(-12+13)	AO39.1	32%	Acceptor	43%	JC
39A(+31+55)	AO39.2	44%	ESE	32%	JC
39D(+04-16)	AO39.3	35%	Donor	31%	JC
44A(+14+38)	AO44.1	64%	ESE	0%	KG
44A(+44+68)	AO44.2	48%	ESE	28%	KG

44D(+19-06)	AO44.3	36%	Donor	27%	KG
45A(+15+39)	AO45.1	68%	ESE	3%	KG
45A(+49+73)	AO45.2	60%	ESE	9%	KG
45A(+87+111)	AO45.3	68%	ESE	0%	KG
45D(+21-04)	AO45.4	52%	Donor	0%	JC
46A(-09+16)	AO46.1	28%	Acceptor	5%	KG
46A(+72+96)	AO46.2	40%	ESE	0%	KG
46D(+12-13)	AO46.3	44%	Donor	10%	KG
46A(-03+22)	AO46.4	32%	Acceptor	0%	JC
47A(-03+20)	AO47.1	26%	Acceptor	11%	JC
47A(+58+77)	AO47.2	60%	ESE	43%	JC
47A(+83+102)	AO47.3	40%	ESE	27%	JC
47D(+05-15)	AO47.4	40%	Donor	0%	JC
47A(+44+68)	AO47.5	48%	ESE	24%	JC
47A(+69+93)	AO47.6	52%	ESE	10%	JC
47D(+24-01)	AO47.7	36%	Donor	0%	JC
47A(+56+80)	AO47.2-25mer	52%	ESE	45%	JC
47A(+53+82)	AO47.2-30mer	47%	ESE	42%	JC
49A(-13+12)	AO49.1	28%	Acceptor	0%	KG
49A(+19+43)	AO49.2	48%	ESE	0%	KG
49A(+83+107)	AO49.3	44%	ESE	0%	KG
52A(+29+53)M	AO52.1 ^m	48%	ESE	40%	KG
52A(+29+53)N	AO52.1 ⁿ	52%	ESE	41%	KG
52A(-08+17)	AO52.2	60%	Acceptor	0%	KG
52D(+13-12)	AO52.3	52%	Donor	37%	KG
52A(-23+02)	AO52.4	44%	Acceptor	0%	KG
52A(+03+27)	AO52.5	52%	ESE	22%	KG
59A(-21+04)	AO59.1	12%	Acceptor	0%	JC
59A(+41+65)	AO59.2	48%	ESE	33%	JC
59A(+86+110)	AO59.3	40%	ESE	0%	JC
59A(+36+60)	AO59.2+5	44%	ESE	17%	JC
59A(+46+70)	AO59.2-5	36%	ESE	15%	JC

Binding sites of 2'OMe-PS AOs.

Table A4.2: Proportion of effective *FBN1* 2'OMe-PS AO based on binding site.

The proportion of AOs targeted to the splice sites or ESEs of the target *FBN1* exons that induce exon skipping.

Annealing site	Skipping		Total
	Yes	No	
Acceptor	5 (33%)	10	15
ESE	24 (63%)	14	38
Donor	7 (44%)	9	16
Total	36 (52%)	33	69

Splice site scores of exons 27 and 49

Table A4.3: The splice site scores for *FBN1* exons 27 and 49.

Splice site scores are an expression of how similar a splice site is to the consensus sequence. The scores were calculated using a Splice Site Score Calculation webtool.²¹⁶

Target	5' splice site Score (donor)	3' splice site Score (acceptor)
Exon 27	9.1	7.1
Exon 49	8.3	12.2
Average for constitutive exons	8.1	7.9

Blanket AO Python script

```
print "Please save sequence data in .txt format"
print "With the Exon sequence in UPPERCASE bookended with 25bp of intron in
lowercase, for example:"
print ">Ex2"
print "agctAGCTagct"
print ">Ex3"
print "agctAGCTagct"
print ""
filename = raw_input("Please enter the filename followed by .txt: ")

print "Processing..."

intron = ["a", "c", "t", "g"]
exon = ["A", "C", "T", "G"]

fin = open(filename, "r")
fout = open("Raw AOs.txt", "w")

print "Enter a gene name: "
gene_name = str(raw_input())

print "enter first exon number, eg 2:"
exon_number = int(raw_input())

for line in fin:
    if line[0] == '>':
        fout.write(line[:])

        print "Processing sequence: ", line
        continue

    ao_raw = list()

    for x in range(0, len(line)-25):
        ao_raw.append(line[x:x+25])

    ao_labeled = list()
    exons = 1
    for ao in ao_raw:
        valid = False
        for ex in exon:
            if ex in ao:
                valid = True
        if not valid:
            continue

        if ao[0] in intron:
            #Label as H_A intron
            introns = 0
            for char in ao:
                if char in intron:
                    introns += 1
            ao_labeled.append(("H{0}A(-{1}+{2})".format(exon_number,
introns, 25-introns), ao))

        elif ao[0] in exon:
            if ao[-1:] in intron:
                #label as H_D
                introns = 0
                for char in ao:
```

```

        if char in intron:
            introns += 1
            ao_labeled.append(("H{0}D(+{1}-{2})".format(exon_number,
25-introns, introns), ao))

            continue
            #Label as H_A exon
            ao_labeled.append(("H{0}A(+{1}+{2})".format(exon_number, exons,
exons+24), ao))
            exons += 1

    exon_number += 1

    for ao in ao_labeled:
        fout.write(">{0} {1} \n{2}".format(gene_name, ao[0], ao[1]))
        fout.write("\n")
        fout.write("\n")

fout.close()
fin.close()

fin = open("Raw AOs.txt", "r")
fout = open("Blanket AOs.txt", "w")

nuc =
{'A':'U', 'T':'A', 'G':'C', 'C':'G', 'K':'M', 'M':'K', 'R':'Y', 'Y':'R', 'S':'W', 'W':
':W', 'B':'V', 'V':'B', 'H':'G', 'D':'C', 'X':'N', 'N':'N'}

def revComp(seq):
    rev = ''
    for i in range(len(seq) - 1, -1, -1):
        rev += nuc[seq[i]]

    return rev

seq = ''
for line in fin:
    if line[0] == ">":
        fout.write(line)
    elif line[0] == "/n":
        continue
    else:
        seq = line.strip()
        fout.write(revComp(seq.upper()))
        fout.write("\n\n")

fout.close()
fin.close()
print "Done Processing..."
print "Raw DNA AOs and final AO sequences stored as 'Raw AOs.txt' and
'Blanket AOs.txt'"

raw_input("Press enter to exit")

```

Figure A4.6: Blanket AO Python script

A simple script written in Python 2.7 that when executed will produce a list of all possible 25-mer antisense oligonucleotides across the provided sequence. The input must be in FASTA format and flanked by 25 bases of intronic sequence. Small changes to the code itself allow for the length of the AO to be altered.

In silico analysis of the mRNA secondary structure of FBN1 exon 32 and 39 using RNAfold

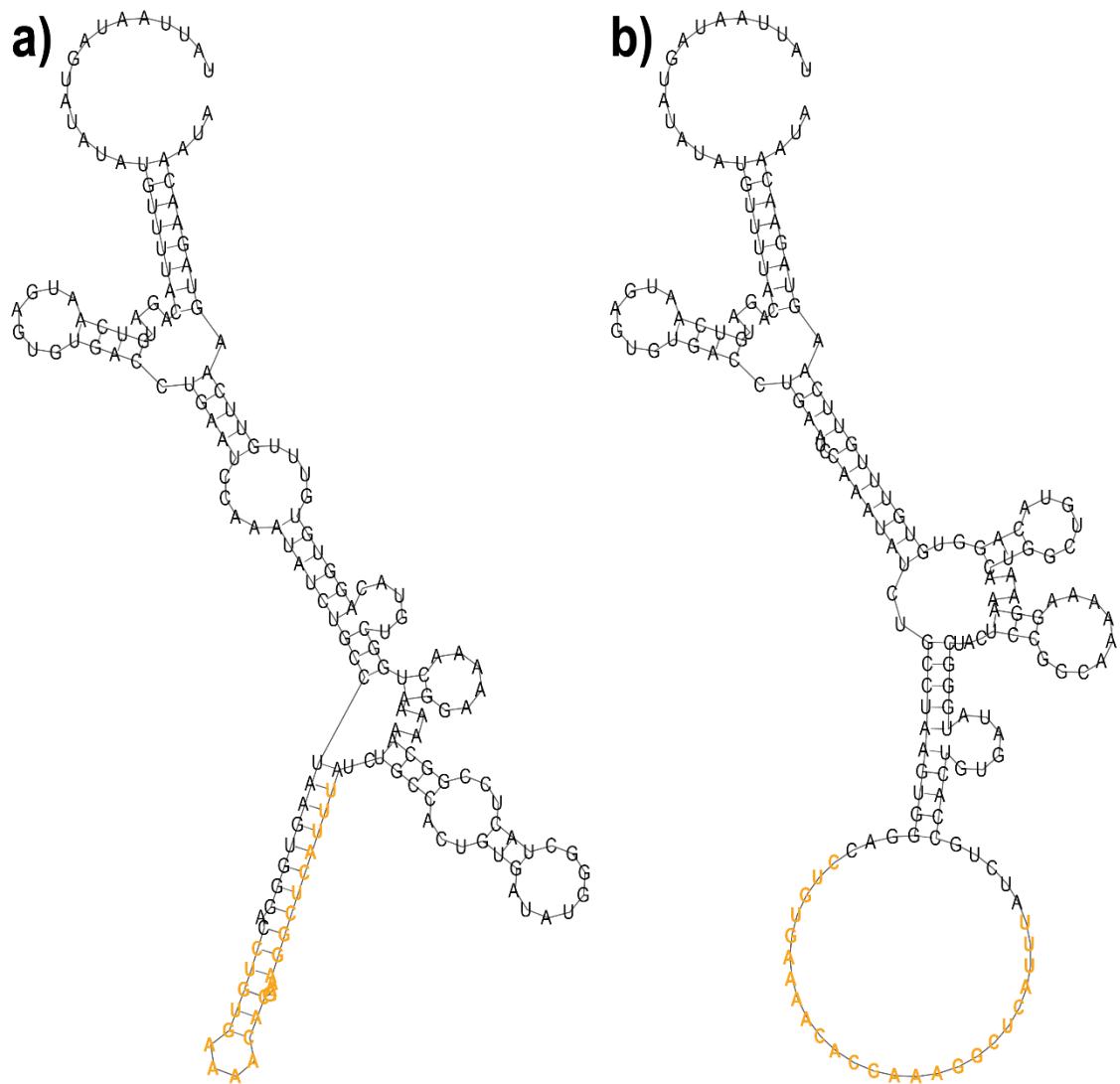


Figure A4.7: *In silico* prediction of the *FBN1* exon 32 mRNA secondary structure using the RNAfold web server²¹⁷

a) the *FBN1* exon 32 sequence without AO annealing, and b) the *FBN1* exon 32 sequence following PMO32 binding. Bases targeted by PMO32 are highlighted in yellow

References

1. Dietz, H. C. *et al.* Marfan syndrome caused by a recurrent de novo missense mutation in the fibrillin gene. *Nature* **352**, 337–339 (1991).
2. Stenson, P. D. *et al.* The Human Gene Mutation Database (HGMD®): optimizing its use in a clinical diagnostic or research setting. *Hum Genet* (2020) doi:10.1007/s00439-020-02199-3.
3. Collod-Bérout, G. *et al.* Update of the UMD-FBN1 mutation database and creation of an FBN1 polymorphism database. *Hum. Mutat.* **22**, 199–208 (2003).
4. Robinson, P. N. *et al.* Mutations of FBN1 and genotype-phenotype correlations in Marfan syndrome and related fibrillinopathies. *Hum. Mutat.* **20**, 153–161 (2002).
5. Corson, G. M., Charbonneau, N. L., Keene, D. R. & Sakai, L. Y. Differential expression of fibrillin-3 adds to microfibril variety in human and avian, but not rodent, connective tissues. *Genomics* **83**, 461–472 (2004).
6. Biery, N. J. *et al.* Revised Genomic Organization of FBN1 and Significance for Regulated Gene Expression. *Genomics* **56**, 70–77 (1999).
7. Romere, C. *et al.* Asprosin, a Fasting-Induced Glucogenic Protein Hormone. *Cell* **165**, 566–579 (2016).
8. Lönnqvist, L., Reinhardt, D., Sakai, L. & Peltonen, L. Evidence for furin-type activity-mediated C-terminal processing of profibrillin-1 and interference in the processing by certain mutations. *Hum. Mol. Genet.* **7**, 2039–2044 (1998).
9. Zhang, H., Hu, W. & Ramirez, F. Developmental expression of fibrillin genes suggests heterogeneity of extracellular microfibrils. *J. Cell Biol.* **129**, 1165–1176 (1995).
10. Sabatier, L. *et al.* Fibrillin-3 expression in human development. *Matrix Biol* **30**, 43–52 (2011).
11. Sakai, L. Y., Keene, D. R. & Engvall, E. Fibrillin, a new 350-kD glycoprotein, is a component of extracellular microfibrils. *J. Cell Biol.* **103**, 2499–2509 (1986).
12. Isogai, Z. *et al.* Latent Transforming Growth Factor β -binding Protein 1 Interacts with Fibrillin and Is a Microfibril-associated Protein. *J. Biol. Chem.* **278**, 2750–2757 (2003).

13. Sengle, G. & Sakai, L. Y. The fibrillin microfibril scaffold: A niche for growth factors and mechanosensation? *Matrix Biol.* **47**, 3–12 (2015).
14. Kielty, C. M. & Shuttleworth, C. A. Fibrillin-containing microfibrils: structure and function in health and disease. *Int. J. Biochem. Cell Biol.* **27**, 747–760 (1995).
15. Ramirez, F., Gayraud, B. & Pereira, L. Marfan syndrome: new clues to genotype-phenotype correlations. *Ann. Med.* **31**, 202–207 (1999).
16. Ramachandra, C. J. A. *et al.* Molecular pathogenesis of Marfan syndrome. *Int. J. Cardiol.* **187**, 585–591 (2015).
17. Reinhardt, D. P., Gambee, J. E., Ono, R. N., Bächinger, H. P. & Sakai, L. Y. Initial steps in assembly of microfibrils. Formation of disulfide-cross-linked multimers containing fibrillin-1. *J. Biol. Chem.* **275**, 2205–2210 (2000).
18. Charbonneau, N. L. *et al.* Fibrillins can co-assemble in fibrils, but fibrillin fibril composition displays cell-specific differences. *J. Biol. Chem.* **278**, 2740–2749 (2003).
19. Pereira, L. *et al.* Targetting of the gene encoding fibrillin-1 recapitulates the vascular aspect of Marfan syndrome. *Nat. Genet.* **17**, 218–222 (1997).
20. Jensen, S. A., Iqbal, S., Lowe, E. D., Redfield, C. & Handford, P. A. Structure and Interdomain Interactions of a Hybrid Domain: A Disulphide-Rich Module of the Fibrillin/LTBP Superfamily of Matrix Proteins. *Structure* **17**, 759–768 (2009).
21. Pereira, L. *et al.* Genomic organization of the sequence coding for fibrillin, the defective gene product in Marfan syndrome. *Hum. Mol. Genet.* **2**, 961–968 (1993).
22. Mellody, K. T. *et al.* Marfan syndrome-causing mutations in fibrillin-1 result in gross morphological alterations and highlight the structural importance of the second hybrid domain. *J. Biol. Chem.* **281**, 31854–31862 (2006).
23. Reinhardt, D. P., Ono, R. N. & Sakai, L. Y. Calcium stabilizes fibrillin-1 against proteolytic degradation. *J. Biol. Chem.* **272**, 1231–1236 (1997).
24. Jensen, S. A., Robertson, I. B. & Handford, P. A. Dissecting the fibrillin microfibril: structural insights into organization and function. *Structure* **20**, 215–225 (2012).

25. Schrijver, I., Liu, W., Brenn, T., Furthmayr, H. & Francke, U. Cysteine substitutions in epidermal growth factor-like domains of fibrillin-1: distinct effects on biochemical and clinical phenotypes. *Am. J. Hum. Genet.* **65**, 1007–1020 (1999).
26. Collod-Bérout, G. & Boileau, C. Marfan syndrome in the third Millennium. *Eur. J. Hum. Genet.* **10**, 673–681 (2002).
27. Ammash, N. M., Sundt, T. M. & Connolly, H. M. Marfan Syndrome-Diagnosis and Management. *Curr Probl Cardiol* **33**, 7–39 (2008).
28. Pyeritz, R. E. Recent progress in understanding the natural and clinical histories of the Marfan syndrome. *Trends Cardiovasc. Med.* **26**, 423–428 (2016).
29. Gray, J. R. *et al.* Ascertainment and severity of Marfan syndrome in a Scottish population. *J Med Genet* **31**, 51–54 (1994).
30. Pyeritz, R. E. The Marfan syndrome. *Annu. Rev. Med.* **51**, 481–510 (2000).
31. de Vries, B. B. A., Pals, G., Odink, R. & Hamel, B. C. J. Homozygosity for a FBN1 missense mutation: clinical and molecular evidence for recessive Marfan syndrome. *Eur. J. Hum. Genet.* **15**, 930–935 (2007).
32. Hilhorst-Hofstee, Y. *et al.* The clinical spectrum of missense mutations of the first aspartic acid of cbEGF-like domains in fibrillin-1 including a recessive family. *Hum. Mutat.* **31**, E1915-1927 (2010).
33. Judge, D. P. & Dietz, H. C. Marfan's syndrome. *Lancet* **366**, 1965–1976 (2005).
34. Loeys, B. L. *et al.* The revised Ghent nosology for the Marfan syndrome. *J. Med. Genet.* **47**, 476–485 (2010).
35. Murdoch, J. L., Walker, B. A., Halpern, B. L., Kuzma, J. W. & McKusick, V. A. Life expectancy and causes of death in the Marfan syndrome. *N. Engl. J. Med.* **286**, 804–808 (1972).
36. Stheneur, C. *et al.* Prognosis factors in probands with an FBN1 mutation diagnosed before the age of 1 year. *Pediatr. Res.* **69**, 265–270 (2011).
37. Ramirez, F. & Dietz, H. C. Marfan syndrome: from molecular pathogenesis to clinical treatment. *Curr. Opin. Genet. Dev.* **17**, 252–258 (2007).

38. McBride, A. R. T. & Gargan, M. Marfan syndrome. *Current Orthopaedics* **20**, 418–423 (2006).
39. Summers, K. M. *et al.* Recent developments in the diagnosis of Marfan syndrome and related disorders. *Med. J. Aust.* **197**, 494–497 (2012).
40. Stheneur, C. *et al.* Identification of the minimal combination of clinical features in probands for efficient mutation detection in the FBN1 gene. *Eur. J. Hum. Genet.* **17**, 1121–1128 (2009).
41. Lipscomb, K. J., Clayton-Smith, J. & Harris, R. Evolving phenotype of Marfan’s syndrome. *Arch. Dis. Child.* **76**, 41–46 (1997).
42. Beighton, P. *et al.* International Nosology of Heritable Disorders of Connective Tissue, Berlin, 1986. *Am. J. Med. Genet.* **29**, 581–594 (1988).
43. De Paepe, A., Devereux, R. B., Dietz, H. C., Hennekam, R. C. & Pyeritz, R. E. Revised diagnostic criteria for the Marfan syndrome. *Am. J. Med. Genet.* **62**, 417–426 (1996).
44. Steinberg, I. A simple screening test for the Marfan syndrome. *Am J Roentgenol Radium Ther Nucl Med* **97**, 118–124 (1966).
45. Walker, B. A. & Murdoch, J. L. The Wrist Sign: A Useful Physical Finding in the Marfan Syndrome. *Arch Intern Med* **126**, 276–277 (1970).
46. Van de Velde, S., Fillman, R. & Yandow, S. Protrusio acetabuli in Marfan syndrome. History, diagnosis, and treatment. *J Bone Joint Surg Am* **88**, 639–646 (2006).
47. De Maio, F., Fichera, A., De Luna, V., Mancini, F. & Caterini, R. Orthopaedic Aspects of Marfan Syndrome: The Experience of a Referral Center for Diagnosis of Rare Diseases. *Advances in Orthopedics* vol. 2016 e8275391 <https://www.hindawi.com/journals/aorth/2016/8275391/> (2016).
48. Forrest, C. R. Chapter 51 - Secondary Management of Posttraumatic Craniofacial Deformities. in *Plastic Surgery Secrets Plus (Second Edition)* (ed. Weinzwieg, J.) 330–339 (Mosby, 2010). doi:10.1016/B978-0-323-03470-8.00051-X.
49. Booms, P. *et al.* Novel exon skipping mutation in the fibrillin-1 gene: two ‘hot spots’ for the neonatal Marfan syndrome. *Clin. Genet.* **55**, 110–117 (1999).

50. Passarge, E., Robinson, P. N. & Graul-Neumann, L. M. Marfanoid-progeroid-lipodystrophy syndrome: a newly recognized fibrillinopathy. *Eur. J. Hum. Genet.* **24**, 1244–1247 (2016).
51. Takenouchi, T. *et al.* Severe congenital lipodystrophy and a progeroid appearance: Mutation in the penultimate exon of FBN1 causing a recognizable phenotype. *Am. J. Med. Genet. A* **161A**, 3057–3062 (2013).
52. Graul-Neumann, L. M. *et al.* Marfan syndrome with neonatal progeroid syndrome-like lipodystrophy associated with a novel frameshift mutation at the 3' terminus of the FBN1-gene. *Am. J. Med. Genet. A* **152A**, 2749–2755 (2010).
53. Glesby, M. J. & Pyeritz, R. E. Association of mitral valve prolapse and systemic abnormalities of connective tissue. A phenotypic continuum. *JAMA* **262**, 523–528 (1989).
54. Greene, V. B. *et al.* Confirmation of ADAMTSL4 mutations for autosomal recessive isolated bilateral ectopia lentis. *Ophthalmic Genet.* **31**, 47–51 (2010).
55. Chandra, A. *et al.* The revised ghent nosology; reclassifying isolated ectopia lentis. *Clin. Genet.* **87**, 284–287 (2015).
56. Loeys, B. L. *et al.* Mutations in fibrillin-1 cause congenital scleroderma: stiff skin syndrome. *Sci Transl Med* **2**, 23ra20 (2010).
57. Le Goff, C. *et al.* Mutations in the TGF β binding-protein-like domain 5 of FBN1 are responsible for acromicric and geleophysic dysplasias. *Am. J. Hum. Genet.* **89**, 7–14 (2011).
58. Faivre, L. *et al.* Homozygosity mapping of a Weill-Marchesani syndrome locus to chromosome 19p13.3-p13.2. *Hum. Genet.* **110**, 366–370 (2002).
59. Rommel, K., Karck, M., Haverich, A., Schmidtke, J. & Arslan-Kirchner, M. Mutation screening of the fibrillin-1 (FBN1) gene in 76 unrelated patients with Marfan syndrome or Marfanoid features leads to the identification of 11 novel and three previously reported mutations. *Hum. Mutat.* **20**, 406–407 (2002).
60. Latasiewicz, M., Fontecilla, C., Millá, E. & Sánchez, A. Marfan syndrome: ocular findings and novel mutations-in pursuit of genotype-phenotype associations. *Can. J. Ophthalmol.* **51**, 113–118 (2016).

61. Schrijver, I. *et al.* Premature termination mutations in FBN1: distinct effects on differential allelic expression and on protein and clinical phenotypes. *Am. J. Hum. Genet.* **71**, 223–237 (2002).
62. Rommel, K. *et al.* Identification of 29 novel and nine recurrent fibrillin-1 (FBN1) mutations and genotype-phenotype correlations in 76 patients with Marfan syndrome. *Hum. Mutat.* **26**, 529–539 (2005).
63. Horn, D. & Robinson, P. N. Progeroid facial features and lipodystrophy associated with a novel splice site mutation in the final intron of the FBN1 gene. *Am. J. Med. Genet. A* **155A**, 721–724 (2011).
64. Jacquinet, A. *et al.* Neonatal progeroid variant of Marfan syndrome with congenital lipodystrophy results from mutations at the 3' end of FBN1 gene. *Eur J Med Genet* **57**, 230–234 (2014).
65. Goldblatt, J., Hyatt, J., Edwards, C. & Walpole, I. Further evidence for a marfanoid syndrome with neonatal progeroid features and severe generalized lipodystrophy due to frameshift mutations near the 3' end of the FBN1 gene. *Am. J. Med. Genet. A* **155A**, 717–720 (2010).
66. Jensen, S. A., Aspinall, G. & Handford, P. A. C-terminal propeptide is required for fibrillin-1 secretion and blocks premature assembly through linkage to domains cbEGF41–43. *Proc. Natl. Acad. Sci. U.S.A.* **111**, 10155–10160 (2014).
67. Faivre, L. *et al.* In frame fibrillin-1 gene deletion in autosomal dominant Weill-Marchesani syndrome. *J. Med. Genet.* **40**, 34–36 (2003).
68. Dietz, H. C. *et al.* Four novel FBN1 mutations: significance for mutant transcript level and EGF-like domain calcium binding in the pathogenesis of Marfan syndrome. *Genomics* **17**, 468–475 (1993).
69. Aoyama, T., Francke, U., Dietz, H. C. & Furthmayr, H. Quantitative differences in biosynthesis and extracellular deposition of fibrillin in cultured fibroblasts distinguish five groups of Marfan syndrome patients and suggest distinct pathogenetic mechanisms. *J. Clin. Invest.* **94**, 130–137 (1994).
70. Ramirez, F. & Pereira, L. The fibrillins. *Int. J. Biochem. Cell Biol.* **31**, 255–259 (1998).

71. Neptune, E. R. *et al.* Dysregulation of TGF-beta activation contributes to pathogenesis in Marfan syndrome. *Nat. Genet.* **33**, 407–411 (2003).
72. Doyle, J. J., Gerber, E. E. & Dietz, H. C. Matrix-dependent perturbation of TGFβ signaling and disease. *FEBS Lett.* **586**, 2003–2015 (2012).
73. Benke, K. *et al.* The role of transforming growth factor-beta in Marfan syndrome. *Cardiol J* **20**, 227–234 (2013).
74. Huang, F. & Chen, Y.-G. Regulation of TGF-β receptor activity. *Cell Biosci* **2**, 9 (2012).
75. Silverman, D. I. *et al.* Life expectancy in the Marfan syndrome. *Am. J. Cardiol.* **75**, 157–160 (1995).
76. Shores, J., Berger, K. R., Murphy, E. A. & Pyeritz, R. E. Progression of aortic dilatation and the benefit of long-term beta-adrenergic blockade in Marfan's syndrome. *N. Engl. J. Med.* **330**, 1335–1341 (1994).
77. Gott, V. L., Pyeritz, R. E., Cameron, D. E., Greene, P. S. & McKusick, V. A. Composite graft repair of Marfan aneurysm of the ascending aorta: Results in 100 patients. *The Annals of Thoracic Surgery* **52**, 38–45 (1991).
78. Rossi-Foulkes, R. *et al.* Phenotypic features and impact of beta blocker or calcium antagonist therapy on aortic lumen size in the Marfan syndrome. *Am. J. Cardiol.* **83**, 1364–1368 (1999).
79. Habashi, J. P. *et al.* Losartan, an AT1 Antagonist, Prevents Aortic Aneurysm in a Mouse Model of Marfan Syndrome. *Science* **312**, 117–121 (2006).
80. Franken, R. *et al.* Beneficial Outcome of Losartan Therapy Depends on Type of FBN1 Mutation in Marfan Syndrome. *Circ Cardiovasc Genet* **8**, 383–388 (2015).
81. Loewenstein, A., Barequet, I. S., De Juan, E. & Maumenee, I. H. Retinal detachment in Marfan syndrome. *Retina (Philadelphia, Pa.)* **20**, 358–363 (2000).
82. Jones, K. B., Erkula, G., Sponseller, P. D. & Dormans, J. P. Spine deformity correction in Marfan syndrome. *Spine* **27**, 2003–2012 (2002).
83. Gao, L. *et al.* The effect of losartan on progressive aortic dilatation in patients with Marfan's syndrome: a meta-analysis of prospective randomized clinical trials. *Int. J. Cardiol.* **217**, 190–194 (2016).

84. Lacro, R. V. *et al.* Atenolol versus losartan in children and young adults with Marfan's syndrome. *N. Engl. J. Med.* **371**, 2061–2071 (2014).
85. Phylactou, L. A. & Kilpatrick, M. W. Potential therapy paradigms for Marfan syndrome. *Expert Opin Investig Drugs* **8**, 983–993 (1999).
86. Komor, A. C., Badran, A. H. & Liu, D. R. CRISPR-Based Technologies for the Manipulation of Eukaryotic Genomes. *Cell* **168**, 20–36 (2017).
87. Zeng, Y. *et al.* Correction of the Marfan Syndrome Pathogenic FBN1 Mutation by Base Editing in Human Cells and Heterozygous Embryos. *Molecular Therapy* **26**, 2631–2637 (2018).
88. Carmody, S. R. & Wenthe, S. R. mRNA nuclear export at a glance. *J. Cell. Sci.* **122**, 1933–1937 (2009).
89. Pan, Q., Shai, O., Lee, L. J., Frey, B. J. & Blencowe, B. J. Deep surveying of alternative splicing complexity in the human transcriptome by high-throughput sequencing. *Nat. Genet.* **40**, 1413–1415 (2008).
90. De Conti, L., Baralle, M. & Buratti, E. Exon and intron definition in pre-mRNA splicing. *Wiley Interdiscip Rev RNA* **4**, 49–60 (2013).
91. Berget, S. M. Exon recognition in vertebrate splicing. *J. Biol. Chem.* **270**, 2411–2414 (1995).
92. Wahl, M. C., Will, C. L. & Lührmann, R. The Spliceosome: Design Principles of a Dynamic RNP Machine. *Cell* **136**, 701–718 (2009).
93. Hall, S. L. & Padgett, R. A. Conserved sequences in a class of rare eukaryotic nuclear introns with non-consensus splice sites. *J. Mol. Biol.* **239**, 357–365 (1994).
94. Burge, C. B., Padgett, R. A. & Sharp, P. A. Evolutionary fates and origins of U12-type introns. *Mol. Cell* **2**, 773–785 (1998).
95. Levine, A. & Durbin, R. A computational scan for U12-dependent introns in the human genome sequence. *Nucleic Acids Res* **29**, 4006–4013 (2001).
96. Turunen, J. J., Niemelä, E. H., Verma, B. & Frilander, M. J. The significant other: splicing by the minor spliceosome. *Wiley Interdiscip Rev RNA* **4**, 61–76 (2013).

97. Rino, J. *et al.* A Stochastic View of Spliceosome Assembly and Recycling in the Nucleus. *PLoS Computational Biology* **3**, e201 (2007).
98. Becerra, S., Andrés-León, E., Prieto-Sánchez, S., Hernández-Munain, C. & Suñé, C. Prp40 and early events in splice site definition. *Wiley Interdiscip Rev RNA* **7**, 17–32 (2016).
99. Douglas, A. G. L. & Wood, M. J. A. RNA splicing: disease and therapy. *Brief Funct Genomics* **10**, 151–164 (2011).
100. Missler, M. & Südhof, T. C. Neurexins: three genes and 1001 products. *Trends Genet.* **14**, 20–26 (1998).
101. Wang, E. T. *et al.* Alternative isoform regulation in human tissue transcriptomes. *Nature* **456**, 470–476 (2008).
102. Wang, Z. & Burge, C. B. Splicing regulation: From a parts list of regulatory elements to an integrated splicing code. *RNA* **14**, 802–813 (2008).
103. Cartegni, L., Chew, S. L. & Krainer, A. R. Listening to silence and understanding nonsense: exonic mutations that affect splicing. *Nature Reviews Genetics* **3**, 285–298 (2002).
104. Ward, A. J. & Cooper, T. A. The pathobiology of splicing. *J. Pathol.* **220**, 152–163 (2010).
105. Hua, Y. *et al.* Antisense correction of SMN2 splicing in the CNS rescues necrosis in a type III SMA mouse model. *Genes Dev* **24**, 1634–1644 (2010).
106. Dominski, Z. & Kole, R. Restoration of correct splicing in thalassemic pre-mRNA by antisense oligonucleotides. *Proc Natl Acad Sci U S A* **90**, 8673–8677 (1993).
107. Mann, C. J. *et al.* Antisense-induced exon skipping and synthesis of dystrophin in the mdx mouse. *PNAS* **98**, 42–47 (2001).
108. Shuttleworth, J. & Colman, A. Antisense oligonucleotide-directed cleavage of mRNA in *Xenopus* oocytes and eggs. *EMBO J* **7**, 427–434 (1988).
109. Dash, P., Lotan, I., Knapp, M., Kandel, E. R. & Goelet, P. Selective elimination of mRNAs in vivo: complementary oligodeoxynucleotides promote RNA degradation by an RNase H-like activity. *Proc Natl Acad Sci U S A* **84**, 7896–7900 (1987).
110. Zeng, Y., Yi, R. & Cullen, B. R. MicroRNAs and small interfering RNAs can inhibit mRNA expression by similar mechanisms. *PNAS* **100**, 9779–9784 (2003).

111. Bielinska, A., Shivdasani, R. A., Zhang, L. Q. & Nabel, G. J. Regulation of gene expression with double-stranded phosphorothioate oligonucleotides. *Science* **250**, 997–1000 (1990).
112. Boiziau, C. *et al.* Inhibition of translation initiation by antisense oligonucleotides via an RNase-H independent mechanism. *Nucleic Acids Res* **19**, 1113–1119 (1991).
113. Dias, N. & Stein, C. A. Antisense oligonucleotides: basic concepts and mechanisms. *Mol. Cancer Ther.* **1**, 347–355 (2002).
114. Paterson, B. M., Roberts, B. E. & Kuff, E. L. Structural gene identification and mapping by DNA-mRNA hybrid-arrested cell-free translation. *Proc Natl Acad Sci U S A* **74**, 4370–4374 (1977).
115. Zamecnik, P. C. & Stephenson, M. L. Inhibition of Rous sarcoma virus replication and cell transformation by a specific oligodeoxynucleotide. *Proc Natl Acad Sci U S A* **75**, 280–284 (1978).
116. Donis-Keller, H. Site specific enzymatic cleavage of RNA. *Nucleic Acids Res* **7**, 179–192 (1979).
117. Shen, X. & Corey, D. R. Chemistry, mechanism and clinical status of antisense oligonucleotides and duplex RNAs. *Nucleic Acids Res.* **46**, 1584–1600 (2018).
118. Summerton, J. E. Morpholino, siRNA, and S-DNA compared: impact of structure and mechanism of action on off-target effects and sequence specificity. *Curr Top Med Chem* **7**, 651–660 (2007).
119. Majlessi, M., Nelson, N. C. & Becker, M. M. Advantages of 2'-O-methyl oligoribonucleotide probes for detecting RNA targets. *Nucleic Acids Res* **26**, 2224–2229 (1998).
120. Summerton, J. E. & Weller, D. D. Uncharged morpholino-based polymers having phosphorous containing chiral intersubunit linkages. (1993).
121. Hudziak, R. M. *et al.* Resistance of morpholino phosphorodiamidate oligomers to enzymatic degradation. *Antisense Nucleic Acid Drug Dev.* **6**, 267–272 (1996).
122. Moulton, J. D. & Jiang, S. Gene Knockdowns in Adult Animals: PPMOs and Vivo-Morpholinos. *Molecules* **14**, 1304–1323 (2009).

123. Mendell, J. R. *et al.* Eteplirsen for the treatment of Duchenne muscular dystrophy. *Ann. Neurol.* **74**, 637–647 (2013).
124. Iversen, P. L., Arora, V., Acker, A. J., Mason, D. H. & Devi, G. R. Efficacy of Antisense Morpholino Oligomer Targeted to c-myc in Prostate Cancer Xenograft Murine Model and a Phase I Safety Study in Humans. *Clin Cancer Res* **9**, 2510–2519 (2003).
125. Devi, G. R. *et al.* In vivo Bioavailability and Pharmacokinetics of a c-MYC Antisense Phosphorodiamidate Morpholino Oligomer, AVI-4126, in Solid Tumors. *Clin Cancer Res* **11**, 3930–3938 (2005).
126. Vlassov, V. V., Blakireva, L. A. & Yakubov, L. A. Transport of oligonucleotides across natural and model membranes. *Biochimica et Biophysica Acta (BBA) - Reviews on Biomembranes* **1197**, 95–108 (1994).
127. Loke, S. L. *et al.* Characterization of oligonucleotide transport into living cells. *Proc Natl Acad Sci U S A* **86**, 3474–3478 (1989).
128. Yakubov, L. A. *et al.* Mechanism of oligonucleotide uptake by cells: involvement of specific receptors? *PNAS* **86**, 6454–6458 (1989).
129. Summerton, J. E. Endo-Porter: a novel reagent for safe, effective delivery of substances into cells. *Ann. N. Y. Acad. Sci.* **1058**, 62–75 (2005).
130. Stein, C. A. *et al.* Efficient gene silencing by delivery of locked nucleic acid antisense oligonucleotides, unassisted by transfection reagents. *Nucleic Acids Res* **38**, e3 (2010).
131. Aung-Htut, M. T., McIntosh, C. S., West, K. A., Fletcher, S. & Wilton, S. D. In Vitro Validation of Phosphorodiamidate Morpholino Oligomers. *Molecules* **24**, (2019).
132. Moulton, H. M. & Moulton, J. D. Morpholinos and their peptide conjugates: Therapeutic promise and challenge for Duchenne muscular dystrophy. *Biochimica et Biophysica Acta (BBA) - Biomembranes* **1798**, 2296–2303 (2010).
133. Amantana, A. *et al.* Pharmacokinetics, Biodistribution, Stability and Toxicity of a Cell-Penetrating Peptide–Morpholino Oligomer Conjugate. *Bioconjugate Chem.* **18**, 1325–1331 (2007).

134. Moulton, H. M., Nelson, M. H., Hatlevig, S. A., Reddy, M. T. & Iversen, P. L. Cellular Uptake of Antisense Morpholino Oligomers Conjugated to Arginine-Rich Peptides. *Bioconjugate Chem.* **15**, 290–299 (2004).
135. Boisguérin, P. *et al.* Delivery of therapeutic oligonucleotides with cell penetrating peptides. *Adv Drug Deliv Rev* **87**, 52–67 (2015).
136. Wu, B. *et al.* Effective rescue of dystrophin improves cardiac function in dystrophin-deficient mice by a modified morpholino oligomer. *Proc Natl Acad Sci U S A* **105**, 14814–14819 (2008).
137. Cutrona, G. *et al.* Effects in live cells of a c- myc anti-gene PNA linked to a nuclear localization signal. *Nature Biotechnology* **18**, 300–303 (2000).
138. Dean, N. M., McKay, R., Condon, T. P. & Bennett, C. F. Inhibition of protein kinase C- α expression in human A549 cells by antisense oligonucleotides inhibits induction of intercellular adhesion molecule 1 (ICAM-1) mRNA by phorbol esters. *J. Biol. Chem.* **269**, 16416–16424 (1994).
139. Singh, N. K., Singh, N. N., Androphy, E. J. & Singh, R. N. Splicing of a Critical Exon of Human Survival Motor Neuron Is Regulated by a Unique Silencer Element Located in the Last Intron. *Mol Cell Biol* **26**, 1333–1346 (2006).
140. FDA grants accelerated approval to first drug for Duchenne muscular dystrophy. *FDA* <https://www.fda.gov/news-events/press-announcements/fda-grants-accelerated-approval-first-drug-duchenne-muscular-dystrophy> (2016).
141. Muntoni, F., Fletcher, S. & Wilton, S. D. Response to ‘Railroading at the FDA’. *Nat. Biotechnol.* **35**, 207–209 (2017).
142. FDA grants accelerated approval to first targeted treatment for rare Duchenne muscular dystrophy mutation. *FDA* <https://www.fda.gov/news-events/press-announcements/fda-grants-accelerated-approval-first-targeted-treatment-rare-duchenne-muscular-dystrophy-mutation> (2019).
143. Anwar, S. & Yokota, T. Golodirsen for Duchenne muscular dystrophy. *Drugs Today (Barc)* **56**, 491–504 (2020).

144. Lim, K. R. Q., Maruyama, R. & Yokota, T. Eteplirsen in the treatment of Duchenne muscular dystrophy. *Drug Des Devel Ther* **11**, 533–545 (2017).
145. Rigo, F. *et al.* Pharmacology of a Central Nervous System Delivered 2'-O-Methoxyethyl-Modified Survival of Motor Neuron Splicing Oligonucleotide in Mice and Nonhuman Primates. *J Pharmacol Exp Ther* **350**, 46–55 (2014).
146. Stein, C. A., Subasinghe, C., Shinozuka, K. & Cohen, J. S. Physicochemical properties of phosphorothioate oligodeoxynucleotides. *Nucleic Acids Res* **16**, 3209–3221 (1988).
147. Furdon, P. J., Dominski, Z. & Kole, R. RNase H cleavage of RNA hybridized to oligonucleotides containing methylphosphonate, phosphorothioate and phosphodiester bonds. *Nucleic Acids Res* **17**, 9193–9204 (1989).
148. Vitravene Study Group. Safety of intravitreal fomivirsen for treatment of cytomegalovirus retinitis in patients with AIDS. *American Journal of Ophthalmology* **133**, 484–498 (2002).
149. Wong, E. & Goldberg, T. Mipomersen (Kynamro). *P T* **39**, 119–122 (2014).
150. Stein, C. A. & Castanotto, D. FDA-Approved Oligonucleotide Therapies in 2017. *Mol Ther* **25**, 1069–1075 (2017).
151. Liu, W., Qian, C. & Francke, U. Silent mutation induces exon skipping of fibrillin-1 gene in Marfan syndrome. *Nat. Genet.* **16**, 328–329 (1997).
152. Reinhardt, D. P. *et al.* Mutations in calcium-binding epidermal growth factor modules render fibrillin-1 susceptible to proteolysis. A potential disease-causing mechanism in Marfan syndrome. *J. Biol. Chem.* **275**, 12339–12345 (2000).
153. Piva, F., Giulietti, M., Nocchi, L. & Principato, G. SpliceAid: a database of experimental RNA target motifs bound by splicing proteins in humans. *Bioinformatics* **25**, 1211–1213 (2009).
154. Piva, F., Giulietti, M., Burini, A. B. & Principato, G. SpliceAid 2: a database of human splicing factors expression data and RNA target motifs. *Hum. Mutat.* **33**, 81–85 (2012).
155. Mann, C. J., Honeyman, K., McClorey, G., Fletcher, S. & Wilton, S. D. Improved antisense oligonucleotide induced exon skipping in the mdx mouse model of muscular dystrophy. *J Gene Med* **4**, 644–654 (2002).

156. Schneider, C. A., Rasband, W. S. & Eliceiri, K. W. NIH Image to ImageJ: 25 years of image analysis. *Nat. Methods* **9**, 671–675 (2012).
157. Wilton, S. D., Lim, L., Dye, D. & Laing, N. Bandstab: A PCR-Based Alternative to Cloning PCR Products. *BioTechniques* **22**, 642–645 (1997).
158. Hollister, D. W., Godfrey, M., Sakai, L. Y. & Pyeritz, R. E. Immunohistologic abnormalities of the microfibrillar-fiber system in the Marfan syndrome. *N. Engl. J. Med.* **323**, 152–159 (1990).
159. Gibson, M. A. *Microfibril-Associated Glycoprotein-1 (MAGP-1) and Other Non-fibrillin Macromolecules Which May Possess a Functional Association with the 10 nm Microfibrils*. (Landes Bioscience, 2013).
160. Ikonomidis John S. *et al.* Expression of Matrix Metalloproteinases and Endogenous Inhibitors Within Ascending Aortic Aneurysms of Patients With Marfan Syndrome. *Circulation* **114**, I–365 (2006).
161. Aubart, M. *et al.* The clinical presentation of Marfan syndrome is modulated by expression of wild-type FBN1 allele. *Hum. Mol. Genet.* **24**, 2764–2770 (2015).
162. Dominski, Z. & Kole, R. Restoration of correct splicing in thalassemic pre-mRNA by antisense oligonucleotides. *Proc. Natl. Acad. Sci. U.S.A.* **90**, 8673–8677 (1993).
163. FDA approves first drug for spinal muscular atrophy. *FDA* <https://www.fda.gov/news-events/press-announcements/fda-approves-first-drug-spinal-muscular-atrophy> (2016).
164. FDA Approves Targeted Treatment for Rare Duchenne Muscular Dystrophy Mutation. *FDA* <https://www.fda.gov/news-events/press-announcements/fda-approves-targeted-treatment-rare-duchenne-muscular-dystrophy-mutation> (2020).
165. Komaki, H. *et al.* Viltolarsen in Japanese Duchenne muscular dystrophy patients: A phase 1/2 study. *Annals of Clinical and Translational Neurology* **7**, 2393–2408 (2020).
166. Moulton, J. D. & Jiang, S. Gene Knockdowns in Adult Animals: PPMOs and Vivo-Morpholinos. *Molecules* **14**, 1304–1323 (2009).
167. Adams, A. M. *et al.* Antisense oligonucleotide induced exon skipping and the dystrophin gene transcript: cocktails and chemistries. *BMC Mol. Biol.* **8**, 57 (2007).

168. McIntosh, C. S., Aung-Htut, M. T., Fletcher, S. & Wilton, S. D. Removal of the Polyglutamine Repeat of Ataxin-3 by Redirecting pre-mRNA Processing. *International Journal of Molecular Sciences* **20**, 5434 (2019).
169. Uhlén, M. *et al.* Proteomics. Tissue-based map of the human proteome. *Science* **347**, 1260419 (2015).
170. Liu, W., Schrijver, I., Brenn, T., Furthmayr, H. & Francke, U. Multi-exon deletions of the FBN1 gene in Marfan syndrome. *BMC Med. Genet.* **2**, 11 (2001).
171. Achelrod, D., Blankart, C. R., Linder, R., von Kodolitsch, Y. & Stargardt, T. The economic impact of Marfan syndrome: a non-experimental, retrospective, population-based matched cohort study. *Orphanet J Rare Dis* **9**, 90 (2014).
172. Blankart, C. R., Milstein, R., Rybczynski, M., Schüler, H. & von Kodolitsch, Y. Economic and care considerations of Marfan syndrome. *Expert Rev Pharmacoecon Outcomes Res* **16**, 591–598 (2016).
173. Altschul, S. F., Gish, W., Miller, W., Myers, E. W. & Lipman, D. J. Basic local alignment search tool. *J. Mol. Biol.* **215**, 403–410 (1990).
174. Burgio, R. G. *et al.* Asymmetric Marfan syndrome. *Am J Med Genet* **30**, 905–909 (1988).
175. Godfrey, M. *et al.* Unilateral microfibrillar abnormalities in a case of asymmetric Marfan syndrome. *Am. J. Hum. Genet.* **46**, 661–671 (1990).
176. Khan, A. O., Bolz, H. J. & Bergmann, C. Results of fibrillin-1 gene analysis in children from inbred families with lens subluxation. *J AAPOS* **18**, 134–139 (2014).
177. Overwater, E. *et al.* Autosomal dominant Marfan syndrome caused by a previously reported recessive FBN1 variant. *Mol Genet Genomic Med* **7**, e00518 (2019).
178. Aubart, M. *et al.* Association of modifiers and other genetic factors explain Marfan syndrome clinical variability. *Eur. J. Hum. Genet.* **26**, 1759–1772 (2018).
179. Sakai, L. Disulfide bonds crosslink molecules of fibrillin in the connective tissue space. in *Elastin: chemical and biological aspects*. (eds. Tamburro, A. & Davidson, J.) 213 (Congedo Editore, 1990).
180. Sengle, G. *et al.* Microenvironmental regulation by fibrillin-1. *PLoS Genet.* **8**, e1002425 (2012).

181. Ono, R. N. *et al.* Latent transforming growth factor beta-binding proteins and fibulins compete for fibrillin-1 and exhibit exquisite specificities in binding sites. *J. Biol. Chem.* **284**, 16872–16881 (2009).
182. Landis, B. J., Veldtman, G. R. & Ware, S. M. Genotype-phenotype correlations in Marfan syndrome. *Heart* **103**, 1750–1752 (2017).
183. Liu, W. *et al.* Mutant fibrillin-1 monomers lacking EGF-like domains disrupt microfibril assembly and cause severe marfan syndrome. *Hum. Mol. Genet.* **5**, 1581–1587 (1996).
184. Järver, P. *et al.* Peptide Nanoparticle Delivery of Charge-Neutral Splice-Switching Morpholino Oligonucleotides. *Nucleic Acid Ther* **25**, 65–77 (2015).
185. Brown, P. K., Qureshi, A. T., Moll, A. N., Hayes, D. J. & Monroe, W. T. Silver Nanoscale Antisense Drug Delivery System for Photoactivated Gene Silencing. *ACS Nano* **7**, 2948–2959 (2013).
186. Hou, S., Ma, H., Ji, Y., Hou, W. & Jia, N. A Calcium Phosphate Nanoparticle-Based Biocarrier for Efficient Cellular Delivery of Antisense Oligodeoxynucleotides. *ACS Appl. Mater. Interfaces* **5**, 1131–1136 (2013).
187. Yin, H. *et al.* Pip5 Transduction Peptides Direct High Efficiency Oligonucleotide-mediated Dystrophin Exon Skipping in Heart and Phenotypic Correction in mdx Mice. *Mol Ther* **19**, 1295–1303 (2011).
188. Shabanpoor, F. *et al.* Identification of a Peptide for Systemic Brain Delivery of a Morpholino Oligonucleotide in Mouse Models of Spinal Muscular Atrophy. *Nucleic Acid Therapeutics* **27**, 130–143 (2017).
189. Karaki, S. *et al.* Lipid-oligonucleotide conjugates improve cellular uptake and efficiency of TCTP-antisense in castration-resistant prostate cancer. *Journal of Controlled Release* **258**, 1–9 (2017).
190. Yang, L. *et al.* Efficient Delivery of Antisense Oligonucleotides Using Bioreducible Lipid Nanoparticles In Vitro and In Vivo. *Molecular Therapy - Nucleic Acids* **19**, 1357–1367 (2020).
191. Kotula, J. W. *et al.* Aptamer-mediated delivery of splice-switching oligonucleotides to the nuclei of cancer cells. *Nucleic Acid Ther* **22**, 187–195 (2012).

192. Hong, S., Sun, N., Liu, M., Wang, J. & Pei, R. Building a chimera of aptamer–antisense oligonucleotide for silencing galectin-1 gene. *RSC Adv.* **6**, 112445–112450 (2016).
193. Roberts, T. C., Langer, R. & Wood, M. J. A. Advances in oligonucleotide drug delivery. *Nature Reviews Drug Discovery* **19**, 673–694 (2020).
194. McNamara, M. E. O. Development of Novel Therapies for Marfan Syndrome using a Human iPSC-disease model. (University of Cambridge, 2019).
195. Price, L. L. Applications of antisense oligonucleotides in designing a therapy for spinal muscular atrophy. (The University of Western Australia, 2017).
196. Drugs@FDA: FDA-Approved Drugs.
<https://www.accessdata.fda.gov/scripts/cder/daf/index.cfm?event=browseByLetter.page&productLetter=A>.
197. Dhuri, K. *et al.* Antisense Oligonucleotides: An Emerging Area in Drug Discovery and Development. *Journal of Clinical Medicine* **9**, (2020).
198. Roshmi, R. R. & Yokota, T. Viltolarsen for the treatment of Duchenne muscular dystrophy. *Drugs Today (Barc)* **55**, 627–639 (2019).
199. Kim, J. *et al.* Patient-Customized Oligonucleotide Therapy for a Rare Genetic Disease. *New England Journal of Medicine* **381**, 1644–1652 (2019).
200. Nollen, G. J. & Mulder, B. J. M. What is new in the Marfan syndrome? *International Journal of Cardiology* **97**, 103–108 (2004).
201. Cao, Y. *et al.* Three Novel Mutations in FBN1 and TGFBR2 in Patients with the Syndromic Form of Thoracic Aortic Aneurysms and Dissections. *Int Heart J* **59**, 1059–1068 (2018).
202. Magyar, I. *et al.* Quantitative sequence analysis of FBN1 premature termination codons provides evidence for incomplete NMD in leukocytes. *Hum. Mutat.* **30**, 1355–1364 (2009).
203. Krawczak, M., Reiss, J. & Cooper, D. N. The mutational spectrum of single base-pair substitutions in mRNA splice junctions of human genes: causes and consequences. *Hum. Genet.* **90**, 41–54 (1992).
204. Aung-Htut, M. T. *et al.* Splice modulating antisense oligonucleotides restore some acid-alpha-glucosidase activity in cells derived from patients with late-onset Pompe disease. *Scientific Reports* **10**, 6702 (2020).

205. Corey, D. R. Nusinersen, an antisense oligonucleotide drug for spinal muscular atrophy. *Nat. Neurosci.* **20**, 497–499 (2017).
206. Evers, M. M. *et al.* Ataxin-3 protein modification as a treatment strategy for spinocerebellar ataxia type 3: Removal of the CAG containing exon. *Neurobiology of Disease* **58**, 49–56 (2013).
207. Adkin, C. F. *et al.* Multiple exon skipping strategies to by-pass dystrophin mutations. *Neuromuscul Disord* **22**, 297–305 (2012).
208. Yokota, T. *et al.* Efficacy of systemic morpholino exon-skipping in Duchenne dystrophy dogs. *Ann Neurol* **65**, 667–676 (2009).
209. Aartsma-Rus, A. *et al.* Antisense-Induced Multiexon Skipping for Duchenne Muscular Dystrophy Makes More Sense. *The American Journal of Human Genetics* **74**, 83–92 (2004).
210. Bérout, C. *et al.* Multiexon skipping leading to an artificial DMD protein lacking amino acids from exons 45 through 55 could rescue up to 63% of patients with Duchenne muscular dystrophy. *Human Mutation* **28**, 196–202 (2007).
211. Fall, A. M. *et al.* Induction of revertant fibres in the mdx mouse using antisense oligonucleotides. *Genet Vaccines Ther* **4**, 3 (2006).
212. Schatzberg, S. J. *et al.* Alternative dystrophin gene transcripts in golden retriever muscular dystrophy. *Muscle & Nerve* **21**, 991–998 (1998).
213. Yokota, T., Duddy, W., Echigoya, Y. & Kolski, H. Exon skipping for nonsense mutations in Duchenne muscular dystrophy: too many mutations, too few patients? *Expert Opin Biol Ther* **12**, 1141–1152 (2012).
214. Nijbroek, G. *et al.* Fifteen novel FBN1 mutations causing Marfan syndrome detected by heteroduplex analysis of genomic amplicons. *Am. J. Hum. Genet.* **57**, 8–21 (1995).
215. Desmet, F.-O. *et al.* Human Splicing Finder: an online bioinformatics tool to predict splicing signals. *Nucleic Acids Res* **37**, e67 (2009).
216. Yada, T. Splice Sites Score Calculation. *Splice Sites Score Calculation* http://rulai.cshl.edu/new_alt_exon_db2/HTML/score.html (1998).
217. Gruber, A. R., Lorenz, R., Bernhart, S. H., Neuböck, R. & Hofacker, I. L. The Vienna RNA Websuite. *Nucleic Acids Research* **36**, W70–W74 (2008).

218. Verma, A. Recent Advances in Antisense Oligonucleotide Therapy in Genetic Neuromuscular Diseases. *Ann Indian Acad Neurol* **21**, 3–8 (2018).
219. Aartsma-Rus, A. & Krieg, A. M. FDA Approves Eteplirsen for Duchenne Muscular Dystrophy: The Next Chapter in the Eteplirsen Saga. *Nucleic Acid Ther* **27**, 1–3 (2017).
220. Harding, P. L., Fall, A. M., Honeyman, K., Fletcher, S. & Wilton, S. D. The Influence of Antisense Oligonucleotide Length on Dystrophin Exon Skipping. *Molecular Therapy* **15**, 157–166 (2007).
221. Corson, G. M., Chalberg, S. C., Dietz, H. C., Charbonneau, N. L. & Sakai, L. Y. Fibrillin binds calcium and is coded by cDNAs that reveal a multidomain structure and alternatively spliced exons at the 5' end. *Genomics* **17**, 476–484 (1993).
222. Handford, P. A. *et al.* Key residues involved in calcium-binding motifs in EGF-like domains. *Nature* **351**, 164–167 (1991).
223. Hogue, J. *et al.* Homozygosity for a FBN1 missense mutation causes a severe Marfan syndrome phenotype. *Clin. Genet.* **84**, 392–393 (2013).
224. Shefer, K., Sperling, J. & Sperling, R. The Supraspliceosome — A Multi-Task Machine for Regulated Pre-mRNA Processing in the Cell Nucleus. *Computational and Structural Biotechnology Journal* **11**, 113–122 (2014).
225. Kessler, O., Jiang, Y. & Chasin, L. A. Order of intron removal during splicing of endogenous adenine phosphoribosyltransferase and dihydrofolate reductase pre-mRNA. *Mol Cell Biol* **13**, 6211–6222 (1993).
226. Ham, K. A., Aung-Htut, M. T., Fletcher, S. & Wilton, S. D. Nonsequential Splicing Events Alter Antisense-Mediated Exon Skipping Outcome in COL7A1. *International Journal of Molecular Sciences* **21**, 7705 (2020).
227. Hutchinson, S., Wordsworth, B. P. & Handford, P. A. Marfan syndrome caused by a mutation in FBN1 that gives rise to cryptic splicing and a 33 nucleotide insertion in the coding sequence. *Hum. Genet.* **109**, 416–420 (2001).
228. Hyytiäinen, M., Penttinen, C. & Keski-Oja, J. Latent TGF- β Binding Proteins: Extracellular Matrix Association and Roles in TGF- β Activation. *Critical Reviews in Clinical Laboratory Sciences* **41**, 233–264 (2004).

229. Shi, M. *et al.* Latent TGF- β structure and activation. *Nature* **474**, 343–349 (2011).
230. Chaudhry, S. S. *et al.* Fibrillin-1 regulates the bioavailability of TGF β 1. *J Cell Biol* **176**, 355–367 (2007).
231. Eder, P. S., DeVine, R. J., Dagle, J. M. & Walder, J. A. Substrate specificity and kinetics of degradation of antisense oligonucleotides by a 3' exonuclease in plasma. *Antisense Res Dev* **1**, 141–151 (1991).
232. Iversen, P. L., Zhu, S., Meyer, A. & Zon, G. Cellular uptake and subcellular distribution of phosphorothioate oligonucleotides into cultured cells. *Antisense Res Dev* **2**, 211–222 (1992).
233. Monia, B. P. *et al.* Evaluation of 2'-modified oligonucleotides containing 2'-deoxy gaps as antisense inhibitors of gene expression. *J Biol Chem* **268**, 14514–14522 (1993).
234. Kurreck, J., Wyszko, E., Gillen, C. & Erdmann, V. A. Design of antisense oligonucleotides stabilized by locked nucleic acids. *Nucleic Acids Res* **30**, 1911–1918 (2002).
235. Frank, D. E. *et al.* Increased dystrophin production with golodirsen in patients with Duchenne muscular dystrophy. *Neurology* **94**, e2270–e2282 (2020).
236. Yin, H. *et al.* Cell-penetrating peptide-conjugated antisense oligonucleotides restore systemic muscle and cardiac dystrophin expression and function. *Hum Mol Genet* **17**, 3909–3918 (2008).
237. Yin, H. *et al.* Functional rescue of dystrophin-deficient mdx mice by a chimeric peptide-PMO. *Mol Ther* **18**, 1822–1829 (2010).
238. Sarepta Therapeutics, Inc. *A Phase 2, Two-Part, Multiple-Ascending-Dose Study of SRP-5051 for Dose Determination, Then Dose Expansion, in Patients With Duchenne Muscular Dystrophy Amenable to Exon 51-Skipping Treatment.* <https://clinicaltrials.gov/ct2/show/NCT04004065> (2021).
239. Sarepta Therapeutics, Inc. *An Open-Label Extension Study for Patients With Duchenne Muscular Dystrophy Who Participated in Studies of SRP-5051.* <https://clinicaltrials.gov/ct2/show/NCT03675126> (2020).

240. Langner, H. K., Jastrzebska, K. & Caruthers, M. H. Synthesis and Characterization of Thiophosphoramidate Morpholino Oligonucleotides and Chimeras. *J. Am. Chem. Soc.* **142**, 16240–16253 (2020).
241. Kole, R. & Krieg, A. M. Exon skipping therapy for Duchenne muscular dystrophy. *Advanced Drug Delivery Reviews* **87**, 104–107 (2015).
242. Tynan, K. *et al.* Mutation screening of complete fibrillin-1 coding sequence: report of five new mutations, including two in 8-cysteine domains. *Hum Mol Genet* **2**, 1813–1821 (1993).
243. Shen, W., Liang, X. & Crooke, S. T. Phosphorothioate oligonucleotides can displace NEAT1 RNA and form nuclear paraspeckle-like structures. *Nucleic Acids Res* **42**, 8648–8662 (2014).
244. Flynn, L. L. *et al.* Interaction of modified oligonucleotides with nuclear proteins, formation of novel nuclear structures and sequence-independent effects on RNA processing. *Preprint at bioRxiv* 446773 (2019) doi:10.1101/446773.
245. Warf, M. B. & Berglund, J. A. The role of RNA structure in regulating pre-mRNA splicing. *Trends Biochem Sci* **35**, 169–178 (2010).
246. Lima, W. F., Monia, B. P., Ecker, D. J. & Freier, S. M. Implication of RNA structure on antisense oligonucleotide hybridization kinetics. *Biochemistry* **31**, 12055–12061 (1992).
247. Fletcher, S. *et al.* Dystrophin expression in the mdx mouse after localised and systemic administration of a morpholino antisense oligonucleotide. *The Journal of Gene Medicine* **8**, 207–216 (2006).
248. Heemskerk, H. A. *et al.* In vivo comparison of 2'-O-methyl phosphorothioate and morpholino antisense oligonucleotides for Duchenne muscular dystrophy exon skipping. *The Journal of Gene Medicine* **11**, 257–266 (2009).
249. Bond, C. S. & Fox, A. H. Paraspeckles: nuclear bodies built on long noncoding RNA. *Journal of Cell Biology* **186**, 637–644 (2009).
250. Naganuma, T. *et al.* Alternative 3'-end processing of long noncoding RNA initiates construction of nuclear paraspeckles. *EMBO J* **31**, 4020–4034 (2012).
251. Heo, Y.-A. Golodirsen: First Approval. *Drugs* **80**, 329–333 (2020).

252. Wilton, S. D., Fletcher, S. & Flanigan, K. M. Dystrophin as a therapeutic biomarker: Are we ignoring data from the past? *Neuromuscular Disorders* **24**, 463–466 (2014).
253. Nicholson, L. V., Johnson, M. A., Bushby, K. M. & Gardner-Medwin, D. Functional significance of dystrophin positive fibres in Duchenne muscular dystrophy. *Arch Dis Child* **68**, 632–636 (1993).
254. Amantana, A. & Iversen, P. L. Pharmacokinetics and biodistribution of phosphorodiamidate morpholino antisense oligomers. *Curr Opin Pharmacol* **5**, 550–555 (2005).
255. Geary, R. S., Norris, D., Yu, R. & Bennett, C. F. Pharmacokinetics, biodistribution and cell uptake of antisense oligonucleotides. *Advanced Drug Delivery Reviews* **87**, 46–51 (2015).
256. Sarepta Therapeutics Announces Positive Clinical Results from MOMENTUM, a Phase 2 Clinical Trial of SRP-5051 in Patients with Duchenne Muscular Dystrophy Amenable to Skipping Exon 51 | Sarepta Therapeutics, Inc. <https://investorrelations.sarepta.com/news-releases/news-release-details/sarepta-therapeutics-announces-positive-clinical-results> (2020).
257. Pyeritz, R. E. Marfan syndrome: 30 years of research equals 30 years of additional life expectancy. *Heart* **95**, 173–175 (2009).
258. Bathen, T., Velvin, G., Rand-Hendriksen, S. & Robinson, H. S. Fatigue in adults with Marfan syndrome, occurrence and associations to pain and other factors. *Am. J. Med. Genet. A* **164A**, 1931–1939 (2014).
259. Zaw, K. *et al.* Consequences of Making the Inactive Active Through Changes in Antisense Oligonucleotide Chemistries. *Front Genet* **10**, (2019).
260. Mitrpant, C. *et al.* Rational Design of Antisense Oligomers to Induce Dystrophin Exon Skipping. *Molecular Therapy* **17**, 1418–1426 (2009).
261. Slijkerman, R. W. *et al.* Antisense Oligonucleotide-based Splice Correction for USH2A-associated Retinal Degeneration Caused by a Frequent Deep-intronic Mutation. *Molecular Therapy - Nucleic Acids* **5**, e381 (2016).
262. Aoki, Y. *et al.* Bodywide skipping of exons 45-55 in dystrophic mdx52 mice by systemic antisense delivery. *Proc Natl Acad Sci U S A* **109**, 13763–13768 (2012).

263. Echigoya, Y. *et al.* Long-term efficacy of systemic multiexon skipping targeting dystrophin exons 45-55 with a cocktail of vivo-morpholinos in mdx52 mice. *Mol Ther Nucleic Acids* **4**, e225 (2015).
264. Yokota, T. *et al.* Extensive and prolonged restoration of dystrophin expression with vivo-morpholino-mediated multiple exon skipping in dystrophic dogs. *Nucleic Acid Ther* **22**, 306–315 (2012).
265. Ham, K. A. *et al.* Cryptic U2-dependent Pre-mRNA Splice Site Usage Induced by Splice Switching Antisense Oligonucleotides. *Preprint at Research Square* (2021) doi:10.21203/rs.3.rs-144809/v1.
266. Domingos, J., Ricotti, V., Martinez, A. E. & Muntoni, F. Severe persistent injection site reactions after subcutaneous 2'-O-methyl phosphorothioate oligonucleotide therapy for Duchenne muscular dystrophy. *Neuromuscul Disord* **28**, 176–177 (2018).
267. Hillhorst, N., Spanoudi-Kitrimi, I., Goemans, N. & Morren, M.-A. Injection site reactions after long-term subcutaneous delivery of drisapersen: a retrospective study. *Eur J Pediatr* **178**, 253–258 (2019).
268. Mendell, J. R., Sahenk, Z. & Rodino-Klapac, L. R. Clinical trials of exon skipping in Duchenne muscular dystrophy. *Expert Opinion on Orphan Drugs* **5**, 683–690 (2017).
269. Pitout, I., Flynn, L. L., Wilton, S. D. & Fletcher, S. Antisense-mediated splice intervention to treat human disease: the odyssey continues. *F1000Res* **8**, (2019).
270. Bailey, J. K., Shen, W., Liang, X.-H. & Crooke, S. T. Nucleic acid binding proteins affect the subcellular distribution of phosphorothioate antisense oligonucleotides. *Nucleic Acids Res* **45**, 10649–10671 (2017).
271. Handford, P. A. Fibrillin-1, a calcium binding protein of extracellular matrix. *Biochimica et Biophysica Acta (BBA) - Molecular Cell Research* **1498**, 84–90 (2000).
272. Kielty, C. M. & Shuttleworth, C. A. The role of calcium in the organization of fibrillin microfibrils. *FEBS Lett* **336**, 323–326 (1993).
273. Dietz, H. C. *et al.* Marfan phenotype variability in a family segregating a missense mutation in the epidermal growth factor-like motif of the fibrillin gene. *J Clin Invest* **89**, 1674–1680 (1992).

274. Hubmacher, D. *et al.* Biogenesis of extracellular microfibrils: Multimerization of the fibrillin-1 C terminus into bead-like structures enables self-assembly. *PNAS* **105**, 6548–6553 (2008).
275. Rurali, E. *et al.* Precise Therapy for Thoracic Aortic Aneurysm in Marfan Syndrome: A Puzzle Nearing Its Solution. *Prog Cardiovasc Dis* **61**, 328–335 (2018).
276. Barré-Sinoussi, F. & Montagutelli, X. Animal models are essential to biological research: issues and perspectives. *Future Sci OA* **1**, (2015).
277. Perlman, R. L. Mouse models of human disease. *Evol Med Public Health* **2016**, 170–176 (2016).
278. Sakai, L. Y., Keene, D. R., Renard, M. & De Backer, J. FBN1: The Disease-Causing Gene for Marfan Syndrome and Other Genetic Disorders. *Gene* **591**, 279–291 (2016).
279. Lima, B. L. *et al.* A New Mouse Model for Marfan Syndrome Presents Phenotypic Variability Associated with the Genetic Background and Overall Levels of Fbn1 Expression. *PLoS One* **5**, (2010).
280. Charbonneau, N. L. *et al.* In vivo studies of mutant fibrillin-1 microfibrils. *J. Biol. Chem.* **285**, 24943–24955 (2010).
281. Picher-Martel, V., Valdmanis, P. N., Gould, P. V., Julien, J.-P. & Dupré, N. From animal models to human disease: a genetic approach for personalized medicine in ALS. *Acta Neuropathologica Communications* **4**, 70 (2016).
282. Chesselet, M.-F. & Carmichael, S. T. Animal Models of Neurological Disorders. *Neurotherapeutics* **9**, 241–244 (2012).
283. Yucel, N., Chang, A. C., Day, J. W., Rosenthal, N. & Blau, H. M. Humanizing the mdx mouse model of DMD: the long and the short of it. *npj Regenerative Medicine* **3**, 1–11 (2018).
284. Fukada, S. *et al.* Genetic Background Affects Properties of Satellite Cells and mdx Phenotypes. *The American Journal of Pathology* **176**, 2414–2424 (2010).
285. Piha-Gossack, A., Sossin, W. & Reinhardt, D. P. The evolution of extracellular fibrillins and their functional domains. *PLoS ONE* **7**, e33560 (2012).

286. Reber-Müller, S., Spissinger, T., Schuchert, P., Spring, J. & Schmid, V. An extracellular matrix protein of jellyfish homologous to mammalian fibrillins forms different fibrils depending on the life stage of the animal. *Dev Biol* **169**, 662–672 (1995).
287. Mayhew, J. E. *et al.* Reliable surrogate outcome measures in multicenter clinical trials of Duchenne muscular dystrophy. *Muscle & Nerve* **35**, 36–42 (2007).
288. Schnell, F. J. *et al.* Development of a validated Western blot method for quantification of human dystrophin protein used in Phase II and III clinical trials of eteplirsen for the treatment of Duchenne muscular dystrophy (DMD) (P5.105). *Neurology* **88**, (2017).
289. Monaco, A. P., Bertelson, C. J., Liechti-Gallati, S., Moser, H. & Kunkel, L. M. An explanation for the phenotypic differences between patients bearing partial deletions of the DMD locus. *Genomics* **2**, 90–95 (1988).
290. Flanigan, K. M. *et al.* Nonsense mutation-associated Becker muscular dystrophy: interplay between exon definition and splicing regulatory elements within the DMD gene. *Hum Mutat* **32**, 299–308 (2011).
291. Muntoni, F., Torelli, S. & Ferlini, A. Dystrophin and mutations: one gene, several proteins, multiple phenotypes. *The Lancet Neurology* **2**, 731–740 (2003).
292. Liang, W.-C., Wang, C.-H., Chou, P.-C., Chen, W.-Z. & Jong, Y.-J. The natural history of the patients with Duchenne muscular dystrophy in Taiwan: A medical center experience. *Pediatr Neonatol* **59**, 176–183 (2018).
293. Brogna, C. *et al.* Long-term natural history data in Duchenne muscular dystrophy ambulant patients with mutations amenable to skip exons 44, 45, 51 and 53. *PLoS One* **14**, (2019).
294. Díaz de Bustamante, A., Ruiz-Casares, E., Darnaude, M. T., Perucho, T. & Martínez-Quesada, G. Phenotypic variability in Marfan syndrome in a family with a novel nonsense FBN1 gene mutation. *Rev Esp Cardiol (Engl Ed)* **65**, 380–381 (2012).
295. Palz, M. *et al.* Clustering of mutations associated with mild Marfan-like phenotypes in the 3' region of FBN1 suggests a potential genotype-phenotype correlation. *Am. J. Med. Genet.* **91**, 212–221 (2000).
296. Dietz Harry C. Potential Phenotype-Genotype Correlation in Marfan Syndrome. *Circulation: Cardiovascular Genetics* **8**, 256–260 (2015).

297. Franken, R. *et al.* Circulating transforming growth factor- β as a prognostic biomarker in Marfan syndrome. *Int J Cardiol* **168**, 2441–2446 (2013).
298. Mullen, M. *et al.* Irbesartan in Marfan syndrome (AIMS): a double-blind, placebo-controlled randomised trial. *The Lancet* **394**, 2263–2270 (2019).
299. Liu, S., Cai, C. & Ning, J. Up-and-down designs for phase I clinical trials. *Contemp Clin Trials* **36**, 218–227 (2013).
300. Storer, B. E. Design and Analysis of Phase I Clinical Trials. *Biometrics* **45**, 925–937 (1989).
301. North, B., Kocher, H. M. & Sasieni, P. A new pragmatic design for dose escalation in phase 1 clinical trials using an adaptive continual reassessment method. *BMC Cancer* **19**, 632 (2019).
302. Körkkö, J., Kaitila, I., Lönnqvist, L., Peltonen, L. & Ala-Kokko, L. Sensitivity of conformation sensitive gel electrophoresis in detecting mutations in Marfan syndrome and related conditions. *J. Med. Genet.* **39**, 34–41 (2002).

Publications Related to this Thesis

Cale, J. M., Fletcher, S. & Wilton, S. D. A Review of the Type-1 Fibrillinopathies: Pathophysiology, Diagnosis and Novel Therapeutic Strategies. *J Genet Syndr Gene Her* **9**, 7 (2018). <https://doi.org/10.4172/2157-7412.1000323>.

Author Contributions:

JC developed the concept, reviewed the literature, interpreted the findings, designed figures, and wrote the manuscript. SDW and SF developed the concept, edited the manuscript and provided supervision. All authors critically reviewed and approved the final version

Cale, J. M., Greer, K., Fletcher, S. & Wilton, S. D. Proof-of-concept: Antisense oligonucleotide-mediated skipping of fibrillin-1 exon 52. *Int J Mol Sci* **22**, 7 (2021). <https://doi.org/10.3390/ijms22073479>.

Submitted: 10/02/2021, *Accepted:* 25/03/2021

Author Contributions:

Conceptualization, J.C. and S.D.W.; methodology, J.C. and K.G.; formal analysis, J.C.; investigation, J.C. and K.G.; writing—original draft preparation, J.C.; writing—review and editing, J.C, K.G., S.F. and S.D.W.; visualization, J.C.; supervision, S.F., S.D.W.; funding acquisition, S.D.W. All authors have read and agreed to the final version of the manuscript.

A Review of the Type-1 Fibrillinopathies: Pathophysiology, Diagnosis and Novel Therapeutic Strategies

Jessica M Cale^{1,2}, Sue Fletcher^{1,2} and Steve D Wilton^{1,2*}

¹Molecular Therapy Laboratory, Centre for Comparative Genomics, Murdoch University, Health Research Building, Discovery Way, Western Australia

²Perron Institute for Neurological and Translational Science, Sarich Neuroscience Institute, University of Western Australia, Verdun Street, Western Australia

*Corresponding author: Steve D Wilton, Centre for Comparative Genomics, Murdoch University, 90 South Street, Murdoch, Western Australia, Tel: +61 8 9360 2305; E-mail: swilton@ccg.murdoch.edu.au

Received date: December 6, 2017; Accepted date: January 12, 2018; Published date: January 20, 2018

Copyright: © 2018 Cale JM, et al. This is an open-access article distributed under the terms of the Creative Commons Attribution License, which permits unrestricted use, distribution, and reproduction in any medium, provided the original author and source are credited.

Abstract

Type-1 fibrillinopathies are a family of connective tissue disorders with major clinical manifestations in the skeletal, ocular and cardiovascular systems. The type-1 fibrillinopathies are caused by mutations in the fibrillin-1 gene (*FBN1*), which encodes fibrillin-1, a large glycoprotein and a major component of the extracellular matrix microfibrils, providing both structural and regulatory support to connective tissues. The type-1 fibrillinopathies have been associated with over 1800 unique mutations within the *FBN1* and demonstrate a wide range of phenotypic variability. This, in conjunction with a number of other factors has impacted on the identification of genotype-phenotype correlations, pathogenesis and diagnostic tests for this family of diseases, leaving many open-ended theories.

Current standard of care relies heavily on surgical intervention and lifelong use of β -blockers to slow disease progression, with research focused heavily on antagonism of transforming growth factor β , which is known to be dysregulated in patients with *FBN1* mutations. Antisense oligonucleotides present a novel therapeutic strategy for the type-1 fibrillinopathies, by mediating the alteration of exon arrangement of both the normal and disease-causing mRNA transcripts, to re-establish the periodicity of fibrillin-1. The induced proteins, while internally truncated, should be homologous and thus be able to form multimer units. This treatment alone or in association with isoform switching, TGF- β antagonism or enhanced/inhibited protein degradation could facilitate the assembly of fibrillin-1 monomers into multimers and consequently a decrease in phenotypic severity.

This review presents a basic overview of the past and current knowledge about the spectrum of type-1 fibrillinopathies with a particular focus on Marfan syndrome, as well as presenting novel potential therapeutic strategies.

Keywords: Type-1 fibrillinopathies; Marfan syndrome; Fibrillin-1; Genetic therapy

Introduction to the Type-1 Fibrillinopathies

The type-1 fibrillinopathies are a family of heritable connective tissue disorders characterised by skeletal, ocular and cardiovascular abnormalities. These diseases are caused by mutations in the fibrillin-1 gene (*FBN1*) [1], with over 1800 unique mutations, spread throughout the *FBN1* sequence, described in the universal mutation database (UMD) [2]. The majority of mutations described are missense mutations, however, insertions, deletions and splice site mutations have also been described [2,3].

FBN1 is one of three distinct genes in the fibrillin family, along with *fibrillin-2* and *fibrillin-3*, all of which share sequence similarities [4]. *FBN1* is a large gene consisting of 66 exons spanning over 200 Kb [5]. While exon 1 of *FBN1* does not directly contribute to the translated product, the exon numbering system used in this review is based on the full 66 exon transcript (GenBank reference sequence NM_000138.4). The remaining 65 exons encode a 2871 amino acid preproprotein, which is cleaved, by the protease furin, into the large glycoprotein fibrillin-1 and the protein hormone asprosin [6,7].

Fibrillin-1 is present in the majority of connective tissues and has both structural and regulatory roles. As a major structural element of microfibrils fibrillin-1 acts as a backbone to which other microfibril associated proteins bind [8,9], while also being essential for the stability of elastic fibres [10,11]. The assembly of fibrillin into microfibrils is initiated immediately after synthesis and secretion when fibrillin-1 monomers aggregate into multimer units, bound by disulphide bonds between the first 4 cysteine residues at the N-terminus [12]. Heterodimers between fibrillin-1 and the other fibrillin monomers have not been observed, suggesting that the proline-rich sequence at the N-terminus (Figure 1), unique to fibrillin-1, provides the specificity responsible for this binding [13].

The structure of fibrillin-1 is complex and highly repetitive, consisting of a number of cysteine-rich repeats (Figure 1). These include 47 epidermal growth factor (EGF)-like repeats, seven transforming growth factor β binding protein-like (TB) domains and two domains that share similarities with both EGF-like and TB domains known as hybrid domains [14,15].

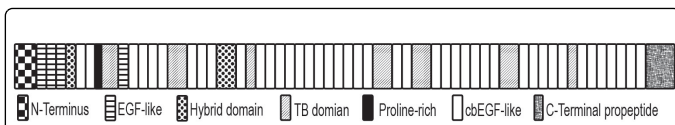


Figure 1: The domain structure of the fibrillin-1 preproprotein. Made up of four EGF-like domains and 43 calcium binding EGF-like (cbEGF-like) domains interspaced with seven TGF- β binding protein-like (TB) domains and two hybrid domains. A proline rich region toward the N-terminus has been implicated in the assembly and specificity of fibrillin-1 multimers [13].

Of the 47 EGF-like repeats, 43 contain a consensus sequence for calcium binding, which is essential for protein stability and protection from proteolysis [16], these repeats are therefore further denoted cbEGF-like domains [15]. Each EGF-like, TB and hybrid domains has 6-8 highly conserved cysteines [14,17] that form disulphide bonds in specific patterns that assist in protein folding and enhance protein function. Mutations that disrupt these bonds are the most common cause of the type-1 fibrillinopathy, Marfan syndrome [18].

Spectrum of Type-1 Fibrillinopathies

Marfan syndrome

Marfan syndrome (MFS, MIM 154700) is the most common of the type-1 fibrillinopathies [19], with a consistent prevalence of 2-3 in 10,000 individuals across gender, ethnicity and geographical distribution [20,21]. MFS is inherited in an autosomal dominant manner with approximately 25% to 30% of mutations arising *de novo* [22,23]. However, despite consistently being referred to as an autosomal dominant condition, as of 2017, twelve cases of homozygous mutations have been recorded in the UMD-*FBN1* database [2]. A number of these cases have an unequivocal autosomal recessive inheritance pattern, with relatives of the proband being asymptomatic heterozygous carriers [24,25]. This suggests that the inheritance pattern of MFS is complex and still not fully understood.

Clinical features

MFS is a multisystem disorder characterised by skeletal, cardiovascular and ocular abnormalities [26,27]. The most noticeable features include increased height with dolichostenomelia and arachnodactyly; the disproportionate overgrowth of long bones and digits respectively, as well as joint hypermobility [26]. Spinal deformities such as scoliosis and dural ectasia, and chest wall deformities are also common features [26,27].

Ocular manifestations include myopia or near sightedness, and ectopia lentis, which is the displacement of the crystalline lens from its natural location [27]. Such features generally present early in disease progression and are therefore important diagnostic indicators, especially for children. However, these features are also common to a multitude of other diseases including a number of other type-1 fibrillinopathies [26].

Cardiovascular abnormalities are the most common cause of death of MFS patients especially in the most severe form, neonatal Marfan syndrome (nMFS), which is characterised by the early onset of cardiovascular manifestations [28,29]. These deaths are typically the result of progressive aortic root enlargement and aortic aneurysm, that

can eventuate into aortic regurgitation, dissection or rupture [30]. Other cardiovascular features include mitral valve prolapse and mitral regurgitation [27]. Due to their late onset and progressive nature, key cardiovascular features are often not present or noticeable in younger patients. However, with advances in technology, features such as aortic enlargement can now be readily detected in suspected MFS patients using echocardiography, allowing for much needed early intervention [20].

Diagnostic odyssey

The diagnosis of MFS and delineation from other type-1 fibrillinopathies is challenging for a number of reasons, including the large size of *FBN1*, number of unique mutations and the lack of defined mutation hotspots [23,31]. These characteristics mean that, despite progress in understanding the genetic basis of MFS, as well as advances in genetic testing techniques, there is still no efficient, time and cost effective molecular test for MFS [19,32]. Molecular diagnosis is most often reserved for patients who either have a clinical diagnosis or a diagnosed relative [33].

There are also diagnostic issues that arise from the extensive phenotypic overlap between MFS and the other type-1 fibrillinopathies, as well as the phenotypic variability observed both between and within affected families [23,31]. The progressive nature of MFS, in particular the late onset of cardiovascular features also adds to the challenge, especially in the diagnosis of children in which the symptoms have not fully developed [34].

To overcome these limitations, the diagnosis of MFS is based on a well-defined set of criteria, known as the Ghent nosology and supplemented with molecular testing when appropriate [20,33]. These criteria were first described by Beighton et al. [35] under the umbrella of the Berlin nosology, which encompassed the diagnosis of a number of connective tissue disorders. This document outlines features considered major or minor in the MFS phenotype, organised according to the organ system involved. The requirements of diagnosis varied, depending on the presence of an affected relative and were based on the involvement of at least 2 organ systems with a number of major and minor manifestations [35].

These diagnostic criteria were subsequently updated in 1996 and reworked into the Ghent nosology that is more specific to the diagnosis of Marfan syndrome. These updated criteria provide more stringent diagnosis for relatives of MFS individuals, revised skeletal involvement and delineation of MFS and MFS-like disorders [36]. In 2010, the Ghent nosology was revised again due to concerns about the sensitivity of diagnosis, especially in regard to age-dependant manifestations and the resulting potential for misdiagnosis of children [27]. The revised criteria place more emphasis on aortic root aneurysm and ectopia lentis, with less emphasis on features such as flat feet and pulmonary artery dilation that are common to other type-1 fibrillinopathies [27]. Current diagnosis of a patient without a diagnosed relative requires the major involvement of at least two organ systems with minor involvement of a third. Individuals with known *FBN1* mutations or a first degree relative with a MFS diagnosis, are diagnosed based on the presence of one major and one minor manifestation in different organ systems [27].

Due to the considerable phenotypic variability amongst individuals with type-1 fibrillinopathies, affected individuals are often classified according to where they sit on the 'Marfan spectrum' [3]. At one end are those diagnosed with neonatal Marfan syndrome, the most severe

form of MFS, characterised by its early onset and life expectancy of less than 24 months [37]. At the other end of the spectrum are those who do not fully meet the Ghent nosology or have additional features not observed in the Marfan phenotype. Such patients are most often diagnosed with other type-1 fibrillinopathies, as described below.

Marfan lipodystrophy syndrome

Marfan lipodystrophy syndrome (MFLS, MIM 616914) is an extremely rare autosomal dominant disease, with only 7 known cases globally [38]. MFLS is characterised by congenital lipodystrophy, the severe lack of fat in the subcutaneous tissues, as well as premature birth and disproportionate growth to weight gain [39]. Affected individuals also have distinctive facial features, including protruding eyes, down slanting palpebral fissures and a posteriorly positioned lower jaw resulting in a severe overbite [39]. Other features overlap with Marfan syndrome including long limbs and digits, hyper extensible joints and myopia [39,40]. Due to these similarities there are cases in which individuals fulfil the Ghent nosology, however due to the characteristic lack of subcutaneous fat tissue are diagnosed with MFLS [40].

MASS syndrome

MASS syndrome (MIM 604308) is the diagnosis given to individuals who have MASS phenotypes involving the Mitral valve, Aorta, Skeleton and Skin, but do not fulfil the Ghent nosology [41]. Despite not meeting the diagnostic criteria of MFS, the MASS phenotype shares a number of features with MFS, including disproportionately long limbs, chest deformities, mitral valve prolapse and aortic root dilation [36,41]. Loeyes et al. [27] suggests caution in the diagnosis of MASS syndrome due to its ambiguity, the lack of understanding of the underlying mutations and the potential for disease progression into classic MFS.

Ectopia lentis syndrome

While ectopia lentis is a key feature of the MFS phenotype, ectopia lentis syndrome (ELS, MIM 129600) describes patients who have ectopia lentis but lack the cardiovascular involvement typical of MFS [27]. ELS has an autosomal dominant inheritance pattern and affected individuals present with dislocation of the lens due to abnormal stretching of the zonular fibres and this can in turn result in acute or chronic impaired vision [42]. Much like MFS, ELS is caused by numerous mutations throughout the *FBNI*, with around 38% of mutations that result in ELS also identified in MFS patients [43].

Stiff skin syndrome

Stiff skin syndrome (SSKS, MIM 184900) is another rare autosomal dominant disorder, characterised by thick and hardened skin that leads to reduced joint mobility [44]. Due to its rarity, the exact cause and pathogenesis of SSKS remains unknown, however using pulse chase analysis Loeyes et al. [44] determined that while SSKS patients have normal levels of fibrillin-1 secretion, they have increased deposition of fibrillin-1; and elastin, in the dermis. The group also observed that patient microfibrils were noticeably shorter than those seen in control samples, suggesting that *FBNI* mutations are implicated in this syndrome [44].

Other type-1 fibrillinopathies

Weill-Marchesani syndrome 2 (WMS2, MIM 608328), acromicric dysplasia (ACMID, MIM 102370) and geleophysic dysplasia 2 (GPHYSD2, MIM 614185) are allelic autosomal dominant disorders characterised by severe short stature, brachydactyly and limited joint movement [45,46]. While all three disorders share skeletal phenotypes, WMS2 patients also present with lens abnormalities including glaucoma and ectopia lentis [46]. GPHYSD2 differs from ACMID as affected patients have additional cardiovascular abnormalities that lower life expectancy [45]. ACMID also has unique craniofacial feature including rounded face, with distinctive well-defined eyebrows and eyelashes, bulbous nose and small mouth with thick lips [45].

Genotype-Phenotype Correlations

Several studies have attempted to correlate mutations in particular regions of *FBNI* with specific phenotypes. However, this has proved difficult due to the high frequency of unique mutations, approximately 60% [2] and the extensive variability in phenotype between and within families [3,47]. Despite these challenges, one trend that is well accepted is the association of neonatal MFS with mutations within exons 25-33 (Figure 2) [18]. However, while the entire region most often quoted as associated with nMFS, Booms et al. [37] reported that evidence actually supports the presence of two nMFS hotspots. The first encompasses exons 25-28 and mainly consists of missense mutations and in-frame insertions [37]. The second hotspot spans exon 32 and 33, in which splice site mutations resulting in exon skipping most often lead to nMFS [37].

Several of the studies attempting to unravel genotype:phenotype associations have noted that the type of mutation, rather than its location, influences the resulting phenotype [18,37,48,49]. A good illustration of this trend is that missense mutations within exons 32 and 33 are most often associated with the classic MFS phenotype [2], while donor or acceptor splice site mutations within this region lead to the severe and early onset phenotype of nMFS [37]. Other examples are the association of premature protein truncation mutations with severe skeletal phenotypes, and cysteine substitutions with ectopia lentis [18,50].

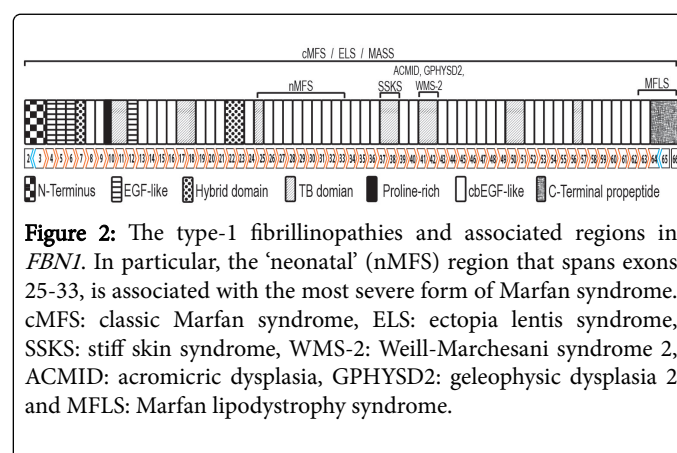


Figure 2: The type-1 fibrillinopathies and associated regions in *FBNI*. In particular, the 'neonatal' (nMFS) region that spans exons 25-33, is associated with the most severe form of Marfan syndrome. cMFS: classic Marfan syndrome, ELS: ectopia lentis syndrome, SSKS: stiff skin syndrome, WMS-2: Weill-Marchesani syndrome 2, ACMID: acromicric dysplasia, GPHYSD2: geleophysic dysplasia 2 and MFLS: Marfan lipodystrophy syndrome.

While mutations causing MFS and ELS are found throughout the *FBNI* sequence, many of the mutations associated with other type-1 fibrillinopathies are clustered within specific regions of *FBNI* (Figure 2). For example, MFLS is associated with mutations that affect the region of *FBNI* that encodes asprosin. The mutations identified to date

include 2 bp, 8 bp and 20 bp deletions in the 65th exon [39,51] as well as mutations resulting in early protein truncation and the loss of the C-terminus [52].

The majority of mutations that have been associated with WMS2, ACMID and GPHYSD2 are within the 42nd and 43rd exons of *FBNI* (Figure 2) [45,53]. It is the effect of these mutations that is thought to result in the phenotypic differences between these diseases. For example, mutations leading to GPHYSD2 have been shown to affect residues with structural roles, such as the cysteines involved in disulphide bond formation, while ACMID mutations are distributed throughout exons 42 and 43 [45]. Le Goff et al. also suggest that short stature and digits are associated with the disruption of the 5th TB domain specifically, while mutations in the other TB domains lead to other phenotypes [45]. For example mutations within the 4th TB domain are associated with SSKS, which shares phenotypic similarity with WMS2, ACMID and GPHYSD2 but lacks the short stature and digits [44].

Models of Pathogenesis

The Marfan phenotype, particularly the cardiovascular manifestations have been observed to progressively worsen with age. The reason for this remains unknown, as the mechanism behind the pathogenesis of MFS, and the other type-1 fibrillinopathies, is still not fully understood. Based on current knowledge, this progression has been attributed to both the compounding weakness of microfibrils and continuing dysregulation of transforming growth factor beta (TGF- β) [54].

Four models of MFS pathogenesis have been proposed to date. The first is known as the dominant negative model, which describes mutations resulting in an altered protein that acts antagonistically against the normal protein [55]. In the case of MFS, this model suggests that aberrant fibrillin-1 monomers bind incorrectly with normal monomers, forming semi- or non-functional multimers and/or prevent the normal assembly of microfibrils. This in turn would lead to the disorganisation of the extracellular matrix and the observed disease phenotype [55]. Therefore, based on this model, the severity of disease is dependent on the level of fibrillin-1 expression [55].

The dominant negative model began to be questioned after the identification of homozygous mutations and an autosomal recessive form of MFS. de Vries et al. [24] studied two related individuals who harboured homozygous c.1453C>T mutation (p.Arg485Cys), and presented with classic MFS. Hilhorst-Hofstee et al. [25] similarly identified a homozygous c.7454A>T mutation (p.Asp2485Val) in three related individuals diagnosed with MFS. Both groups observed that in the heterozygous state these mutations did not have a dominant negative effect, conflicting with the dominant negative model [24,25]. de Vries et al. [24] suggested that in such cases the pathogenesis is more in line with a haploinsufficiency model. That is a lack of microfibrils or fibrillin-1 resulting from protein degradation, intermolecular cross-linking or reduced fibrillin-1 synthesis [24,56].

The second model suggests that mutations in *FBNI* increase the sensitivity of fibrillin-1 to proteolysis, resulting in a steady decline in microfibrils, parallel to the progression of disease severity [16]. This model is particularly relevant to mutations affecting cbEGF-like repeats, as calcium has been shown to be involved in the formation of microfibrils, and specifically in their stabilisation and protection from proteolysis [11].

The third model suggests that the major roles of fibrillin-1 is to maintain tissue homeostasis and therefore MFS is a result of a loss of homeostasis [11]. This model was based on findings from two mouse models showing that MFS, which caused a typical phenotype in the vesicular tissue and resulted in death, did not affect elastic fibres in other tissues [11]. Therefore, the authors came to the conclusion that the primary role of fibrillin-1 was not in the assembly of elastic fibres, rather in maintaining homeostasis of existing elastic fibres [11]. The model also suggests, a critical threshold of functional microfibrils required for tissue homeostasis, therefore mutations in *FBNI* result in a decrease in microfibril abundance resulting in MFS [11]. This hypothesis was based on observations of the two mouse models showing that the ultimate outcome of both dominant negative and hypomorphic mutations is a similar decrease in the abundance of functional microfibrils [57].

The fourth model was proposed in the early 2000s, in light of more recent research that linked decreased fibrillin-1 deposition with the dysregulation of TGF- β , a multifunctional cytokine with a role in cell signalling and survival and subsequently with the development of phenotypic features associated with MFS [58]. The study by Neptune et al. [58] identified that the dysregulation of TGF- β lead to apoptosis in the lung during development. However, when TGF- β activation was neutralised lung apoptosis was reduced and alveolar development was rescued [58]. A number of other studies have now supported these findings, providing more evidence that TGF- β dysregulation is the main cause of pathogenesis in Marfan syndrome, favouring the fourth model and directing research focus [8,59].

Mutations in *FBNI* lead to an increase in active TGF- β by disrupting the interaction between latent TGF- β binding protein (LTBP) and fibrillin-1 [60]. In the absence of organised microfibril lattices, the large latent complex (LLC), made up of TGF- β , latency-associated protein and LTBP, is unable to anchor to microfibrils and as a result the components of the LLC remain uncomplexed [60]. This leaves free TGF- β to bind to its receptor, activating a phosphorylation cascade and a number of downstream effects [60,61]. One such effect is increased expression of matrix metalloproteinases leading to the degradation of elastin and the resulting loss of extracellular matrix stability [62].

The initial disruption of LTBP/fibrillin-1 interaction, could be the result of a number of different factors and is likely dependant on the type and position of a mutation. Aoyama et al. [56] suggested that the majority of *FBNI* mutations can be categorised into 5 groups depending on their effects on the synthesis and/or deposition of fibrillin-1. The group also suggested that *FBNI* mutations result in reduced synthesis and/or deposition in different ways, supporting dominant negative effects, haploinsufficiency and protein degradation, all of which are likely to result in the dysregulation of TGF- β [56].

Life Expectancy and Current Treatments

The mean age of death for Marfan patients was predicted in 1972 to be 32 years, with cardiovascular complications associated with aortic dilation the main cause [28]. A continuation of this study in 1995 found that the mean age of death had increased significantly to 41 years, with the average life expectancy increasing several decades [63]. The increased survival was attributed to an overall increase in life expectancy for the general population, an increase in the proportion of individuals diagnosed with milder phenotypes due to increased molecular genetic testing, and significant advances in medical

intervention, specifically cardiovascular surgery [63]. There is, however, still a significant burden on the livelihood and quality of life of MFS patients and currently no cure [21].

The management of Marfan syndrome is multidisciplinary, most often involving geneticists, ophthalmologists, orthopaedists and cardiologists [26]. Current standard of care consists of lifelong use of β -adrenergic receptor blockade or β -blockers [26], which have been shown to slow progressive aortic dilation and reduce the associated complications [64,65]. This is coupled with numerous surgical interventions aimed at correcting major abnormalities in the chest, eye, spine and cardiovascular system [20,26].

The progressive nature of type-1 fibrillinopathies means that constant re-evaluation is required throughout life. For example, ocular features such as lens dislocation are most often managed with corrective lenses, however with increasing severity surgical intervention such as aphakia, removal of the lens, may be required [66]. Similarly, progressive scoliosis is initially managed with bracing, however, patients are monitored throughout development and surgical stabilisation is often required [67].

Following the implication of TGF- β dysregulation in the pathogenesis of MFS, research into potential ways to antagonise TGF- β has been the main research focus for potential therapeutics. The most notable outcome of which is trials into the use of Losartan, a drug that is currently used to treat hypertension [59]. Studies in mouse models have shown that treatment with Losartan can prevent aortic root aneurysm, as well as partially rescue lung structure [68]. However, clinical trials comparing Losartan with β -blockers have shown that while treatment with Losartan significantly reduces aortic dilation, there was no significant difference in the outcome between the two treatment groups [69,70].

Novel Therapies for Type-1 Fibrillinopathies

Due to the nature of MFS as a progressive multisystem disease, with a dominant genetic basis, conventional therapeutic techniques such as cell or gene replacement are unlikely to be applicable. The wide range of causes of MFS also reduce the applicability of such techniques, for example, while gene replacement has potential for cases of haploinsufficiency, it would not be appropriate for *FBNI* mutations resulting in dominant negative effects. Similarly, techniques such as siRNA induced allele specific silencing has potential for patients with dominant negative mutations, however, MFS is also known to be caused by insufficiency of *FBNI* expression, therefore reduction in fibrillin-1 expression is likely to result in disease. For these reasons, the majority of current treatment options specifically target particular clinical features. Antisense oligonucleotides provide a novel therapeutic approach with the potential to treat many mutation types by targeting the pre-mRNA directly.

The primary gene transcript (pre-mRNA) of a gene must be processed in a number of ways, before the mature mRNA can be translated into a protein. These include 5' capping, splicing of exons and removal of intervening sequences, cleavage, polyadenylation of the 3' end and finally export to the cytoplasm [71]. The splicing of non-coding regions (introns) and the subsequent joining of coding regions (exons) is a highly complex and coordinated process that must take place for most human gene transcripts. It is estimated that 95% of multi-exon genes also undergo an additional process called alternative splicing [72]. This process allows for further diversification of gene expression in a highly regulated tissue or development specific manner.

Antisense oligonucleotides (AOs) are single stranded nucleic acid analogues that can be used to achieve a number of outcomes to modify gene expression, including exon skipping for reading frame restoration, isoform switching and gene transcript knockdown. AOs are typically 20-25 bp long and may be designed to bind specifically to a targeted motif within the pre-mRNA of a gene of interest. There are two broad classes of AOs; those that promote the degradation of targeted mRNA, such as RNase H-dependent oligonucleotides or siRNAs and those that physically block or inhibit the splicing or translational machinery, steric-blocker oligonucleotides [73].

Antisense oligonucleotides, in particular steric blockers, have therapeutic applications for a number of diseases. One notable case is a splice-switching phosphorodiamidate morpholino oligomer, now called Exondys51, that was granted accelerated approval by the Food and Drug Administration as a treatment for Duchenne muscular dystrophy [74]. Exondys51 was designed to induce skipping of dystrophin exon 51 to restore the mRNA reading frame around frame-shifting deletions that flank exon 51. Removal of dystrophin exon 51 from these amenable deletions allows translation of an internally truncated dystrophin isoform, similar to that observed in patients with the phenotypically milder Becker's muscular dystrophy [75,76].

Targeted switch splicing could also have potential therapeutic applications for the type-1 fibrillinopathies. We hypothesise that the skipping of exons harbouring disease-causing mutations from *FBNI*, along with the corresponding exon from the normal transcript, could re-establish periodicity of fibrillin-1 monomers. Due to their homology, monomers from all transcripts should therefore be able to correctly aggregate into multimer units forming an organised and functional microfibril backbone.

There is also potential for therapeutic strategies by designing AOs against associated targets. For example, an AO that inhibits the activation of TGF- β could have therapeutic potential because while Losartan proved no more effective than β -blockers, the antagonistic effect of Losartan on TGF- β is effective at preventing aortic root aneurysm and decreasing aortic dilation [68-70]. In particular, TGF- β antagonism works efficiently in patients with *FBNI* mutations that result in haploinsufficiency [77].

Another example is isoform switching, which is a potential way of increasing the expression of fibrillin-1. Burchett et al. [78] identified two alternative isoforms, *54A-FBNI* and *57A-FBNI*, that arise from the incorporation of cryptic exons from introns 54 and 57 respectively. *57A-FBNI* in particular was observed to make up a significant portion of the total number of *FBNI* transcripts, approximately 10-40% depending on the tissue and developmental stage [78]. Antisense oligonucleotides can be designed to block inclusion of these cryptic exons, pushing expression toward the normal transcript thus increasing the abundance of normal fibrillin protein.

Lastly components of the protein degradation pathway could be targeted in two ways depending on the pathogenesis of a mutation. For patients who harbour dominant negative mutations, enhanced proteolysis of aberrant fibrillin-1 would theoretically lead to a higher portion of normal protein that could assemble into functional multimers, as long as there was an increase in expression. Conversely for mutations that result in increased proteolytic sensitivity, inhibiting protein degradation could lead to increased fibrillin-1 abundance and thus a decrease in disease severity. Along with targets within *FBNI* itself these alternative targets mean there are numerous ways in which

AOs could be used as a treatment for individuals suffering from MFS and the other type-1 fibrillinopathies.

Final Remarks

Type-1 fibrillinopathies are a family of connective tissue disorders, of which Marfan syndrome is the most common, with a prevalence of 2-3 in 10,000 individuals. These diseases are caused by mutations in *FBNI*, which encodes fibrillin-1, a major component of the extracellular matrix microfibrils providing both structural and regulatory support. The type-1 fibrillinopathies have variable ages of onset and are progressive in nature, affecting multiple body systems with major clinical manifestations in the skeletal, ocular and cardiovascular systems.

Current standard of care relies heavily on surgical intervention and lifelong use of β -blockers to slow disease progression. Antisense oligonucleotides present a novel therapeutic strategy for the type-1 fibrillinopathies, by mediating the alteration of exon structure of both the normal and disease-causing mRNA transcripts to re-establish the periodicity of fibrillin-1. Resulting proteins, while internally truncated, would be homologous thus may be able to form functional multimer units. This treatment alone or in association with isoform switching, TGF- β antagonism or enhanced/inhibited protein degradation could facilitate the assembly of fibrillin-1 monomers into multimers increasing the abundance of microfibrils and decreasing phenotypic severity.

References

1. Dietz HC, Cutting GR, Pyeritz RE, Maslen CL, Sakai LY, et al. (1991) Marfan syndrome caused by a recurrent *de novo* missense mutation in the fibrillin gene. *Nature* 352: 337-339.
2. Collod-Beroud G, Le Bourdelles S, Ades L, Ala-Kokko L, Booms P, et al. (2003) Update of the UMD-*FBNI* mutation database and creation of an *FBNI* polymorphism database. *Hum Mutat* 22: 199-208.
3. Robinson PN, Booms P, Katzke S, Ladewig M, Neumann L, et al. (2002) Mutations of *FBNI* and genotype-phenotype correlations in Marfan syndrome and related fibrillinopathies. *Hum Mutat* 20: 153-161.
4. Corson GM, Charbonneau NL, Keene DR, Sakai LY (2004) Differential expression of fibrillin-3 adds to microfibril variety in human and avian, but not rodent, connective tissues. *Genomics* 83: 461-472.
5. Biery NJ, Eldadah ZA, Moore CS, Stetten G, Spencer F, et al. (1999) Revised genomic organization of *FBNI* and significance for regulated gene expression. *Genomics* 56: 70-77.
6. Romere C, Duerrschmid C, Bournat J, Constable P, Jain M, et al. (2016) Asprosin, a fasting-induced glucogenic protein hormone. *Cell* 165: 566-579.
7. Lonnqvist L, Reinhardt D, Sakai L, Peltonen L (1998) Evidence for furin-type activity-mediated C-terminal processing of profibrillin-1 and interference in the processing by certain mutations. *Hum Mol Genet* 7: 2039-2044.
8. Sengle G, Sakai LY (2015) The fibrillin microfibril scaffold: A niche for growth factors and mechanosensation? *Matrix Biol* 47: 3-12.
9. Sakai LY, Keene DR, Engvall E (1986) Fibrillin, a new 350 kD glycoprotein, is a component of extracellular microfibrils. *J Cell Biol* 103: 2499-2509.
10. Kiely CM, Shuttleworth CA (1995) Fibrillin-containing microfibrils: Structure and function in health and disease. *Int J Biochem Cell Biol* 27: 747-760.
11. Ramirez F, Gayraud B, Pereira L (1999) Marfan syndrome: New clues to genotype-phenotype correlations. *Ann Med* 31: 202-207.
12. Reinhardt DP, Gambia JE, Ono RN, Bachinger HP, Sakai LY, et al. (2000) Initial steps in assembly of microfibrils. Formation of disulfide-cross-linked multimers containing fibrillin-1. *J Biol Chem* 275: 2205-2210.
13. Trask TM, Ritty TM, Broekelmann T, Tisdale C, Mecham RP, et al. (1999) N-terminal domains of fibrillin 1 and fibrillin 2 direct the formation of homodimers: A possible first step in microfibril assembly. *Biochem J* 340: 693-701.
14. Jensen SA, Iqbal S, Lowe ED, Redfield C, Handford PA, et al. (2009) Structure and interdomain interactions of a hybrid domain: A disulphide-rich module of the fibrillin/LTBP superfamily of matrix proteins. *Structure* 17: 759-768.
15. Pereira L, D'Alessio M, Ramirez F, Lynch JR, Sykes B, et al. (1993) Genomic organization of the sequence coding for fibrillin, the defective gene product in Marfan syndrome. *Hum Mol Genet* 2: 961-968.
16. Reinhardt DP, Ono RN, Sakai LY (1997) Calcium stabilizes fibrillin-1 against proteolytic degradation. *J Biol Chem* 272: 1231-1236.
17. Jensen SA, Robertson IB, Handford PA (2012) Dissecting the fibrillin microfibril: Structural insights into organization and function. *Structure* 20: 215-225.
18. Schrijver I, Liu W, Brenn T, Furthmayr H, Francke U, et al. (1999) Cysteine substitutions in epidermal growth factor-like domains of fibrillin-1: Distinct effects on biochemical and clinical phenotypes. *Am J Hum Genet* 65: 1007-1020.
19. Collod-Beroud G, Boileau C (2002) Marfan syndrome in the third Millennium. *Eur J Hum Genet* 10: 673-681.
20. Ammash NM, Sundt TM, Connolly HM (2008) Marfan syndrome-diagnosis and management. *Curr Probl Cardiol* 33: 7-39.
21. Pyeritz RE (2016) Recent progress in understanding the natural and clinical histories of the Marfan syndrome. *Trends Cardiovasc Med* 26: 423-428.
22. Gray JR, Bridges AB, Faed MJ, Pringle T, Baines P, et al. (1994) Ascertainment and severity of Marfan syndrome in a Scottish population. *J Med Genet* 31: 51-54.
23. Pyeritz RE (2000) The Marfan syndrome. *Annu Rev Med* 51: 481-510.
24. de Vries BB, Pals G, Odink R, Hamel BC (2007) Homozygosity for a *FBNI* missense mutation: Clinical and molecular evidence for recessive Marfan syndrome. *Eur J Hum Genet* 15: 930-935.
25. Hilhorst-Hofstee Y, Rijlaarsdam ME, Scholte AJ, Swart-van den Berg M, Versteegh MI, et al. (2010) The clinical spectrum of missense mutations of the first aspartic acid of cbEGF-like domains in fibrillin-1 including a recessive family. *Hum Mutat* 31: E1915-1927.
26. Judge DP, Dietz HC (2005) Marfan's syndrome. *Lancet* 366: 1965-1976.
27. Loeys BL, Dietz HC, Braverman AC, Callewaert BL, De Backer J, et al. (2010) The revised Ghent nosology for the Marfan syndrome. *J Med Genet* 47: 476-485.
28. Murdoch JL, Walker BA, Halpern BL, Kuzma JW, McKusick VA (1972) Life expectancy and causes of death in the Marfan syndrome. *N Engl J Med* 286: 804-808.
29. Stheneur C, Faivre L, Collod-Beroud G, Gautier E, Binquet C, et al. (2011) Prognosis factors in probands with an *FBNI* mutation diagnosed before the age of 1 year. *Pediatr Res* 69: 265-270.
30. Ramirez F, Dietz HC (2007) Marfan syndrome: from molecular pathogenesis to clinical treatment. *Curr Opin Genet Dev* 17: 252-258.
31. McBride ART, Gargan M (2006) Marfan syndrome. *Current Orthopaedics* 20: 418-423.
32. Summers KM, West JA, Hattam A, Stark D, McGill JJ, et al. (2012) Recent developments in the diagnosis of Marfan syndrome and related disorders. *Med J Aust* 197: 494-497.
33. Stheneur C, Collod-Beroud G, Faivre L, Buyck JF, Gouya L, et al. (2009) Identification of the minimal combination of clinical features in probands for efficient mutation detection in the *FBNI* gene. *Eur J Hum Genet* 17: 1121-1128.
34. Lipscomb KJ, Clayton-Smith J, Harris R (1997) Evolving phenotype of Marfan's syndrome. *Arch Dis Child* 76: 41-46.

35. Beighton P, de Paepe A, Danks D, Finidori G, Gedde-Dahl T, et al. (1988) International nosology of heritable disorders of connective tissue, Berlin, 1986. *Am J Med Genet* 29: 581-594.
36. De Paepe A, Devereux RB, Dietz HC, Hennekam RC, Pyeritz RE (1996) Revised diagnostic criteria for the Marfan syndrome. *Am J Med Genet* 62: 417-426.
37. Booms P, Cislser J, Mathews KR, Godfrey M, Tiecke F, et al. (1999) Novel exon skipping mutation in the fibrillin-1 gene: Two 'hot spots' for the neonatal Marfan syndrome. *Clin Genet* 55: 110-117.
38. Passarge E, Robinson PN, Graul-Neumann LM (2016) Marfanoid-progeroid-lipodystrophy syndrome: A newly recognized fibrillinopathy. *Eur J Hum Genet* 24: 1244-1247.
39. Takenouchi T, Hida M, Sakamoto Y, Torii C, Kosaki R, et al. (2013) Severe congenital lipodystrophy and a progeroid appearance: Mutation in the penultimate exon of *FBNI* causing a recognizable phenotype. *Am J Med Genet A* 161A: 3057-3062.
40. Graul-Neumann LM, Kienitz T, Robinson PN, Baasanjav S, Karow B, et al. (2010) Marfan syndrome with neonatal progeroid syndrome-like lipodystrophy associated with a novel frameshift mutation at the 3' terminus of the *FBNI*-gene. *Am J Med Genet A* 152A: 2749-2755.
41. Glesby MJ, Pyeritz RE (1989) Association of mitral valve prolapse and systemic abnormalities of connective tissue. A phenotypic continuum. *JAMA* 262: 523-528.
42. Greene VB, Stoetzel C, Pelletier V, Perdomo-Trujillo Y, Liebermann L, et al. (2010) Confirmation of ADAMTSL4 mutations for autosomal recessive isolated bilateral ectopia lentis. *Ophthalmic Genet* 31: 47-51.
43. Chandra A, Patel D, Aragon-Martin JA, Pinard A, Collod-Beroud G, et al. (2015) The revised ghent nosology; reclassifying isolated ectopia lentis. *Clin Genet* 87: 284-287.
44. Loeys BL, Gerber EE, Riegert-Johnson D, Iqbal S, Whiteman P, et al. (2010) Mutations in fibrillin-1 cause congenital scleroderma: stiff skin syndrome. *Sci Transl Med* 2: 23ra20.
45. Le Goff C, Mahaut C, Wang LW, Allali S, Abhyankar A, et al. (2011) Mutations in the TGFbeta binding-protein-like domain 5 of *FBNI* are responsible for acromicric and geleophysic dysplasias. *Am J Hum Genet* 89: 7-14.
46. Faivre L, Megarbane A, Alswaid A, Zylberberg L, Aldohayan N, et al. (2002) Homozygosity mapping of a Weill-Marchesani syndrome locus to chromosome 19p13.3-p13.2. *Hum Genet* 110: 366-370.
47. Rommel K, Karck M, Haverich A, Schmidtke J, Arslan-Kirchner M, et al. (2002) Mutation screening of the fibrillin-1 (*FBNI*) gene in 76 unrelated patients with Marfan syndrome or Marfanoid features leads to the identification of 11 novel and three previously reported mutations. *Hum Mutat* 20: 406-407.
48. Latasiewicz M, Fontecilla C, Milla E, Sanchez A (2016) Marfan syndrome: ocular findings and novel mutations-in pursuit of genotype-phenotype associations. *Can J Ophthalmol* 51: 113-118.
49. Schrijver I, Liu W, Odom R, Brenn T, Oefner P, et al. (2002) Premature termination mutations in *FBNI*: distinct effects on differential allelic expression and on protein and clinical phenotypes. *Am J Hum Genet* 71: 223-237.
50. Rommel K, Karck M, Haverich A, von Kodolitsch Y, Rybczynski M, et al. (2005) Identification of 29 novel and nine recurrent fibrillin-1 (*FBNI*) mutations and genotype-phenotype correlations in 76 patients with Marfan syndrome. *Hum Mutat* 26: 529-539.
51. Goldblatt J, Hyatt J, Edwards C, Walpole I (2011) Further evidence for a marfanoid syndrome with neonatal progeroid features and severe generalized lipodystrophy due to frameshift mutations near the 3' end of the *FBNI* gene. *Am J Med Genet A* 155A: 717-720.
52. Jacquinet A, Verloes A, Callewaert B, Coremans C, Coucke P, et al. (2014) Neonatal progeroid variant of Marfan syndrome with congenital lipodystrophy results from mutations at the 3' end of *FBNI* gene. *Eur J Med Genet* 57: 230-234.
53. Faivre L, Gorlin RJ, Wirtz MK, Godfrey M, Dagoneau N, et al. (2003) In frame fibrillin-1 gene deletion in autosomal dominant Weill-Marchesani syndrome. *J Med Genet* 40: 34-36.
54. Achelrod D, Blankart CR, Linder R, von Kodolitsch Y, Stargardt T, et al. (2014) The economic impact of Marfan syndrome: A non-experimental, retrospective, population-based matched cohort study. *Orphanet J Rare Dis* 9: 90.
55. Dietz HC, McIntosh I, Sakai LY, Corson GM, Chalberg SC, et al. (1993) Four novel *FBNI* mutations: significance for mutant transcript level and EGF-like domain calcium binding in the pathogenesis of Marfan syndrome. *Genomics* 17: 468-475.
56. Aoyama T, Francke U, Dietz HC, Furthmayr H (1994) Quantitative differences in biosynthesis and extracellular deposition of fibrillin in cultured fibroblasts distinguish five groups of Marfan syndrome patients and suggest distinct pathogenetic mechanisms. *J Clin Invest* 94: 130-137.
57. Ramirez F, Pereira L (1999) The fibrillins. *Int J Biochem Cell Biol* 31: 255-259.
58. Neptune ER, Frischmeyer PA, Arking DE, Myers L, Bunton TE, et al. (2003) Dysregulation of TGF-beta activation contributes to pathogenesis in Marfan syndrome. *Nat Genet* 33: 407-411.
59. Doyle JJ, Gerber EE, Dietz HC (2012) Matrix-dependent perturbation of TGFbeta signaling and disease. *FEBS Lett* 586: 2003-2015.
60. Benke K, Agg B, Szilveszter B, Tarr F, Nagy ZB, et al. (2013) The role of transforming growth factor-beta in Marfan syndrome. *Cardiol J* 20: 227-234.
61. Huang F, Chen YG (2012) Regulation of TGF-beta receptor activity. *Cell Biosci* 2: 9.
62. Ramachandra CJ, Mehta A, Guo KW, Wong P, Tan JL, et al. (2015) Molecular pathogenesis of Marfan syndrome. *Int J Cardiol* 187: 585-591.
63. Silverman DI, Burton KJ, Gray J, Bosner MS, Kouchoukos NT, et al. (1995) Life expectancy in the Marfan syndrome. *Am J Cardiol* 75: 157-160.
64. Rossi-Foulkes R, Roman MJ, Rosen SE, Kramer-Fox R, Ehlers KH, et al. (1999) Phenotypic features and impact of beta blocker or calcium antagonist therapy on aortic lumen size in the Marfan syndrome. *Am J Cardiol* 83: 1364-1368.
65. Shores J, Berger KR, Murphy EA, Pyeritz RE (1994) Progression of aortic dilatation and the benefit of long-term beta-adrenergic blockade in Marfan's syndrome. *N Engl J Med* 330: 1335-1341.
66. Loewenstein A, Barequet IS, De Juan E, Jr., Maumenee IH (2000) Retinal detachment in Marfan syndrome. *Retina* 20: 358-363.
67. Jones KB, Erkula G, Sponseller PD, Dormans JP (2002) Spine deformity correction in Marfan syndrome. *Spine (Phila Pa 1976)* 27: 2003-2012.
68. Habashi JP, Judge DP, Holm TM, Cohn RD, Loeys BL, et al. (2006) Losartan, an ATI antagonist, prevents aortic aneurysm in a mouse model of Marfan syndrome. *Science* 312: 117-121.
69. Gao L, Chen L, Fan L, Gao D, Liang Z, et al. (2016) The effect of losartan on progressive aortic dilatation in patients with Marfan's syndrome: A meta-analysis of prospective randomized clinical trials. *Int J Cardiol* 217: 190-194.
70. Lacro RV, Dietz HC, Sleeper LA, Yetman AT, Bradley TJ, et al. (2014) Atenolol versus losartan in children and young adults with Marfan's syndrome. *N Engl J Med* 371: 2061-2071.
71. Carmody SR, Wente SR (2009) mRNA nuclear export at a glance. *J Cell Sci* 122: 1933-1937.
72. Pan Q, Shai O, Lee LJ, Frey BJ, Blencowe BJ (2008) Deep surveying of alternative splicing complexity in the human transcriptome by high-throughput sequencing. *Nat Genet* 40: 1413-1415.
73. Dias N, Stein CA (2002) Antisense oligonucleotides: basic concepts and mechanisms. *Mol Cancer Ther* 1: 347-355.
74. Muntoni F, Fletcher S, Wilton S (2017) Response to "Railroading at the FDA". *Nat Biotechnol* 35: 207-209.
75. Lim KR, Maruyama R, Yokota T (2017) Eteplirsin in the treatment of Duchenne muscular dystrophy. *Drug Des Devel Ther* 11: 533-545.
76. Mendell JR, Rodino-Klapac LR, Sahenk Z, Roush K, Bird L, et al. (2013) Eteplirsin for the treatment of Duchenne muscular dystrophy. *Ann Neurol* 74: 637-647.

-
77. Franken R, den Hartog AW, Radonic T, Micha D, Maugeri A, et al. (2015) Beneficial outcome of Losartan therapy depends on type of *FBNI* mutation in Marfan syndrome. *Circ Cardiovasc Genet* 8: 383-388.
78. Burchett ME, Ling IF, Estus S (2011) *FBNI* isoform expression varies in a tissue and development-specific fashion. *Biochem Biophys Res Commun* 411: 323-328.



Article

Proof-of-Concept: Antisense Oligonucleotide Mediated Skipping of Fibrillin-1 Exon 52

Jessica M. Cale ¹, Kane Greer ¹, Sue Fletcher ^{1,2,3}  and Steve D. Wilton ^{1,2,*}

¹ Centre for Molecular Medicine and Innovative Therapeutics, Health Futures Institute, Murdoch University, Murdoch, WA 6150, Australia; jessica.cale@murdoch.edu.au (J.M.C.); K.Greer@murdoch.edu.au (K.G.); S.Fletcher@murdoch.edu.au (S.F)

² Centre for Neuromuscular and Neurological Disorders, Perron Institute for Neurological and Translational Science, The University of Western Australia, Nedlands, WA 6009, Australia

³ PYC Therapeutics, Nedlands, WA 6009, Australia

* Correspondence: s.wilton@murdoch.edu.au; Tel.: +61-8-9360-2305

Abstract: Marfan syndrome is one of the most common dominantly inherited connective tissue disorders, affecting 2–3 in 10,000 individuals, and is caused by one of over 2800 unique *FBN1* mutations. Mutations in *FBN1* result in reduced fibrillin-1 expression, or the production of two different fibrillin-1 monomers unable to interact to form functional microfibrils. Here, we describe in vitro evaluation of antisense oligonucleotides designed to mediate exclusion of *FBN1* exon 52 during pre-mRNA splicing to restore monomer homology. Antisense oligonucleotide sequences were screened in healthy control fibroblasts. The most effective sequence was synthesised as a phosphorodiamidate morpholino oligomer, a chemistry shown to be safe and effective clinically. We show that exon 52 can be excluded in up to 100% of *FBN1* transcripts in healthy control fibroblasts transfected with PMO52. Immunofluorescent staining revealed the loss of fibrillin 1 fibres with ~50% skipping and the subsequent re-appearance of fibres with >80% skipping. However, the effect of exon skipping on the function of the induced fibrillin-1 isoform remains to be explored. Therefore, these findings demonstrate proof-of-concept that exclusion of an exon from *FBN1* pre-mRNA can result in internally truncated but identical monomers capable of forming fibres and lay a foundation for further investigation to determine the effect of exon skipping on fibrillin-1 function.

Keywords: Marfan syndrome; fibrillin-1; antisense oligonucleotides; exon skipping; splice-switching



Citation: Cale, J.M.; Greer, K.; Fletcher, S.; Wilton, S.D. Proof-of-Concept: Antisense Oligonucleotide Mediated Skipping of Fibrillin-1 Exon 52. *Int. J. Mol. Sci.* **2021**, *22*, 3479. <https://doi.org/10.3390/ijms22073479>

Academic Editors: Salvador F. Aliño and Luis Sendra

Received: 10 February 2021

Accepted: 25 March 2021

Published: 27 March 2021

Publisher's Note: MDPI stays neutral with regard to jurisdictional claims in published maps and institutional affiliations.



Copyright: © 2021 by the authors. Licensee MDPI, Basel, Switzerland. This article is an open access article distributed under the terms and conditions of the Creative Commons Attribution (CC BY) license (<https://creativecommons.org/licenses/by/4.0/>).

1. Introduction

Marfan syndrome (MFS, MIM 154700) is one of the most common dominantly inherited connective tissue diseases, affecting an estimated 2–3 in 10,000 individuals [1,2], in a family of disorders called the type-1 fibrillinopathies [3]. Marfan syndrome is characterised by extreme height with disproportionate limb and digit length in comparison to the torso, coupled with a myriad of other skeletal, ocular, skin and cardiovascular abnormalities [4]. However, it is the progressive growth of the aorta often eventuating into aortic dissection and rupture that is the most common cause of death [5].

Marfan syndrome was linked in the early 1990s to mutations in the, then recently discovered [6], fibrillin-1 gene (*FBN1*) [7,8]. Since then, over 2800 disease-causing mutations have been reported [9]. Fibrillin-1 encodes a large 350 kDa glycoprotein of the same name that is secreted from the cell and deposited into the extracellular matrix (ECM) [6]. In a healthy individual, fibrillin-1 monomers aggregate into multimer units within the first few hours after secretion [10]. Fibrillin-1 multimers form the backbone of microfibrils [6] that are essential in the majority of connective tissues and to which many microfibril associated proteins bind [11]. It is in the microfibril form that fibrillin-1 exerts its structural and regulatory roles, providing a backbone for microfibrils [12], maintaining the stability of elastic

fibres [13], and regulating the bioavailability of signalling proteins such as transforming growth factor-beta (TGF- β) [14,15].

In a Marfan syndrome patient, the disease-causing *FBN1* mutation results in a lack of functional microfibrils, in turn leading to instability of the ECM that is further compounded by the dysregulation of TGF- β [12,16]. An increase in bioavailable TGF- β activates a signalling cascade resulting in, among other outcomes, increased expression of matrix metalloproteinase [15] that degrade fibrillin-1 and other matrix proteins leading to further destabilisation of the ECM [15,17]. The initial loss of functional microfibrils is theorised to depend on the type of mutation. In general, missense mutations, which do not affect a conserved cysteine, as well as splicing mutations are thought to exert dominant negative effects. Such mutations result in the production of a dominant aberrant monomer that disrupts the assembly of the wild-type protein into microfibrils [18]. In contrast, many nonsense and frameshifting mutations are associated with haploinsufficiency [19,20]. This haploinsufficiency is the result of transcript instability that leads to degradation and thus reduced fibrillin-1 expression [21]. A small subgroup of nonsense and frameshift mutations that affect the C-terminal region can produce stable transcripts that are translated into protein rather than being degraded [22,23]. Such mutations have been associated with intracellular retention of fibrillin-1, the outcome of which is a similar lack of microfibrils in the ECM [20,22].

The most common type of mutations are missense mutations that result in the disruption of a cysteine residue [9,24]. The fibrillin-1 protein has several repeated domains including 47 epidermal growth factor (EGF)-like domains, 43 of which are involved in calcium-binding (cbEFG-like), seven TGF- β binding protein-like (TB) domains and two hybrid domains [25,26]. Each of these domains are cysteine-rich with six to eight conserved cysteine residues that play a critical role in the folding and stability of the fibrillin-1 protein [25,27]. Mutations affecting a conserved cysteine have been shown to either increase the susceptibility of fibrillin-1 to proteolysis [28,29] or disrupt the folding and secretion of fibrillin-1 leading to intracellular retention [30]. The outcome of either scenario is a similar decreased microfibril stability and abundance.

Following the discovery that mutations in fibrillin-1 result in TGF- β dysregulation, a research area emerged focussing on the antagonism of TGF- β as a therapeutic strategy [31,32]. However, no breakthroughs have yet been made in the field and treatment of MFS patients remains heavily focused on symptom management. The current standard of care includes surgical correction of scoliosis, ectopia lentis, pectus deformities and aortic dilatation, as well as pain management and the use of β -Blockers [33–35] or more recently angiotensin II receptor type 1 blockers [1,31,36] to slow aortic growth. Here, we propose that personalised medicines using antisense oligonucleotides (AO) to alter *FBN1* exon selection during the splicing process, may be an appropriate therapeutic approach for some individuals with Marfan syndrome.

Antisense oligonucleotides (AO) are short sequences, generally between 15 and 30 bases in length, that are single-stranded analogues of nucleic acids. An AO is designed to be complementary to the region of interest binding to the target RNA or DNA through Watson-Crick base pairing. When bound to the target sequence and depending upon the chemistry, AOs can alter transcripts through two main mechanisms; recruiting RNase-H to cleave the target leading to degradation [37,38] or physically blocking the binding of regulatory factors or machinery of the transcription [39], translation [40] or splicing [41,42] processes. Several studies have outlined the potential of AOs in the treatment of genetic diseases. Several notable examples—eteplirsen [43,44], nusinersen [45,46] and more recently golodirsen [47], viltolarsen [48] and casimersen [49]—have now been approved by the United States Food and drug authority (FDA). All four drugs are a class of AO commonly referred to as splice switching. Splice switching AOs function by blocking the splicing machinery or regulatory features, altering the normal splicing process.

Splicing is an essential process for all multi-exon genes; removing the non-coding introns and re-joining the coding exons, before the transcript can be translated. The splicing

process is, therefore, tightly regulated by several *cis*- and *trans*-acting elements. The majority of multi-exon genes, however, also undergo a process called alternative splicing [50]. Alternative splicing allows the production of multiple transcripts, and thus proteins, from a single gene, significantly increasing genetic complexity and diversity. To maintain the precise removal of introns, as well as supporting alternative splicing, the regulation of these processes is multi-layered and complex while maintaining a level of flexibility in the definition of an exon. Utilising the inherent flexibility of exon definition AOs can be targeted to motifs involved in exon recognition and processing, such as the acceptor and donor splice sites, as well as hotspots for splicing enhancers either in the intron or exon. Targeting enhancer sites can block the binding of positive splicing factors, thus decreasing the definition and recognition of an exon sufficiently to result in its exclusion [51,52]. Contrariwise, targeting exonic splicing silencer or intronic splicing silencer sequences can inhibit the binding of negative splicing factors, increasing exon recognition leading to inclusion [52,53].

The affinity, specificity, efficiency, stability and tolerance of an AO can be increased by modifying the chemical structure of the monomers and the backbone. Two widely used chemistries were utilised in this study. First of which has 2'-O-methyl (2'OMe) ribose ring modifications on a negatively charged phosphorothioate (PS) backbone. The resulting 2'OMe-PS compounds are robust RNase-H independent AOs that are nuclease resistant and relatively cost-effective to synthesise. The second chemistry is the phosphorodiamidate morpholino oligomer (PMO) that completely replaces the ribose sugar moiety with a morpholine ring and has phosphorodiamidate linkages [54]. The PMO chemistry is RNase-H independent, and has a neutral charge that precludes interaction with proteins, greatly reducing the possibility of off-target effects [55,56]. While the PMO chemistry is both more technically challenging and costly to synthesise than 2'OMe-PS AOs, PMOs are generally recognised as both safe and effective in a clinical setting, making it a promising chemistry for drug development [43,57].

As described previously, fibrillin-1 monomers are secreted from the cell and rapidly aggregated into multimer units to form the backbone of fibrillin-1 microfibrils [10]. Mutations in *FBN1* disrupt the formation of microfibrils, ultimately leading to a disease phenotype; either Marfan syndrome or another type-1 fibrillinopathy. Therefore, we propose that removal of a mutation-associated exon from all *FBN1* transcripts during the splicing process could result in the production of fibrillin-1 proteins that are able to form functional microfibrils, restoring ECM stability. To assess the viability of this hypothesis, we addressed three preliminary questions using *FBN1* exon 52 as a model. (1) Can an exon be specifically removed from *FBN1* pre-mRNA using antisense oligonucleotides, (2) Can sufficient exon skipping be achieved, and (3) can the internally truncated fibrillin-1 protein form microfibrils.

2. Results

2.1. The *FBN1* Transcript and Antisense Oligonucleotide Design

The fibrillin-1 transcript (LRG_778t1; NM_000138.4) contains 11,695 bases separated into 66 exons, 65 of which encode the 350 kDa fibrillin-1 protein (Figure 1a). Exon 52 of *FBN1* encodes a total of 22 amino acids and makes up a portion of the sixth, of seven TB domains. Over 20 disease-causing mutations have been reported to affect exon 52, the majority of which result, or are predicted to result, in aberrant exon 52 splicing [9,24]. To excise exon 52, along with the flanking introns during the splicing process, five AOs were designed to target the acceptor, and donor splice sites as well as exonic splice enhancer (ESE) and intronic splice enhancer (ISE) sites across exon 52, predicted using the webtool SpliceAid [58] (Figure 1c). SpliceAid examines the exonic and intronic sequence of interest and determines associated silencer and enhancer sites. Each site is given a score of 1 to 10 that indicates the strength of the site, with the value closest to 10 being the strongest ESE sites.

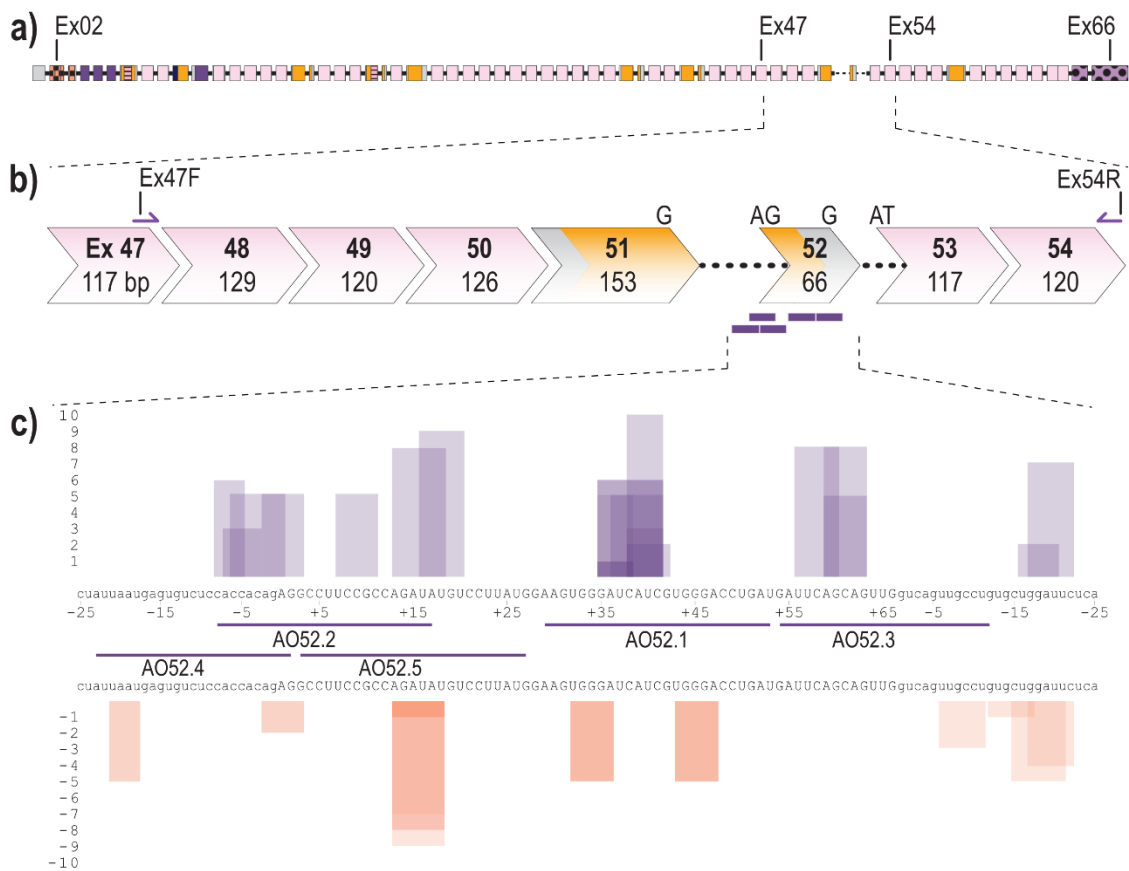


Figure 1. Schematic of *FBN1* pre-mRNA highlighting the region between exons 47 and 54 as well as AO binding sites (a) Full fibrillin-1 pre-mRNA transcript with each box representing an exon. The solid black line represents introns (not to scale); (b) highlighting the region between exons 47 and 54; showing forward and reverse primers and antisense oligonucleotide binding sites (purple bars). Chevron sides indicate exons bounded by partial codons. Pink and yellow fill indicate regions encoding cbEGF-like and TB domains, respectively. The black dotted line indicates partial introns 51 and 52.; (c) Antisense oligonucleotide binding sites and the regulatory motifs they target predicted using spliceAid [58]. Each box represents a predicted enhancer (purple) or silencer (orange) site. The height of the box represents the strength of the site with 1 being the weakest and 10 being the strongest. Exonic and intronic sequences are shown in upper- and lower-case, respectively.

2.2. Evaluation of AOs to Induce Exon 52 Skipping from *FBN1* Transcripts

Initial AO screening was performed using AOs composed of 2'OMe-PS molecules. An unrelated control AO that does not anneal to any transcript was included in all transfections as a sham treatment to observe any chemistry or delivery related effects on cell health and transcript abundance. A complete list of AOs can be found in Table 1.

All 2'OMe-PS AOs were transfected into fibroblasts, derived from a healthy control subject, at three concentrations (200 nM, 100 nM and 50 nM) and incubated for 24 h before collection for RNA extraction and RT-PCR analysis to assess exon skipping efficiencies. The 24-h transfection incubation period was chosen after a time course of 24, 48 and 72 h revealed negligible differences in skipping efficiency over time (data not shown). However, treated cells, in particular those treated with the higher AO concentration, showed changes in morphology and began to die after 48 h (data not shown).

Table 1. Antisense oligonucleotide binding coordinates and sequences.

Nomenclature (FBN1 H...)	Name	Sequence (5'-3')	Chemistry
52A(+29+53)N	AO52.1 ⁿ	AUC AGG UCC CAC GAU GAU CCC ACU U ATC AGG TCC CAC GAT GAT CCC ACT T	2'OMe-PS PMO
52A(+29+53)M	AO52.1 ^m	AUC AGG UCC CAC AAU GAU CCC ACU U	2'OMe-PS
52A(-08+17)	AO52.2	UAU CUG GCG GAA GGC CUC UGU GGU G	2'OMe-PS
52D(+13-12)	AO52.3	CAG GCA ACU GAC CAA CUG CUG AAU C	2'OMe-PS
52A(-23+02)	AO52.4	CUC UGU GGU GGA GAC ACU CAU UAA U	2'OMe-PS
52A(+03+27)	AO52.5	CAU AAG GAC AUA UCU GGC GGA AGG C	2'OMe-PS
Control AO	Ctrl	GGA UGU CCU GAG UCU AGA CCC UCC G	2'OMe-PS
GeneTools Control	GTC	CCT CTT ACC TCA GTT ACA ATT TAT A	PMO

Analysis of PCR amplicons revealed the presence of two products in several samples; the expected full length (FL) product between exon 47 forward and exon 54 reverse primers, as well as a smaller product corresponding to the expected size after skipping of exon 52 ($\Delta 52$) (Figure 2a). The identity of the amplicons was confirmed by band purification and Sanger sequencing, confirming the precise removal of all 66 bases of exon 52 (Figure 2b,c).

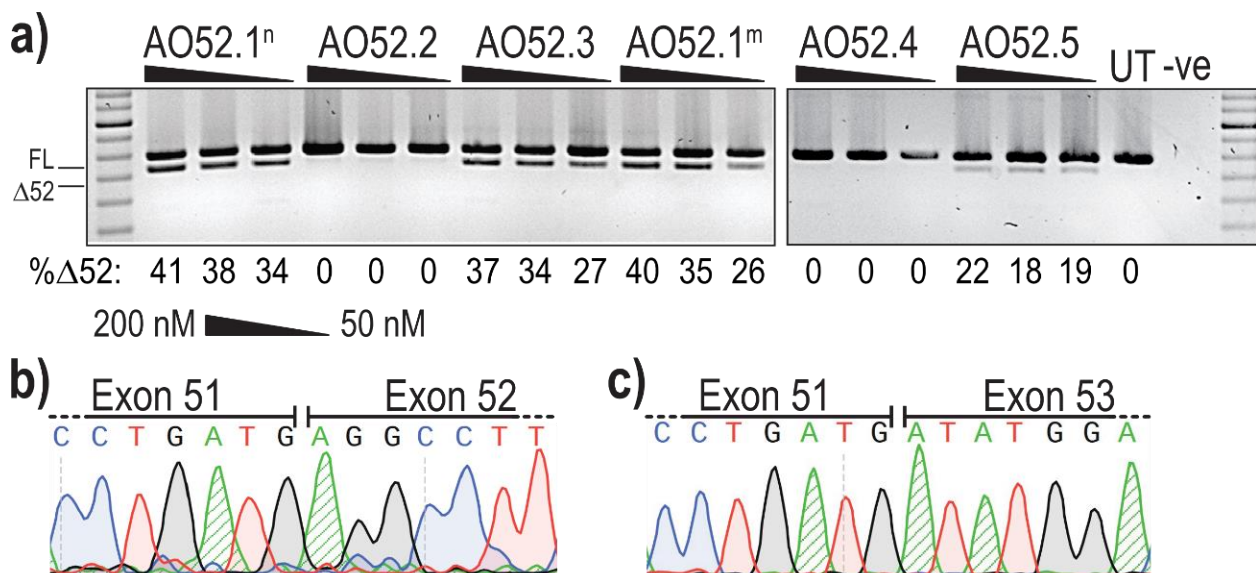


Figure 2. Evaluation of AOs designed to induce *FBN1* exon 52 skipping. (a) Screening of 2'OMe-PS AOs targeting exon 52. Healthy control fibroblasts were transfected with AOs as lipoplexes at three concentrations, 200, 100 and 50 nM. The values below each gel image indicate the percentage of exon 52 skipped ($\Delta 52$) transcripts in each sample. Ctrl: an unrelated sequence used as a sham treatment, UT: untreated control, -ve: RT-PCR negative control. 100 bp molecular marker used for size reference. The gels were cropped for presentation. Full gel images are presented in Figure S1; (b) Sanger sequencing analysis showing the junction between exons 51 and 52 in full-length transcripts (FL, 859 bp); (c) Sanger sequencing analysis showing the junction between exon 51 and 53 exon 52-skipped transcripts ($\Delta 52$, 793 bp).

The most efficient exon 52 skipping was induced by AO52.1ⁿ, with 41% of transcripts lacking exon 52 after transfection at 200 nM (Figure 2a). However, three other sequences, AO52.1^m, AO52.3 and AO52.5 were also relatively efficient, inducing up to 40%, 37% and 22% skipping, respectively (Figure 2a). The remaining two sequences did not induce any measurable exon 52 skipping. The sequences AO52.1ⁿ and AO52.1^m differ by a single base, with each being an exact complementary pair for the wild-type and a known Marfan syndrome patient cell line, respectively. This AO was designed in the hopes of understanding the mechanism behind the mutation that is known to cause mis-splicing of

exon 52. The one base-pair mismatch did not greatly reduce the efficiency of AO52.1^m in healthy control cells.

Following initial AO screening, removal of exon 52 was deemed an appropriate option. In an attempt to further enhance exon exclusion, two AOs targeting *FBN1* exon 52 were combined into cocktails and evaluated. This method has previously been shown to boost skipping efficiency through synergy between the two AOs [59]. Six of the eight cocktails tested, induced between 23% and 42% exon 52 skipping, suggestive of an additive or baseline effect, similar to that achieved with a single AO. The combination of AO52.1ⁿ with AO52.2 or AO52.3 was antagonistic resulting in no measurable exon skipping (Figure S2). No synergistic cocktails were identified, therefore AO52.1ⁿ was chosen as the most promising candidate and the sequence was synthesised as a PMO for further analysis (Table 1).

2.3. PMO52 Induces Efficient Exon 52 Skipping and an Increase in Fibrillin-1 Microfibrils Determined by Immunofluorescent Staining

To both confirm the efficiency of the AO52.1ⁿ sequence as a PMO, and to assess the effect of exon 52 skipping on fibrillin-1 microfibril formation, PMO52 was transfected into healthy control fibroblasts. An electroporation-based transfection method, nucleofection, was used to deliver PMO52 into control cells at two concentrations, 250 and 50 μ M, as calculated in a 20 μ L cuvette. Transfected cells were plated either directly into 24 well plates or onto coverslips and incubated for 72 h before cells were collected for RNA analysis and coverslips fixed for immunofluorescent staining.

Representative results of healthy control cells treated with PMO52 are presented in Figure 3a. These representative RT-PCR results reflect exon 52 removal from approximately 100% of transcripts, with no measurable FL product remaining. The lower AO concentration was observed to induce approximately 50% skipping, with no endogenous exon 52 skipping observed in either the control or untreated samples (Figure 3a). Analysis of RT-PCR amplicons across four replicates revealed relatively consistent dose-dependent exon 52 skipping. On average Δ 52 transcripts constituted 91% of total *FBN1* transcripts from cells transfected at the higher concentration and 55% at the lower concentration (Figure 3b). The lowest skipping efficiency at the highest concentration was 74%; in the same experiment, the lower concentration maintained the average 55% skipping efficiency (Figure 3b).

Fibrillin-1 protein was detected through immunofluorescent staining using a fibrillin-1 specific primary antibody and a fluorescently tagged secondary. Staining of the untreated sample revealed the long-thin extracellular fibre-like formations expected of fibrillin-1 (Figure 3c iii). Notably, the morphology of fibres in the sample with more than 90% skipping is trending toward those seen in the untreated healthy control (Figure 3c i,iii). The abundance of fibrillin-1 staining, as well as the abundance of fibre-like formations is, however, noticeably reduced in the 250 μ M-treated samples. In contrast to the fibre formation in both untreated and high concentration of PMO52, healthy control cells treated with 50 μ M of PMO52, present with a complete loss of fibrillin-1 fibres and an overall reduction in fibrillin-1 staining (Figure 3c ii).

Following successful exon 52 skipping in healthy control fibroblasts, PMO52 was further assessed in fibroblasts derived from an individual with Marfan syndrome obtained from the NIGMS Human Genetic Cell Repository at the Coriell Institute for Medical Research. The patient fibroblasts (MFS Δ 52) were reported to harbour a silent c.6354C > T, p.(Ile2118Ile) mutation in *FBN1* that was found to result in the in-frame skipping of exon 52 [60]. PMO52 was nucleofected into the MFS Δ 52 and healthy control fibroblasts and collected for RNA and protein analysis after 4 days. The PMO52 sequence resulted in robust skipping in both cell lines and a strong dose response was observed. Treatment with 50 μ M resulted in 64% and 41% exon 52 skipping in MFS Δ 52 and healthy control fibroblasts, respectively (Figure 4a). Increasing the concentration to 250 μ M resulted in 92% skipping in both cell lines (Figure 4a).

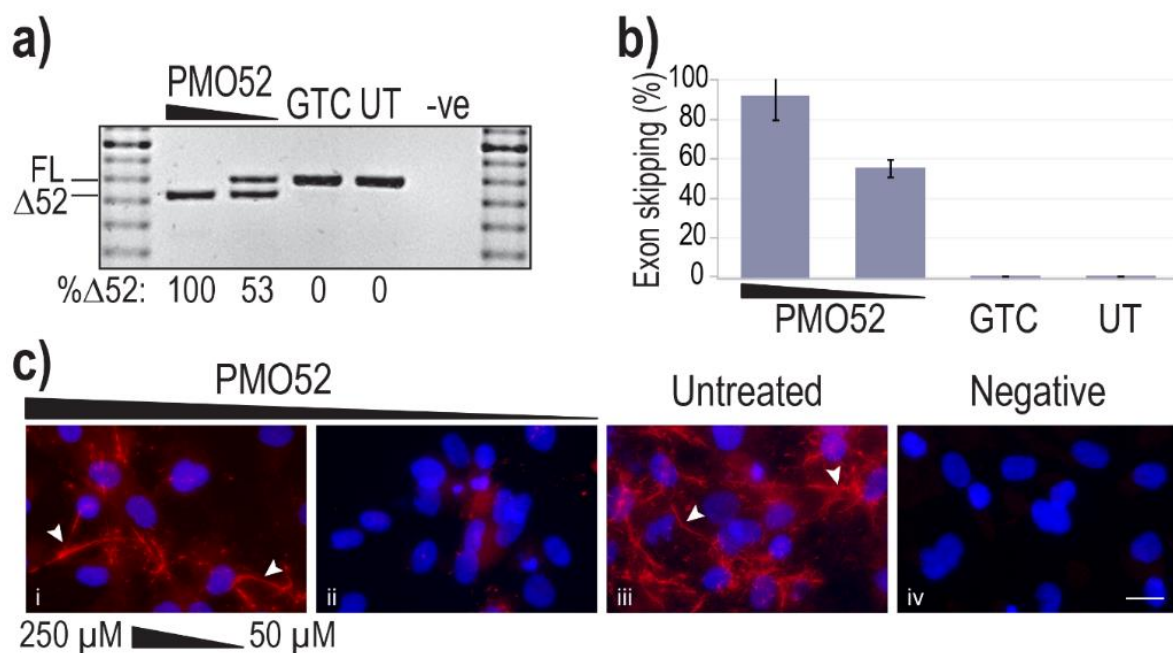


Figure 3. Efficiency and effect of PMO52. Healthy control fibroblasts were harvested for protein and RNA analysis, 72 h after nucleofection with PMO52 at concentrations of 250 μM and 50 μM ; calculated in a 20 μL cuvette. (a) Agarose gel fractionation of *FBN1* exons 47 to 54 amplicons showing full-length (FL, 859 bp) and exon 52-skipped ($\Delta 52$, 793 bp) transcripts. The values below the gel image indicate the percentage of $\Delta 52$ transcripts. GTC: Gene Tools control PMO, UT: Untreated control, -ve: RT-PCR negative control, 100 bp molecular marker used as a size reference. The gels were cropped for presentation. Full gel images are presented in Figure S1 (b) The percentage of full-length transcript relative to total *FBN1* transcript across four biological replicates (means plus error bars. Error bars = standard deviation, $n = 4$). (c) Fibrillin-1 protein analysed via immunofluorescent staining. Merged fluorescence images of Hoechst staining of the nucleus (blue) and fibrillin-1 (red) with ‘healthy’ fibre-like morphology of fibrillin-1 indicated by white arrowheads. Negative: no primary antibody added, to control for non-specific binding of the secondary antibody. Untreated: no PMO added. Scale bar = 20 μm . The images were cropped for presentation. Full images are presented in Figure S3.

Immunofluorescence once again revealed the strong fibre-like structures formed by fibrillin-1 in the untreated, and GTC treated, healthy control fibroblasts. These fibres were completely lost when 41% skipping was induced (Figure 4b vi). The staining pattern mirrored that observed in the untreated $\text{MFS}^{\Delta 52}$ fibroblasts with no fibre formation and minimal diffuse fibrillin-1 staining (Figure 4b iv). The minor increase in the proportion of skipped products after treatment of $\text{MFS}^{\Delta 52}$ fibroblasts with 50 μM of PMO52, did not alter the fibrillin-1 staining pattern (Figure 4b ii). In both cell lines, treatment with 250 μM of PMO52 resulted in the formation of fibrillin-1 fibres. In the healthy control cells, these fibres, while of high staining intensity, were fragmented and reduced in abundance compared to the untreated healthy control sample (Figure 4b v,viii). However, in $\text{MFS}^{\Delta 52}$ cells treated with the 250 μM , fibrillin-1 fibres had a continuous, non-fragmented morphology trending toward those seen in the untreated healthy control (Figure 4b i,viii). The fibres are also relatively abundant filling the majority of the field-of-view; however, they are not as plentiful as those seen in the untreated healthy control that form a multi-layered lattice (Figure 4b i,viii). Similar staining patterns were seen across multiple biological replicates representative images of one replicate are presented in Figure S4.

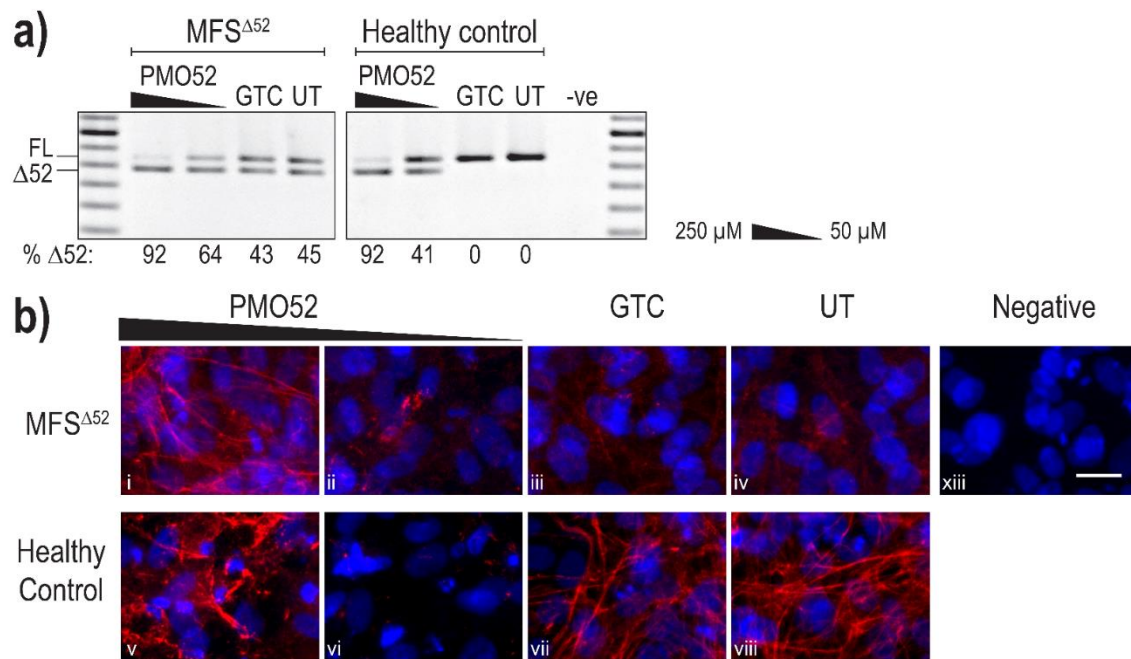


Figure 4. Evaluation of PMO52 in *MFS*^{Δ52} fibroblasts. Healthy control and *MFS*^{Δ52} patient fibroblasts were transfected with PMO52 (250 μM and 50 μM), GTC or left untreated. Cells were collected 4 days post-transfection. **(a)** RT-PCR analysis of *FBNI* exons 47 to 54 amplicons showing full-length (FL, 859 bp) and exon 52-skipped (Δ52, 793 bp) transcripts. The relative abundance (%) of Δ52 amplicons are shown below each gel image. GTC: Gene Tools control PMO, UT: untreated control, -ve: RT-PCR negative control, 100 bp molecular marker used as a size reference. The gels were cropped for presentation. Full gel images are presented in Figure S1 **(b)** Representative images showing fibrillin-1 (red) and nuclei (blue) in *MFS*^{Δ52} or healthy control fibroblasts treated with (i,v) 250 μM of PMO52, (ii,vi) 50 μM of PMO52, (iii,vii) 250 μM of GTC or (iv,viii) left untreated. (xiii) negative control with no primary antibody added. Scale bar = 20 μm. The images were cropped for presentation. Full images are presented in Figure S3.

3. Discussion

Although Marfan syndrome is well established as an inherited connective tissue disorder caused by mutations in the fibrillin-1 gene, the exact mechanism of pathogenesis has not been fully resolved. Current understanding suggests that the pathogenesis is dependent on the mutation type with an overarching basis that a lack of functional fibrillin-1 microfibrils leads to *TGF-β* dysregulation, further compounding ECM destabilisation [15,61]. Therefore, we propose that removal of a mutation-associated exon from all *FBNI* transcripts could result in the production of internally truncated fibrillin-1 proteins that retain some function and are able to form microfibrils. We addressed this hypothesis by designing antisense oligonucleotides to induce exon 52 exclusion from unaffected *FBNI* pre-mRNA. We suggest that many fibrillin-1 gene lesions will be amenable to the removal of the affected exon for two main reasons. Firstly, fibrillin-1 is highly repetitive suggesting the possibility of functional redundancy. Secondly, excluding exons 2, 3, 64, 65 and 66, the majority of fibrillin-1 exons are in-frame, and therefore can be removed without disrupting the reading frame.

Here, we describe evidence for the efficient removal of *FBNI* exon 52. Of the five 2'OMe-PS AOs tested three were found to induce exon 52 skipping. Earlier dystrophin screening studies similarly found that two out of three AOs induced some skipping, albeit at different efficiencies [59]. The different delivery methods, concentration and length of incubation that were used when assessing the 2'OMe-PS and PMO sequences, make it impossible to directly compare their efficiencies. However, our data show that the proportion of Δ52 transcripts induced is greater when using the PMO sequence, this is likely in-part because a higher PMO concentration and longer incubation period could be used without a large decrease in cell viability. A higher concentration is generally re-

quired for the PMOs as the neutral charge of the chemistry hinders cellular uptake [62,63]. Immunofluorescent staining of fibrillin-1 in treated cells supports the hypothesis that fibrillin-1 Δ 52 proteins can interact to form multimers. We observed fibre formation, mirroring that of the untreated control cells, when more than 92% exon 52 skipping was induced in either the healthy control or MFS Δ 52 patient fibroblasts. We also established that inducing approximately 50% exon 52 skipping results in a complete loss of fibrillin-1 fibre staining in healthy control fibroblasts mimicking the disease-like state caused by splicing mutations. Together, these results demonstrate proof-of-concept that the internally truncated fibrillin-1 Δ 52 proteins produced through efficient exon 52 skipping are able to form multimers.

Of particular interest, is the total loss of microfibril formation that results from the induction of a combination of wild-type and *FBN1* Δ 52 transcripts after sub-optimal levels of PMO-induced exon skipping. This finding demonstrates the inability of the heterogeneous population of Δ 52 fibrillin-1 proteins to form microfibrils, supporting the dominant-negative pathogenic mechanism [64]. We observed a similar lack of extracellular fibrillin-1 as that reported by Liu et al. [65] resulting from the c.6354C > T mutation that leads to 41% fibrillin-1 synthesis and only 5% deposition of fibrillin-1 in the extracellular matrix. However, this finding also has relevance to mapping of amenable *FBN1* exons that could be targeted in a splice intervention therapy. The elimination of microfibrils and subsequent formation with increased skipping efficiency could prove to be an invaluable tool in optimisation of fibrillin-1 AO sequences as well as identification of potential target exons for therapeutic intervention. Importantly, being able to induce a disease-like state would allow the use of healthy control cells, rather than specific patient cells, for the identification of exons that when removed do not affect the expression or function of fibrillin-1. Furthermore the occurrence and severity of dominant negative effects depend on the mutation type and location [66]. For example, duplications causing a mouse model of tight skin syndrome, result in a larger fibrillin-1 protein that has been shown to only form microfibrils in the presence of wild-type fibrillin-1 [67]. While the co-polymerisation of the two fibrillin-1 isoforms forms functionally deficient microfibrils, the outcome is a mild phenotype lacking vascular involvement [67]. Identification of such naturally occurring co-polymerisation events that lead to a mild phenotype could reveal potential therapeutic strategies to assess in the future.

We predict that the AOs reported here can manipulate *FBN1* splicing such that, at lower skipping efficiencies disease characteristics can be induced in unaffected cells and upon increased efficiency, sufficient skipping can be induced to reduce the key phenotype of MFS. This prediction is based on the dominant-negative model that suggests that in the presence of two protein isoforms, the aberrant protein disrupts the formation of microfibrils by the wild-type protein [18]. It is unknown exactly what ratio of wild-type to aberrant proteins would negate the dominant negative effects. However, the results presented here suggest that this tolerable threshold may be approximately 95%. We demonstrate that fibrillin-1 fibres can be formed when exon 52 skipping is sufficient, likely >90% skipping, such that more than 95% of total multimers that are formed would be of the fibrillin-1 Δ 52-fibrillin-1 Δ 52 structure. We also note, however, that *FBN1* mutations resulting in haploinsufficiency lead to disease. Therefore, we believe that the abundance of microfibrils has to be maintained, as a minimum, above that observed in haploinsufficiency patients [19,21]. It is also important to note that while this exon skipping strategy relies on excluding the target exon from both the mutation-harboring and healthy *FBN1* transcripts, the exon skipping is at the mRNA level, and therefore not permanent as would be the case for other techniques such as gene therapy.

While we demonstrated efficient and consistent exon skipping using PMO52, the concentrations used are relatively high, when compared to similar studies targeting other genes [59,68]. One of the possible explanations for the high concentration required is the abundance of fibrillin-1 transcripts. Fibrillin-1 RNA is expressed in the vast majority of cell types and is maintained at relatively high levels throughout the body [69]. We

noted the efficient PCR amplification of *FBN1* transcripts; requiring 20 or fewer rounds of amplification coupled with the need for very low template concentrations (25 ng). While the in vitro PMO transfection concentrations used seem relatively high, we noticed no changes in morphology or health of cell cultures up to four days post-transfection with PMO52. The PMO chemistry is generally considered to be safe with no off-target effects nor toxicity [43,57,62]. Nevertheless, while the PMO chemistry may be safe and a higher concentration required due to the level of fibrillin-1 expression, there are still several ways in which the efficiency of an AO can be improved, including optimisation of AO delivery, sequence, length and chemistry. Further optimisation could allow for the use of a significantly lower dosage that in turn would not only reduce the possibility of off-target effects or toxicity but also lower the cost of treatment.

The fibrillin-1 protein produced by excising exon 52 is predicted to be internally truncated, fibrillin-1^{Δ52}, and lack the last seven amino acids of the sixth TB domain. This isoform has only been reported in the context of exon 52 mutations, where it is known to act in a dominant-negative manner against the wild-type protein and result in a severe lack of functional microfibrils [60,65]. Liu et al. [65] also reported that an exon 52 splicing mutation leads to reduced fibrillin-1 synthesis, less than 50% of that observed in healthy controls, while the mutant mRNA levels remain unchanged, suggesting that the fibrillin-1^{Δ52} proteins are unstable. Liu et al. [65] suggests this instability may result from the partial deletion of a TB domain that leads to misfolding of the fibrillin-1 protein increasing its susceptibility to proteolysis. If this is the case then attempts to induce exon skipping of other exons encoding partial TB domains; 10, 11, 17, 18, 38, 39, 42, 43 and 51, would likely face the same issue. It is possible that removal of the two exons encoding the TB domain as a pair could solve this problem. However, our findings suggest that the fibrillin-1^{Δ52} proteins produced through exon 52 skipping are able to be synthesised, secreted from the cell and form fibre-like structures in both healthy control and MFS^{Δ52} patient fibroblasts. Nevertheless, the synthesis, deposition and function of fibrillin-1^{Δ52}, especially in the absence of wild-type fibrillin-1, needs to be investigated further.

Here, we illustrate that when fibrillin-1^{Δ52} is the predominant product it is able to be both synthesised and secreted from the cell, with no evidence of intracellular staining. We also demonstrate that fibrillin-1^{Δ52} proteins can form fibres, provided that *FBN1*^{Δ52} transcripts make up more than 90% of total *FBN1* transcripts. These results suggest that the fibrillin-1^{Δ52} protein is at least partially functional, although further protein analysis is required to assess if the fibres formed can interact with the microfibril associated proteins with which fibrillin-1 naturally interacts. The ability of fibrillin-1^{Δ52} proteins to sequester TGF-β also needs to be assessed. If removal of exon 52 disrupts the regulation of TGF-β, then regardless of the high skipping efficiency and fibre formation that is observed, symptoms such as aortic growth would continue to progress with no benefit from this treatment. To assess the effect of *FBN1* exon skipping and the function of the induced fibrillin-1 isoform especially the impacts on TGF-β signalling, surrogate markers such as the phosphorylation of Smad2 can be analysed [70,71]. The level of active and total TGF-β can similarly be assessed as a measure of functionality [61,71,72]. Such assays were outside the scope of the current study and will be the focus of further research.

As previously noted, our results support the hypothesis that fibrillin-1^{Δ52} can form fibres. However, while the morphology of fibres is superficially similar to that of the untreated, healthy control, their abundance is reduced. The reduction in abundance could be the result of the experimental design and protocols. For example, nucleofection can cause cell stress potentially reducing fibrillin-1 expression, or the transfection incubation time could be insufficient to allow more efficient formation of microfibrils after treatment. However, it is likely that, as reported by Liu et al. [65], fibrillin-1^{Δ52} synthesis is reduced in comparison to the wild-type. Western blotting analysis of intracellular and extracellular fibrillin-1 was attempted, however, due to poor signal and resolution in samples from healthy control fibroblasts we were unable to confirm any changes in fibrillin-1 abundance. Further optimisation of the Western blot protocol to produce reliable results is required

before the effect of *FBN1* exon skipping on the abundance of fibrillin-1 can be assessed. While restoring microfibril abundance and function to a 'normal' state would be ideal, this may not be possible. We believe that any increase in functional microfibrils could provide a therapeutic benefit by reducing disease progression and severity.

As discussed earlier, the current standard of care for individuals living with MFS relies heavily on invasive surgical interventions and the lifelong use of medicines such as β -adrenergic receptor blockades that slow the progression of aortic dilation [33–35]. These interventions have proven lifesaving, as well as life-extending [5,73]. However, the burden of MFS on quality of life, and the economic stress, for both patients and their families, remains substantial [74,75]. In more recent years major efforts have been made to discover and develop therapeutics for MFS [31–33,76]. Research has focused on slowing aortic growth as well as a continued improvement upon current treatment strategies for the main symptoms of MFS. With FDA approval of AO therapeutics to restore gene function in spinal muscular atrophy [45] and Duchenne muscular dystrophy [77–79], we suggest that antisense oligonucleotide-mediated splice switching as described here could be an appropriate direction for the development of therapies for Marfan syndrome.

In conclusion, this study assessed the ability of a suite of AOs to induce targeted exon 52 skipping from full-length *FBN1* mRNA transcripts expressed in healthy control fibroblasts. The most efficient sequence, and the consequences of splice modification, was further evaluated in both healthy control and MFS $\Delta 52$ patient fibroblasts. We showed in vitro, that AO52.1ⁿ, AO52.1^m and AO52.3 as well as PMO52 induced dose-dependent exon 52 skipping. Encouragingly the presence of more than 90% of one transcript type; wild-type or *FBN1* $\Delta 52$, corresponded with the formation of fibrillin-1 fibres in both cell lines. In contrast, a mixed transcript pool resulted with the complete loss of fibrillin-1 fibres, mimicking the disease-like state.

While this study is a preliminary, in vitro investigation, our candidate PMO consistently induces efficient exon 52 exclusion while maintaining fibrillin-1 $\Delta 52$ fibre formation. With increasing numbers of AO therapeutics being approved for clinical use, our results suggest that PMO52 may be an attractive therapeutic option for the treatment of Marfan syndrome caused by mutations in fibrillin-1 exon 52. This study provides proof-of-concept and a foundation for the further development of antisense oligonucleotide therapies for Marfan syndrome.

4. Materials and Methods

4.1. Design and Synthesis of Antisense Oligonucleotides

Antisense oligonucleotides were designed to target splicing regulatory motifs at the exon-intron junctions as well as exonic splicing enhancer sequences predicted using the SpliceAid web tool [58]. AO sequences were also analysed using NCBI nucleotide BLAST (NCBI, Bethesda, MD, USA) [80] to identify any possible off-target annealing. Antisense oligonucleotides with 2'OMe-PS chemistry were purchased from TriLink biotechnologies (Maravai LifeSciences, San Diego, CA, USA), and PMOs were purchased from GeneTools LLC (Philomath, OR, USA). The nomenclature of AOs is based on that described by Mann et al. [42] and provides information on the gene, exon, annealing co-ordinates and species. A full list of AOs used in this study are provided in Table 1. The *FBN1* exon nomenclature was determined with respect to the NCBI Reference Sequence NM_000138.4, in which the translation start codon is in the second of 66 exons.

4.2. Cell Culture and Transfection

Fibroblasts were originally sourced from a dermal biopsy derived from a healthy volunteer with informed consent. The following cell line was obtained from the NIGMS Human Genetic Cell Repository at the Coriell Institute for Medical Research: GM21941 (Camden, NJ, USA). The use of human cells for this research was approved by the Murdoch University Human Ethics Committee, approval numbers 2013_156 (25 October 2013) and 2017_101 (12 May 2017) and The University of Western Australia Human Research Ethics

Committee, approval number RA/4/1/2295 (21 April 2009). Healthy control fibroblasts were maintained in Dulbecco's Modified Essential Medium (DMEM, Gibco; Thermo Fisher Scientific, Melbourne, Australia) supplemented with 10% foetal bovine serum (FBS, Scientifix, Melbourne, Australia). The MFS^{Δ52} patient fibroblasts were maintained in DMEM supplemented with 15% FBS (Scientifix, Melbourne, Australia) and 1% glutaMax (Gibco; Thermo Fisher Scientific, Melbourne, Australia). Both cell lines were maintained at 37 °C with 5% CO₂.

Antisense oligonucleotides (2'OMe-PS chemistry) used for target site screening were transfected into healthy control fibroblasts using Lipofectamine 3000 (L3K, Life Technologies, Melbourne, Australia). Transfections were prepared by incubating the AO with 3 μL of L3K, at room temperature in 50 μL of Opti-MEM (Gibco; Thermo Fisher Scientific, Melbourne, Australia), according to manufacturer's protocol. The transfection mixture was then diluted to the desired AO concentration in a final volume of 1 mL and applied to cells. Transfected cells were incubated for 24 h before collection.

The PMO was delivered using the 4D-Nucleofector™ and P3 nucleofection kits (Lonza, Melbourne, Australia). One microliter of stock PMO (5 mM), either undiluted (250 μM) or diluted 1:4 in sterilised water (50 μM), was added into a cuvette along with 300,000 fibroblasts resuspended in 19 μL of pre-warmed transfection solution. The mixture of fibroblasts and PMO was subsequently nucleofected using the pulse code, CA 137, previously optimised in our laboratory for dermal fibroblasts. Nucleofected fibroblasts were maintained in DMEM supplemented with 5% FBS before collection after 3 or 4 days.

4.3. RNA Extraction and RT-PCR Analysis

Total RNA was extracted using MagMax™ nucleic acid isolation kits (Thermo Fisher Scientific, Melbourne, Australia) as per the manufacturer's protocol. Total RNA concentration and purity were determined using a Nanodrop 1000 spectrophotometer (Thermo Fisher Scientific, Melbourne, Australia). Transcripts were amplified using one-step SuperScript® III reverse transcriptase (Thermo Fisher Scientific, Melbourne, Australia) with 25 ng of total RNA as a template. To assess exon 52 skipping, *FBN1* transcripts were amplified using exon 47 Forward (5'-GGTTTCATCCT-TTCTCACAAC-3') and exon 54 Reverse (5'-TCACATGTCATCATTGGACC-3') primers (Integrated DNA Technologies, Sydney, Australia). The cycling conditions were as follows; 55 °C for 30 min, 94 °C for 2 min followed by 20 cycles of 94 °C for 30 s, 55 °C for 30 s and 68 °C for 1 min. The PCR amplicons were fractionated on 2% agarose gels in Tris-Acetate-EDTA buffer. Relative exon skipping efficiency was estimated through densitometric analysis of images using ImageJ (version 1.8.0_112) imaging software (NIH, Bethesda, MD, USA) [81] and reported as the proportion of FL or Δ52 transcript products relative to the sum of products.

4.4. Immunofluorescence

Immediately after nucleofection, 100,000 fibroblasts were seeded into each well of a 24-well plate lined with a 13 mm #0 round uncoated glass coverslip. Cells were incubated for 72 h before being fixed in ice-cold acetone: methanol (1:1, *v:v*) and allowed to air dry. Fixed cells were washed once with PBS to rehydrate before blocking with 10% goat serum in PBS for 1 h at room temperature. The primary antibody, Anti-fibrillin-1 antibody clone 26 (Merck Millipore, Sydney, Australia), was applied at a dilution of 1:100 in 1% goat serum-PBS and incubated overnight at 4 °C. Secondary antibody; AlexaFluor568 anti-mouse IgG (Thermo Fisher Scientific, VIC, Australia) was applied, 1:400, for 1 h at room temperature, and co-stained with Hoechst 33,342 (Sigma-Aldrich, Sydney, Australia) for nuclei detection (1 mg/mL diluted, 1:125). Coverslips were mounted using ProLong™ Gold antifade mountant (Thermo Fisher Scientific, Melbourne, Australia). Fibrillin-1 was detected using a Nikon 80i microscope with NIS-Elements software (Nikon, Adelaide, Australia). The brightness and contrast of individual channel images were altered equally for each image, then merged. The merged image was cropped from the original

1280 × 1024 pixel image using Adobe Photoshop CC. A 20 µm scale bar was added using ImageJ software (NIH, Bethesda, MD, USA) [81].

Supplementary Materials: The following are available online at <https://www.mdpi.com/article/10.3390/ijms22073479/s1>, Figure S1: Full gel images for figures listed, Figure S2: Evaluation of AO cocktails designed to induce *FBN1* exon 52 skipping, Figure S3: Full immunofluorescence staining images for figures listed, Figure S4: Additional evaluation of PMO52.

Author Contributions: Conceptualization, J.M.C. and S.D.W.; methodology, J.M.C. and K.G.; formal analysis, J.M.C.; investigation, J.M.C. and K.G.; writing—original draft preparation, J.M.C.; writing—review and editing, J.M.C., K.G., S.F. and S.D.W.; visualization, J.M.C.; supervision, S.F., S.D.W.; funding acquisition, S.D.W. All authors have read and agreed to the published version of the manuscript.

Funding: This research was funded by NHMRC, grant number APP 1144791. J.C. received a Research Training Program scholarship from Murdoch University. This work was conducted in Perth, Australia.

Institutional Review Board Statement: Primary dermal fibroblasts derived from a healthy volunteer after informed consent. The MFS^{Δ52} patient fibroblasts were obtained from the NIGMS Human Genetic Cell Repository at the Coriell Institute for Medical Research (Cat#: GM21941). The use of human cells for this research was approved by the Murdoch University Human Ethics Committee, approval numbers 2013_156 (25 October 2013) and 2017_101 (12 May 2017) and The University of Western Australia Human Research Ethics Committee, approval number RA/4/1/2295 (21 April 2009).

Informed Consent Statement: Informed consent was obtained from all subjects involved in the study.

Data Availability Statement: Not applicable.

Conflicts of Interest: The authors declare no conflict of interest.

References

1. Ammash, N.M.; Sundt, T.M.; Connolly, H.M. Marfan Syndrome-Diagnosis and Management. *Curr. Probl. Cardiol.* **2008**, *33*, 7–39. [[CrossRef](#)] [[PubMed](#)]
2. Pyeritz, R.E. Recent Progress in Understanding the Natural and Clinical Histories of the Marfan Syndrome. *Trends Cardiovasc. Med.* **2016**, *26*, 423–428. [[CrossRef](#)]
3. Collod-Bérout, G.; Boileau, C. Marfan Syndrome in the Third Millennium. *Eur. J. Hum. Genet.* **2002**, *10*, 673–681. [[CrossRef](#)]
4. Loeys, B.L.; Gerber, E.E.; Riegert-Johnson, D.; Iqbal, S.; Whiteman, P.; McConnell, V.; Chillakuri, C.R.; Macaya, D.; Coucke, P.J.; De Paepe, A.; et al. Mutations in Fibrillin-1 Cause Congenital Scleroderma: Stiff Skin Syndrome. *Sci. Transl. Med.* **2010**, *2*, 23ra20. [[CrossRef](#)]
5. Murdoch, J.L.; Walker, B.A.; Halpern, B.L.; Kuzma, J.W.; McKusick, V.A. Life Expectancy and Causes of Death in the Marfan Syndrome. *N. Engl. J. Med.* **1972**, *286*, 804–808. [[CrossRef](#)]
6. Sakai, L.Y.; Keene, D.R.; Engvall, E. Fibrillin, a New 350-KD Glycoprotein, Is a Component of Extracellular Microfibrils. *J. Cell Biol.* **1986**, *103*, 2499–2509. [[CrossRef](#)]
7. Dietz, H.C.; Cutting, G.R.; Pyeritz, R.E.; Maslen, C.L.; Sakai, L.Y.; Corson, G.M.; Puffenberger, E.G.; Hamosh, A.; Nanthakumar, E.J.; Curren, S.M. Marfan Syndrome Caused by a Recurrent de Novo Missense Mutation in the Fibrillin Gene. *Nature* **1991**, *352*, 337–339. [[CrossRef](#)]
8. Hollister, D.W.; Godfrey, M.; Sakai, L.Y.; Pyeritz, R.E. Immunohistologic Abnormalities of the Microfibrillar-Fiber System in the Marfan Syndrome. *N. Engl. J. Med.* **1990**, *323*, 152–159. [[CrossRef](#)]
9. Stenson, P.D.; Mort, M.; Ball, E.V.; Chapman, M.; Evans, K.; Azevedo, L.; Hayden, M.; Heywood, S.; Millar, D.S.; Phillips, A.D.; et al. The Human Gene Mutation Database (HGMD[®]): Optimizing Its Use in a Clinical Diagnostic or Research Setting. *Hum. Genet.* **2020**. [[CrossRef](#)] [[PubMed](#)]
10. Reinhardt, D.P.; Gambee, J.E.; Ono, R.N.; Bächinger, H.P.; Sakai, L.Y. Initial Steps in Assembly of Microfibrils. Formation of Disulfide-Cross-Linked Multimers Containing Fibrillin-1. *J. Biol. Chem.* **2000**, *275*, 2205–2210. [[CrossRef](#)] [[PubMed](#)]
11. Gibson, M.A. *Microfibril-Associated Glycoprotein-1 (MAGP-1) and Other Non-Fibrillin Macromolecules Which May Possess a Functional Association with the 10 Nm Microfibrils*; Landes Bioscience: Austin, TX, USA, 2013.
12. Sengle, G.; Sakai, L.Y. The Fibrillin Microfibril Scaffold: A Niche for Growth Factors and Mechanosensation? *Matrix Biol.* **2015**, *47*, 3–12. [[CrossRef](#)]
13. Kielty, C.M.; Shuttleworth, C.A. Fibrillin-Containing Microfibrils: Structure and Function in Health and Disease. *Int. J. Biochem. Cell Biol.* **1995**, *27*, 747–760. [[CrossRef](#)]

14. Isogai, Z.; Ono, R.N.; Ushiro, S.; Keene, D.R.; Chen, Y.; Mazziere, R.; Charbonneau, N.L.; Reinhardt, D.P.; Rifkin, D.B.; Sakai, L.Y. Latent Transforming Growth Factor β -Binding Protein 1 Interacts with Fibrillin and Is a Microfibril-Associated Protein. *J. Biol. Chem.* **2003**, *278*, 2750–2757. [[CrossRef](#)] [[PubMed](#)]
15. Ramachandra, C.J.A.; Mehta, A.; Guo, K.W.Q.; Wong, P.; Tan, J.L.; Shim, W. Molecular Pathogenesis of Marfan Syndrome. *Int. J. Cardiol.* **2015**, *187*, 585–591. [[CrossRef](#)] [[PubMed](#)]
16. Doyle, J.J.; Gerber, E.E.; Dietz, H.C. Matrix-Dependent Perturbation of TGF β Signaling and Disease. *FEBS Lett.* **2012**, *586*, 2003–2015. [[CrossRef](#)] [[PubMed](#)]
17. Ikonomidis, J.S.; Jones, J.A.; Barbour, J.R.; Stroud, R.E.; Clark, L.L.; Kaplan, B.S.; Zeeshan, A.; Bavaria, J.E.; Gorman, J.H.; Spinale, F.G.; et al. Expression of Matrix Metalloproteinases and Endogenous Inhibitors Within Ascending Aortic Aneurysms of Patients With Marfan Syndrome. *Circulation* **2006**, *114*, I-365. [[CrossRef](#)]
18. Dietz, H.C.; McIntosh, I.; Sakai, L.Y.; Corson, G.M.; Chalberg, S.C.; Pyeritz, R.E.; Francomano, C.A. Four Novel FBN1 Mutations: Significance for Mutant Transcript Level and EGF-like Domain Calcium Binding in the Pathogenesis of Marfan Syndrome. *Genomics* **1993**, *17*, 468–475. [[CrossRef](#)]
19. de Vries, B.B.A.; Pals, G.; Odink, R.; Hamel, B.C.J. Homozygosity for a FBN1 Missense Mutation: Clinical and Molecular Evidence for Recessive Marfan Syndrome. *Eur. J. Hum. Genet.* **2007**, *15*, 930–935. [[CrossRef](#)]
20. Aoyama, T.; Francke, U.; Dietz, H.C.; Furthmayr, H. Quantitative Differences in Biosynthesis and Extracellular Deposition of Fibrillin in Cultured Fibroblasts Distinguish Five Groups of Marfan Syndrome Patients and Suggest Distinct Pathogenetic Mechanisms. *J. Clin. Invest.* **1994**, *94*, 130–137. [[CrossRef](#)]
21. Aubart, M.; Gross, M.-S.; Hanna, N.; Zabot, M.-T.; Sznajder, M.; Detaint, D.; Gouya, L.; Jondeau, G.; Boileau, C.; Stheneur, C. The Clinical Presentation of Marfan Syndrome Is Modulated by Expression of Wild-Type FBN1 Allele. *Hum. Mol. Genet.* **2015**, *24*, 2764–2770. [[CrossRef](#)] [[PubMed](#)]
22. Jensen, S.A.; Aspinall, G.; Handford, P.A. C-Terminal Propeptide Is Required for Fibrillin-1 Secretion and Blocks Premature Assembly through Linkage to Domains CbEGF41-43. *Proc. Natl. Acad. Sci. USA* **2014**, *111*, 10155–10160. [[CrossRef](#)]
23. Graul-Neumann, L.M.; Kienitz, T.; Robinson, P.N.; Baasanjav, S.; Karow, B.; Gillessen-Kaesbach, G.; Fahsold, R.; Schmidt, H.; Hoffmann, K.; Passarge, E. Marfan Syndrome with Neonatal Progeroid Syndrome-like Lipodystrophy Associated with a Novel Frameshift Mutation at the 3' Terminus of the FBN1-Gene. *Am. J. Med. Genet. A* **2010**, *152A*, 2749–2755. [[CrossRef](#)]
24. Collod-Bérout, G.; Le Bourdelles, S.; Ades, L.; Ala-Kokko, L.; Booms, P.; Boxer, M.; Child, A.; Comeglio, P.; De Paepe, A.; Hyland, J.C.; et al. Update of the UMD-FBN1 Mutation Database and Creation of an FBN1 Polymorphism Database. *Hum. Mutat.* **2003**, *22*, 199–208. [[CrossRef](#)] [[PubMed](#)]
25. Jensen, S.A.; Iqbal, S.; Lowe, E.D.; Redfield, C.; Handford, P.A. Structure and Interdomain Interactions of a Hybrid Domain: A Disulphide-Rich Module of the Fibrillin/LTBP Superfamily of Matrix Proteins. *Structure* **2009**, *17*, 759–768. [[CrossRef](#)] [[PubMed](#)]
26. Pereira, L.; D'Alessio, M.; Ramirez, F.; Lynch, J.R.; Sykes, B.; Pangilinan, T.; Bonadio, J. Genomic Organization of the Sequence Coding for Fibrillin, the Defective Gene Product in Marfan Syndrome. *Hum. Mol. Genet.* **1993**, *2*, 961–968. [[CrossRef](#)] [[PubMed](#)]
27. Jensen, S.A.; Robertson, I.B.; Handford, P.A. Dissecting the Fibrillin Microfibril: Structural Insights into Organization and Function. *Structure* **2012**, *20*, 215–225. [[CrossRef](#)]
28. Reinhardt, D.P.; Ono, R.N.; Sakai, L.Y. Calcium Stabilizes Fibrillin-1 against Proteolytic Degradation. *J. Biol. Chem.* **1997**, *272*, 1231–1236. [[CrossRef](#)] [[PubMed](#)]
29. Ramirez, F.; Gayraud, B.; Pereira, L. Marfan Syndrome: New Clues to Genotype-Phenotype Correlations. *Ann. Med.* **1999**, *31*, 202–207. [[CrossRef](#)]
30. Schrijver, I.; Liu, W.; Brenn, T.; Furthmayr, H.; Francke, U. Cysteine Substitutions in Epidermal Growth Factor-like Domains of Fibrillin-1: Distinct Effects on Biochemical and Clinical Phenotypes. *Am. J. Hum. Genet.* **1999**, *65*, 1007–1020. [[CrossRef](#)] [[PubMed](#)]
31. Habashi, J.P.; Judge, D.P.; Holm, T.M.; Cohn, R.D.; Loeys, B.L.; Cooper, T.K.; Myers, L.; Klein, E.C.; Liu, G.; Calvi, C.; et al. Losartan, an AT1 Antagonist, Prevents Aortic Aneurysm in a Mouse Model of Marfan Syndrome. *Science* **2006**, *312*, 117–121. [[CrossRef](#)]
32. Gao, L.; Chen, L.; Fan, L.; Gao, D.; Liang, Z.; Wang, R.; Lu, W. The Effect of Losartan on Progressive Aortic Dilatation in Patients with Marfan's Syndrome: A Meta-Analysis of Prospective Randomized Clinical Trials. *Int. J. Cardiol.* **2016**, *217*, 190–194. [[CrossRef](#)] [[PubMed](#)]
33. Rossi-Foulkes, R.; Roman, M.J.; Rosen, S.E.; Kramer-Fox, R.; Ehlers, K.H.; O'Loughlin, J.E.; Davis, J.G.; Devereux, R.B. Phenotypic Features and Impact of Beta Blocker or Calcium Antagonist Therapy on Aortic Lumen Size in the Marfan Syndrome. *Am. J. Cardiol.* **1999**, *83*, 1364–1368. [[CrossRef](#)]
34. Shores, J.; Berger, K.R.; Murphy, E.A.; Pyeritz, R.E. Progression of Aortic Dilatation and the Benefit of Long-Term Beta-Adrenergic Blockade in Marfan's Syndrome. *N. Engl. J. Med.* **1994**, *330*, 1335–1341. [[CrossRef](#)]
35. Judge, D.P.; Dietz, H.C. Marfan's Syndrome. *Lancet* **2005**, *366*, 1965–1976. [[CrossRef](#)]
36. Franken, R.; den Hartog, A.W.; Radonic, T.; Micha, D.; Maugeri, A.; van Dijk, F.S.; Meijers-Heijboer, H.E.; Timmermans, J.; Scholte, A.J.; van den Berg, M.P.; et al. Beneficial Outcome of Losartan Therapy Depends on Type of FBN1 Mutation in Marfan Syndrome. *Circ. Cardiovasc. Genet.* **2015**, *8*, 383–388. [[CrossRef](#)] [[PubMed](#)]
37. Shuttleworth, J.; Colman, A. Antisense Oligonucleotide-Directed Cleavage of mRNA in Xenopus Oocytes and Eggs. *EMBO J.* **1988**, *7*, 427–434. [[CrossRef](#)] [[PubMed](#)]

38. Dash, P.; Lotan, I.; Knapp, M.; Kandel, E.R.; Goelet, P. Selective Elimination of MRNAs in Vivo: Complementary Oligodeoxynucleotides Promote RNA Degradation by an RNase H-like Activity. *Proc. Natl. Acad. Sci. USA* **1987**, *84*, 7896–7900. [CrossRef]
39. Bielinska, A.; Shivdasani, R.A.; Zhang, L.Q.; Nabel, G.J. Regulation of Gene Expression with Double-Stranded Phosphorothioate Oligonucleotides. *Science* **1990**, *250*, 997–1000. [CrossRef]
40. Boiziau, C.; Kurfurst, R.; Cazenave, C.; Roig, V.; Thuong, N.T.; Toulmé, J.J. Inhibition of Translation Initiation by Antisense Oligonucleotides via an RNase-H Independent Mechanism. *Nucleic Acids Res.* **1991**, *19*, 1113–1119. [CrossRef]
41. Dominski, Z.; Kole, R. Restoration of Correct Splicing in Thalassaemic Pre-mRNA by Antisense Oligonucleotides. *Proc. Natl. Acad. Sci. USA* **1993**, *90*, 8673–8677. [CrossRef]
42. Mann, C.J.; Honeyman, K.; Cheng, A.J.; Ly, T.; Lloyd, F.; Fletcher, S.; Morgan, J.E.; Partridge, T.A.; Wilton, S.D. Antisense-Induced Exon Skipping and Synthesis of Dystrophin in the Mdx Mouse. *Proc. Natl. Acad. Sci. USA* **2001**, *98*, 42–47. [CrossRef]
43. Mendell, J.R.; Rodino-Klapac, L.R.; Sahenk, Z.; Roush, K.; Bird, L.; Lowes, L.P.; Alfano, L.; Gomez, A.M.; Lewis, S.; Kota, J.; et al. Eteplirsen for the Treatment of Duchenne Muscular Dystrophy. *Ann. Neurol.* **2013**, *74*, 637–647. [CrossRef]
44. FDA Grants Accelerated Approval to First Drug for Duchenne Muscular Dystrophy. Available online: <https://www.fda.gov/news-events/press-announcements/fda-grants-accelerated-approval-first-drug-duchenne-muscular-dystrophy> (accessed on 29 October 2020).
45. Rigo, F.; Chun, S.J.; Norris, D.A.; Hung, G.; Lee, S.; Matson, J.; Fey, R.A.; Gaus, H.; Hua, Y.; Grundy, J.S.; et al. Pharmacology of a Central Nervous System Delivered 2'-O-Methoxyethyl-Modified Survival of Motor Neuron Splicing Oligonucleotide in Mice and Nonhuman Primates. *J. Pharmacol. Exp. Ther.* **2014**, *350*, 46–55. [CrossRef]
46. FDA Approves First Drug for Spinal Muscular Atrophy. Available online: <https://www.fda.gov/news-events/press-announcements/fda-approves-first-drug-spinal-muscular-atrophy> (accessed on 11 February 2021).
47. FDA Grants Accelerated Approval to First Targeted Treatment for Rare Duchenne Muscular Dystrophy Mutation. Available online: <https://www.fda.gov/news-events/press-announcements/fda-grants-accelerated-approval-first-targeted-treatment-rare-duchenne-muscular-dystrophy-mutation> (accessed on 29 October 2020).
48. FDA Approves Targeted Treatment for Rare Duchenne Muscular Dystrophy Mutation. Available online: <https://www.fda.gov/news-events/press-announcements/fda-approves-targeted-treatment-rare-duchenne-muscular-dystrophy-mutation> (accessed on 27 January 2021).
49. FDA Approves Targeted Treatment for Rare Duchenne Muscular Dystrophy Mutation. Available online: <https://www.fda.gov/news-events/press-announcements/fda-approves-targeted-treatment-rare-duchenne-muscular-dystrophy-mutation-0> (accessed on 4 March 2021).
50. Pan, Q.; Shai, O.; Lee, L.J.; Frey, B.J.; Blencowe, B.J. Deep Surveying of Alternative Splicing Complexity in the Human Transcriptome by High-Throughput Sequencing. *Nat. Genet.* **2008**, *40*, 1413–1415. [CrossRef]
51. Cartegni, L.; Chew, S.L.; Krainer, A.R. Listening to Silence and Understanding Nonsense: Exonic Mutations That Affect Splicing. *Nat. Rev. Genet.* **2002**, *3*, 285–298. [CrossRef] [PubMed]
52. Ward, A.J.; Cooper, T.A. The Pathobiology of Splicing. *J. Pathol.* **2010**, *220*, 152–163. [CrossRef]
53. Singh, N.K.; Singh, N.N.; Androphy, E.J.; Singh, R.N. Splicing of a Critical Exon of Human Survival Motor Neuron Is Regulated by a Unique Silencer Element Located in the Last Intron. *Mol. Cell Biol.* **2006**, *26*, 1333–1346. [CrossRef]
54. Summerton, J.E.; Weller, D.D. Uncharged Morpholino-Based Polymers Having Phosphorous Containing Chiral Intersubunit Linkages. U.S. Patent No 5,185,444A, 9 February 1993.
55. Summerton, J.E. Morpholino, siRNA, and s-DNA Compared: Impact of Structure and Mechanism of Action on off-Target Effects and Sequence Specificity. *Curr. Top. Med. Chem.* **2007**, *7*, 651–660. [CrossRef]
56. Moulton, J.D.; Jiang, S. Gene Knockdowns in Adult Animals: PPMOs and Vivo-Morpholinos. *Molecules* **2009**, *14*, 1304–1323. [CrossRef] [PubMed]
57. Iversen, P.L.; Arora, V.; Acker, A.J.; Mason, D.H.; Devi, G.R. Efficacy of Antisense Morpholino Oligomer Targeted to C-Myc in Prostate Cancer Xenograft Murine Model and a Phase I Safety Study in Humans. *Clin. Cancer Res.* **2003**, *9*, 2510–2519. [PubMed]
58. Piva, F.; Giulietti, M.; Nocchi, L.; Principato, G. SpliceAid: A Database of Experimental RNA Target Motifs Bound by Splicing Proteins in Humans. *Bioinformatics* **2009**, *25*, 1211–1213. [CrossRef] [PubMed]
59. Adams, A.M.; Harding, P.L.; Iversen, P.L.; Coleman, C.; Fletcher, S.; Wilton, S.D. Antisense Oligonucleotide Induced Exon Skipping and the Dystrophin Gene Transcript: Cocktails and Chemistries. *BMC Mol. Biol.* **2007**, *8*, 57. [CrossRef]
60. Liu, W.; Qian, C.; Francke, U. Silent Mutation Induces Exon Skipping of Fibrillin-1 Gene in Marfan Syndrome. *Nat. Genet.* **1997**, *16*, 328–329. [CrossRef]
61. Neptune, E.R.; Frischmeyer, P.A.; Arking, D.E.; Myers, L.; Bunton, T.E.; Gayraud, B.; Ramirez, F.; Sakai, L.Y.; Dietz, H.C. Dysregulation of TGF-Beta Activation Contributes to Pathogenesis in Marfan Syndrome. *Nat. Genet.* **2003**, *33*, 407–411. [CrossRef] [PubMed]
62. Amantana, A.; Iversen, P.L. Pharmacokinetics and Biodistribution of Phosphorodiamidate Morpholino Antisense Oligomers. *Curr. Opin. Pharmacol.* **2005**, *5*, 550–555. [CrossRef] [PubMed]
63. Iversen, P.L.; Aird, K.M.; Wu, R.; Morse, M.M.; Devi, G.R. Cellular Uptake of Neutral Phosphorodiamidate Morpholino Oligomers. *Curr. Pharm. Biotechnol.* **2009**, *10*, 579–588. [CrossRef] [PubMed]
64. Dietz, H. Marfan Syndrome. In *GeneReviews*[®]; Adam, M.P., Ardinger, H.H., Pagon, R.A., Wallace, S.E., Bean, L.J., Stephens, K., Amemiya, A., Eds.; University of Washington, Seattle: Seattle, WA, USA, 1993.

65. Liu, W.; Schrijver, I.; Brenn, T.; Furthmayr, H.; Francke, U. Multi-Exon Deletions of the FBN1 Gene in Marfan Syndrome. *BMC Med. Genet.* **2001**, *2*, 11. [[CrossRef](#)]
66. Faivre, L.; Collod-Beroud, G.; Loeys, B.L.; Child, A.; Binquet, C.; Gautier, E.; Callewaert, B.; Arbustini, E.; Mayer, K.; Arslan-Kirchner, M.; et al. Effect of Mutation Type and Location on Clinical Outcome in 1,013 Proband with Marfan Syndrome or Related Phenotypes and FBN1 Mutations: An International Study. *Am. J. Hum. Genet.* **2007**, *81*, 454–466. [[CrossRef](#)] [[PubMed](#)]
67. Gayraud, B.; Keene, D.R.; Sakai, L.Y.; Ramirez, F. New Insights into the Assembly of Extracellular Microfibrils from the Analysis of the Fibrillin 1 Mutation in the Tight Skin Mouse. *J. Cell Biol.* **2000**, *150*, 667–680. [[CrossRef](#)] [[PubMed](#)]
68. McIntosh, C.S.; Aung-Htut, M.T.; Fletcher, S.; Wilton, S.D. Removal of the Polyglutamine Repeat of Ataxin-3 by Redirecting Pre-mRNA Processing. *Int. J. Mol. Sci.* **2019**, *20*, 5434. [[CrossRef](#)]
69. Uhlén, M.; Fagerberg, L.; Hallström, B.M.; Lindskog, C.; Oksvold, P.; Mardinoglu, A.; Sivertsson, Å.; Kampf, C.; Sjöstedt, E.; Asplund, A.; et al. Proteomics. Tissue-Based Map of the Human Proteome. *Science* **2015**, *347*, 1260419. [[CrossRef](#)]
70. Lin, M.; Zhao, S.; Liu, G.; Huang, Y.; Yu, C.; Zhao, Y.; Wang, L.; Zhang, Y.; Yan, Z.; Wang, S.; et al. Identification of Novel FBN1 Variations Implicated in Congenital Scoliosis. *J. Hum. Genet.* **2020**, *65*, 221–230. [[CrossRef](#)] [[PubMed](#)]
71. Le Goff, C.; Mahaut, C.; Wang, L.W.; Allali, S.; Abhyankar, A.; Jensen, S.; Zylberberg, L.; Collod-Beroud, G.; Bonnet, D.; Alanay, Y.; et al. Mutations in the TGFβ Binding-Protein-like Domain 5 of FBN1 Are Responsible for Acromicric and Geleophysic Dysplasias. *Am. J. Hum. Genet.* **2011**, *89*, 7–14. [[CrossRef](#)] [[PubMed](#)]
72. Chaudhry, S.S.; Cain, S.A.; Morgan, A.; Dallas, S.L.; Shuttleworth, C.A.; Kielty, C.M. Fibrillin-1 Regulates the Bioavailability of TGFβ1. *J. Cell Biol.* **2007**, *176*, 355–367. [[CrossRef](#)] [[PubMed](#)]
73. Silverman, D.I.; Burton, K.J.; Gray, J.; Bosner, M.S.; Kouchoukos, N.T.; Roman, M.J.; Boxer, M.; Devereux, R.B.; Tsipouras, P. Life Expectancy in the Marfan Syndrome. *Am. J. Cardiol.* **1995**, *75*, 157–160. [[CrossRef](#)]
74. Achelrod, D.; Blankart, C.R.; Linder, R.; von Kodolitsch, Y.; Stargardt, T. The Economic Impact of Marfan Syndrome: A Non-Experimental, Retrospective, Population-Based Matched Cohort Study. *Orphanet J. Rare Dis.* **2014**, *9*, 90. [[CrossRef](#)]
75. Blankart, C.R.; Milstein, R.; Rybczynski, M.; Schüler, H.; von Kodolitsch, Y. Economic and Care Considerations of Marfan Syndrome. *Expert Rev. Pharmacoecon. Outcomes Res.* **2016**, *16*, 591–598. [[CrossRef](#)]
76. Mullen, M.; Jin, X.Y.; Child, A.; Stuart, A.G.; Dodd, M.; Aragon-Martin, J.A.; Gaze, D.; Kiotsekoglou, A.; Yuan, L.; Hu, J.; et al. Irbesartan in Marfan Syndrome (AIMS): A Double-Blind, Placebo-Controlled Randomised Trial. *Lancet* **2019**, *394*, 2263–2270. [[CrossRef](#)]
77. Lim, K.R.Q.; Maruyama, R.; Yokota, T. Eteplirsen in the Treatment of Duchenne Muscular Dystrophy. *Drug Des. Dev. Ther.* **2017**, *11*, 533–545. [[CrossRef](#)]
78. Anwar, S.; Yokota, T. Golodirsen for Duchenne Muscular Dystrophy. *Drugs Today* **2020**, *56*, 491–504. [[CrossRef](#)]
79. Roshmi, R.R.; Yokota, T. Viltolarsen for the Treatment of Duchenne Muscular Dystrophy. *Drugs Today* **2019**, *55*, 627–639. [[CrossRef](#)] [[PubMed](#)]
80. Altschul, S.F.; Gish, W.; Miller, W.; Myers, E.W.; Lipman, D.J. Basic Local Alignment Search Tool. *J. Mol. Biol.* **1990**, *215*, 403–410. [[CrossRef](#)]
81. Schneider, C.A.; Rasband, W.S.; Eliceiri, K.W. NIH Image to ImageJ: 25 Years of Image Analysis. *Nat. Methods* **2012**, *9*, 671–675. [[CrossRef](#)] [[PubMed](#)]